A 3D RADIOLOGICAL STUDY OF AGE-RELATED QUANTITATIVE AND MORPHOLOGICAL DIFFERENCES IN THE HUMAN FEMUR: CLINICAL AND ANTHROPOLOGICAL APPLICATIONS

By

Jacqueline Lee Hislop-Jambrich

Submitted in total fulfillment of the requirements of the degree of
Doctor of Philosophy

April 2010

Melbourne Dental School

The University of Melbourne
Australia

ABSTRACT

The establishment of a valid scientific instrument for the non-destructive analysis of age-related change in the human femur is essential for the disciplines of clinical medicine and anthropology. The overall aim of this thesis was therefore to develop novel and scientifically verifiable methods for using multiple detector-row computed tomographic (MDCT) data to produce a population-based, morphometric and densitometric record of age-related differences in human femoral bone. The resulting study of contemporary urban Australians is the first to use MDCT data to produce a contemporary model of age-related differences of the human femur.

Four independent empirical studies were performed, each of which established the validity of the mortuary-sourced MDCT data, and then reported the age-related radiological findings. The adult population used for this work was taken from the high-resolution MDCT scans performed routinely at the Victorian Institute of Forensic Medicine (VIFM) in Melbourne Victoria Australia. The scans were therefore from those who died unexpectedly in the state of Victoria, and who had no disease or pathology involving the femur.

The first study engaged clinical quantitative computed tomography (QCT) software to create a model of the bilateral three-dimensional (3D) densitometric characteristics of the population. The hypothesis was that clinical software may be used effectively on mortuary-based MDCT data to derive population-based assessments of quantitative bone characteristics. Aspects of reproducibility, quality assurance and calibration were all extensively investigated. Clinical ionising-radiation dose estimation software was also used to compare the effective dose delivered during the mortuary MDCT acquisition, to what may be expected in implementing a similar protocol on the living. Results established that a non-destructive QCT technique may be effectively employed using mortuary MDCT data for the purposes of an adult population-based analysis.

Results also demonstrated significant differences in gender and age-based expressions of bone mineral and spatial QCT characteristics. Ionising radiation dose calculations showed little variance between the VIFM and theorised clinical protocols.

The second study used those same MDCT data to produce 3D image-renders of the bilateral femora. The hypothesis was that there were predictable morphologic age, gender and symmetry related differences within a contemporary predominantly urban adult population spanning 80 years. A series of novel and adapted caliper-type measurements, designed to evaluate age-related differences were implemented. Results were then compared in terms of the physical features of the individuals, such as weight, height and age. A study of femoral symmetry was also completed. Results demonstrated large variability of symmetry in individuals and of deep and surface morphometry across the group generally. Results also demonstrated that irrespective of age, all morphological variables tested were discriminating for gender.

The third study used results from an analysis of 17 right-sided femoral specimens from the Melbourne Femur Collection (MFC), to assess the impact of three different MDCT scanning conditions on spatial and quantitative measurements of bone. The hypothesis was that alterations in the scanning conditions and environment would produce little change in the spatial assessments, and consistent variation for the quantitative evaluations. Results demonstrated a strong and predictable correlation in all scanning conditions for both spatial and quantitative assessments.

The fourth study produced an epidemiological review of all hip fractures in bodies admitted to the VIFM for autopsy in 2008, as well as a QCT and morphometric assessment from 14 unilateral hip fracture cases. The hypothesis was that the fracture cases would present with dissimilar QCT and morphometric assessments as the normal or un-fractured control group from the first two research chapters. While results demonstrated no difference in morphometric

features between the fractured and normal groups, there were significant differences (p<0.005) for BMD, bone mass and cortical depth variables. The findings indicate a high sensitivity of these 3D variables for the determination of relative risk of femoral neck fracture. The cortical depth comparison also demonstrated that there were definite “safe” and “unsafe” levels expressed in this variable, in terms of low and high probability of femoral neck fracture. This high-level distinction is not currently available clinically using 2D bone assessments.

Assessing individual biological-age from the femora after they have reached skeletal maturity has previously been recognised as problematic. Results from this study have however demonstrated that it is possible to use non-destructive modified clinical and anthropological techniques on mortuary-based MDCT data to quantify age-related differences in a contemporary urban population of diverse racial backgrounds.

DECLARATION

This is to certify that

(i) this thesis comprises only my original work towards the PhD except where indicated,

(ii) due acknowledgement has been made in the text to all other materials used,

(iii) the thesis is less than 100 000 words in length exclusive of tables, maps, bibliographies and appendices.

Jacqueline L Hislop-Jambrich

…….. 30th day of April 2010

PREFACE

The results of these studies have been communicated in the following publications and at the scientific meetings listed:

Refereed Journal Publications:

J.L. Hislop-Jambrich, Do bones get wrinkles? An overview of current understanding of bone biology. Journal of ANZ Nuclear Medicine, Dec 2009, Vol. 40, No.4 pp. 12-14

Book Contribution:

Specialist Consultant and Editor for *Radiology and Imaging* entries in: Mosby's Dictionary of Medicine Nursing & Health Professions, ANZ 2nd Ed. 2009 ISBN 9780729539098 (hardback edition)

Conference Presentations with Published Abstracts:

J.L. Hislop-Jambrich, C.D.L. Thomas, C.D. Briggs, S. Blau, C.J. Hall, J.G. Clement (2009)

The MDCT evaluation of human femoral bones symmetry in aging, using QCT and anthropological measurements: A cross sectional mortuary-based study. In Proceedings of the 2nd Joint Meeting of the **International Bone and Mineral Society and Australian and New Zealand Bone and Mineral Society**, Sydney Australia March 21-25 2009: abs#317Page S107 doi:10.1016/ j.bone.2009.01.233 (Poster)

J.L. Hislop-Jambrich, C.D.L. Thomas, C.D. Briggs, C.J. Hall, J.G. Clement (2009)

Using QCT and Adapted Anthropological Techniques to Determine Age-Related Changes in the Human Femur: A cross sectional mortuary-based study. In Proceedings of the 1st Joint Meeting of **RANZCR, AIR, FRO and ACPSEM**, Brisbane Australia October 22-25 2009: abs#073 Page A116 doi:10.1111/journal of medical imaging and radiation oncology.2009..01207 (Oral Presentation)

Conference Presentations:

J.L. Hislop-Jambrich, C.D.L. Thomas, C.J. Hall, A.G. Peele, J.G. Clement (2007)
Hierarchical 3D X-ray imaging of human femoral cortical bone in aging. In Proceedings of the ASRP/Australian Synchrotron Users Meeting 2007, Melbourne Australia December 12-14 2007: 32 (Poster)

J.L. Hislop-Jambrich, C.D.L. Thomas, C.J. Hall, J.G. Clement (2008)
Synchrotron Based Micro-CT of Bone. How the Findings Relate to Clinical CT Methods. In Proceedings of the 5th Clare Valley Bone Meeting 2008, Clare Valley South Australia, 30th March – 3rd April 2008: O22 (Poster)

J.L. Hislop-Jambrich (2008)
How Synchrotron Micro-CT Research is Guided by Clinical CT Imaging in the Study of Bone. In Toshiba CT User Group Meeting, Conrad Jupiter's Gold Coast Queensland, 24th July 2008: IS3 (Invited Speaker) (Oral Presentation)

J.L. Hislop-Jambrich, C.D.L. Thomas, C.D. Briggs, C.J. Hall, J.G. Clement (2008)
Using Mortuary CT Data to Evaluate Age Related Bone Changes in the Hip. In Proceedings of the ANZBMS/Australian and New Zealand Bone and Mineral Society, Melbourne Australia August 28-30 2008: P58 (Peer Reviewed) (Poster)

Thomas CDL, Hislop-Jambrich J, Hall CJ, Peele A Hannah K, and Clement JG (2008)
Hierarchical Tomography of Human Bone. In AusTomo II, Second Australian Tomography Workshop, Melbourne November 13-14th 2008 (Poster)

J.L. Hislop-Jambrich, C.L. Thomas, C.D. Briggs, C.J. Hall, J.G. Clement (2009)
Femoral Bone Aging, MDCT Research. In Proceedings of the CRC-BID Education Seminar, Cooperative Research Centre of Biomedical Imaging Development, North Melbourne June 18-19th 2009 (Invited Oral Presentation)

J.L. Hislop-Jambrich, C.L. Thomas, C.D. Briggs, C.J. Hall, J.G. Clement (2010) Using QCT Techniques to Determine Age-Related Fracture Risk in the Human Femur: The Potential for Synchrotron MicroCT. In Proceedings of the 10th International Conference on Biology and Synchrotron Science and the 6th International Conference on Medical Applications of Synchrotron Radiation, Melbourne, February 15-18 2010: abs#108 (Peer Reviewed) (Oral Presentation)

J.L. Hislop-Jambrich, C.D.L. Thomas, C.D. Briggs, C.J. Hall, S. Blau, J.G. Clement (2010) ***(*Awarded National ANZFSS Student Award)*** Using mortuary CT data to establish age and stature from the femur. In Proceedings of ANZ Forensic Science Society, 20th International Symposium on the Forensic Sciences, Sydney, September 5th – 9th 2010, abs# 268 (Peer Reviewed) (Oral Presentation)

Meeting Presentations of Research:

Victorian Institute of Forensic Medicine (VIFM) Pathologist Meeting, 8.00 - 9.00am Thursday July 9th 2009. Video linked with Canberra Forensic Services.

University of Melbourne School of Dentistry, PhD completion seminar on Friday 28 May from 11.30 – 12.30pm in Wylie Lecture Theatre, ground floor, 720 Swanston Street.

ACKNOWLEDGEMENTS

I am exceedingly grateful to Professor John Clement and Mr. David Thomas for their enthusiasm and guidance in completing this manuscript. Their boundless interest in the ageing of bones, and their support generally has allowed me the freedom to construct a project that is both interesting and valuable. I am also especially grateful to Associate Professor Chris Briggs and Dr Chris Hall, who not only supported my physics and anthropological knowledge and skills development respectively, but also helped me feel like the project was always moving forward.

I am extremely grateful for the financial assistance, in the form of a full PhD scholarship from the Cooperative Research Centre in Biomedical Imaging Development (CRCBID). Thanks especially to Dr Gerry Roe and Sonia Mailer for reminding me that I would eventually finish. The support of the entire CRCBID team has been a powerful motivator, and I thank these wonderfully positive and very clever people for their help in getting the manuscript finished within three years.

I want to also express my extreme gratitude to the Victorian Institute of Forensic Medicine (VIFM) staff, especially Sarsha Collette, Trish O'Brian, Vicky Winship, Dr Soren Blau, Dr Chris O'Donnell, and especially Dr Jodie Leditschke for the respect and knowledgeable regard over which they supervised my data collection. The group at the VIFM is the most professional medical team with whom I have ever had the privilege to work.

I want to sincerely thank Keenan Brown at Mindways Inc™ for supporting the use of the companies' hardware and software in my non-clinical environment. His advice and support will remain one of my fondest memories, especially of the early part of this work, when I was finding my way. 3D evaluation is the most sensible way to move forward our understanding of the ageing process in the hip.

Thanks to Martin Coyne from Toshiba Medical Australia, who assisted me in making sense of CT imaging procedures conducted in a uniquely complicated imaging environment. His openness and readiness to assist in technical detail gathering, scanning wet-bone specimens and assessing quality assurance measures has been instrumental to the technical accuracy of this work.

Thanks also to Dr Ken Poole, Dr Nigel Loveridge and Dr Paul Mayhew at Addenbrookes Hospital in Cambridge for their jolly humor and for helping me understand the limitations of what I was trying to do. Nothing is quite so simple as it seems, and nor should it be so.

Thanks too to Anthony Wallace and Lisa Mong for their assistance in performing quality assurance on the CT equipment at the VIFM, and to Chris Owen for his assistance in getting our scientific posters ready to present to the world. Thanks also to all of the Melbourne Dental School staff and postgraduate students for their kind words of encouragement at all stages, especially Kim Hanson, Dr Peter Clause, Dr Sherrie Blackwell and Dr Rebecca Taylor.

Thanks to Dr Kathleen Gray who provided a gender balance to my all-male supervising team, and who supported my caffeine addiction. Kathleen is a most remarkable and inspiring woman. I will always treasure her wisdom, and remember her encouragement.

To Joanne Hislop-Kelso, thank you for assisting me to present this thesis with a sense of the rigor that the work deserves. To the rest of my immediate family Robert, Elizabeth, Tania and Matthew Hislop, and especially Lesa Hislop-Miller; thank you for your unwavering support, even though I am sure none of you never really understood why I was doing it. I had my doubts too!

Finally, I want to thank my husband and partner Tom Jambrich, without whom this dissertation would not have been. Tom sees me the way I want to be, which helped to provide the motivation to both start and finish this work. We make a great team, and everything is indeed possible.

LIST OF FIGURES

LIST OF TABLES

LIST OF APPENDICIES

ABBREVIATIONS

2D	two-dimensional
3D	three-dimensional
aBMD	areal bone mineral density
AEC	automatic exposure control
AIP	average intensity projection
ANOVA	analysis of variance
AP	antero-posterior
ARPANSA	Australian Radiation Protection and Nuclear Safety Agency
BIT	bone investigation tool
BMAD	bone mineral apparent density
BMD	bone mineral density
BMI	body mass index
BMU	bone modelling unit
BR	buckling ratio
CaHAP	calcium hydroxyapatite
CBCT	coned beam computed tomography
COD	cause of death

CSA	cross sectional area
CSMI	cross sectional moment of inertia
CT	computed tomography
CTDI	computed tomography dose index
CTXA™	computed tomography x-ray absorptiometry
DA%	directional asymmetry percentage
DAP	dose area product
dB	decibel
DHS	Department of Human Services
DICOM	digital imaging and communications in medicine
DLP	dose length product
DTB	Donor Tissue Bank
DVI	disaster victim identification
DXA	dual energy x-ray absorptiometry
E	effective dose
ECG	electrocardiograph
FDA	Federal Drug Authority (USA)
FH	femoral head
fMRI	functional magnetic resonance imaging
FN	femoral neck
FOV	field of view
FWHM	full width at half maximum
HAS	hip structural analysis
HU	Hounsfield units
HREC	Human Research Ethics Committee
Hz	hertz
ICMP	International Commission for Missing Persons
IT	inter-trochanteric
IT	information technology
IV	intra-venous
kVp	kilovolt peak
lp/cm	line pairs per centimeter
mA	milliamp
mAs	milli-amperage second
MDCT	multiple detector-row CT
MFC	Melbourne Femur Collection
MFI	mass fatality incident
MIP	maximum/minimum intensity projection
MPR	multi-planar reconstruction
MRI	magnetic resonance imaging
MRPB	Medical Radiation Practitioner's Board
mSv	milli-sievert
MTF	modulation transfer function
MUSCOT	multislice cone-beam tomography
NAS	network attached storage
NOF	neck of femur
OA	osteoarthritis

OP	osteoporosis
PA	postero-anterior
PACS	picture archive and communication system
pixel	picture element
QA	quality assurance
QCT	quantitative computed tomography
RAID	redundant array of independent discs
RAM	random access memory
ROI	region of investigation/interest
RSNA	Radiological Society of North America
SD	standard deviation
SE QCT	single energy quantitative computed tomography
SSD	surface shaded display
Sv	sievert
TCOT	true cone-beam tomography
TGA	Therapeutic Goods Administration (Australia)
THR	total hip replacement
TLD	thermo-luminescent dosimetry
μ	linear x-ray attenuation coefficient
UK	United Kingdom
USA	United States of America
VAR	volume artifact reduction
vBMD	volumetric bone mineral density
VIFM	Victorian Institute of Forensic Medicine
voxel	volume element
VR	volume render
WHO	World Health Organisation
Z	section modulus

TABLE OF CONTENTS

CHAPTER 1

INTRODUCTION

"To be 70 years young is sometimes far more cheerful and hopeful than to be 40 years old."

~ Oliver Wendel Holmes Jr. ~

1.1 Introduction

The central aim of this thesis is to describe population-based age-related differences in the human cadaveric femur using clinical computed tomography (CT) technology, and thereby contribute to a greater understanding of age-related change. The goal is to design a reliable and valid scientific instrument to measure age-related differences. The intention is to apply the novel radiological methods to data from a representative Australian, predominantly urban population, identify, and then quantify the age-related differences. The rationale behind the study is that an accurate theoretical model of age-related change will more accurately predict fracture risk in contemporary urban populations, and assist in the classification of biological-age characteristics generally.

The study of age-related change is important as populations in developed countries like Australia continue to experience increased life expectancy, and the associated financial and physical costs of ageing continue to grow (1).

Anthropologists and clinical physicians approach the question of how bones age from different perspectives, although generally they evaluate similar data through their observations. Anthropology uses bones as an indicator of bio-cultural history (2). The skeleton can provide powerful evidence of skeletal dynamics, bio-cultural influences including evolution, gait, diet and exercise, as well as a means for estimating age at death.

Clinical medicine primarily evaluates bone to establish the presence or absence of disease and trauma. Early interventional strategies for the treatment of

disease or trauma in the living provide positive outcomes in terms of faster healing and ultimately improved productivity from a social perspective. The development and application of medical imaging technologies are guided by the interests of the patient in terms of safety (i.e. do no harm), and access or availability, which inevitably includes cost. Clinical medicine's considerations for bone imaging in the living are therefore very similar to the philosophy of anthropological bone investigation, though with an awareness of the ionising radiation burden. Rarely however do the two disciplines compare results, or share technological platforms.

This thesis establishes the feasibility of using high-resolution multiple detector-row computed tomography (MDCT) techniques from recent mortuary-based full-body scans to build a radiological model of human femoral-ageing in a contemporary predominantly urban Australian population. The study describes and quantifies the age-related differences from a cross-sectional heterogeneous sample of male and female individuals covering 80-years of the adult lifespan, though novel assessments using clinical software, and adapted anthropological measurements. The study presents a model of the age-related characteristics of the human femur for the modern Australian urban population using regressions and observational analysis.

1.2 Study Background

The femur was chosen for this study because clinically the femoral neck is commonly involved in age-related fractures which are linked with high mortality and morbidity rates (3). The femur is also frequently examined morphologically for establishing biological-identity, as it is a large weight-bearing bone that often survives intact for long periods of time, even after events such as fire and animal predation (4).

The primary clinical tool for measuring bone mineral density (BMD) and morphometry are 2D dual x-ray absorptiometry (DXA) and plain film x-ray

respectively. This is also true in the anthropology discipline, though they are utilised less often. The problem with 2D imaging techniques is that bones are complicated 3D structures, and should be studied as such. This dissertation uses 3D data generated by a commercial MDCT clinical unit. The MDCT technique represents a non-destructive means of evaluating both surface and internal structures of the dense and complex 3D biological structure of the femur.

The research presented in this thesis also uses commercially available clinical software in a series of empirical studies to develop novel and scientifically verifiable methods for using MDCT data to produce morphometric and densitometric models of age-related differences in the human femur. A significant advantage of the volumetric MDCT dataset is that it provides a permanent record of the individual. These data may also be reprocessed for further analysis without rescanning, providing the potential to perform both superficial and deep structural assessments including those related to biomechanical assessments using 3rd party software.

Morphological assessments of the femur in anthropology are usually performed by direct bone measurements made using calipers. Direct caliper measurements require that the bone is defleshed prior to evaluation. Even then, this assessment method can only provide surface examination of the structure. Only very limited work has only recently been published describing the application of 3D imaging techniques such as MDCT for establishing direct (i.e. still only surface) measurements for morphological assessments in anthropology.

While skeletal ageing in the sub-adult human skeleton follows a relatively predictable pathway, the process of ageing, especially after peak bone mass (occurring in the third decade), is far less predictable. Skeletal ageing is influenced by a range of environmental, nutritional, gender and genetic factors including ethnicity (5). Osteoporosis is the term defined by the World Health Organization (WHO), to describe an age-related reduction in bone, with an associated deterioration in bone architecture. That is, the older the person, the

more likely they are considered osteoporotic. Modern urban populations are diverse, and whether the term *osteoporosis* is an expression of normal skeletal ageing for an individual or population, or a quantifiable and treatable disease; skeletal health generally is an important issue globally. Presently however there is no agreed unit for *bone quality*, or reliable measure of fracture risk. There are no criteria for determining "good" bone from "bad" (6), which is a problem, as longevity becomes more common in all parts of the world.

Humans are living longer than at any other time in history, and we are likely observing the expression of that longevity through an increased number of people presenting with age-related conditions. We will also likely continue to increase average life-expectancy as medicine, nutritional and environmental support systems advance. The Australian Bureau of Statistics (ABS) currently projects the population in Australia in the year 2051 will be between 25 and 33 million, with almost 50% of those people being over the age of 50 years (7). From an historical perspective, in 1900, the average life expectancy of both men and women in Australia was 53 years, and it took until 1940 for that average life-expectancy to reach the current retirement age of 65 years (8). Contrast with those data, the projection that one in four children born today in the early part of the 21st century can expect to reach the age of 100 years, and the notion of an *ageing population* has huge financial, social and health-related implications. Simply put, the fastest growth in the population data is expected to be in the 85-plus age group, who currently represent 1.6% of the Australian population, but who are likely to represent 7.1% (2.3 million people) in approximately 40 years' time (9).

The cadaveric MDCT data used for the scientific investigations conducted throughout was obtained under ethics approval using a clinical MDCT unit co-located in a civilian metropolitan mortuary. The Victorian Institute of Forensic Medicine (VIFM) has provided ethical oversight to the project via the human research ethics committee (HREC). The VIFM is one of only a few mortuaries in the world where such technology is routinely used to augment the conventional

autopsy. The VIFM MDCT imaging site has provided the rare opportunity to evaluate an adult, urban population that includes both sexes and encompasses data from individuals aged between 15 and 95, in significant numbers. The clinical nature of the data has also afforded the opportunity to use clinical software for analysis, which is invaluable in terms of linking these data with the comparable living population.

This thesis describes the development of radiological methods for evaluating the femurs from a diverse, contemporary, urban population. It presents practical techniques for combining the knowledge, skills and imaging attributes from medicine and anthropology in ways not previously done, and thereby has produced data with a much broader utility than would otherwise have been the case.

1.3 Thesis Central Aim and Scope

The central aim of this thesis is to investigate and document population-specific age-related changes in human femora using existing clinical equipment and software applied in novel ways. The study uses an 80-year range of adult femoral image-based samples from both sexes in empirical studies of densitometric and morphometric radiologic expressions. Aspects relating to scientific error, accuracy and reproducibility for the novel techniques developed are also assessed and presented. Furthermore this thesis will present a descriptive and quantitative model (through regressions and observations) of the ageing adult human femur from a predominantly urban Australian population.

This study has been prepared under the assumption that adapted 3D radiological imaging analysis methods from anthropological and clinical medicine disciplines may be combined to produce a more complete morphological and structural understanding of the human femur. This represents an innovative viewpoint from which to evaluate age-related change. It also represents a challenge in terms of writing and presenting the study, as it must address the needs of a variety of different audiences. As a consequence some parts of the thesis will be

unnecessary for some readers, but for others the background is imperative in conveying the complexities of the general assumptions made.

The scope of the thesis does not include a detailed investigation of degenerative bone and joint conditions or skeletal trauma, though both conditions logically arise in discussing advancing years in the human and the ageing process generally. Chapter seven however presents evaluations from 14 neck of femur (NOF) fracture cases. This thesis also does not include a discussion of congenital diseases of the skeleton such as *osteogenisis imperfecta*, and *Paget's disease*, and all reasonable efforts have been made to exclude any cases involving such conditions from the evaluation. Background information such as prior medical history, level of physical activity, diet and ethnicity were not available, and this will therefore limit the scope for discussion of the findings.

What is currently possible in imaging the dead may not be possible in the living, due mainly to concerns regarding excessive ionising radiation. A detailed comparison of clinical and mortuary-based radiation dose is therefore also presented in chapter 4.3.2. Future developments in CT technology may change the current limitations on both technique and application, leading to the possibility of an optimisation and widespread adoption of the techniques explained in this study. The novel techniques developed have therefore been optimised such that they may easily be replicated using any MDCT or serial CT scanner in either the living or the dead, consequently enhancing the broad utility of the data and results produced.

1.4 Thesis Objectives and Overview

Objective 1: To describe the characteristics of MDCT and determine its utility to collect cross-sectional images of the human cadaveric femora. (Chapters 3, 4, 5 and 6)

Objective 2: To develop novel 3D MDCT-based techniques to evaluate osteological differences of the femora in the adult population (Chapters 4, 5 and 6).

Objective 3: To use adapted morphological measurements and clinical QCT to describe age-related characteristics related to the surface and internal structures visible on high-resolution CT scans of the femora (Chapters 4 and 5).

Objective 4: To describe the differences of symmetry of the femoral bones related to morphological and QCT characteristics such as spatial measurements and bone mineralisation (Chapters 4 and 5).

Objective 5: To produce prediction models of age, stature, gender and fracture characteristics of the human femur from MDCT data (Chapters 4, 5 and 7).

The **first chapter** outlines the reason for the investigation using clinical and anthropological radiologically-based methods to evaluate femoral-ageing, and establishes why it is an important area of research for both the medical and anthropological disciplines. The chapter also contains an outline of the aim of the thesis and defines the scope and parameters to which the investigation has been bound.

The **second chapter** presents a literature review of human skeletal development and an overview of the literature in the determinants of bone health and ageing. The chapter includes background on the health and ageing statistics currently available in Australia, and for the state of Victoria.

The **third chapter** describes the materials and methods common to research chapters four, five, six and seven. The chapter describes in detail the MDCT scanner and includes key definitions used throughout the thesis.

The **fourth chapter** establishes that it is possible and practical to use the routine collection of mortuary-based high-resolution MDCT datasets for the assessment of femoral structure. The chapter describes a comprehensive 3D model of gender and age-specific bone densitometry using the contemporary and predominantly urban Australian adult population from datasets collected at the VIFM. As the method employed was clinically based, a comparison of ionising radiation dose in the living is also included.

The **fifth chapter** establishes the utility of the MDCT database examined in chapter four for surface and deep morphometric femoral measurements. The chapter describes a comprehensive 3D morphometric model of the differences between those aged 50 years and under and those aged between 51 and 95 years, and includes predictive modelling.

The **sixth chapter** compares three sets of different MDCT imaging conditions and quantifies their effect on the spatial and quantitative MDCT assessments.

The **seventh chapter** combines the findings from the previous three investigative chapters and compares these studies of normal femurs with that of 14 unilateral age-related femoral fracture cases. The chapter also includes an epidemiological evaluation of hip fracture and death using 2008 VIFM statistical data.

The **eighth chapter** assimilates the findings from the preceding four research chapters and explains their relationship and significance. The chapter also discusses some of the radiological imaging problems still confronting the clinical and anthropological disciplines, in particular the wide-scale adoption of the techniques developed. The chapter also includes an assessment of the age-related model developed, and concludes with suggestions for further research and the cross-disciplinary engagement crucial for the further advancement of QCT-based technologies.

CHAPTER 2

LITERATURE REVIEW AND BACKGROUND

"Reports that say that something hasn't happened are always interesting to me because as we know there are known knowns; that is to say we know there are some things we do not know. But there are also unknown unknowns – the ones we don't know we don't know."

~ ***Donald Rumsfeld*** ~

Chapter two consists of three parts which provide a comprehensive background to the subject materials examined throughout the thesis.

- **Part A** contains a background discussion based on the literature regarding the biology of bone tissue including structure and normal development. The section then discusses ageing and fracture. This section puts into perspective the complexities involved in working towards a better understanding of bone tissue, and introduces the subsequent challenges in producing valid radiologically-based testing tools and methods.
- **Part B** presents a critical review of the literature centering on the radiological evaluation of bone in the clinical and anthropological disciplines. Specific evaluations of the literature are also contained as part of each research chapter introduction.
- **Part C** provides an analysis of the available Australian health and ageing statistics. This section provides the context through which the clinical study of bone-related-ageing for an Australian, predominantly urban population may be viewed, and the anthropological perspective for which future comparisons may be made. The section is included last because this study began with a split anthropological and clinical focus on documenting age-related change. It became apparent however in chapter seven that a significant advantage of the techniques developed lay in their use for determining fracture-risk in the elderly.

2.1 Part A. Introduction to Bone Biology

Bone is a living material that adapts to its internal and external environment to provide the body with a rigid frame (10). Bone also functions to regulate minerals, produce red and white blood cells, support the production of sound (through the tiny bones of the inner ear), maintain acid base-balance, as well as detoxify the body via the storage and gradual secretion of heavy metals. Living cells such as those in bone, can maintain normal activity as long as they receive the nutrients required for cell maintenance. They also require a working transport system for the removal of waste products created as a by-product of cell action.

Bones come in a variety of shapes and sizes, all of which are optimised to provide suitable levels of support, while being light-weight and adaptive to the needs of the mobile organism. A number of methodologies have been used to determine a characteristic molecular structure of bone. These include wet chemical methods, x-ray diffraction (XRD), neutron diffraction, infrared (IR) and Raman spectroscopy, and nuclear magnetic resonance (NMR) spectroscopy. A conclusive structural molecular blueprint however has remained elusive (11). A molecular model of bone and an associated non-invasive clinical analogue remain vital steps in further developing treatments for bone-related pathological conditions, and for understanding the processes under which normal bones ages.

2.1.1 Phases or Components of Bone

The basic structure of bone comprises three components or phases: mineral, organic-protein (in the form of collagen) and water. The mineral phase of bone is formed predominately of calcium phosphate, but also includes calcium carbonate, sodium, magnesium and fluoride in the chemical arrangement of impure hydroxyapatite. The mineralised phase represents around 65% of the bone mass, and provides bone with its strength and stiffness characteristics. The material properties of the femoral bone provide a high level of compressive strength, though it is less able to tolerate tensile forces. The proximal and distal

ends of the femur experience axial and shear forces during walking and exercising, while the diaphysis experiences the least (12).

The organic-protein phase of bone comprises around 30% of the bone mass. The toughness of bone is chiefly contributed by the level of collagen-binding of the organic-matrix. Almost all of the organic-phase of the bone-matrix consists of type I collagen, which is made intracellularly as tropocollagen, and exported where it associates into fibrils. The collagen fibres in bone measure between 80-100 nm in diameter and provide the nucleus for mineralisation and growth, as well as act as reinforcement for the mineral component by providing toughness. The presence of collagen however does not appear to have any effect on bone stiffness generally (13), though age-related modifications in the cross-link patterns may alter the mechanical properties (14). The remaining organic-phase components are various growth factors of which little is currently known except for the presence of glycosaminoglycans, osteocalcin, cell attachment factor, bone sialo-protein and osteonectin (15).

Water is also present in the bone-matrix, though it comprises only 5% of the mass. Water is found within the collagen fibres, in the pores and in the mineral structures. Investigation specifically into the water component indicate that a loss of water in the collagen-component decreases the toughness of bone, whereas a loss of water associated with the mineral-phase decreases both bone strength and toughness (16). There also appears to be a role for water on the mineral surface in mediating mineral-organic-matrix interactions (11).

2.1.2 Bone Formation

The formation of bone during the fetal stage of development occurs as either intra-membranous ossification, such as in the flat bones of the skull, or as endochondral ossification, as in the case of the long bones. Endochondral ossification begins with the formation of ossification centres within the cartilage through the swelling of chondrocytes, and the subsequent mineralisation of the cartilage matrix in the bone rudiments. Osteoclasts and osteoblasts then invade

and begin the bone shaping (and later remodelling) process. Osteoblasts are the cells responsible for bone-building, and arise from pluripotent mesenchymal stem cells of the marrow. Osteoclasts, which are the cells responsible for bone-resorption, arise from haematopoietic granulocyte-macrophage colony forming units. Cortical bone (also described as compact) forms 80% by mass of the skeleton, and the remaining 20% is trabecular bone (also described as cancellous or spongy).

The difference visually between trabecular and cortical bone is largely made on the type of porosity and microstructure. Trabecular bone forms a rod and plate array that lightens the bone, and provides room for blood vessels and marrow to exist. The network of vertical and horizontal struts in trabecular bone confers strength by its ability to deform while absorbing and dissipating energy.

Cortical bone is dense and forms the outer walls of the bones where it provides a high moment of inertia that prevents bending. Cortical bone consists of repeating structural units known as osteons which include an interstitial area and concentric rings of lamellae. The thickness and shape of the cortex is the result of periosteal and endosteal growth with varying degrees of contribution of each aspect during ageing (17).

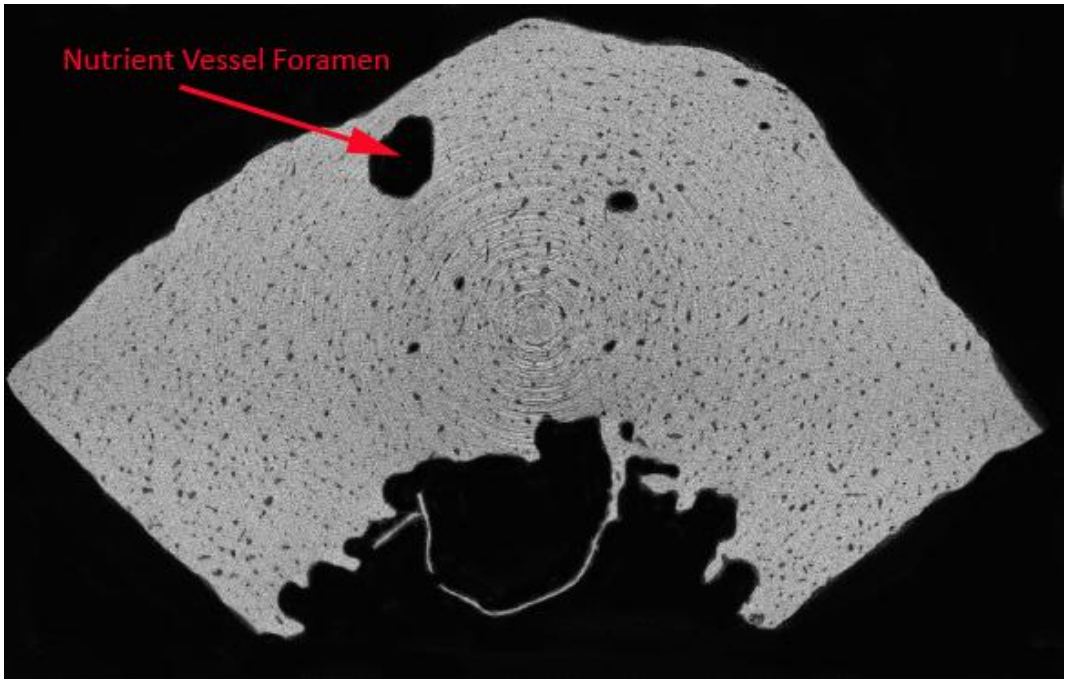

Figure 1 Axial femoral synchrotron MicroCT image from the SPring8 Japan

Posterior quadrant of cortical femur from MFC590 formed using Synchrotron Micro-CT. The large pore is for the *diaphysial* nutrient artery.

Osteons are approximately cylindrical structures that are around 100µm in diameter, and contain at their centre, a Haversian canal, which contains blood vessels, a nerve and some space that is filled with fluid (18). The walls of the canal are covered with cells, are connected to the osteocyte by a network of canaliculi. The canaliculi form passages between the disc shaped lacunae, which contain osteocytes. The space between osteons is known as the cement line. The cement line denotes the limit of new tissue, or where bone removal has ceased (*resting phase)* and the construction of a new osteon and associated bone deposition is now taking place. Canaliculi rarely cross the cement line, and evidence as to their anatomical distribution has not yet been investigated (19).

Cortical and trabecular bone are in contact with marrow which serves as a source of bone cells, and which contains blood vessels and nerves. The marrow is either of two kinds, fatty (yellow) or hematopoietic (red). Hematopoietic marrow is a primary element in the production of blood. In infancy all marrow is hematopoietic, and gradually with increasing age, the marrow becomes progressively fatty. The change in marrow as a person ages may be imaged using

magnetic resonance spectroscopic (MRS) methods. The application MRS demonstrates a gradual progression from red to yellow marrow in the femur, with the diaphysis first affected (1-10 years), then the distal metaphysis (10-20 years), with an adult pattern by age 24 years (20). Clinical studies have shown the age-related fatty change in marrow to be inversely proportional to bone mineral measurements (21), i.e. when bone is lost, it is replaced by marrow. Only the tiny bones of the middle ear do not contain pores, and as such also do not contain marrow.

2.1.3 Woven and Lamellar Bone and Periosteum

Bone is classified as either woven or lamellar types. Lamellar or secondary bone is a highly organised structure consisting of lamellae of either orthogonal or heliocoidal orientation of fibres. This type of bone is structured much like plywood, and has a high resistance to force but requires a significant amount of time to build. Woven or primary bone is built much quicker than lamellar, and as such the fibre arrangement is significantly more random. Woven bone plays an important part in fracture healing as it links the fractured ends together. Woven bone also forms the embryonic skeleton, and predominates at the sites of the growth plates in young mammals (15).

The periosteum is not considered bone tissue. It is a fibrous layer that surrounds all bone surfaces apart from those involved in synovial joints and ligament attachment. The periosteum contributes a vital role to the blood supply and lymphatic drainage of the bone, especially in the event of a fracture and during skeletal development (22). The periosteum is attached to the bone through strong collagenous fibres known as Sharpey's fibres (William Sharpey 1802 – 1880). The thickness of the periosteum diminishes as age increases, but it retains its role in bone remodelling throughout life, and has a pivotal role in fracture healing (23). The periosteum also contains a rich supply of nerve fibres, though little is known about the actions of the periosteal cell-lining during adulthood. The osteogenic cells of the periosteum however are known to control the outer

layer of the cortical endosteum, and animal studies have shown that periosteal cells actively remodel; absorbing and forming bone (22).

2.1.4 Bone Building and Replacement

Frost postulated in the 1960s that bone turnover occurs in anatomically discrete foci, and that the remodelling process occurs over a period lasting 4-6 months (24). Frost was also responsible for the phrase "*bone modelling unit"* or BMU, though the *M* has stood for *multi-cellular* and *metabolising* in subsequent publications. Recently BMU has stood for *basic multicellular unit*.

The structural order of the modelling and remodelling of bone is achieved by the coordination of cellular activity within each BMU. If modelling and remodelling activities were activated as separate and independent cellular functions, it should be a simple process to determine if age-related bone loss was caused by an overactive osteoclastic activity or an underactive osteoblastic one (25). The close relationship both temporally and spatially between them however requires a deeper understanding of the cellular balancing act that Frost called *activation frequency,* or how often cells are replaced.

At the commencement of a remodelling cycle, osteoclasts appear on an otherwise inactive surface, and over a period of around two to three weeks, a tunnel is constructed in cortical bone, or lacunae on the surface of trabecular bone. The osteoclasts are then replaced by osteoblasts which replace the resorption cavity over a period of approximately 100 days to create a new bone structural unit. During skeletal development, and fracture repair, bone formation predominates (24). Osteoclast activity is either up-regulated or down-regulated by the growth factors interleukin-1, colony-stimulating factor, and transforming growth factor. The regulation of bone resorption is also affected by both local and systemic factors that induce the formation and activation of osteoclasts. Osteoblasts produce interleukin-6, interleukin-1, prostaglandins, and colony-stimulating factors (CSFs), which induce the formation of osteoclasts. Accessory

cells such as the T cells can produce cytokines that can inhibit the formation of osteoclasts, such as interleukin-4, interleukin-18, and interferon-y (26).

As animals age, it is thought that periosteal modelling rates decline whereas Haversian modelling rates increase. Moderate amounts of mechanical loading are thought however to have little effect on stimulating either of these processes (27). The animal study supports the idea that mechanical loading on the skeleton prior to maturity has a greater effect on the development of stronger skeletal structure than similar mechanical actions on the mature skeleton; but also that such loadings may act to produce osteons with smaller Haversian canals, leading to a less porous cortical bone (28).

As early as the 1870s Julius Wolff (1836 – 1902) and others noted that bones were affected by mechanical loading, and that there may be a predictable relationship between bone structure and function (29). Though often stated as *Wolff's Law*, his explanation of bone shape being formed by interactions with its mechanical environment is neither a law nor is it completely accurate (30, 31). *Wolff's* so-called *law* describes how the orientations of trabeculae in areas such as the proximal femur come to be during the phases of growth. A number of exceptions and flaws however make it of little practical use in developing and understanding of the factors modulating the adaptation of bone in particular anatomical sites, and in resolving the forces experienced by bone in day-to-day activities (19, 32). However Wolff's work bought the idea of bone as an adaptive material that responds to its environment to prominence.

Bones respond adaptively to the environment through an internal process of modelling, and externally through the co-ordination of muscles, and the functional strains that movement produces (33). Wilhelm Roux in the late 1800s first discussed the idea of dependent differentiation or functional adaptation of bone to mechanical loading over time (31).

Three key concepts from the 19th century are still the subject of testing in the 21st century:

1. Bone is absorbed and deposited for optimised strength and weight.
2. Trabecular bone patterns tend to line up along lines of principle stressors.
3. Numbers one and two occur through self-regulated processes that respond to mechanical loading.

Mature adult bone almost certainly exhibits signs of micro-damage, but this in and of itself does not completely explain why it becomes progressively weaker as it ages (34). Evidence also exists that some combination of collagen and hydroxyapatite crystals undergo chemical changes during ageing that render bones less able to withstand tensile and compressive loads (35).

Mechanical stress improves bone strength by influencing the alignment of collagen fibres as the bone is forming (36). Cortical bone located in areas of high tensile stresses has a greater proportion of fibres aligned along the bone axis, while in areas of compressive forces, the collagen fibres align in a more transverse plane in relation to the long axis of the bone (37). Any relevance to genetic influence or functional adaptation, and fibre orientation in collagen is currently unknown. However muscle induced loading likely has a considerable role in both the geometry and the recovery of bone mineral mass after a fracture of a load-bearing long bone (38). Adaptation to loading may be shown to occur through changes in bone geometry, without any change in the areal or volumetric BMD (39). BMD is used as a surrogate for bone strength; however there are other parameters such as geometry, for evaluating the mechanical properties of bone, including resistance to fracture.

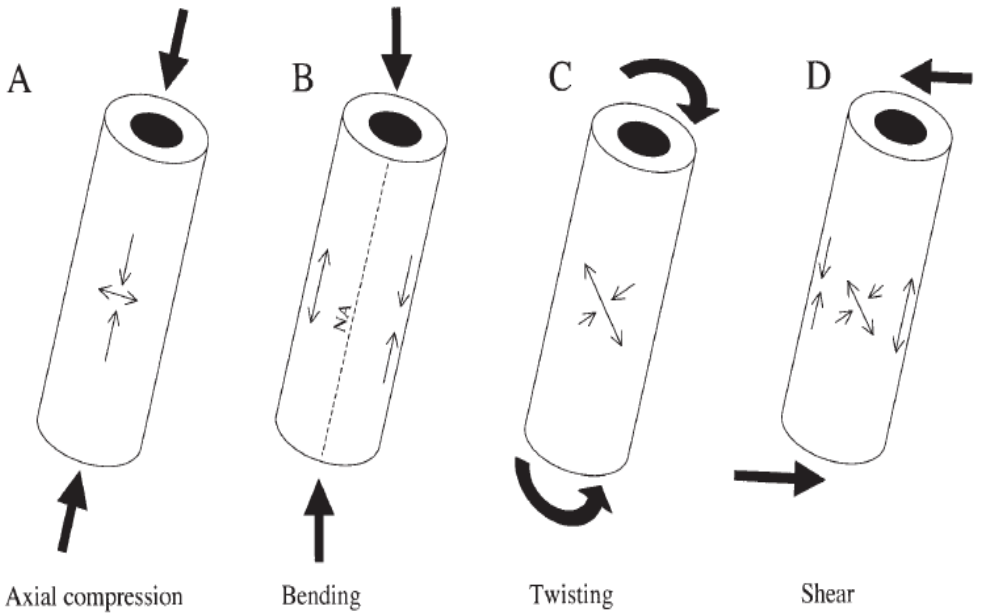

Figure 2 Forces on bone in movement

Beam and cross-section views of the forces and strain distributions on bone tissue (30).

Figure 2 demonstrates the various forces that act on bone through body movement. Long bones such as the femur are loaded in both axial compression and in bending. The forces exerted on bone in axial compression are distributed uniformly over the cross-section, and the ability of bone to resist axial compressive forces is directly proportional to the mineralisation of that cross-section. The forces exerted in bending are however quite different. In the femur, the proximal aspect is forced in tension, while the distal sections are forced in compression. The femur through evolution has therefore been fashioned to resist bending and compressive forces, as well as being light enough to provide efficient locomotion. Animal studies indicate that modelling and remodelling rates in bone are greatly reduced in outer cortical bone as the animal matures skeletally (27). The animal studies in bone are therefore of limited value in studying ageing human bone in terms of biomechanical effects.

A classic experiment by Chalmers and Ray in 1962 grew a mechanically unloaded rat femur inside a spleen. The result was a bone with thinner cortices, a short and widened femoral neck, less organised trabeculae, and no diaphysial curvature (40). The finding strengthens the assertion that a purely genetic

predetermination of bone shape is unlikely, but rather bone shape and structure are more largely determined by intrinsic mechanical actions and extrinsic nutrition and general health factors. This hypothesis also explains, in part, why the bones of astronauts, even after resistance generating exercise in space, can lose up to 7% of their bone mass as determined by DXA (41, 42). Localised bone loss is also widely reported in people who have limb immobilisation after fracture, amputation and subsequent immobility; or in the case of the mandible, tooth loss. All of these immobilisation conditions cause a loss in the normal pattern of bone mechanical loading due to the changing loading conditions.

Mouse studies involving Botox used to paralyze the hind limb document the poorly understood modulation of bone homeostasis as a function of muscle action (43). Losses in both trabecular and cortical bone have been reported in these Botox studies, primarily through the action of bone resorption. The combination of a rapid rise in the application of neuromuscular inhibiters for long term pain management clinically, and the mice-based results indicating a possible associated bone loss, should raise concern over the management of bone resorption side effects for patients under long-term pain management.

2.1.5 Bone Vascularity and Blood Flow

Long bones have been shown to exhibit age-related changes in blood flow characteristics in both human and animal models (44-46). Long bones are characteristically perfused through the epiphysial, metaphysial and diaphysial nutrient arteries, where the diaphysial is more commonly referred to as the principle nutrient artery (PNA) (47). The PNA perfuses the cortex and marrow of the long bones, and the flow rates through bone, like those in other parts of the body, are determined by resistance arteries. The impact of a flow resistance control mechanism has a profound effect on the vascular health of the bone as it acts as a fluid filtration system into the bone interstitium, which effects interstitial fluid flow and shear forces acting on the bone cells (47). Endosteal and periosteal vessels follow a mainly longitudinal path inside the Haversian canals

(25-75µm wide) parallel with the long axis of the bone, with radial connections made following Volkmann's canals (19).

The diaphysial arteries in long bones are homologous with the nutrient-vessels of the major organs within the body, as they generally arise from an adjacent major systemic artery. In the case of the femur, the vessel enters the nutrient foramen located around the level of the mid-shaft. The vessel then proceeds directly through into the medullary cavity where it divides into ascending and descending branches (48). The intra-medullary cavity pressure is greater than that of the periosteal area, and it is this pressure gradient that is responsible for maintaining a centrifugal circulation (18).

It was previously thought that inner circulation of long bones were serviced by the medullary branches, and the more superficial surfaces were derived from the periosteal circulation (49). Brooks and Harrison in 1957 however postulated that in youth, the circulation of the long bone cortex is from the medullary circulation, and more recent research has established that in people below 35 years of age, there is no periosteal blood supply to the cortex, rather a centrifugal circulation exists (48). As vessels increasingly become affected by ageing and disease, the periosteal circulation becomes the principle arterial blood supply for the long bones (50).

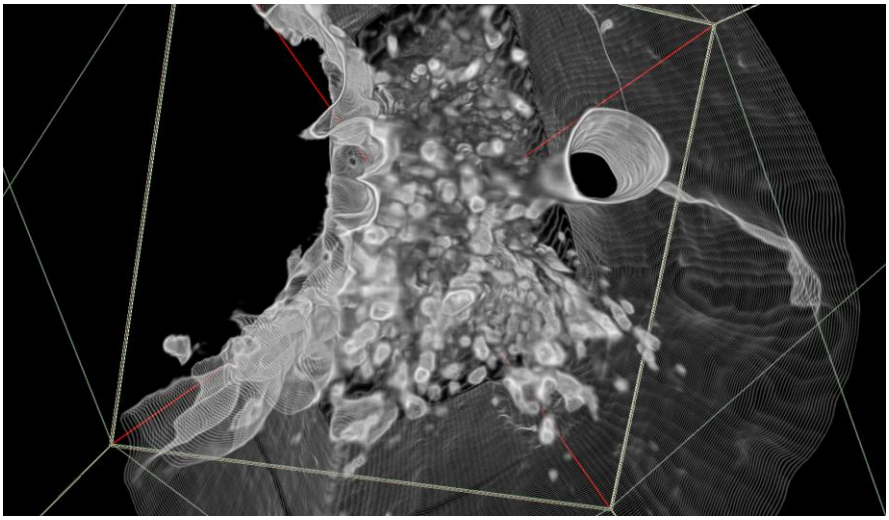

Figure 3 Bone Vasculature - 20mm wide bone specimen from MFC590

The large circular structure represents the principle nutrient artery of the femur feeding off into smaller pores.

Intravascular hydrostatic pressures have been measured in the human tibia to be 123 ±15mm Hg before it enters the bone, 16mm Hg in the diaphysis, 27mm Hg in the metaphysis and 19mm Hg in the vein (19). Higher medullary canal pressures result from the contraction of muscle leading to an increased compartmental pressure onto the bone during muscular contraction.

A classic 1953 paper by Trueta examined the vascular supply of the human femur in an age-range of 20-100 years. One of his key findings was that there appeared no noticeable decrease in the level of patency of the femoral vascular tree with ageing (51). Vascular distribution patterns in the femur that are established during the normal growth phase remain largely intact throughout the lifespan (51, 52). The lamellar bone system constituting the border of epiphysial and metaphysial regions in the femoral head, may be seen as a type of scar that lies on the epiphysial side of where the growth cartilage was in childhood (51). Figure 4 demonstrates the presence of the *epiphysial scar* in the proximal femur (red arrow).

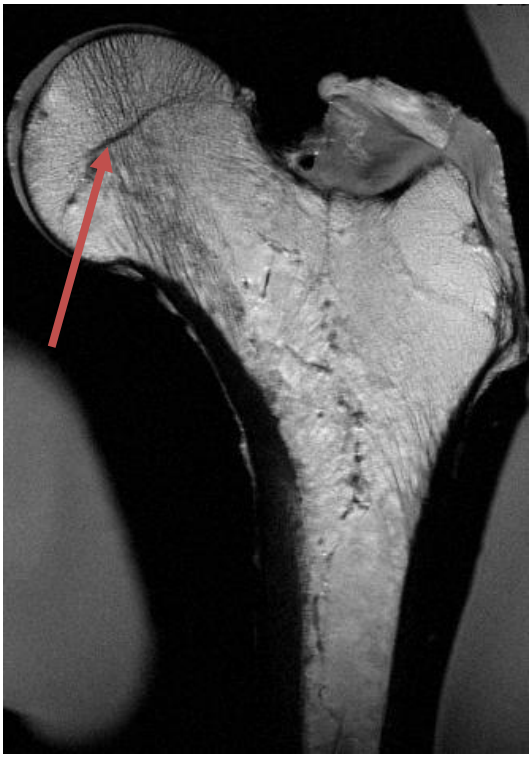

Figure 4 Lamellar scar on specimen MFC590

T1 weighted coronal magnetic resonance (MR) image of MFC590 demonstrating the concentration of lamellae bone superficial to the epiphysial plate. The age of the person is 45 years.

Variations of vascular attributes between different bones and bone types has been postulated as a key factor in determining intrinsic and extrinsic bone-based responses that regulate bone turnover. This is likely as it is also thought that the recruitment of osteoclastic activity is borne through blood-based precursors (53). Hence the vascular networks in bones are extremely important in understanding how bone ages.

Pore Structure

The pores of bone form an inter-connected network. Current research into pore structure is based on investigating an increasing complexity as age increases (54-57). In both trabecular and cortical bone there are four types of bone porosity; vascular, lacunar-canalicular, inter-trabecular and collagen-apatite porosity (19).

Cortical bone, which as previously mentioned, makes up approximately 80% by mass of the mature human skeleton, does not have the same highly-networked

pores as trabecular bone. The pores of cortical bone consist of Haversian canals (Clopton Havers, 1657 – 1702) which are a series of interconnecting, longitudinal channels in bone tissue, through which blood vessels, nerve fibres, and lymphatics are able to pass. The canals communicate with osteocytes in lacunae through canaliculi. The transverse connections within the osteons of the Haversian canals are called Volkmann's canals (Alfred Wilhelm Volkmann, 1801–1877), which connect with the periosteum.

Osteonal and Volkmann's canals form the vascular porosity (PV) and contain blood vessels nerves and bone fluid. The canal structure is highly-permeable, which allows fluids to pass freely. The capillary walls within the Osteonal and Volkmann's canals have no smooth muscle layer, and a thin endothelium. The canal vasculature operates at 40-60mm Hg pressure.

Lacunar-Canalicular Porosity

All space in the lacunae and the canaliculi is collectively termed the lacunar-canalicululular porosity (PLC). The PLC porosity is considered the most important porosity related to the mechanical and mechano-sensory effects observed in bone (19). The PV acts as a low pressure reservoir for the PLC for the exchange of bone fluids. The area between the cell membrane of the osteocyte and the walls of the canaliculi and lacunae are filled with a surface mineral-matrix or cell glycocalyx, which is thought to function as a gel (19).

Intratrabecular-Space Porosity

The intra-trabecular-space porosity (PIT) is associated with the area external to and surrounding cancellous bone trabeculae, and as such is extremely variable in size, with smaller pores existing near load-bearing outer regions of bone. The PIT pore is connected to the medullary cavity (where the larger pores exist), and as such it may contain marrow, fat and blood vessels.

Collagen-Apatite Porosity

The spaces between the collagen and crystallites of the mineral-apatite make up the collagen-apatite porosity (PCA). The size of the PLA is in the order of 10µm,

and there is very little movement of bone fluids within this pore, as water is bound by ionic-interactions with the collagen-apatite structure.

2.1.6 Bone Biology and Age

Age is an independent risk factor for fracture, and the exact reasons for this, as previously mentioned, are uncertain. Fracture risk may be related to an accumulation of micro-fractures, or a decline in osteocyte density or in the number of osteocytes, a combination of these factors, and/or some other, as yet unknown cause. An active network is known to exist between an osteoclast and an osteocyte, and perhaps the dead osteocyte is a signal to the osteoclast to begin resorption (58).

At the organ level, data exists demonstrating that increased cortical-porosity and decreased cortical-thickness are associated with increased fracture-risk (54, 59, 60). A dominant relationship exists between increasing age, increased cortical porosity and a decrease in cortical thickness generally. Small increases in porosity translate into a large decrease in bone-strength and conversely a larger increase in fracture-risk (61). An age-related increase in porosity has however (perhaps erroneously) been referred to as *trabecularisation* of the cortical bone. The mechanism for increased porosity appears to be a fusion of simple osteons into a complex osteonal pattern, with an enlargement of the Haversian canals, or an increase in pore-density (55). The over simplification of the process implied using "*trabecularisation"* would therefore seem inappropriate as the bone tissue is not changing types.

2.1.7 Proximal Femur Fractures

One in two women and one in four men over the age of 60 years will suffer an osteoporotic fracture over the period of their lifetime (62). The critical feature of bone in terms of its resistance to fracture is its toughness, or its' ability to absorb energy. There is however no standard way in which bone toughness in the living may be evaluated (63), so x-ray techniques remain the most commonly used method for inferring both fracture-risk and fracture presence.

Threshold values the force required to fracture for various bones have been explored (64). If a force is applied to a bone, and that force is greater than the bone's strength, it will fracture. If the force is less than the threshold strength value; the bone, while perhaps still sustaining injury or damage; will not fracture. The effect of force on bones is related to the way or ways in which bones dissipate energy from a fall or knocks. It is also related to the load sharing that occurs between the outer cortical and inner trabecular bone division, the integration of which is of particular importance in weight-bearing vertebral body and femoral neck structures.

Femoral neck fracture usually occurs in the elderly as a result of a low-energy impact or in the case of *"normal"* bone density or the young, a high-energy impact such as a motor-vehicle collision. Metastatic, infective and metabolic diseases (i.e. Paget's disease) may also result in fracture, but are less common.

A fracture of the proximal femur is classified relative to the anatomical location. The classifications are sub-capital, transcervical (commonly what is meant when referred to as a neck of femur (NOF) fracture), inter-trochanteric and sub-trochanteric. Each of these fractures may also be referred to as either intra-capsular or extra-capsular which refers to either the involvement or non-involvement of the synovial joint capsule. Only fractures involving the trochanteric regions alone are considered extra-capsular. An intra-capsular fracture has a higher incidence of non-union and avascular necrosis, and these complications are highly related to the degree of displacement of the bone fragments. Each hip fracture presents clinically in a slightly different way.

Sub-capital fractures are often a subtle fracture that is frequently impacted, and there is often a need to look closely at the cortical rim on an x-ray to see the deformity. **Trans-cervical** fractures frequently present with varus deformity and associated limb-shortening. An **inter-trochanteric** fracture may involve a separation of one or both of the trochanters from other fragments. An associated fragmentation of the posterior cortex of the femoral neck makes the

inter-trochanteric fracture extremely unstable. A fracture located below the trochanters, and perhaps extending in the shaft of the femur is called a **sub-trochanteric** fracture.

While there are several methods for classifying femoral neck fractures, the Garden classification system (65) is most commonly used to denote the relative stability of the neck of femur fracture, though the characterisation is not without its critics (66). The four types of femoral neck fractures under this system are:

Type 1: stable with impaction in valgus.
Type 2: complete fracture though non-displaced.
Type 3: displaced but not entirely disconnected (often with rotation and angulation of the lower limb) with varus displacement.
Type 4: completely displaced or fragmented.

Bone mass declines in an affected limb after a fracture (38, 67-69), with the loss up to 5-times the rate of the age matched population (70), though the loss may be partly or fully reversed. Part of the bone loss seen after fracture is thought to be caused by immobilisation, though the only consistent correlation that predicts the changes in BMD after a fracture is the baseline BMD before the fracture (71), and this information is not always available.

Rapid and specific intervention in relation to rehabilitation is essential in the management of osteoporotic fractures of weight-bearing bone, as the decreased strains of immobilisation will lead to further bone mass loss and altered bone geometry (38). Further adding to the need for prompt rehabilitative action in fracture cases is evidence that after fracture, not only does aBMD decrease at a rate higher than the normal age matched population; a loss occurs both in the affected and unaffected limbs (72) .

Contraction of the *gluteus medius* may provide some degree of protection against fracture of the hip (73). There is also evidence supporting adult physical

programs that support balance and co-ordination, thereby reducing the chances of fall and fracture (74). Preventing fracture is obviously a primary goal in clinical medicine with regard to age-related bone loss. However, the application of effective management of those fractures that cannot be prevented, has a profound effect on the degree to which bone recovers from the fracture, and hence forecasts the longer term outcome for the patient. Being able to accurately quantify the efficacy of a specific rehabilitative treatment regime for fracture through non invasive means is therefore of paramount importance.

2.1.8 Nutrition, Genetics, and Hormones

Modern lifestyles and the trend towards greater life expectancies in both men and women are exposing the biological cost of our adaptation to evolutionary forces. Previously these forces acted on human populations that lived much shorter lives under the effect of more rigorous selective pressures (2). Apart from the biomechanical influences discussed previously, other important factors such as genetics, nutrition and hormones influence bone health, and therefore greatly impact on the ways in which bones age.

A 2004 population-based study of 1363 older women showed that the 24% who achieved the highest physical activity and dietary calcium intakes had a 5.1% higher hip BMD than those who did not. The finding provides strong evidence of a positive impact in the development of bone mineral density from good nutrition and lifestyle practices (75).

Conversely another recent study involving the BMD evaluation of 73 women who survived the holocaust, demonstrated that these women had a significantly higher level of osteoporosis within their numbers when compared to age-matched individuals from the general population. (76). This finding highlights the negative impact of poor nutrition and environmental factors such as exposure to sunlight, in influencing early bone development but affecting the entire lifespan

Studies investigating the genetic influences on bone formation and turnover have come mainly from maternal offspring pairs (77) and monozygotic and dizygotic twin investigations (78-80). Studies demonstrate a difference in the heritability of bone mineral density characteristics in relation to skeletal location and gender (79). Recent studies of adult Caucasian twins has also quantified genetic variation in elements responsible for bone loss in twins as being as low as 40% (78) and as high as 56% (80).

As previously mentioned, under disuse of bone appears to uncouple the normal course of bone formation from resorption. Both animal and human studies have shown that when bone is lost due to disuse, remobilisation for periods of 2-3 times that of the period of disuse are required to rebuild bone to the quality prior to immobilisation (81-83). Studies of the femurs of the North American hibernating grizzly bears however demonstrate a decreased bone turnover with a balanced formation and resorption, which reduces the bone porosity, and maintains the geometric and mechanical properties throughout the hibernation period. The mechanisms by which the bears prevent bone loss throughout hibernation are not clearly understood, but may involve parathyroid hormone (84) which is the primary regulator of calcium levels in the blood. The bear obviously possesses a unique regulatory mechanism that prevents bone loss during disuse, and understanding the mechanism may offer opportunities to treat osteoporosis (85), and manage bone conditions generally.

Systemic hormones such as parathyroid hormone (PTH), 1.25-dihydroxyvitamin D_3 and thyroxine (T_4) stimulate the formation of osteoclasts by inducing the expression of receptor activator of nuclear factor-κB ligand (RANK L) on marrow stromal cells and osteoblasts. The sex-hormones also have an effect on bone, and are discussed in Part B.

The adult human contains calcium and magnesium outside of the skeleton in blood plasma (86). The prevalent calcium in the body is however located predominantly (99%) in the mineral phase of bone tissue as hydroxyapatite

$[Ca_{10}(PO_4)_6(OH_2)]$, with the remainder located not only in blood, but also in extracellular fluids and within soft-tissues. The body's magnesium is also located predominantly (66%) within the skeleton, but is also located in the cells (33%) and in the extra-cellular fluids including blood (1%). The intracellular and extracellular concentrations of both calcium and magnesium are tightly regulated by factors that are not very well understood (87), though it is known that systemic hormones help to regulate both calcium and phosphate.

The ionised form of calcium acts on several aspects of metabolism such as blood coagulation, cell membrane permeability, neuromuscular activity and enzyme-based processes (88). Calcium levels within the body are tightly regulated in blood plasma with the mobilisation of calcium overriding skeletal reserves due to functional deficiencies of the body such as renal disease, mal-absorption, or a poor calcium diet, leading eventually to bone loss, which is mediated generally by elevated levels of PTH (5).

Calcium also forms the primary focus of radiological bone imaging techniques. The natural diets of all mammals are rich in calcium, with normal human serum levels of 8.5 to 10.2 mg/dL. These normal human levels of serum calcium are much lower than those found in other organisms such as many marine-based animals. These animals have around 4 times that of humans, which indicates an adaptation over a long period by humans to lower calcium levels (2).

2.2 Part B. Literature Review of Bone Measurement

Presently there are no diagnostic examinations that can be used to assess the degree of bone weakening in any individual, beyond which normally occurring stresses and force will cause fracture. This represents a clinical problem. Age-related bone changes increase the risk of fracture; but that change alone does not in and of itself cause the fracture. Also, the rate and nature of bone-ageing is not consistent across the adult lifespan, and is not consistent between the sexes

2.2.1 Osteoporosis

Osteoporosis is a term used to describe a decrease in bone mineral mass and a deterioration of the micro-architecture of bone. Osteoporosis has no one cause, and is more apt to be described as a micro-structural failure likely leading to fracture, than a disease process (89). Osteoporosis is a condition which, in its extreme expression, dramatically increases the chance of fracture. The prevalence of osteoporosis increases with age, and an osteoporotic fracture subsequently puts the incumbent at risk of death or permanent disablement, and an increased risk for a subsequent fracture (90). The World Health Organization (WHO) defines determines that an individual is osteoporotic if they have a bone mineral density (BMD) 2.5 standard-deviations below the mean for young adults (91). The WHO t-score evaluation is shown in table 1 on page 32. The WHO system was initially formulated as a tool for the evaluation of a population, but has subsequently been adapted by clinical medicine as a tool for individualised patient assessment.

Osteoporosis can be manifested in three ways. Least commonly, the disease takes the form of a reduced peak bone mass evidenced in early adulthood, and this condition is known as ***juvenile*** osteoporosis. Osteoporosis may also occur as a ***secondary*** disease related directly to the treatment of other disease processes, such as those involving cortisol and its synthetic analogues; which is specifically termed *glucocorticoid-induced osteoporosis*. The most common and most widely studied form of osteoporosis presents in the ageing population **(primary)** where it affects women more prevalently after menopause.

History

The term osteoporosis has its origins in France in the early 1820s where it was broadly used as a description of a pathological state of bone, but it was not until the early 20th century that the term came to be used in English medical vocabulary (92). The definition of osteoporosis has altered over the years as scientific endeavors have sought to describe physiological and clinical changes observed in the process of bone-ageing. The socioeconomic impacts of an

increase in fracture risk, and the subsequent increased morbidity and mortality risks are now also part of this age-related condition. In the past, osteoporosis was a diagnosis that was achieved by exclusion, in that it was pronounced only after a person sustained a fracture that was not able to be explained by any other cause (93). Today the term broadly represents a multi-factorial condition of bone turnover imbalance.

Osteoporosis is also not a new challenge for humans, and in fact has been identified in bones derived from archeological excavations such as the nearly 800 skeletons of the Wadi Halfa area of Lower Nubia in the Sudan, dating from 350 BCE to 1400 CE. It was during this investigation conducted in the 1960s that some of the first examples of osteoporosis rates in prehistoric bone samples were published (94). Results indicated that females in that population showed significantly lower BMD levels when compared with that of the males. The reported rate of age-related bone loss in the ancient population indicated that osteoporosis occurred at an earlier age, and advanced more rapidly than currently occurs in the 21st century. A 51 year old Nubian femur for example, was said to have characteristics of a 60-year-old modern femur (94).

Another example of an archeological excavation that examined femora for the presence of osteoporosis, involved the 1729-1852 crypt at the Christ Church, Spitalfields, London. This study also yielded results indicating that an average modern-day 70-year-old has a lower BMD than a woman of the same age living 200 years ago (95). Archeological evaluations however do not reveal consistent findings. Bone material from the 3rd and 4th centuries in Britain indicate that women then had a greater postmenopausal cortical bone loss than a modern reference population, and thus an increased prevalence in osteoporotic fractures (96). Contemporary data also indicates significant variation in the osteoporosis rates in different geographical locations across an economically advanced country (97).

T-Score, Z-Score and Relative Risk

The World Health Organization classification of osteoporosis is documented as table 1. The associated Mayo Clinic classification system is also included as table two.

Normal: BMD within 1 SD of a "normal" (T-Score at -1.0 and above)

Low Bone Mass (Osteopenia): BMD between 1 and 2.5 SD below that of a "normal" (T-Score between -1 and -2.5)

Osteoporosis: BMD 2.5 SD or more below that of a "normal" (T-Score at or below -2.5).

Severe Osteoporosis: BMD 2.5 SD or more below that of a "normal" (T-Score at or below -2.5), and the presence of one or more fragility fractures.

*WHO Study Group Report. WHO Technical Report Series 843; 1994 (98)

Table 1 World Health Organization Osteoporosis Classification

Mayo Clinic Classification

Type I: Postmenopausal Osteoporosis (oestrogen deficient cause)

- 55 – 75 years old, 6:1 ratio of female to male affected, and commonly fractures wrist and spine.
- Bone re-absorption exceeds bone formation at each BMU, resulting in a net bone loss.

Type II: Age-Related or Senile Osteoporosis (universal phenomenon)

- 75 years old, 2:1 ratio of female to male affected, and commonly fractures spine and femoral neck.
- Affects bone micro-architecture or trabecular connectivity of bone.

*(Riggs, Melton 1986)(99)

Table 2 Mayo Clinic Osteoporosis Classification

$$T - Score = \frac{\text{Measured BMD} - \text{Young Mean BMD}}{\text{Young BMD } SD}$$

Equation 1 T-score formula

T-scores are said to be useful in the estimation of the relative risk of fracture (RRF), using a guiding principle that fracture-risk doubles with every standard deviation (SD) decrease in the BMD (100). It is interesting that RRF is used in the context of the T-score, as "relative" risk indicates that there is a score for which no fracture is expected, and yet there is **no recognised *safe* T-score**.

Using BMD values derived by DXA technology and the WHO endorsed guide, the risk of fracture increases as BMD decreases, however significant rates of fracture are seen in individuals with osteopenic and normal BMD values (101). The substantial Rotterdam fracture surveillance study for example demonstrated that over half of the women and one-fifth of the men with femoral neck fractures had T-scores that were within the normal range (102). Using these data it may be presumed that using the -2.5 T-score as a fracture predictor is likely to result in missing treatment and therapy opportunities for well over half of those people who **will** eventually fracture. Conversely, it also means providing pharmacological treatment, with all the associated side-effects, for a great number who don't need it.

$$RRF = 2^{T-score}$$

Equation 2 Relative Risk Factor

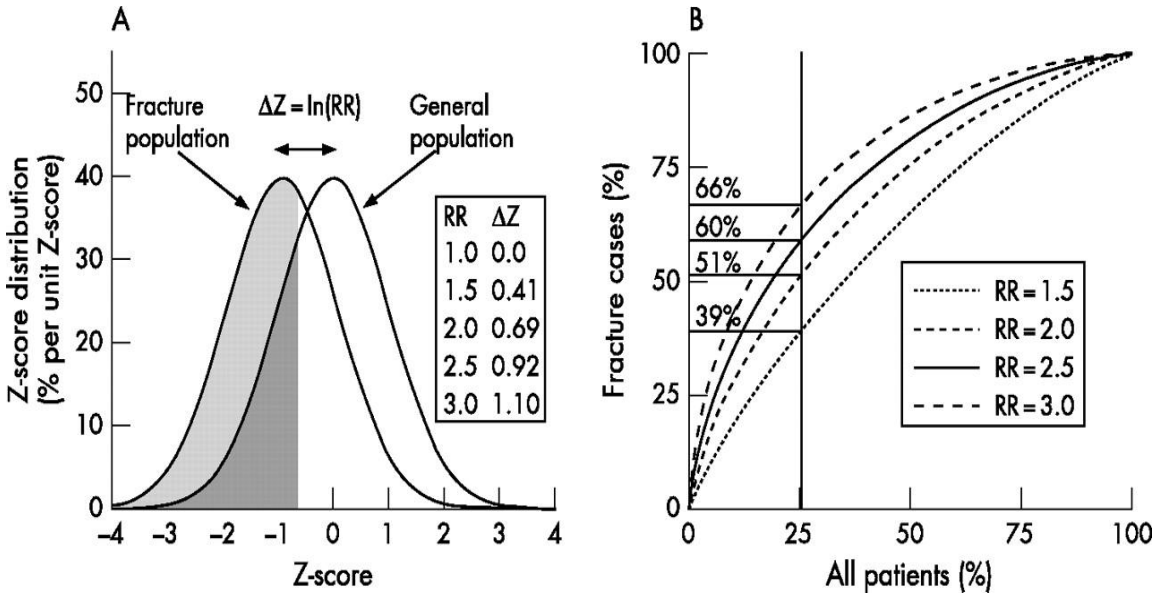

Figure 5 Z-Score in Fracture Population

(A) RR is relative risk. Note the overlap of the two groups. (B) The ROC (receiver operating characteristic) of the areas under the two curves shown in (A), demonstrating that in the lowest quartile of BMD values, the RR values (1.5, 2.0. 2.5 and 3.0) of fracture are 39%, 51%, 60% and 66% (103)

According to this method, a proximal femur DXA scan that reveals a T-score of -3 is therefore 8 times more likely to fracture than a person who records a *normal* or 0 T-score value. No data for relative risk as a function of age exists.

Z scores are similar to T scores except that the BMD result is compared to that of his or her peers rather than that of the young adult mean.

$$Z - Score = \frac{\text{Measured BMD} - \text{Age and Sex Matched Mean BMD}}{Age\ and\ Sex\ Matched\ SD}$$

Equation 3 Z-score formula

Osteoporosis in Women

Menopause refers to cessation of menstruation, and occurs as a result of the gradual decline in ovarian hormone production. The process begins late in the 4th decade and usually progresses until sometime in the 5th decade. Women loose considerably more bone mass in the period just following menopause (or after surgical oophorectomy) than at any other time in their lives, with a rate of loss around 3-times that of a premenopausal woman (104). There is no equivalent

period of accelerated bone loss demonstrated in the adult lifespan of men, who loose bone continually from the time of skeletal maturity.

An estrogen lead decline in hormone production is therefore the central factor in a woman's development of an osteoporotic condition (105). A more accelerated bone loss is also strongly linked to a low body mass at the time of menopause (106, 107). A loss in body mass likely further complicates the assessment of osteoporosis using DXA based screening procedures as the differences in adipose tissue of the abdomen and pelvic apron confound serial evaluations using this technology (108).

Osteoporosis in Men

Studies have shown that osteoporosis rates in men have a bimodal-distribution with peaks occurring around the age of 50 (as ***secondary*** osteoporosis) and after the age of 70 (***primary*** or age-related osteoporosis) (109). Osteoporosis in men is becoming increasingly recognised as an important public health issue due to increased longevity, and the differences in the expression of the condition between men and women have assisted in developing a better understanding of bone biology generally (110). Men do show similar trends of bone loss to women as young adults, but as mentioned, do not exhibit the same rapid loss that women do directly after the period of menopause, rather the loss occurs more consistently over time. The reasons for the differences in both skeletal development and bone-ageing patterns between the sexes are unclear, but likely they arise from the differences in sex-steroid actions.

The incidence of hip fracture in men from developed countries is around half the rate in women of the same age. Taking into account the current lower average-life-expectancy of men, their lifetime risk of proximal femur and other osteoporotic fractures is about one-third that of women. Osteoporotic fracture rates in elderly men however has a similar to the pattern with increasing age as seen in women, though it occurs at least 5 to 10-years later in men (110). Recent

studies also demonstrate a positive correlation between a high lean body-mass and high BMD (111).

2.2.2 Peak Bone Mass

At any given age, an individual's overall bone mass is a function of peak bone mass at skeletal maturity, and the subsequent rate of bone loss during the process of ageing. The term peak bone mass is defined as the amount of bone-based tissue at the time of skeletal maturation (112). On average, men have a higher peak bone mass than women, independent of their size.

Studies evaluating specific differences in the attainment of peak bone mass demonstrate that it is largely dependent on racial origin (113) and difficult to quantify a relevance to subsequent age-related fracture risk (114). Clinical studies have shown that juveniles who exercise regularly, build more bone mass than do children who do very little exercise, with exercise being effective longer-term when engaged in around the time of puberty (115). Exercise enhanced juvenile bone-building results in a higher peak bone mass as young adults, and translates to a higher peak bone mass overall, which is shown to reduce the risk of osteoporotic bone fracture later in life (116-118).

The racial differences in children have been shown to more positively affect bone accrual in terms of a higher level of physical activity, calcium intake and lean body mass, for Caucasians in comparison to children of Asian ethnicity (119). While overall bone strength, which is greater in overweight children, has been shown to be due to a greater muscle area in the overweight, rather than as a consequence of the greater bulk contributed by fat (120).

Peak bone mass has been shown using CT and DXA methods to be reached by sexual maturity, but may rise further after longitudinal-growth has completed (121). The variation in the DXA based assessment of peak bone mass (and bone mineral mass generally) may be partly explained by the influence of x-ray field inhomogenieties induced by differences in the adjacent soft-tissues. Variation in

bone structure and soft-tissue correction using DXA is a known source of error in bone mineral assessment (122).

2.2.3 Radiological Bone Evaluation

At any age, a person's skeleton is a representation of everything that has occurred to it from conception to peak bone mass, and into old age (123). The radiological technologies used to investigate bone have advanced rapidly over the years, though the enormous accumulation of information has done very little to produce a set of criteria from which a gold standard of bone-health or fracture-risk may be determined. Bone and bones are very complicated and still poorly understood structures.

The diagnostic challenge in radiological techniques for quantitative bone evaluation has, in the past, been that evaluation involved an essentially analogue technique (93). The principle of 2D-photon transmission worked well in the 1895 demonstration of Rontgen's wife's hand, but bones are 3-dimensional.

Bone Mineral Density

Bone density is analogous to the *mineral ash weight ratio*, which refers to the product formed from a technique where bone is heated to a point where all organic and water components are burned off, leaving only the mineral solid. The term *ashed bone* is therefore commonly used to describe the product. The remaining *dry* non-volatile sample of the process of *ashing* consists of salts and some oxides depending on the burn temperature. The remains are weighed, and that weight compared with the weight of the original *wet* bone, providing an estimate of bone mineral density, expressed in g/cm^3. Water in this evaluation method therefore represents a density of $0g/cm^3$, as the entire molecule is vaporised in heating, leaving no solid material. Methods for establishing the calibration and accuracy of microCT techniques to ash weight are limited (124, 125).

Early attempts at bone-densitometry occurred in the 1960s. These methods involved monochromatic low-energy photon beams, which investigators derived from radioactive sources, like iodine-125 at 27.3 keV and americium-241 at 59.6 keV (126), and gadolinium-153 was also used (127). In these early studies, Cameron and Sorenson used scintillation detectors to derive bone density measurements, and claimed an accuracy of 3%. Unfortunately these early techniques lacked the penetration required to evaluate the spine and hip, and the uneven nature (i.e. soft-tissue compositions not consistently expressed across any two individuals) of these anatomical areas made using a tissue equivalent material problematic for single-energy techniques.

Technological advances since early BMD evaluations have been significant. Bone mineral densitometry however continues to be limited in terms of being able to provide a definitive scale of age-related change in an individual, because of the large inter-individual variance. Indeed much of the hesitancy in the development of ***bone-health*** investigative methods, apart from the fact that there is no agreed definition for the term, arises from the uncertainty of what variable or variables need to be measured (93) and how. Geometry, material properties and BMD can all provide information on the likelihood of a fracture, but measuring these factors non-invasively and at adequate resolution is difficult at the moment.

DXA

Dual energy x-ray absorptiometry (DXA) techniques provide an assessment of the areal density of mineralised bone or aBMD. A 2D-image is analysed with all soft-tissue structures superimposed over the bone, then the soft-tissue is subtracted using a correction algorithm. DXA involves the formation of a 2D projection image of a 3D object. This inevitably confounds bone geometry and mineral density. The variability of biological materials using a 2D technique also affects the precision and accuracy of DXA as well as the ability for inter-calibration when different calibration techniques are used (108, 122, 128).

The aBMD measurement relates to the area from which the measurement was taken, notwithstanding errors related to the operator usage, patient positional differences, the presence of more than two biological tissues in the image, and equipment variations. Any correlation between areal bone mass and bone strength is therefore highly contentious (129).

aBMD peaks at around age 20-years in the proximal femur, while total skeletal-mass continues to increase for another 6 to 10-years (130). Importantly when discussing aBMD, the relative size of a bone is not taken into consideration when the mineral mass is expressed as an absolute weight, (i.e. a large bone could weigh 300g, and so could a very dense smaller bone). The calculation of mineral mass provided by DXA techniques is only partly compensated for in an areal density (gm/cm^2) expression. The expression of mineral mass that takes full consideration of the size of the bone, is volumetric bone mineral density vBMD (gm/cm^3), though to call vBMD a *true density* rather than *apparent density* is also erroneous. Aspects relating to *apparent* and *true density* will be discussed further in chapter six.

Cortical bone has an internal pore structure that does not contain any mineralised component. The voids in trabecular bone are much larger and contain marrow. The very small *hypo-dense* areas such as those in bone (i.e. no mineralisation), have the capacity to *confound* the 3D-evaluation of absolute mineral values, leading to what is known as the *partial volume effect (131).* Where hyper-dense (mineral) and hypo-dense (pores) areas exist in the one imaging volume element (voxel), an average attenuation-related greyscale value is created, which leads to the concept of an *"apparent"* value. It is therefore appropriate to indicate an ***apparent*** density in the radiological expression of either *a*BMD or *v*BMD. The guiding principle of *apparent density* is that, the smaller the voxel, the more accurate the density estimation, hence techniques such as synchrotron microCT is used on bone specimens.

Figure 6 shows a copy of the tabled results of a repeat DXA clinical examination of five patients performed 2 to 12 days apart. The study used a DXA unit with an aBMD accuracy of 1%, and a 2-3% for total body fat (132). The sample size is very small (*n*=5), but in all but one of the results (the youngest patient, and the only measurement completed using an automated edge detector) the difference in two of the three measurements is well above the 1% variation allowed for in the mainstream application of the technology.

Gender	Age	Lumbar spine	Femoral neck	Distal wrist
F	41	- 0.9	+ 0.8	- 1.0
F	50	- 3.1	- 1.2	+ 1.4
M	54	- 1.3	0.0	+ 3.0
F	62	+ 0.7	+ 2.4	+ 1.8
F	66	+ 3.2	+ 6.6	- 0.3
F	83	+ 8	+ 3.9	- 0.4

Figure 6 Table from NZ DXA Review Study

Difference (expressed as percentage) between the initial DXA scan and that of the subsequent scan. (133)

The stated accuracy in the repeated measurement case is therefore only applicable to younger individuals suited to the application of the automated edge detection, as they likely have more defined margins of bone. Generally however the great bulk of DXA examinations performed globally are on older individuals who, depending on their osteoporotic state, do not express these radiological characteristics. The sole reliance on technologies such as DXA to provide meaningful data on bone mineral density would therefore be unwarranted and perhaps invalid without due consideration of the associated pitfalls (129).

QCT

Contemporary CT-related techniques such as quantitative computed tomography (QCT) build densitometry measurements from a three-dimensional volumetric acquisition processed to separate out overlying soft-tissue structures, and provide a 3D-estimation of the measurement site (134). There is evidence supporting the long-term precision and accuracy of the modern CT unit for QCT

evaluations (135). The QCT bone mineral assessment technique requires the use of a bone calibration phantom, to account for the polychromatic nature of the CT photons. Various known concentrations of bone equivalent materials are used both for calibration and quality assurance (QA) to establish a predictive assessment of bone density (136). The QCT technique is discussed in detail in chapters 3 and 4.

MicroCT techniques such as peripheral quantitative computed tomography (pQCT) involve imaging small samples at high-resolution, while QCT techniques use clinical CT scanners to evaluate larger samples at lower resolutions. Each technique however requires care in assessing geometric and densitometric variations across populations and/or time points (137). This is especially important as the application of various slice reconstruction algorithms will influence the *calibration* of the image qualities used to determine densitometric values. This point is further discussed in chapter 6.

CT-based finite element analysis which incorporates information of both 3D-architecture and bone density distribution, will also likely achieve a more precise assessment of proximal femur strength than BMD factors only (138). Work on developing automated segmentation for the separation of bone types (i.e. trabecular or cortical) is also showing considerable progress (139), furthering the utility of the data. The limitations of clinical MDCT systems in differentiating trabecular from cortical bone are discussed in chapter 7.

2.2.4 Ionising Radiation Dose

The cultural response to nuclear radioactivity after the explosions at Nagasaki and Hiroshima, has been described as “miasmic dread” (140). Much of what we currently know about the deleterious effects of radiation comes from the experiences of the survivors of those bombs (141). The present increasing use, and subsequent increase in ionising radiation burden of the general population for the purposes of diagnostic CT imaging is raising concern (142).

Recent evaluations of ionising radiation dose, based on a per-capita-burden, estimated that 3.6-billion radiological medical evaluations are performed worldwide annually (143). Diagnostic procedures account for 3.1-billion procedures, dental 0.5-billion and nuclear medicine 37-million. The evaluation estimates that in just over 20-years, the net increase in the average effective dose delivered by medicine has risen from 0.5mSv to 3.0mSv annually. The result is significant; especially considering that the average background dose from the Australian environment is 3.0mSv annually. A comprehensive description of the units used to measure ionising radiation dose are contained in chapter 3.

Scientific articles outlining the relative benefits of using DXA scans for determining bone mineral density, invariably state that the 2D-technology has a 1 to 10 magnitude lower ionising radiation burden than that of the 3D CT-based studies (144-146). Importantly that does not mean that the appropriate use of CT technology will cause deleterious medical outcomes as a result of the radiation dose. There are also very few reports in the literature that make any distinction between effective and absorbed-dose, or attempt to try and tease apart the meaning behind these units and how they apply to bone densitometry. Outside of cardiac screening and pediatric studies, very little has been recently published regarding MDCT radiation dose generally. Some articles that do quantitatively discuss the issue of radiation dose, do not clearly define the dose units (effective or absorbed) used, and often read more like an advertisement for DXA than a scientific analysis. One such *scientific* article even includes various images directly from the advertising brochures of the manufacturers (147).

Absorbed dose is measured using the unit Gray (Gy), which corresponds to the equivalent of one joule of energy deposited into one kilogram of biological material. The lethal dose for 50% of subjects (LD_{50}) for ionising radiation delivered over one or two months for a human is between 3-5 Gy. Because radiation interacts differently depending on the type of radiation being delivered, an additional unit known as the Sievert (Sv) is used to describe the effective dose (E). The Sv provides a determinate of the absorbed dose

multiplied by the effectiveness factor of the type of radiation delivered. The effective dose is therefore an expression of dose that reflects the biological sensitivity of the tissue being irradiated (148).

CT scans are performed for the purposed of clinical decision making every day all over the world. One expects that the vast majority of those CT scans performed are being used to positively direct patient management. Surely the key question about what diagnostic test to perform relates to the test that has the most chance of answering the clinical question. Dismissing CT-based techniques for determining bone assessments on the basis of *"excessive"* radiation dose concerns, serve only to limit the prospect to search for better ways to individualise treatment and therapy options.

Cancers related to exposure to ionising and non-ionising radiation including medical procedures, have been estimated to account for up to 2% of all cancer deaths (149). Research conducted into cancer cases of workers in the nuclear industry also report that estimates of between 1-2% of deaths from cancer are attributable to occupational exposure to radiation (150). Research into work-related dose-effects; note that it is very difficult to subtract causes other than those from radiological imaging or radiation work generally from the results of any study into cancer. An actuarial approach to cancers induced by medical procedures is therefore problematic generally.

Changes involving marrow content or type as bone ages have also not been extensively investigated using MRI despite an obvious advantage over radiological imaging, with only a few recent articles exploring the link between bone ageing and fatty composition (21, 151, 152). The usefulness of the MRI technique to the work documented in this thesis is therefore at its infancy. The technique however is potentially extremely relevant, as shown in a recent evaluation of marrow changes in anorexia nervosa (153). Figure 7 demonstrates bone bruising associated with an anterior cruciate ligament tear.

2.2.5 Femoral Morphometry and Gait

At birth the femoral neck lies at an angle greater than 106° to the diaphysis, and reaches 130° - 135° deflection well before the age of skeletal maturity (32). As growth occurs, the femoral neck increases in length, causing an increased angle of pull on the abductor muscles, and on the attached fascia. Eventually this action causes the epiphysial cartilaginous plate to rotate where it eventually lies perpendicular to the equilibrant force in the femoral neck (73).

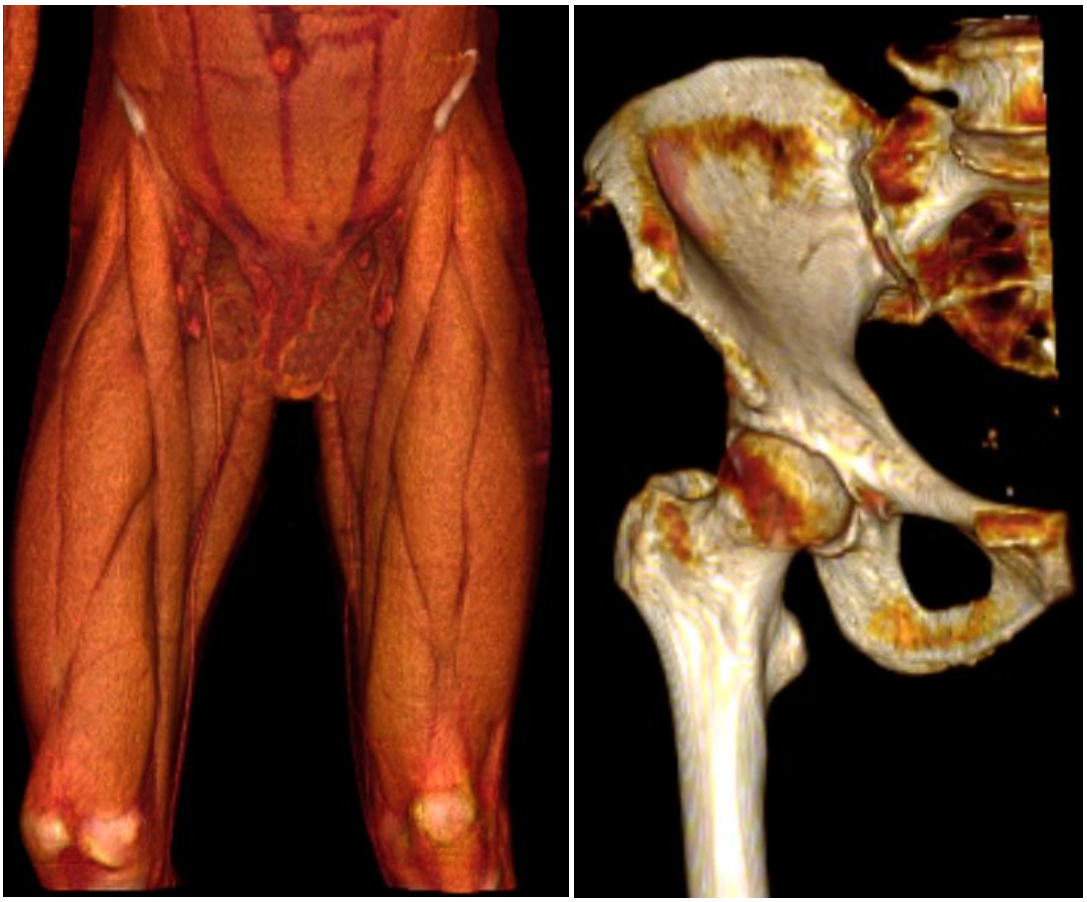

Figure 7 CT soft and hard tissue renders of the lower limb

Renders of the muscles and hemi-pelvis of the proximal lower limbs from the VIFM CT scans. All of the muscles act from the time of first walking to finalise the hip structure.

The loadings of the hip are heavily scrutinized, with much of the inquiry directed toward advancing positive outcomes for total hip arthroplasty (154). It has been demonstrated that in ageing long bones, the cortical cross-sectional area declines, while the total area increases due to periosteal apposition (22, 155-157). This finding suggests that the expansion of the outer diameter of bone

partly compensates for the net loss of BMD in relation to maintaining a long bone's resistance to compression and bending. It does not however explain the geometric variations seen after a fracture (38). It also does little to describe from a biomechanical perspective, why BMD can be a predictor of fragility of bone (158), as aBMD decrease with age, but as a function of an increased periosteal envelope, as well as through bone loss (159). Meaning that during ageing, if more bone is reabsorbed than is deposited, the effect on the bones overall strength is negligible if the deposition taking place occurs on the periosteal surface (160). The effect of ageing does however make a sudden and catastrophic failure more likely.

The complex mechanical interactions between hard and soft-tissues in studies of gait and mechanical loading are over simplified if the structural components (muscle and bone) have been treated as separate structural objects (12). In the hip, it is the force of the abductor muscles and the tension on the *iliotibial tract* that holds the pelvis in equilibrium during stance and in motion. The attachments of the *gluteus medius* and *minimus* at the greater trochanters support the coordinated support of the pelvis during motion.

Evidence in the literature, demonstrates that in order to maintain equilibrium, a person with an amputation below the level of the knee (BKA) experiences a 10% increase in energy expenditure as measured in the contralateral *gluteus medius* muscle, compared with that of an intact individual. This additional energy is used to maintain equilibrium during unilateral stance. The above knee amputee (AKA) requires 40% more energy (161). Knee joint flexion during stance determines, in concert with other factors such as pelvic displacement (73) and *iliotibial band* transaction (32), gait. A combination of factors is responsible for the changes in energy requirement for the BKA and the AKA, and these need to be considered together to construct a realistic determination of the forces applied to the femur, and the subsequent responses of bone to force in a normal presentation. Given that the ageing process also affects both muscle, it may also be important to

consider the sites of muscular and ligamentous insertion in an age-related evaluation of fracture risk.

2.2.6 aBMD Assessment and Drug Therapy

One of the main components in the delivery of healthcare to an ageing population centers on the supply and access to drug-related therapies. BMD analysis is commonly used to evaluate the efficacy of drug-based treatments for osteoporosis, as well as establishing the baseline from which treatment decisions are made. Pharmaceutical therapy in the case of a low BMD usually involves a class of drugs known as *bisphosphonates* or *diphosphonates*.

Bisphosphonates are a widely utilised class of drugs used to treat a number of bone-based diseases. They are stable analogs of inorganic pyrophosphate, and hence have a high affinity for the hydroxyapatite crystals and bind selectively to mineralised bone surfaces (162). After being absorbed, the bisphosphonate drug selectively disrupts osteoclastic activity by blocking some of the steps in cholesterol synthesis. The disruption results in a decreased bone turnover rate. Bisphosphonates have also been suggested to also have a positive effect on osteoblastic activity through inhibiting apoptosis in osteoblasts and osteocytes (163). The bisphosphonate drugs are presented in either a non-nitrous, or more commonly and more potent nitrous forms (164).

Bone mass has been reported to increase during treatment using bisphosphonates (165). Meta-analysis of the efficacy of anti-resorptive therapies has shown that these treatments significantly reduce the incidence of fracture, but the number of fractures prevented cannot be explained by increase in the aBMD alone. Scientific evidence exists for both a strong correlation (166), and very little correlation, (167) in non-vertebral areas such as the femoral neck for the efficacy of bisphosphonates generally in terms of the BMD. The present thinking therefore in terms of the delivering therapy and treatment for osteoporosis, has shifted from evaluating bone mass to analysing “bone quality”

(168). As previously discussed however, this is confusing as the term has no commonly agreed meaning.

Trials of oral bisphosphonates over 7 to 10 years duration (without continuous placebo comparison groups) produce convincing evidence that drugs like *Risedronate* are generally well tolerated, and as well as significantly increasing BMD, also shows signs of reducing bone turnover activity (169, 170). The dog model has been used in a trial demonstrating the prevention of immobilisation induced increased bone turnover using the bisphosphonate *Pamidronate* (171).

In Australia, from the 1st of April 2007 the Federal Government introduced a Medicare rebate for DXA scans for anyone over the age of 70. If their BMD is very low (i.e. a T-Score of -3 or less), the patient is able to obtain either of the *Alendronate,* or *Risedronate* drugs subsidised under the pharmaceuticals benefit scheme (PBS). Other drugs are sure to follow in the $225 million rollout of access to subsidised osteoporosis medications, expected to reach 40 000 Australians over the next few years (172).

Establishing a regime for the safe long-term use of osteoporosis drugs requires a deeper understanding of the ways in which these drugs interfere with the micro-architecture of bone than is currently available (168). Physicians also require a clinically reliable method of evaluating the efficacy of any therapy used to decrease an individual's chances of suffering a fragility fracture. There are however studies demonstrating significant concern over the long-term use of bisphosphonates (173).

2.3 Part C. Australian Health Statistics Literature

Population statistics from the Australian Bureau of Statistics (ABS) indicate that during the years 1881-1890, the average life-expectancy at birth was 47.2 years for males and 50.9 years for females (8). One-hundred-years later it was 73.9

years for males and 80.1 for females, while projected figures have a child born today having a one in four chance of living past 100 years.

An ageing population has extensive economic consequence from the perspective of a government economy-supply projections, and this forms the Australian Governments 3P's framework; population, participation and productivity (174). Figure 8 presents the current projections from the ABS on the births and deaths in Australia to 2056 (7). The figure shows the changing nature of the Australian population as medical interventions assist in keeping people alive significantly longer than previously would have been expected.

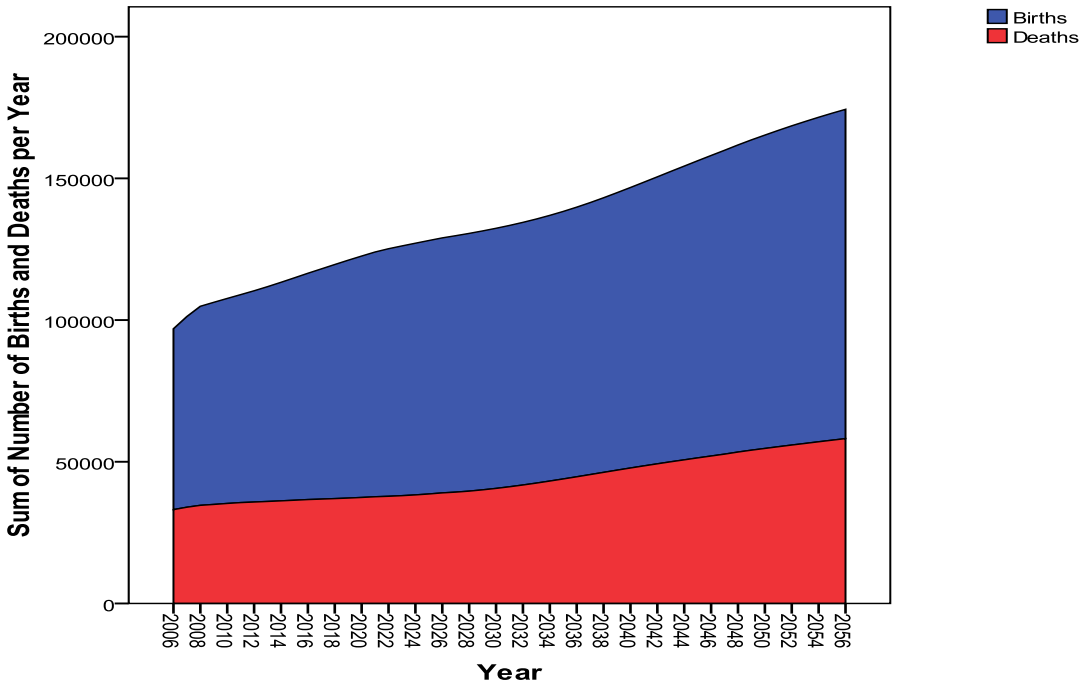

Figure 8 Birth and death projections for Australia (7)

Note the less steep gradient of the deaths compared to the more steep births.

2.3.1 Life-Expectancy and Healthcare Spending

Current life-expectancy data indicates that healthcare spending is an area that will require significant increases in funding to manage an increasingly aged population (9). The current data represents a growing and pressing health obligation.

Half of all older adults suffer from a geriatric condition such as incontinence, vision impairment dizziness and falling (175). Impairments affect the quality of an older person's life by restricting their ability to perform routine activities such as bathing, dressing and eating, and results in them being dependent on others for their care. The ageing population is an issue therefore that will affect more people, both directly and indirectly in the future. Figure 9 presents Australian Treasury data outlining the population age composition from 1967 projected to 2047 (9).

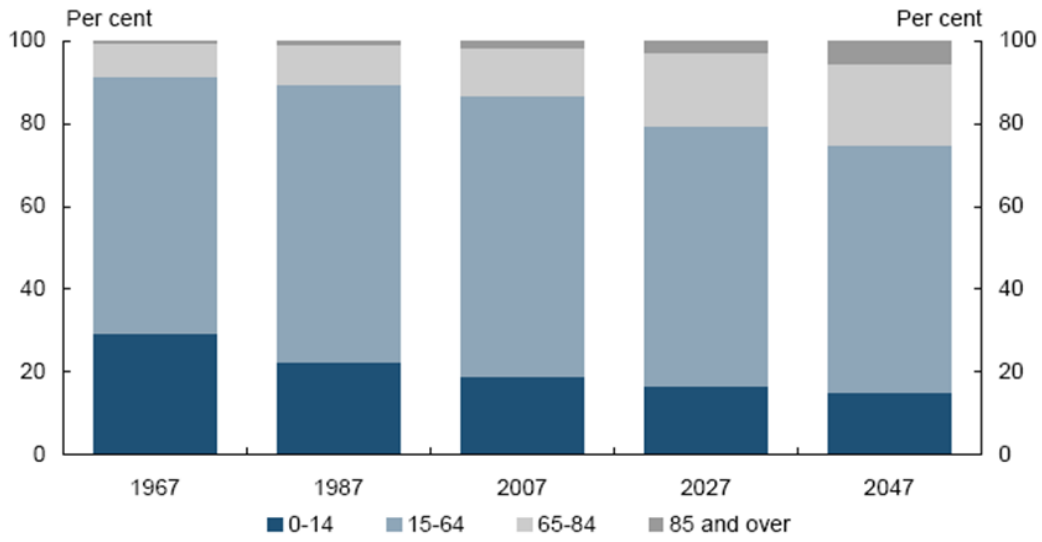

Source: Australian Bureau of Statistics Historic Australian Population Statistics 3105.0.65.001 Table 19 and Treasury projections.

Figure 9 Australian Population Age Demographics

Note the present rate and projected rise in 65-84 and 85 and over categories, and the opposing decline in the 0-14 and 15-64 years categories.

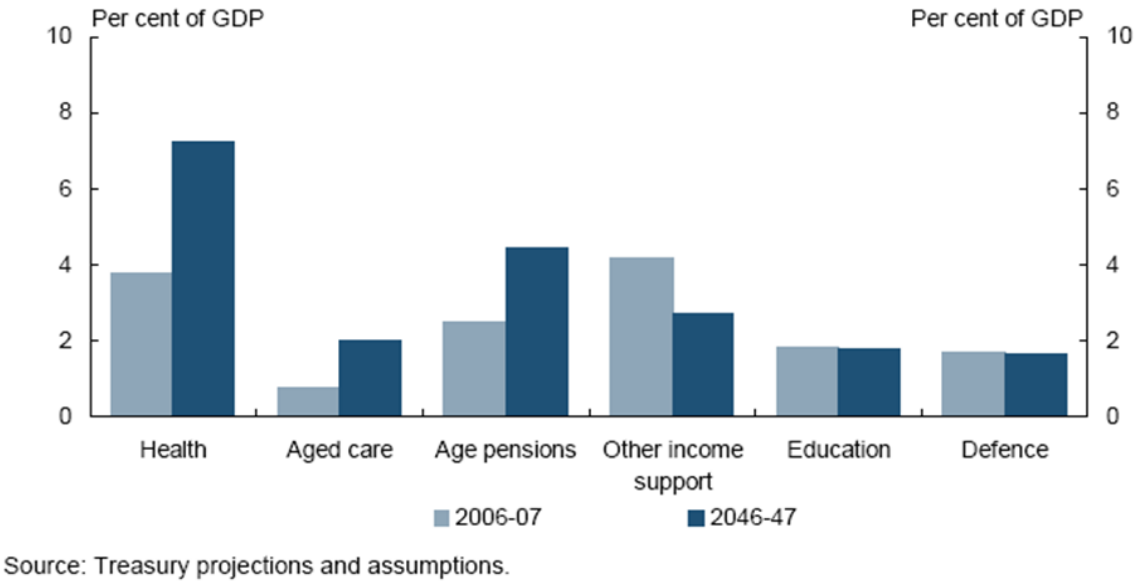

Source: Treasury projections and assumptions.

Figure 10 Australian Government Health Spending

Figure 10 demonstrates the projected impact on healthcare and aged support pensions as a result of a population with fewer and fewer of their number being of working age. Working age individuals are documented in red in figure 11 (7).

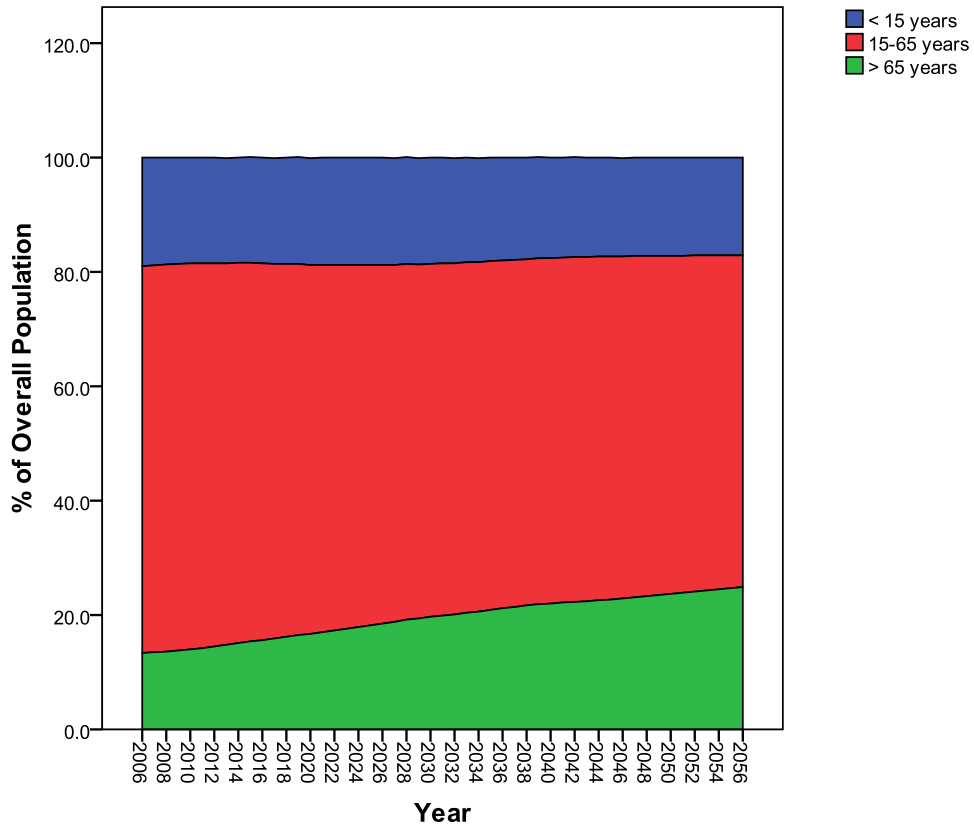

Figure 11 ABS projection data demonstrating the population by age (7)

Currently 2.2 million Australians are considered to have osteoporosis, resulting in one hospital admission every 5-6 minutes; of which 25% are expected to die within 12 month of their initial fracture (176).

The overall aim of this thesis is to develop novel and scientifically verifiable methods for using multiple detector-row computed tomographic (MDCT) data to produce a population-based, morphometric and densitometric record of age-related differences in human femoral bone. The broad objective is to contribute to a greater understanding of the ways in which the femora of a current predominantly urban population ages; which may then be used to improve the evaluation of the ageing process in bone, especially for determining fracture risk, and to therefore improve the quality of life for our ageing population. The subsequent benefits of the age-modelling conducted will also greatly benefit anthropology in terms of the non-destructive evaluation of biological age and stature characteristics using the femur, and relevant population based comparisons.

CHAPTER 3

COMMON MATERIALS AND METHODS

"The whole is more than the sum of its parts."

~ Aristotle ~

Chapter three presents a comprehensive description of the common materials and methods used for the collection of data in the research chapters to follow. It is presented in three parts.

Part A describes the physical and practical characteristics of computed tomography (CT) for the production of cross-sectional x-ray images. This is extremely important as many observations in following chapters are predicated on a clear understanding of the influences that technical parameters have on the quantitative aspects of CT data. The section also includes detailed descriptions of the technical terms used.

Part B outlines the materials and methods used for the calibration and performance testing conducted for the experimentation.

Part C describes in detail the materials and methods involved in the collection, manipulation and storage of the CT data used throughout the thesis. Part C also describes the difficulties involved in obtaining CT data from a busy metropolitan mortuary, and the issues associated with using these data to establish cross-sectional bone analysis methods and records using clinical software.

3.1 Part A: CT Instrumentation

3.1.1 Introduction

QCT based techniques may be used for the evaluation of bone structure and density. The differentiation of tissues using CT is achieved by applying a mathematical algorithm to an accumulated dataset of x-ray attenuations called ray-paths. The attenuated photons hit a solid-state detector where their energy is converted into a series of positional and intensity-related maps. It is from a series of these projections covering the entire 360° circumference of the body, that a CT-image is produced. The image-based intensity information is measured using a scale of Hounsfield units (Sir Godfrey Newbold Hounsfield 1919-2004) or CT-numbers, which assigns a greyscale element. The visual imaging of the greyscale is defined by an operator setting a window width (the number of greys included in the display) and window level (the zero-point upon which the window width is applied).

Attenuation is a factor of both the absorption and scatter of radiation by the material under investigation. The two main mechanisms of scatter are called Compton scatter (Arthur Holly Compton 1892-1962), and the photoelectric effect. The scale by which both affect the interactions of the x-rays on the material, depends largely on the atomic density of the material under investigation, and the energy (or range of energies in the case of CT) of the x-ray photons. In the production of CT-based images, the Compton scatter effect is largely independent of the photon energy levels, whereas the photoelectric effect is strongly determined by the energies used (177). Figure 12 demonstrates the two mechanisms of scatter.

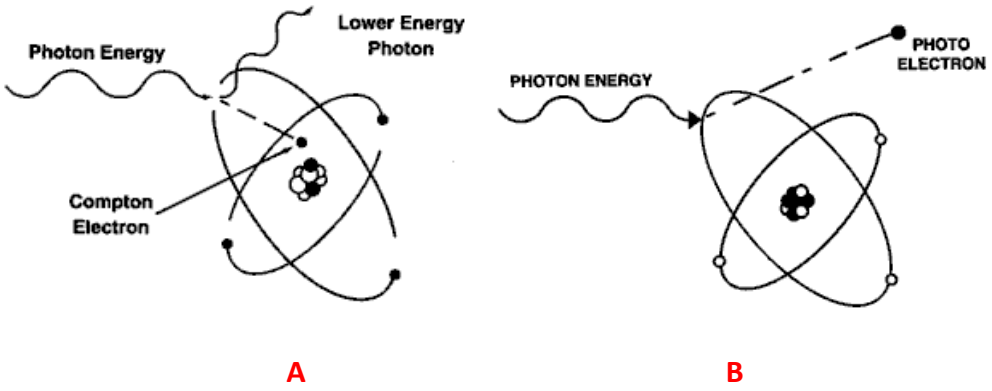

Figure 12 Compton scatter and photoelectric effect

Compton scatter A (decreases with increased photon energies) and the photoelectric effect B (mainly occurs at lower energies i.e. less than 50keV)

Body composition (the distribution of bone, muscle, fat etc.) influences scatter depending on the energy of the photons. The polychromatic nature of the photon flux used for CT will also affect the nature of the scatter.

3.1.2 Clinical CT Origins and Development

Computerised Axial (or Assisted) Tomography (CAT) scanning was introduced into clinical practice in 1972. It was used to demonstrate a large frontal lobe cystic tumor in a living person (178). No deep tumor had ever been verified previously without cutting into the body. Generational advances, especially in computerisation speed and detector technology since then, have supported the broad use of CT for both clinical and research imaging. Clinical CT scans that took hours to mathematically process and reconstruct in the 1970s, occur today in almost real time. Examples of the images produced using original and current technology are presented as figure 13.

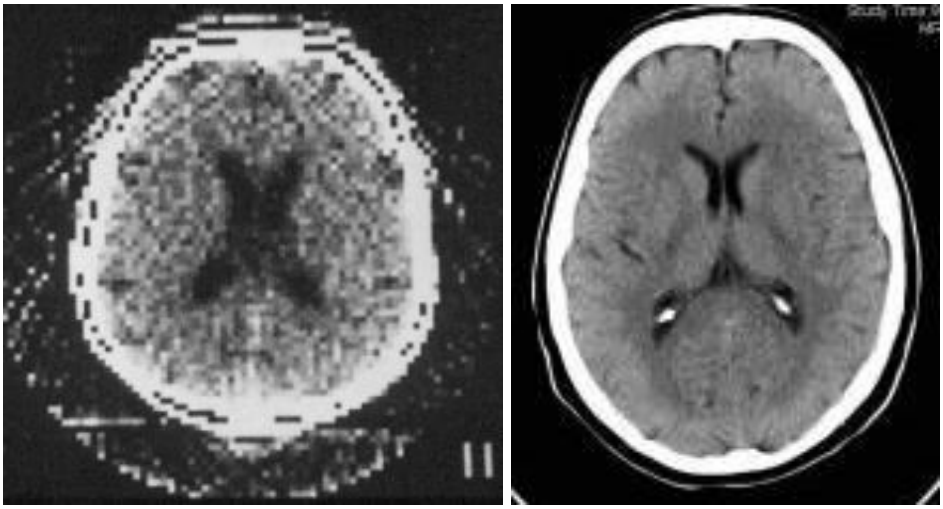

Figure 13 Historical CT comparison

Comparison of axial brain images between an 80 x 80 image matrix (left) used in the 1970s and which took several minutes to reconstruct, and the 512 x 512 matrix (right) routinely used today, and which may be scanned and reconstructed in a fraction of a second.

Advances in modern computing and the application of innovative clinical methods have seen CT-based technology outlive the dire predictions of the 1980s, that the then new and non-ionising form of imaging, magnetic resonance imaging (MRI) would replace it completely (179). The low point in the design and development of CT instrumentation saw little technological advancement, apart from those associated with decreased mathematical computation speed. It was the introduction of helical CT in the 1990s that led to the current and lasting renewal of interest in CT (180).

One of the reasons that it is important to consider the development of CT techniques in the context of the emergence of magnetic resonance applications is the delivery of ionising radiation by the former. Each new generation of CT has bought new ways of reducing dose and speeding up scan and image processing times. Chapter four will present a comprehensive evaluation the effective doses for a QCT examination of the proximal femur as protocols for both living and deceased are discussed.

3.1.3 Spiral / Helical CT/MDCT

Helical and spiral CT technologies are identical and as such either term may be used. Both names refer to the shape of the x-ray scan path on the patient that underpins the production of the axial slice information. As there is no place in the scan trajectory where 360°s of slice information is obtained, helical or spiral CT is termed a volumetric data acquisition. This means that axial CT slices (i.e. the images seen on the screen) are interpolated from a helical volume of data rather than being individually acquired through back projection techniques. The interpolative reconstructive process makes assumptions on the behaviour of the ray-path as it is attenuated, and these assumptions are proprietary.

Single slice helical CT-technology was introduced in the early 1990s and involved the application of slip-ring technology to produce a situation where the continuous movement of the x-ray tube and opposing single detector-row bank could occur. Slip ring technology does not use cables, but rather carbon fibre brushes to transmit the required power to the x-ray tube and detectors. The technology enables continuous power delivery and a constant data acquisition stream. The slip-ring advancement in technology was instrumental in significantly lowering scan times and radiation dose.

Multiple detector-row CT (MDCT) units became available commercially in 1994 (dual slice) and were advanced in 1998 (4-detectors). The length of one helical CT acquisition is expressed as the z-axis length. The multiple detector-row configuration further increased the clinical application of CT through faster data acquisition, and longer volumes acquisitions which were able to be reconstructed at finer slice intervals (179). The technology driven increase in z-axis coverage continues today with the release of a 320-slice unit (32 x 0.5mm detectors providing 16cm of z-axis coverage in one rotation) bought to market in late 2007, and setting the next benchmark for the next technical advance (181).

Traditional definitions of technical performance and data output now require further explanation, especially as the z-axis coverage increases. One obvious

effect in increasing z-axis coverage is the ability to capture a large image volume in a short amount of time. Unwanted movement of an involuntary nature such as cardiac motion, and that of a voluntary nature such as breathing, have all been significantly reduced by the introduction of multiple detector-row volume-based CT. Acquisitions of the entire chest performed in one breath-hold, and contrast enhanced, electrocardiograph (ECG) gated studies of the heart are two clinical examples of the application of MDCT technology.

The way helical CT operates seems very simple, (i.e. volumetric rather than slice by slice acquisition) though the data output and how it is used to construct an image are less so. Figure 14 compares the acquisition of 2D slice information and the helical acquisition.

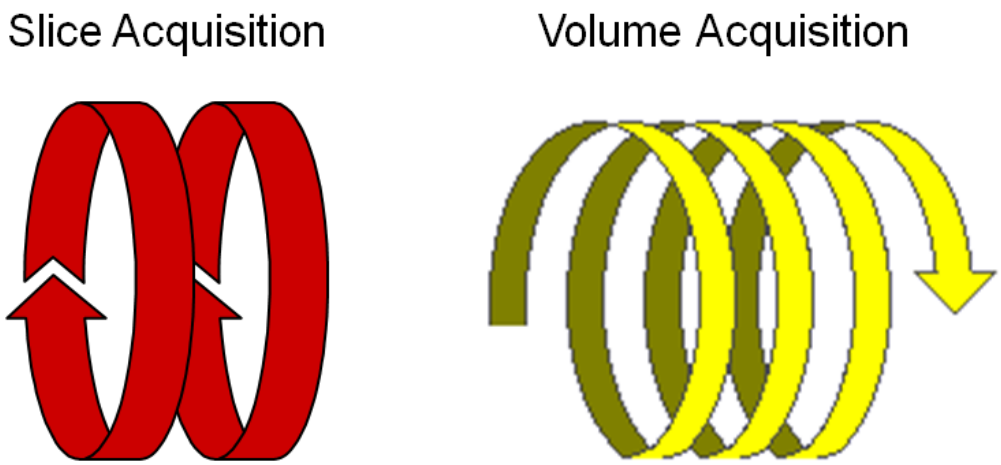

Figure 14 Standard and helical CT acquisition comparisons

Note that a virtual slice is required to be constructed from the raw helical data using a complex method of interpolation of the characteristics of the several rotations of the x-ray tube.

MDCT units are capable of delivering better than 330ms rotational times, which as previously discussed, dramatically decreases the scan time. In doing so however, the rotational action creates approximately 30G of centrifugal force (179), which may limit further advancement of current technology.

The x-ray tube and detector bank on any CT unit may also be used in a fixed orientation (either 90° or 180°) to produce scout or 2D-images. From one or a series of 2D images, the acquisition may be planned by the operator depending on the requirements of the investigation.

3.1.4 Interpolation

In producing an image or series of images from a helical acquisition, two separate mathematical processes must be applied to the projection data. The first involves extracting the raw slice information from a helix of data points, and is described throughout the thesis as interpolation. During the interpolation process the data points from the helix are transformed using various cone-beam and distance-dependent weightings to form raw CT sinogram information (182). Figure 15 demonstrates the formation of raw axial slice information from a volumetric data acquisition.

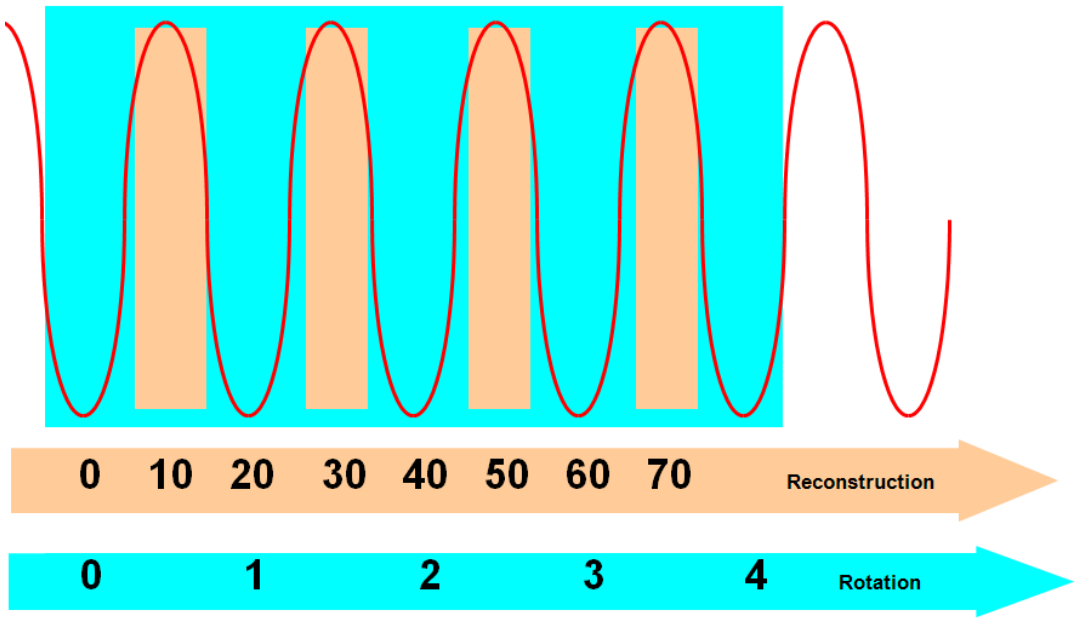

Figure 15 Helical data interpolation

Helical acquisition set to reconstruct 10mm slices thickness every 20mm.

No 180° or 360° complete rotation occurs at any given slice specific site during a helical acquisition, so a traditional back projection algorithm alone is not sufficient to produce an image. Interpolations are applied to the helical data to

form axial scans using one of either of the two methods illustrated in figures 16 and 17. All MDCT units may also be used in a *"traditional", "step and shoot"* or "*axial"* mode if required.

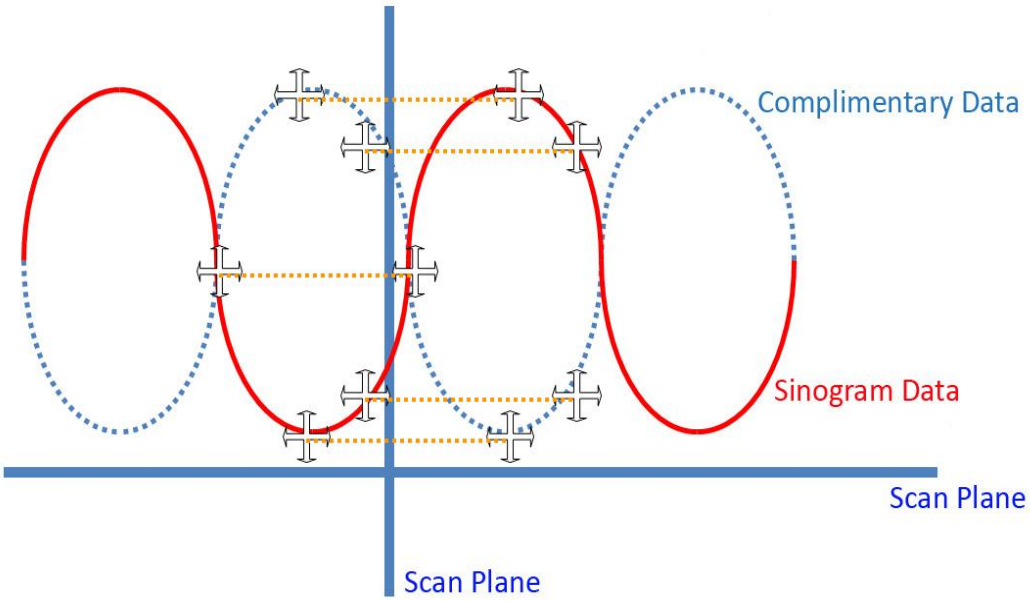

Figure 16 Interpolation using a 180° interpolation method

180° interpolator used to produce slice information. Note the use of complimentary data to support the application of a type of back projection.

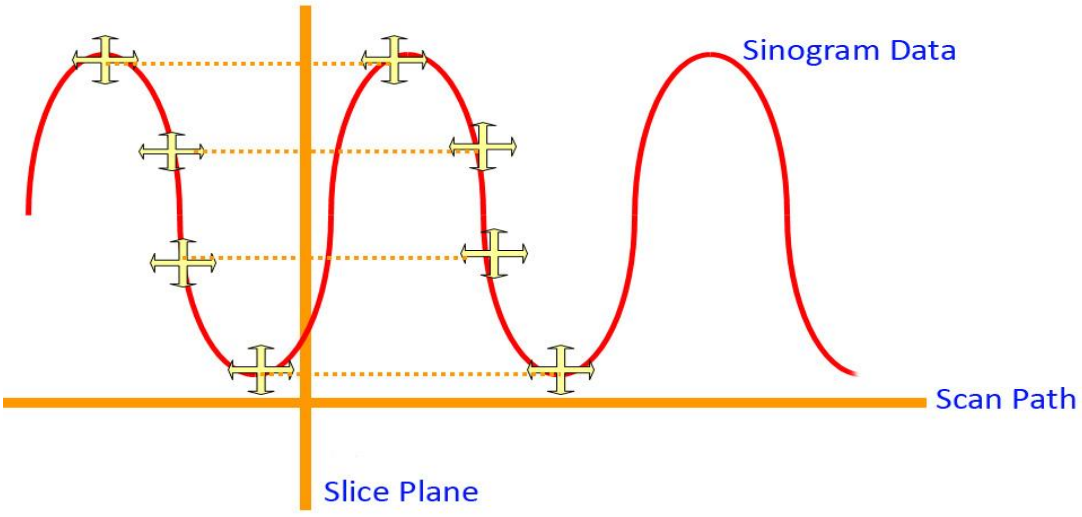

Figure 17 Interpolation using a 360° interpolation method

360° interpolator used to produce slice information. Note that point to point information from either side of the reconstruction slice plane is used.

Conceptually the production of axial images or slices from a volume acquisition is challenging to explain. The point of difference between an axial scan and a helical acquisition is the volumetric attribution to the later. An axial acquisition still has a z-axis only it is set in the collimator rather than by an arithmetic process. The detector-bank for the collection of attenuation data used in a MDCT unit is set in multiple rows along the z-axis. This means that although a body area is not in the central rotational axis for 180° or 360°, a collection of data-points immediately in front of and behind the central-point are interpolated in much the same way that a nut works to hold a bolt as it passes through the windings.

Information on how these interpolators are applied are considered proprietary by the manufacturers and so there are limitations in gauging any effect a particular interpolator has on the data collected. The Toshiba Aquilion™ units, like all currently in the marketplace, use a modified Feldkamp algorithm. The multislice cone-beam tomography (MUSCOT), filtered back projection and true cone-beam tomography (TCOT) are available to use retrospectively on the raw sinogram data if deemed appropriate by the operator (183). For all scans conducted for this study, no alteration to the manufacturer's interpolation method or application recommendation was made.

3.1.5 Cone-Beam

Cone-beam algorithms allow 2D-data to be used to produce a projectional image. As x-rays leave the target, they exist as a point or coned-source, and then gradually fan out until the beam reaches the target (patient) and eventually the detector. The effect can be conceptualised as a light and shadow effect as the object (patient) is located at various distances from the screen (detector-bank). Cone-beam algorithms correct for the geometric distortion that occurs as the ray-path fans out along the z-axis. The cone-beam characteristic of MDCT reconstructions is increasing complex as z-axis lengths increase with every generational change in the equipment.

3.1.6 Image Reconstruction

The second mathematical process that must be applied to the interpolated data is in the creation of an actual slice image and will be referred to as the slice reconstruction algorithm. An image or slice reconstruction algorithm is applied to projectional data, irrespective of whether it is a helical or single slice acquisition. The slice reconstruction algorithm represents the way in which the positional and intensity-related data is manipulated to form an image.

One of the primary strengths in the application of MDCT clinically is the ability to produce additional image series using alternate slice reconstruction algorithms and slice thicknesses, without rescanning the patient. Worth noting is that the ability to alter the slice thickness at the reconstruction level is determined by the configuration of the detectors, which is why manufacturers place the smallest detectors (0.5mm) in the centre of the detector bank. The informed use of reconstruction algorithms is extremely important in the application of quantitative measures on the data produced, and as such will be discussed at length as appropriate.

3.1.7 Isotropic Imaging

A CT image consists of three dimensions from which the scanned information may be viewed. Each picture element (pixel) of computerised image display is constructed from a scanned volume element (voxel) primarily comprised of the x-ray attenuations detected in the x, y and z-axis. The z-axis resolution is always expressed as the slice thickness. The slice thickness is usually the largest value, and is set in the collimator of the CT unit or detector element. The x and y- pixel measurements are derived from the matrix values set in the series acquisition and are governed by the size of the field-of-view (FOV) selected by the operator. The matrix sizes used most commonly for MDCT are either 256 x 256 or 512 x 512, though a 1024 x 1024 is also commonly available. The data used for this study used the 512 x 512 matrix size for all acquisitions. Equation 4 demonstrated the pixel size.

$$\text{Pixel Size} = \frac{\text{Field of View}}{\text{Matrix Size}}$$

Equation 4 Pixel Size

Isotropic imaging is where all three elements of the voxel in the matrix measure equally as demonstrated in figure 18.

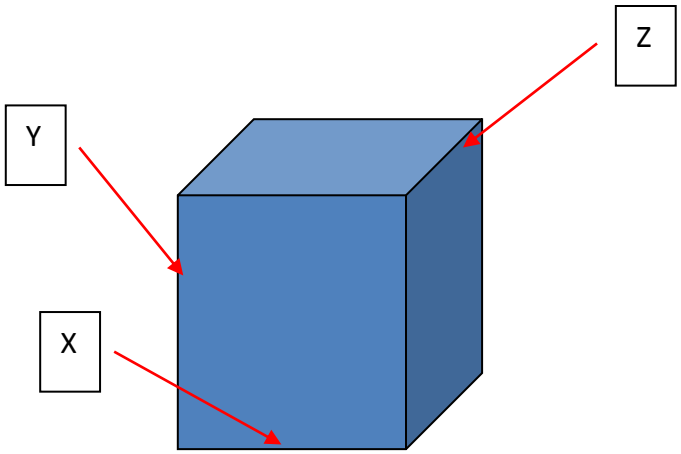

Figure 18 CT Voxel

Anisotropic imaging: slice thickness (z) is larger than the values of x and y in the image.

$$x = y \neq z$$

Isotropic imaging: slice thickness (x) is the same as the values of x and y.

$$x = y = z$$

Equation 5 Isotropic and non-isotropic equations

Pixel size selection has an obvious influence on image quality, mainly in terms of image noise as it relates to the number of photons counted, though the choice of reconstruction algorithm will also influence image quality.

3.1.8 Fixed and Adaptive Matrix Detector Array

The application of fixed matrix and adaptive detector arrays in MDCT units has supported the introduction of isotropic imaging into clinical CT. Using these detectors, the slice thickness which is set in the collimator, may be split or combined by altering the detector array arrangement used during image acquisition. For example, an MDCT acquisition using a 10mm collimated slice

thickness may be processed after scanning into thinner slice thicknesses (i.e. 5mm) by separating the exposures across a number of detectors in the z-axis (e.g. 4 X 0.5mm and 3 X 1mm detectors for an adaptive array or 10 X 0.5mm for a fixed array detector).

Reprocessing is undertaken on the RAW (sinogram space interpolation data) CT data. For the 1mm thick slices performed every 1mm which were used for this study, the central 16 X 0.5mm detector elements were combined to form 8 X 1mm arrays, with an additional 4 elements from left and right of the mid-section forming the other 8 channels of data. Therefore at every rotation of the x-ray tube, 16 effective slices were obtained.

The x-ray collimator also has an important role in MDCT reconstructions, as it controls the effective slice thickness, and hence partial volume artifacts. The collimator does not however control the location of the reconstructed slice (184). The technical aspects under the control of the x-ray tube collimator will be discussed further under the section *slice thickness*.

The detector material used in the Toshiba Aquilion™ is Gd_2O_2S:Pr which has a decay time of 3µsec and uses an emission wavelength of 512nm. The detector is a scintillator and photodiode type and is documented as Figure 19.

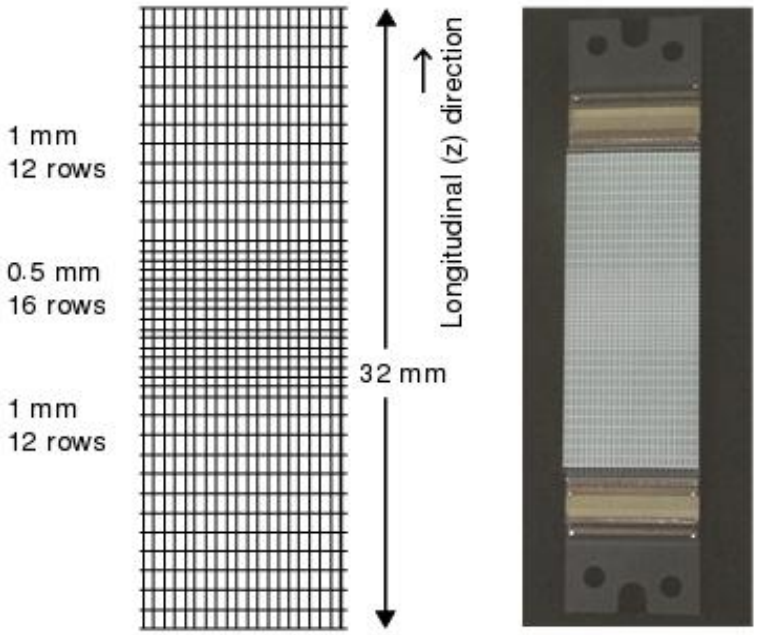

Figure 19 Toshiba Aquilion16™ detector bank (185)

Fixed matrix array. Small detectors may be combined to form larger units, or the greater divided out to form thinner slice widths. Reprinted with permission Toshiba Medical Australia

There are 896 detector elements in total in the Aquiion16 ™ unit, with 40 of those located along the z-axis, creating an effective detector aperture of 0.407mm in the x-y direction at intervals of 0.5mm and 1mm along the z-axis. The dynamic range of the detectors is 20 bits, and for the 500mm FOV used for most of the scan data used, all 896 detector elements were used for the acquisition. The mathematical manipulations involved to manage the production of 16 X 1mm slices of reconstructed axial data at every rotation of the x-ray tube, are extremely complicated.

3.1.9 Partial Volume Effect

The partial volume effect in CT occurs where multiple coefficients of attenuation exist within the one voxel area, and hence the values are averaged for the image display. If for example one tissue produces attenuation intensity I_1 and another tissue located in the same voxel space produces attenuation intensity I_2, then the attenuation intensity of that voxel is $I_1 + I_2$. The CT number however is calculated from the logarithm (ln) of each intensity, and $I_1 + I_2 \neq \ln I_1 + \ln I_2$ and as such the resulting image is quantitatively inaccurate for either tissue type.

The partial volume effect is therefore a consequence of finite spatial resolution. It does not of itself decrease spatial resolution; it is merely a product of a biological material being of a finite size. The partial volume effect does however create uncertainty in measuring the density of a voxel if more than one material is present. For example, a clinical CT voxel (0.5mm at best, but realistically 1-5mm in terms of slice thickness) of bone represents much more than one element of mineralised trabeculae, because of the degree of porosity. In cortical bone however (much smaller pores), a small voxel is more likely to contain the one type of mineralised material assisting in an accurate quantitative assessment. Ageing cortical bone however becomes more porous, thinner and more like trabecular bone with increasing age. The cortex in an elderly woman's hip for example may be significantly less than 0.5mm thick, and hence, ageing cortical bone becomes more difficult to capture in one or even several voxels.

The partial volume effect may be corrected for in some regard by using voxels as small as possible (isotropic imaging), and by using so called correction algorithms in the image reconstruction phase (186), but the use of these algorithms increases dose. The increased dose is required to maintain the signal to noise ratio, as some signal is lost in the image manipulation process.

The general use of "*image enhancement techniques*" clinically acts to increase the aesthetic qualities of the image. The application of these algorithms may however complicate the determination of quantitative derivatives from the CT measurements, which will be explored extensively in chapter six.

3.1.10 Pitch Factor and Slice Thickness

When developing an MDCT scanning protocol, a compromise is usually made between collimation or slice thickness and pitch factor. The objective being to keep the dose as low as reasonably achievable (ALARA), while maintaining an appropriate signal to noise ratio for diagnostic results.

The pitch factor is defined as the distance the table moves through the gantry during one rotation of the x-ray tube, divided by the collimator thickness as shown in equation 6. Collimation and pitch ratio are important in MDCT techniques as they influence the amount of image noise.

$$\text{Pitch Factor} = \frac{\text{Table transport distance (mm)}}{\text{Collimation (mm)}}$$

Equation 6 Definition of CT pitch factor

A scan using slices 10mm thick at 10mm intervals (i.e. contiguous) would usually employ a pitch factor of 1. This simply means that in one rotation of the x-ray tube, the table moves 10mm. At a pitch factor of 1.5, the table in the example above, would move 15mm during one rotation, remembering that the 10mm slices may be interpolated from the volumetric data.

Varying the pitch modulates the dose which effects image quality in terms of the signal to noise ratio. Toshiba, like other manufacturers have several recommended optimised pitch settings for various examinations (185, 187). The selection of pitch factor also has an effect on the life-expectancy of the x-ray tube, especially when scanning the entire body as in the case of the VIFM.

Beam collimation settings and the translocation of the table during one rotation of the x-ray tube, determines the amount of z-axis coverage. The slice reconstruction interval represents the midpoint distance along the z-axis between each sequential transverse reconstruction. If slice thickness and interval are identical, then the acquisition is termed contiguous. For 3D imaging, resolution is enhanced by the acquisition of overlapping slices where the slice interval is 50% smaller than the slice thickness (188) and this is termed an overlapping acquisition (e.g. 1mm slice thickness at 0.5mm slice interval).

The slice reconstruction protocol used at the VIFM is different to clinical protocols, in that while the body is scanned at contiguous 1mm intervals, slice

reconstructions are produced at 2mm thickness every 1.6mm; representing a 20% overlap. Toshiba applications specialists indicate that the TCOT algorithm used on the Aquilion16 requires only 20% overlap for adequate 3D reconstructions (189). The data acquired at the VIFM is used in this way to save on data storage space, which is important when considering that they produce approximately 5000 whole body scans annually.

Nominal slice thickness represents the section thickness set in the collimator. It affects the z-axis resolution, and therefore has a significant effect on image quality. As mentioned earlier, the collimator setting does not necessarily set the slice reconstruction thickness in an MDCT acquisition, and therefore there is the concept of effective slice thickness.

When using MDCT for quantitative CT analysis, it is important to differentiate between nominal and effective slice thickness, especially if using a pitch-factor of more than one. The consequence on image quality from effective slice thickness influences both quantitative and visual-based image analysis.

The term effective slice thickness encompasses the slice-broadening effects of the table speed and z-axis interpolation method (190). Most manufacturers include the effective slice thickness in the header of the scan menu. A general rule is that the effective slice thickness increases by 30% when the pitch factor is doubled. Figure 20 demonstrates the consequence of altering the pitch on effective slice thickness for different interpolation methods.

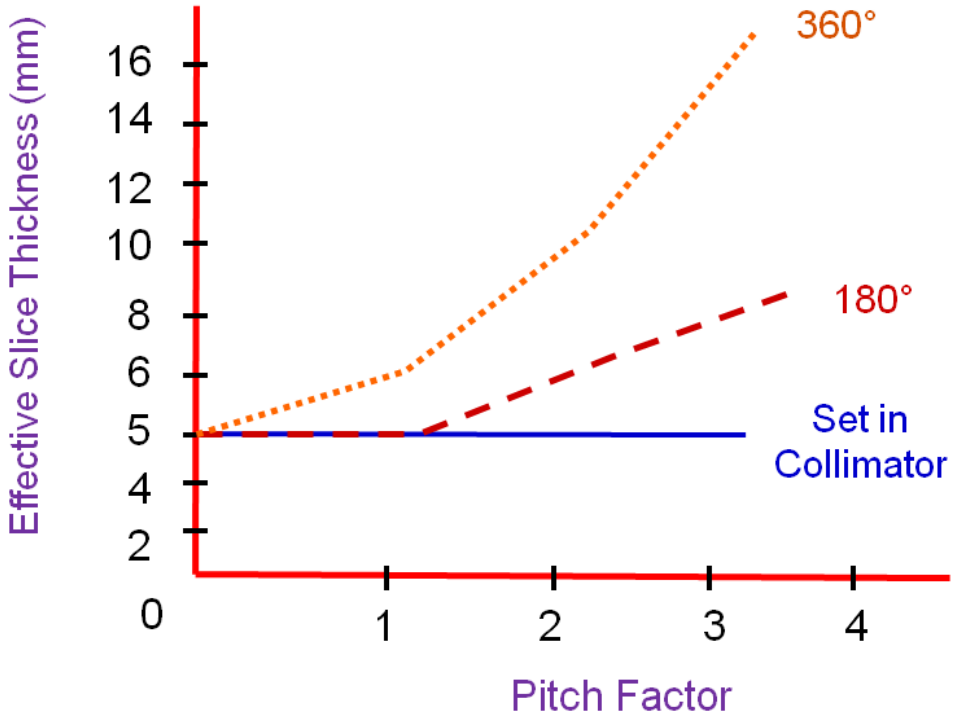

Figure 20 Effective slice thickness

Effect on slice thickness for 180° and 360° linear interpolators, and various pitch settings.

Figure 21 demonstrates the subtle visual effect of effective slice thickness on an axial slice of the brain. The effect is most obvious visually in soft tissue but will affect the image characteristics of bone as well. Both brain scans were performed using a pitch factor of 1, but using a 180° interpolation method has resulted in an image with an effective slice thickness of 5mm, whereas the 360° method has produced an image with the characteristics of a 7mm slice. Note the increased noise using the thinner effective slice thickness.

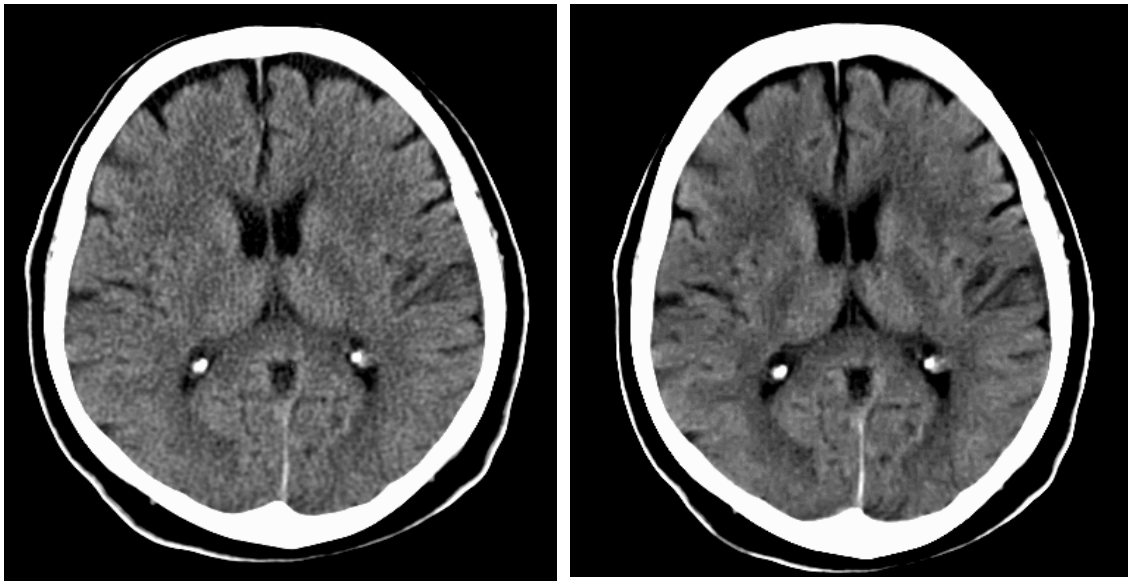

Figure 21 Effective slice thickness image effects

Note the image quality in relation to signal to noise in identical acquisitions other than using different linear interpolators.

VIFM scanning protocols minimise effective slice thickness impacts by using a pitch factor of 1.

3.1.11 Image Artifacts

Other than the partial volume effect previously discussed, a number of other artifacts affect MDCT acquisitions. Broadly, artifacts degrade image quality and have a deleterious effect on the perception of image detail (191). A common artifact encountered during measurement for this study was the beam hardening or streak artifact. Beam hardening is always present when using a spectrum of photon energies as with CT, and is most obvious in the femoral region when there is a hip prosthesis present. Figure 22, documents a number of the hard materials were found when imaging the mortuary specimens.

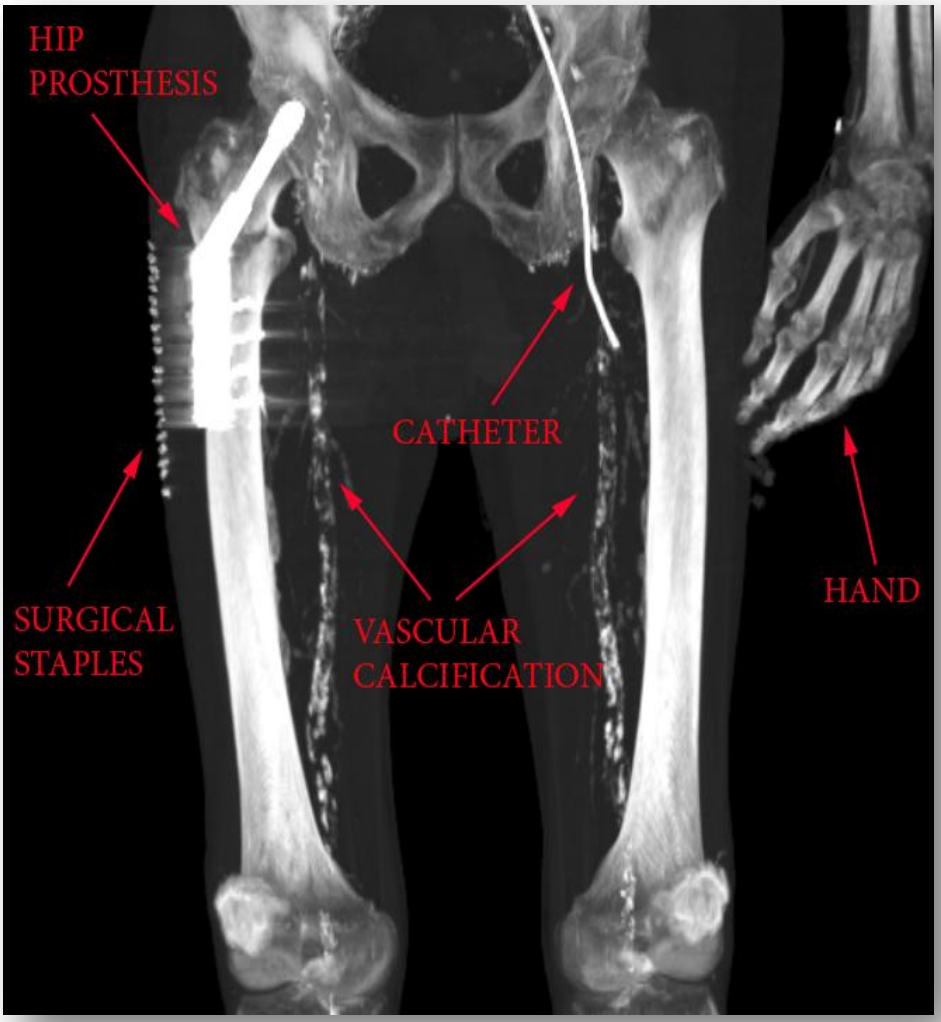

Figure 22 Hard materials found during VIFM imaging

Note the streaking around the right hip pin which has been inserted to support a femoral neck fracture. The iliac, femoral and popliteal vessels are heavily calcified in this 78 year old male.

Another example of artifact encountered during VIFM data collection was seen when the field of view (FOV) used to scan the body was too small to include all body parts. The resultant data clipping (usually of the arms) resulted in an image reconstruction artifact, which either subtly or grossly degraded the image quality around the hip. The data clipping artifact is caused by a loss in projectional data from those areas outside the FOV and was especially significant when the dense long bone of the humerus was involved. Scans exhibiting this effect were usually culled from the data collection, and an example of the gross effect is demonstrated in figure 23.

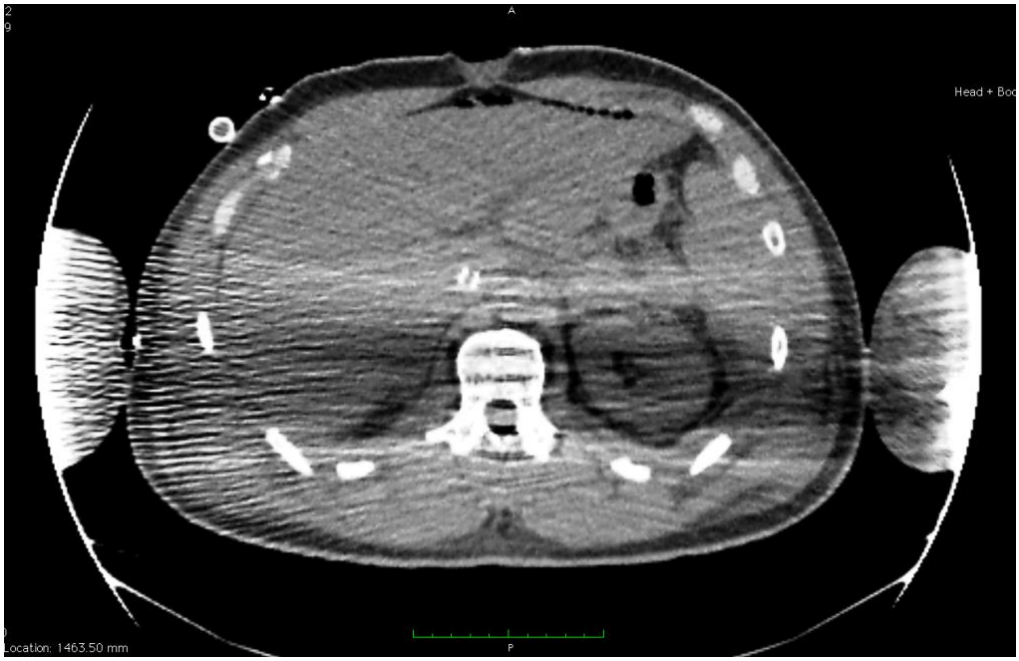

Figure 23 Projectional data clipping artifact

The circular ring on the lateral aspects is the FOV.

3.1.12 Scout Image

For the purposes of this study, the 2D images taken prior to the application of the 3D CT scanning protocol will be referred to as the scout acquisition. Most companies have a proprietary name for these scans which are performed using the x-ray tube and detectors in a fixed 90 degree (AP) or 180 degree (Lateral) configuration while the body is driven through the gantry. Scouts are used to plan the CT acquisition. Figure 24 documents an AP scout image from the VIFM.

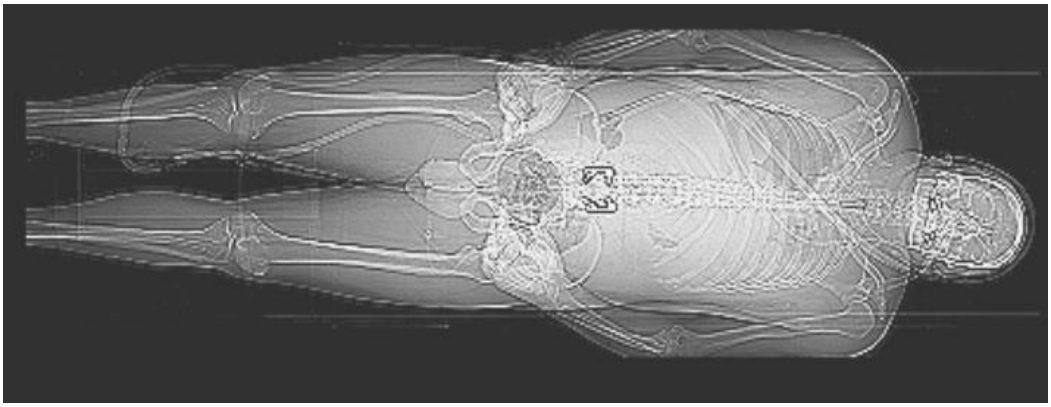

Figure 24 AP scout image of MFC590

3.1.13 Multiplanar Reconstructions (MPR)

One of the major extensions from the introduction of helical CT technology has been the creation of 3D-volumetric applications, improving the utility of CT data (192). MPR's are 3D-displays created using the combined axial slice information. They are produced for visual assessment and are not usually used for quantitative evaluations. The images are useful because the gross alignment of body parts is not always apparent when using an axial scan plane. The reformations of slice data created by MPR manipulations may be displayed in various orientations depending on the requirement. Common presentations are the maximum intensity projection (MIP), volume render (VR), and surface shaded display (SSD) (193); all of which may also be presented as a moving image file, further enhancing usability. The average intensity projection (AIP) reformat may be used in combination with radiological contrast agents. All image manipulations use threshold values of the CT number to enhance image characteristics, and figure 25 documents a femoral tumour from the VIFM scans.

Figure 25 Multi-planar reconstruction (MPR)

The MPR cut away technique has been applied through the distal anterior femoral demonstrating a calcified tumor in the marrow cavity.

3.1.14 Image Segmentation

Segmentation involves the selection of material for image display. Selected structures are either included or withdrawn from the overall image using various methods such as shape recognition or threshold setting. Segmentation is a useful technique to remove objects to provide an unobstructed viewpoint. Figure 26 demonstrates the application of segmentation to the femoral head used by the QCT software described in chapter four.

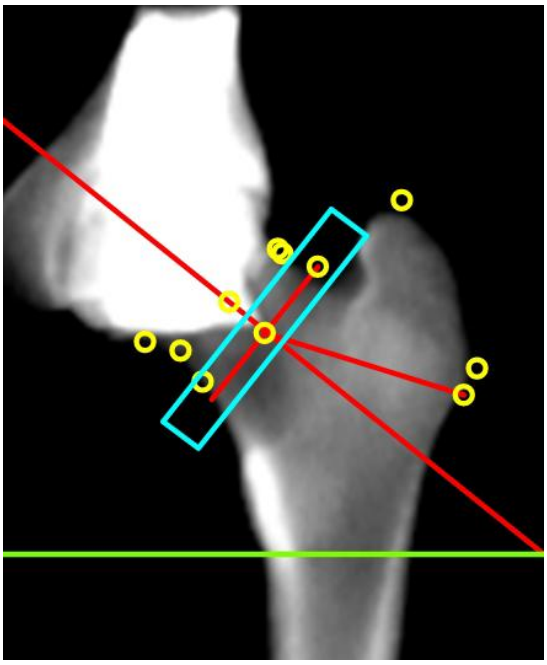

Figure 26 Image segmentation

3.1.15 Toshiba Aquilion16™ MDCT Unit

The CT unit used for this study was the Toshiba Aquilion™ 16 operated by the VIFM. The Aquilion™ 16 is a MDCT unit supporting whole body CT scanning (183). The VIFM MDCT unit is a conventional clinical scanner with no additional features to provide for the increased workload of the unit with respect to serial image reconstruction and tube cooling. The unit is worked at significantly higher intensities, though for shorter periods, than would be expected in the clinical environment. Figure 27 documents the equipment inside the VIFM MDCT room.

Figure 27 VIFM MDCT, heavy lifting apparatus and ceiling suspended x-ray unit

3.1.15 X-ray Exposure Factors

CT scans produced at the VIFM are performed by mortuary technologists who undertake approved training prior to acquiring a limited radiation user licence, valid only in the state of Victoria in Australia.

The x-ray exposure factors and scanning technique are controlled via the application of a protocol loaded into the system by the manufacturer. Alterations to the standard protocol are performed in conjunction with specialist staff at the VIFM when required. The bodies are routinely scanned inside a plastic body bag, to preserve the condition of the CT couch and table. Appropriate tube warm-up procedures are conducted by staff to maximise the lifespan of the x-ray tube and components, and to ensure the safe discharge of the unit generally. A plastic sheet is also used (after warm up) to cover the base of the gantry aperture to prevent any liquid or fine solid products from entering the gantry housing.

A typical representation of exposure factors used for each image acquisition:

Scan type	Helical
Pitch Factor	1.0
Slice thickness	2.0mm
Pixel spacing	0.976mm/0.976mm (averaged)
Typical kVp	120
Typical tube current	180mAs (adjustable)
Typical field of view (FOV)	500mm
Matrix size	512 x 512 pixels
Typical resolution	1.025 pixels per mm (averaged)
Focal spot size	1.6mm x 1.4mm
Kernel	FC01 Body
Patient position	Supine feet first
Number of slices	approx 400 (torso)

The standard VIFM protocol differs from the clinical environment only in relation to the FOV, (larger), and the slice thickness and spacing (thinner and closer). Of course the total body area acquired is also much larger than would be used clinically.

3.2 Part B: Calibration and Performance Estimation

The following is a description of the calibration and performance testing performed. This section is important as the primary focus of clinical CT methods is on assessing the image-based characteristics visually, while much of the thesis evaluates the CT data quantitatively. Comprehensive understandings of the factors that differentiate these aspects of analysis are therefore crucial.

3.2.1 Scanner Performance Analysis

The MDCT unit at the VIFM is maintained under an Australian vendor maintenance and service agreement.

The scanner performance analysis for this study was conducted under the supervision and direction of a registered medical physicist from a local teaching hospital. This person volunteered their services, and facilitated the loan of the calibration and testing phantom used.

A Catphan-600™ (Serial Number 611219) phantom was sourced for testing at the VIFM CT site. The test scans were performed as per the manual in both axial and helical modes (194). The Catphan-600™ unit is a specially designed and engineered series of axial and helical scanning test phantoms embedded in an acrylic housing. The unit is scanned using parameters set by the operator and matched to clinical protocols. The resultant series of slice reconstruction data are then fed into the proprietary software and an analysis for each of the following is provided:

- Alignment of laser guidance system for patient positioning
- Scan slice geometry (slice width)
- Scan incrimination (axial distance feed per tube revolution)
- Circular symmetry (FOV)
- Spatial linearity (pixel size)
- Sensitometry (CT number linearity)
- Line pair resolution
- Modulation Transfer Function (MTF)
- Slice sensitivity profile
- Low contrast resolution
- Image uniformity

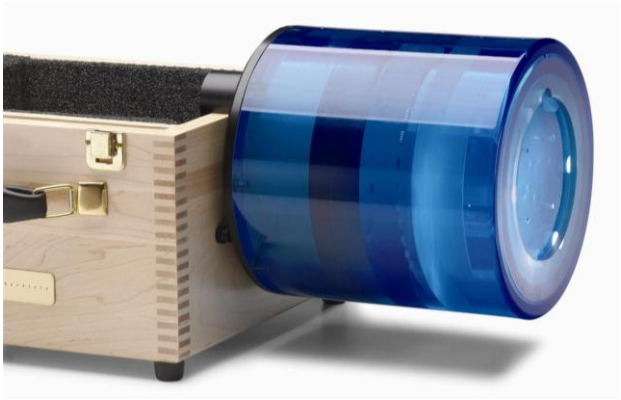

Figure 28 Catphan 600™ testing device

The box suspends the blue phantom in the gantry at the end of the CT table.

Testing was performed on the VIFM MDCT unit and a comparable clinical unit for comparison. This clinical unit was considered as representing the criterion standards against which the study instrument (i.e. the MDCT unit at the VIFM) was being compared. This unit was considered appropriate as it conformed to all Australian standards and is regularly tested for compliance as per Australian Radiation and instrumentation standards (195).

The image quality aspects tested were within the expected ranges both for axial and helical acquisitions for all variables except those related to the reconstruction algorithm and resolution which is discussed in section 3.2.3. A full copy of the results for both MDCT units is included as appendix 3C and 3D. Pertinent testing results are described in the following sections. Figure 29 documents one image-based output obtained using Catphan600™ testing.

The testing procedure was performed only once throughout the 6-month period of data collection, as access to the VIFM MDCT for testing was limited due to the nature of the workflow.

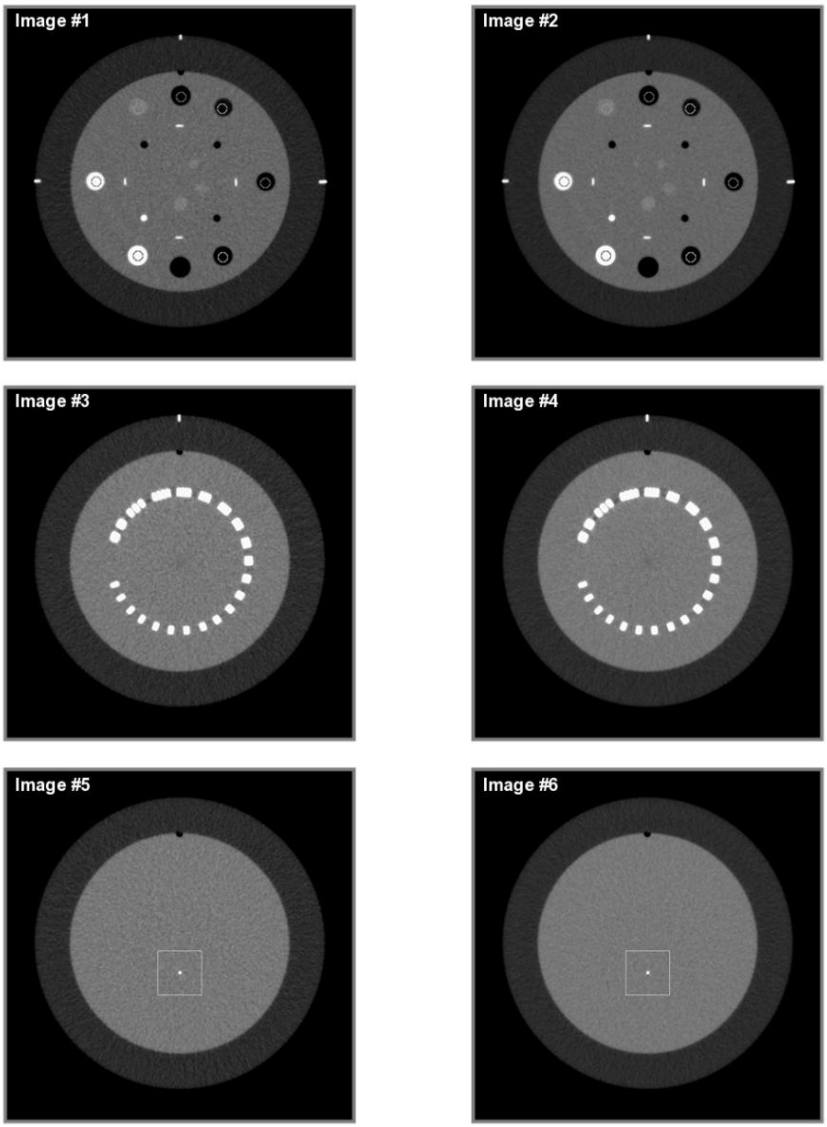

Figure 29 Catphan™ image testing results

Sensitometry (top row), line pair resolution (second row) and slice sensitivity profile (final row). Two scans per test were performed and hence both images were used for analysis.

3.2.2 Noise and Uniformity

Image noise may be broadly described as the standard deviation of voxel values derived from a scan of a homogeneous phantom (most typically water). A more comprehensive evaluation takes into account the scale of parameters available in the scanner (196) but principally the noise in an image will be dependent on factors such as tube voltage, exposure time, tube current, slice thickness, reconstruction algorithm, pitch, focal spot size and detector efficacy.

An example of the effect of noise may be demonstrated via the manipulation of tube current. A doubling of tube current effectively decreases noise by approximately 40%, and halving the same photon flux conversely increases noise by about 40% (197). Figures 30 and 31 present the VIFM unit performance in relation to image noise at two levels of tube current (100 and 200mA) at 5 different spatial locations within the scan area (represented by five x-y coordinates A-E).

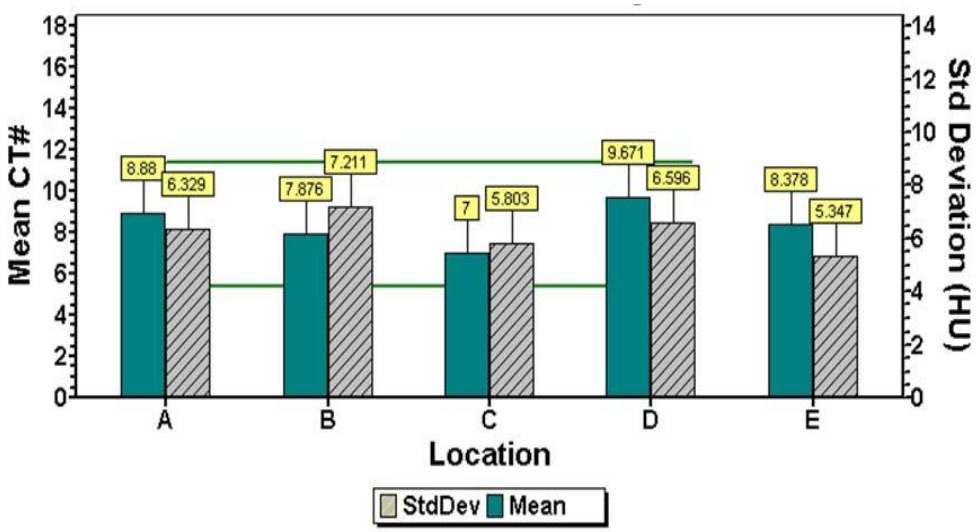

Figure 30 Noise uniformity VIFM unit at 100mA

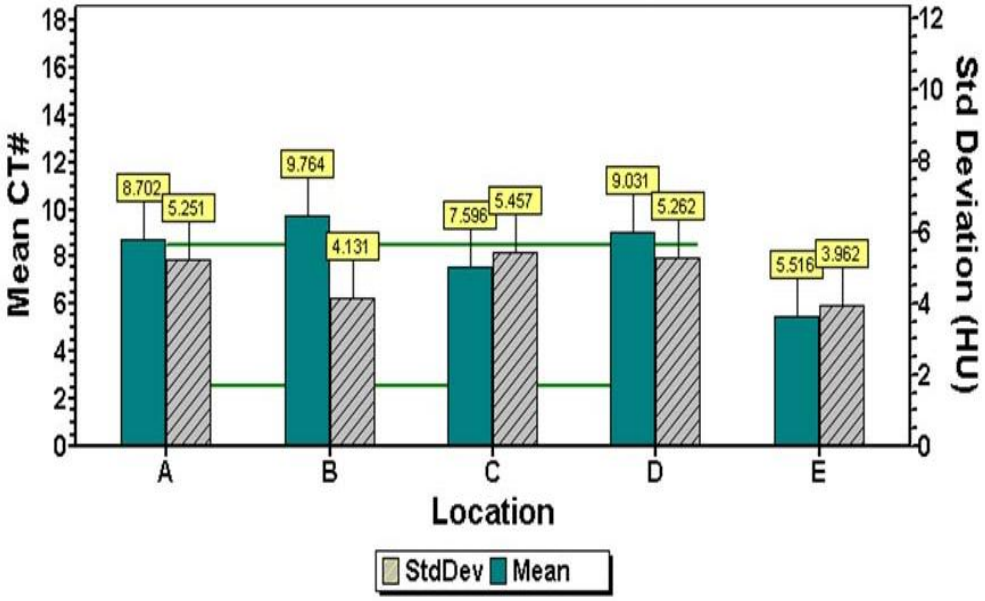

Figure 31 Noise uniformity VIFM unit at 200mA

The variation in noise levels across the FOV demonstrated in these observations could be caused by a number of physical parameters such as detector wear, temperature variation and tube fluctuations. The spatial variations may also be related to the slice reconstruction algorithm applied. The results are however within normal limits.

3.2.3 Resolution

Spatial resolution (also called high contrast resolution) is determined using the modulation transfer function (MTF). MTF is a curve that demonstrates the system's ability to faithfully record information as a function of line pairs per cm (lp/cm) and relative amplitude of the signal received (184). A score of one represents a perfect representation.

The results from the evaluation of MTF on the VIFM unit were unexpected, and therefore the testing process was reproduced on an identical clinical scanner using identical imaging parameters. Figure 32 is the result from a clinical CT unit identical to that of the VIFM scanner. It demonstrates the expected MTF performance using the "body" slice reconstruction algorithm. The green vertical line represents the Nyquist limit of the system.

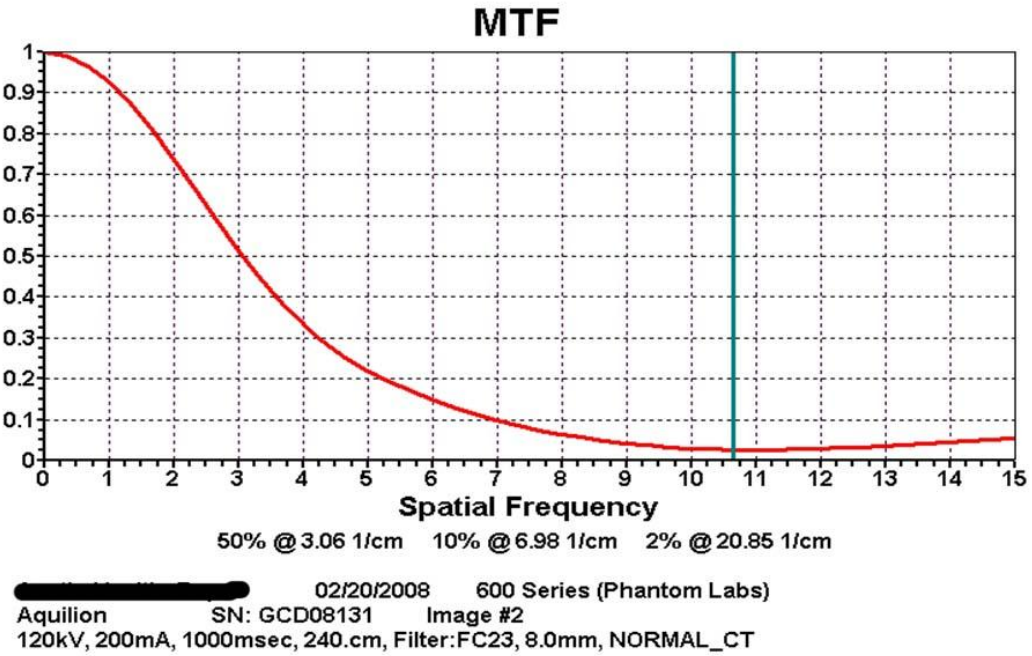

Figure 32 MTF curve from hospital reference data

The shape of the MTF curve is mostly determined by the choice of slice reconstruction algorithm, selected by the operator in a compromise between low contrast object detection and high contrast object detection. A graph such as documented in figure 32 with a shallow gradient terminating at almost 11lp/cm represents a typical readout from a clinical scan condition.

Figure 33 documents the VIFM MTF result. It shows effect of using an algorithm strongly biased towards low contrast resolution rather than spatial resolution.

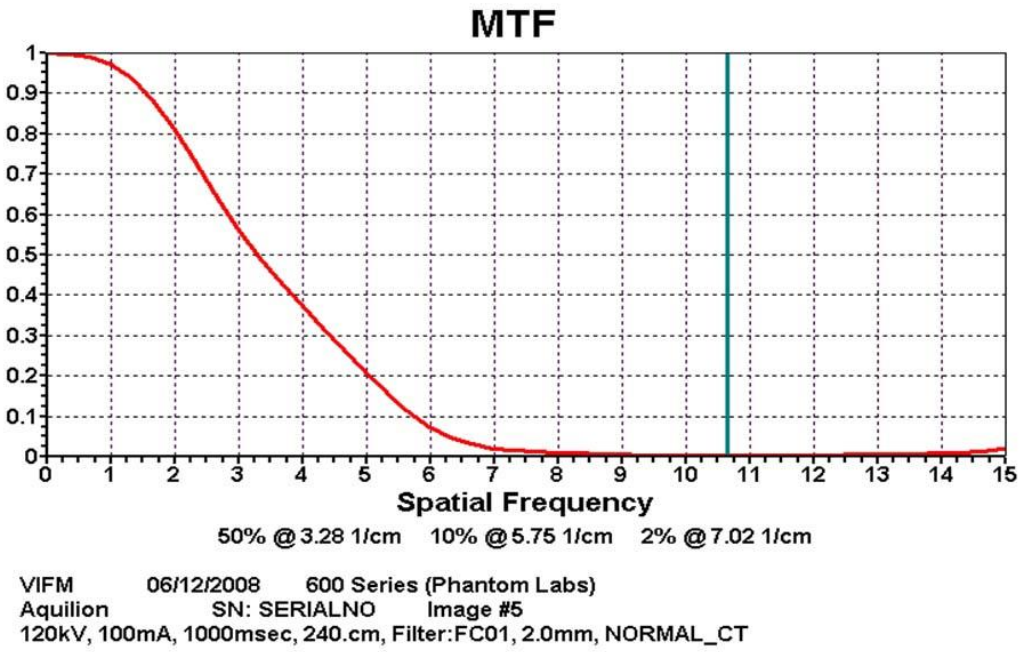

Figure 33 MTF curve from VIFM QA testing

Note the extreme drop-off of the signal which reaches baseline at a spatial frequency of 7. It was not possible to alter the algorithm used for image reconstructions, and further discussion is made in the recommendations for research using a mortuary-based MDCT in chapter 8.

Low contrast resolution is a measure of a systems ability to differentiate between objects of similar attenuation characteristics. Typically CT systems are evaluated at varied spacing's (mm) and contrast levels (% variation). Results are a function of how the reconstruction algorithm deals with issues of object size, object contrast characteristics from background levels, and system noise (184).

Low contrast resolution performance at the VIFM was slightly superior to that generated from the hospital testing, again reflecting the choice of slice reconstruction algorithm by the VIFM to preferentially detect low contrast attenuation differences. The results from the VIFM analysis of low contrast resolution are included as Figure 34.

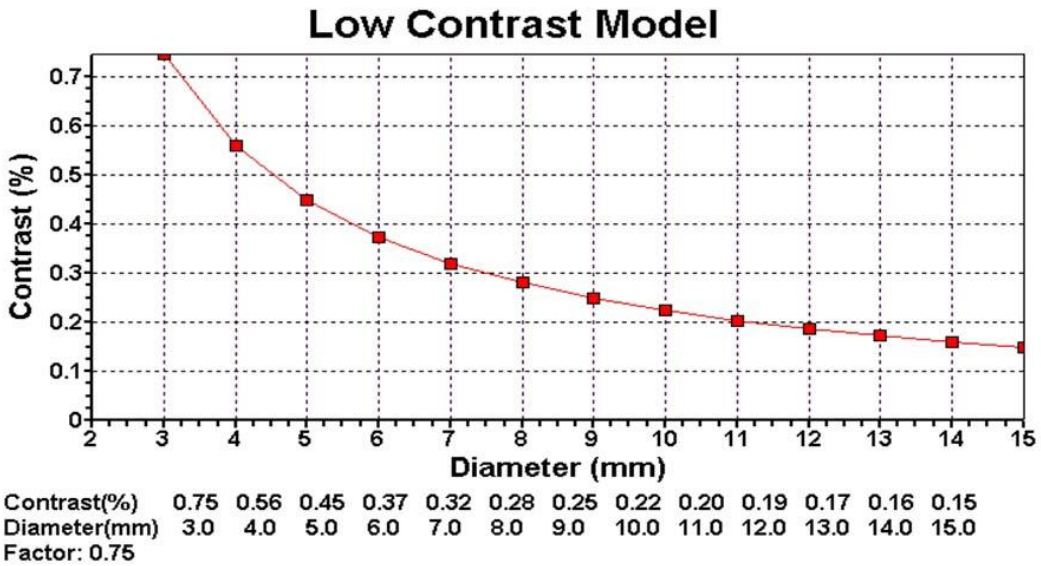

Figure 34 Low contrast resolution object detection for VIFM

The combined low contrast and MTF testing results suggest the implementation by the VIFM of a scanning protocol targeted primarily at the differentiation of soft-tissue. This would seem an obvious choice when presented with the challenge of identifying subtle post mortem variations.

While there are a number of commercial manufacturers of CT equipment, there is very little testing information available for the various interpolation algorithms (198), which would assist to better quantify any effect other than visible changes to the image. An example of the trade-off in signal to noise ratio from the application of the various commercial algorithms is documented figure 35. The lack of proprietary information, as well as an inability to review existing raw MDCT data with alternate algorithms has therefore limited the scope of this study.

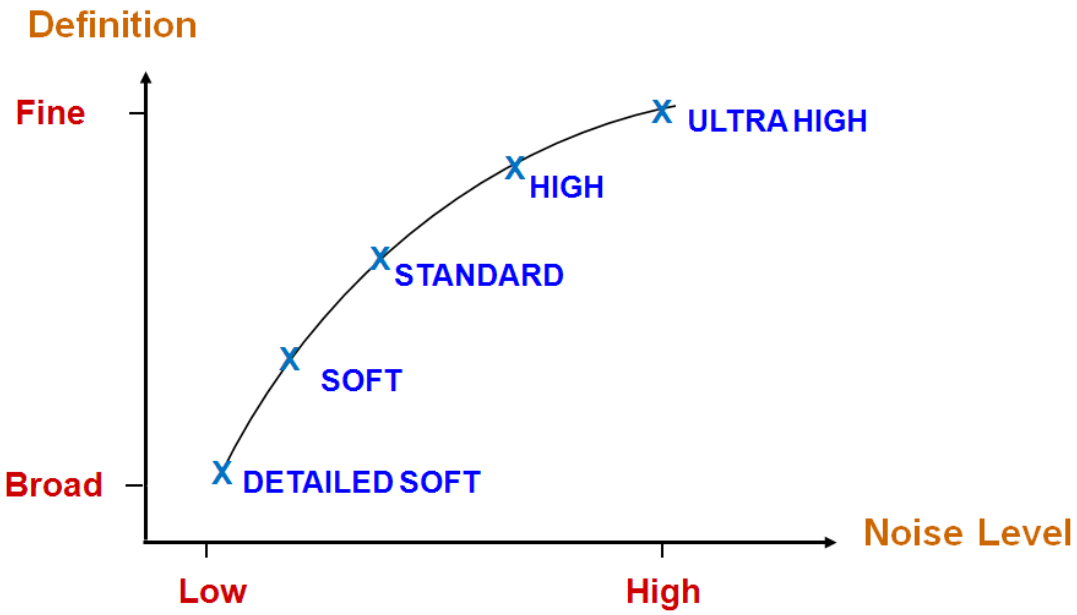

Figure 35 Image definition v image noise

Image definition and noise characteristics using various CT algorithms

3.2.4 *Sensitometry*

Sensitometry refers to the performance of the CT scanner in relation to CT number linearity. It records the relationship between the CT numbers and the underlying linear attenuation coefficients of various materials (199). The test therefore represents the so called “trueness” of the CT number in relation to the material under investigation. Figure 36 represents the results from the analysis of the VIFM unit in relation to sensitometry. It demonstrates adequate registration of the biological equivalent materials, as can be seen in the relationship of actual readings (red dots) to the expected results (green line).

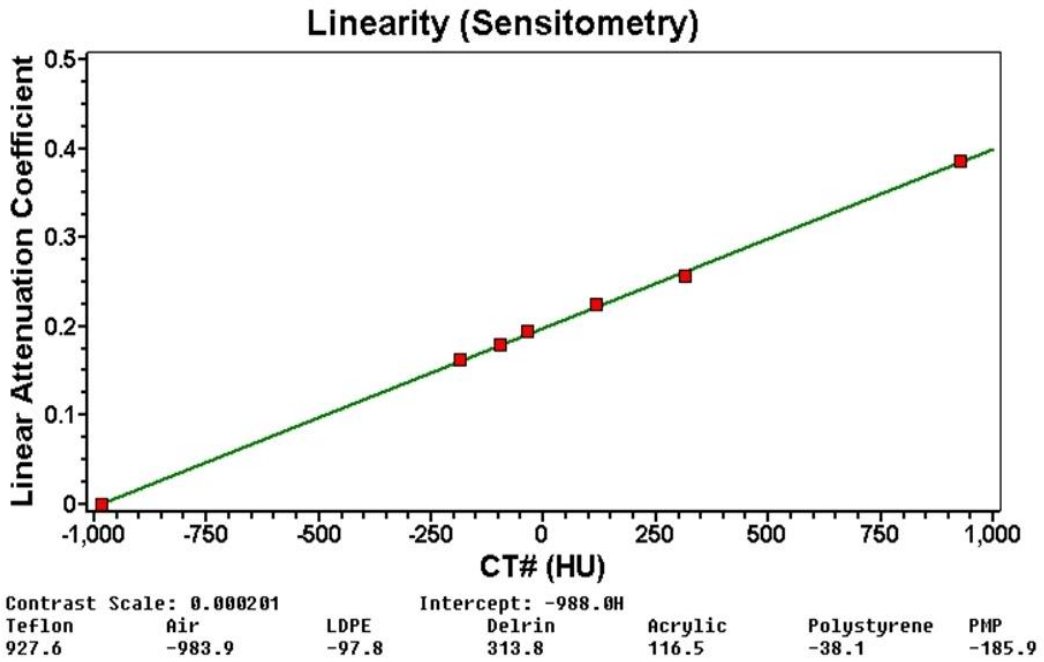

Figure 36 Sensitometry result from the VIFM QA series

Results are presented in Hounsfield units V linear attenuation co-efficient.

Commercial units employ a range of beam-shaping and filtration methods which will all impact on the results from the sensitometry evaluation. The exact relationship between the CT number and attenuation coefficient is also complicated by the fact that the CT system delivers a polychromatic spectrum of x-ray energies.

3.2.5 Window Width and Level

Window manipulation in CT involves the control of the window width (WW), (number of grey scales [Hounsfield units] in the display), and the window level (WL), (central point on which those grey scales are applied). Applying different window width and level does not require that the data be reprocessed, though, as described previously, using alternative algorithms can often be a powerful tool in the production of CT images (191). Figure 37 illustrates window width and level application in the pelvis.

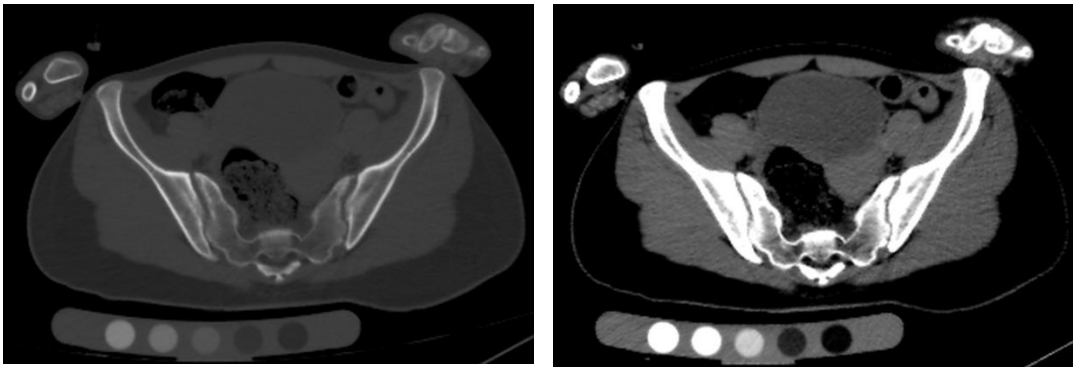

WW 1500 WL 300 WW 350 WL 45

Figure 37 Bone and soft-tissue windowing

Note the definition of the soft-tissue structures using a narrow width and a level close to zero. The housed solid rods in the image are the bone calibration phantom.

3.2.6 kV (tube voltage) and mA (tube current)

Kilo-voltage (kV) and milli-amperage (mA) may be managed by the CT operator. kV determines photon energy, while mA controls the amount of photons or flux available (197). The kV setting for the acquisitions in this study was fixed at 120kV. The mA was varied via an automated exposure control (AEC) system to optimise detector output, and delivered within a range of between 100-200mA. The selection of both tube current and voltage impacts on the ionising radiation dose delivered.

The selection of tube current and voltage have an effect on the image quality by virtue of their influence on the noise the characteristics of the image. Figure 38 represents two cross-sectional images of the abdomen at the level of the liver and spleen. Note the increased noise in the image created using a low tube current. The liver lesions (blackened regions) are evident, but may be seen with more clarity when imaged using a higher tube current. This is an important feature in the discussion about CT technology as much emphasis is placed by the clinician on how the image looks in terms of its diagnostic value.

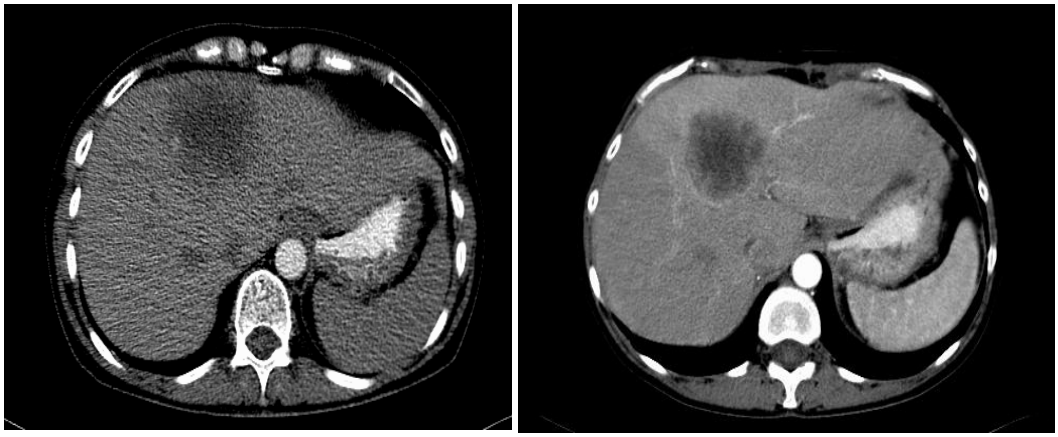

25 mAs 200 mAs

Figure 38 Effect of mAs on image signal to noise

Note the 200mA image is also enhanced by the introduction of intra-venous (IV) contrast.

3.2.7 CT and Radiation Dose

Like every other organism on earth, humans are exposed to some degree of ionising radiation from normal background sources. Additional sources of radiation may also be delivered through air travel and through radiological imaging procedures like DXA and CT. The following section describes units of dose used in CT.

The ionising radiation dose delivered using CT are higher than conventional and fluoroscopic radiological examinations, yet the widespread clinical use of CT continues to grow (200). Although the radiation burden is not a primary concern for individuals from which data was collected for this research, the implications this research has for clinical outcomes make a consideration of dose important.

As previously mentioned in chapter 2, absorbed dose is measured using the unit Gray (Gy), which corresponds to the equivalent of one joule of energy deposited into one kilogram of biological material. The lethal dose for 50% of subjects (LD_{50}) for ionising radiation delivered over one or two months for a human is between 3-5 Gy. Because radiation interacts differently depending on the type of radiation being delivered, an additional unit known as the Sievert (Sv) is used to describe the effective dose (E). The Sv provides a determinate of the absorbed

dose multiplied by the effectiveness factor of the type of radiation delivered. The effective dose is therefore an expression of dose that reflects the biological sensitivity of the tissue being irradiated (148).

The effective dose unit is applied to dose distributions which are not homogeneous; which describes all CT examinations. The unit is designed to provide an overall risk of *potential harm* caused by the radiation. It provides a estimate of comparative risk between differing CT protocols, but cannot be said to provide a *"true"* risk. Organ specific effective dose is preferred for the establishment of *"true"* risk for CT procedures (201). Dose assessments performed using Monte Carlo simulation and thermo-luminescent dosimetry (TLD) measurements have demonstrated differences of up to 100% (skin dose) for effective doses delivered using a 16 slice helical CT scanner (202).

As previously mentioned, the ALARA principle directs the use of radiation for diagnostic irradiation. The computed tomography dose index (CTDI) is the primary tool for assessing dose in CT. The CTDI represents the average absorbed dose along the z-axis measured in one axial rotation of the x-ray tube (203).

$$CTDI = \frac{1}{NT} \int_{-\infty}^{\infty} D\ z\ dz$$

Equation 7 CTDI

D(z) = radiation dose along the z-axis
N = number of tomographic sections or data channels used
T = width of tomographic section along the z-axis by one channel (*MDCT units often couple detector element to form one channel, but on single row detectors T is the nominal slice thickness)

The CTDI may also be expressed as term referring to the accumulated dose at the centre of a 100mm scan ($CTDI_{100}$), a weighted variation across a field of view ($CTDI_W$) or as a volumetric expression of a series of scans used in a protocol ($CTDI_{VOL}$) (142). The dose length product (DLP) provides an overall perspective of the energy delivered by a given protocol along the length of the scan, taking into account the absorbed dose (203).

The primary methods of controlling radiation dose in CT are through beam filtration, beam collimation, mA modulation through automatic exposure control (AEC), detector array efficiencies and avoiding noise reduction algorithms (142).

3.2.8 Bone Calibration Phantom

The intensity or brightness of an x-ray image is known to have a relationship to the physical properties of the material under investigation. X-ray attenuation is predominantly affected by the atomic number and electron density of the material. The linear x-ray attenuation coefficient (μ) of a voxel is calibrated from the $\mu Water$ which is derived from the linear x-ray attenuation coefficient of distilled water at room temperature (204).

CT density is expressed in Hounsfield units (HU) or as the CT number. Water is ascribed a CT number of 0HU and air -1000HU.

$$\text{CT Number} = \frac{\mu - \mu Water}{\mu Water} . 1000\ in\ HU$$

Equation 8 CT number

Where μ = attenuation coefficient of the material under investigation and μWater is the attenuation co-efficient for water.

The densities for volumetric bone mineral density (g/cm^3) are calculated by comparing the measured HU of the bone, and comparing that to the known densities of a bone calibration phantom (205). The density values obtained provide an *apparent* bone density estimate. The reason it is expressed as an *apparent* density is that voids within the bone tissue are averaged along with the mineralised bone in any given voxel. The non-uniform nature of bone, along with the finite size of the voxel combines to confound an absolute or true assessment. One of the primary limitations in using CT as a tool for investigating bone is that morphometric analysis is limited to an order of 0.3 – 1.0mm resolution, when the mineralised bone structure is many orders of magnitude smaller.

Liquid calibration phantoms composed of dipotassium hydrogen phosphate (K_2HPO_4) were initially used for clinical CT-based BMD analysis, but were found to unstable in solution long-term, and are now are only used in some micro-CT bone studies (206). Solid calcium hydroxyapatite (CaHAP) equivalent phantoms such as the Mindways™ product used in this study are commonly used to generate data for comparison with published reference ranges (207).

Figure 39 provides the density values for each of the 5 calibration rods of the Mindways™ phantom, and an equivalent density table for water and K_2HPO_4 for the specified phantom.

Rod	Water Equivalent Density (ρ_{Water}, mg/cc)	K_2HPO_4 Equivalent Density (ρ_{K2HPO4}, mg/cc)
A	1012.25 ± 2.27	-51.83 ± 0.12
B	1056.95 ± 1.94	-53.40 ± 0.10
C	1103.57 ± 1.69	58.88 ± 0.09
D	1119.52 ± 1.82	157.05 ± 0.26
E	923.20 ± 2.12	375.83 ± 0.86

Figure 39 Mindways™ bone calibration density data sheet

The rods are configured down the z-axis of the phantom and are positioned relative to the patient as demonstrated in the figure 40. Note that in this example, the analysis software has locked onto the rod location (green rectangle and circles) and is now waiting for the operator to positions the calculation field (green box) for analysis.

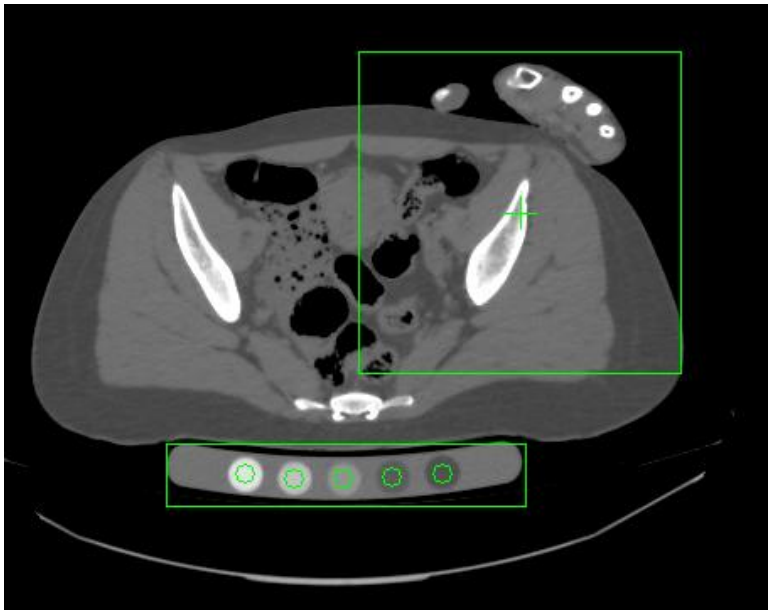

Figure 40 Mindways™ bone calibration phantom position

Each commercial bone calibration phantom and associated QA phantom has a tracking code requiring entry at the time of the first analysis. The testing procedure provides data from which a calibration slope is calculated and entered into the evaluation program. It is from these data that the baseline quantitative analysis of the individual patient occurs. A comprehensive discussion of the Mindways application occurs in chapter 4.

3.3 Part C: CT Data Collection Materials and Methods

The novel imaging and analysis methods documented are based with two separate but parallel considerations. The first consideration is for the living, and these discussions are based in age-related differences by considering variations of morphology, which may be associated with fracture risk. Necessarily for the living, aspects of potential harm related to ionising radiation burden are also included. The second consideration is that of the deceased. For the dead the consideration is presented as an examination of age-related 3D morphology relating to biological-identity and anthropological aspects or history. These two considerations are very much an intimate partner of one another in studying ageing, though their novel combination for the purposes of this thesis was not without challenge.

The software used to perform the bone mineral assessments was sourced from clinical medicine, and using it with human remains in various body orientations required a non-standard application of the analysis technique. The following is a detailed discussion explaining the ways in which the various obstacles of this work were tackled. The author has significant experience using MDCT units clinically, and is registered with the Medical Radiation Practitioner's Board (MRPB) in Victoria. She also holds a license to use diagnostic x-ray equipment from the Department of Human Services (DHS) in Victoria Australia.

Fluoroscopic and conventional radiographic techniques are well established for the routine examination of the deceased, and are used to assist in determining the cause of death (COD) (208). CT techniques are also used for identification, localisation of foreign materials such as bullet fragment, and localisation of gaseous trapping. CT anatomy of the deceased is different from that of a live person predominantly in terms of the soft-tissue presentation. The changes that occur in the soft tissues commence shortly after death, and while appearing grossly abnormal in life, are recognised as representative of the normal patterns of decomposition in death (208).

3.3.1 Ethics and Project Approval

Two separate ethics applications; one prospective (EC9/2007) and one retrospective (EC10/2007) were made to the VIFM in relation to CT data retrieval. Ethics approvals for the collection of bone under the Melbourne Femur Collection (MFC) research had been obtained previously (EC26/2000, HREC 980139), and these approvals were linked for this project. The author was added to the ethics approval for the previously acquired permissions at the commencement of enrolment. Copies of the ethics approval documents are listed as appendix 3A and 3B.

Retrospective ethics permission was sought to obtain the CT reconstructed slices from the 17 MFC specimens used in the experiments of chapter 6. The MFC is an extensive assemblage of human proximal femora acquired with permission at

the time of death. The specimens come from those who have died from causes unrelated to the femora. The bones have been acquired under ethics approval from the VIFM, which also provided plain film or digital x-rays with the bone tissue. A Toshiba Aquilion 16™ unit was installed at the VIFM in May of 2005 at the VIFM (208), and since the installation, full-body high-resolution CT scans are performed on each admission. The 17 MFC specimens had full-body CT files from 2006, which were located by VIFM Information Technology (IT) staff on their picture archive and communication system (PACS), transferred to the Vitrea™ workstation, and then downloaded to disc. These 17 cases were chosen as the only MFC specimen samples that could be identified as having had a CT scan upon their admission to the VIFM. The scans were performed without the bone calibration phantom.

The prospective ethics application requested permission for the insertion of a bone equivalent calibration phantom underneath the mattress of the CT couch, and the subsequent downloading of all appropriate lower limb CT files. One of the conditions of ethics approval was that no alteration be made to ongoing CT scanning protocols used routinely for the conduct of the VIFM CT virtual autopsy. This requirement was made on the basis that no interference may be made to the routine collection of coronial evidence. It was also agreed that the installation of the bone equivalent calibration phantom would not interfere with the usage of the CT scans for the forensic examination, and that the installation meant no additional workload for the mortuary staff. Relevant discussions were conducted after installation to ensure compliance.

3.3.2 CT Imaging of the Femora

CT evaluations of the femora are used clinically, predominantly for the differentiation of borderline pathological assessments (209). Conventional x-ray imaging is the study of choice for the initial evaluation of hip fracture. CT, MRI and nuclear medicine bone scans are useful in cases where the fracture is complicated, or difficult to differentiate from other disease processes. DXA

technology is routinely used for bone mineral evaluation of the hip for osteoporosis diagnosis.

To visualise the femoral neck in the living, a specific orientation of the leg is employed to ensure that the projected image does not foreshorten the femoral neck. This positioning requires that the lower limbs be rotated medially approximately 30 degrees (210), and is often described as the *"Charlie Chaplin"* view. The position is achieved on the supine patient by rotating both lower limbs inward with the ankles slightly apart and the great toes touching. This lower limb orientation is used clinically for all investigations of the hip and pelvis, whether plain film or CT. The positioning cannot always be implemented when imaging a patient with a fracture however.

In the case of the VIFM CT scans used for this study, no effort was made to position the lower limbs, and indeed the bodies are not usually *positioned* in any radiologically recognised way. This aspect of image quality, though necessary, did become increasingly important as a study design shortcoming when using the QCT software, and limited the ability to analyze some of the CT data.

3.3.3 MDCT Scanning at the VIFM

The imaging methods and protocols used at the VIFM placed significant constraint on data acquisition. The Mindways™ QCT software is designed for use with the living in a particularly standardised way with at least some compliance from the patient in achieving an appropriate body position. Using scanned data from the dead was always going to be problematic. The following section is an account of those workings. It is provided in an effort to bring some understanding to the nature of the choices made in the conduct of this study in relation to the data. A comprehensive table of the issues and resolutions undertaken in using these data may be found in appendix 3E.

The MDCT unit at the VIFM is currently one of only 5-7 (units in Brisbane and Kuala Lumpur are currently in advanced stages of installation) units co-located in

civilian mortuaries around the world. The VIFM is run by the Victorian state government, and performs approximately 4700 full-body CT examinations per annum (211). Not all deceased persons can be imaged however. Size, weight, body condition and postural limitations exist when imaging the dead, as well as when imaging the living.

Bodies are scanned supine on the CT couch in a feet first (FF) orientation, without the normal clinical headrest. The headrest contains metallic elements that would obscure the lower cervical spine if used. The FF orientation allows the use of a heavy-duty lifting unit, and maximises the scan length possible (i.e. 1800mm). The body is scanned without any adjustment to position. Most bodies presented with a partial flexion of one hip (usually the right), representing an equivalent position of someone lying comfortably supine in bed.

Scanning is routinely undertaken with the body in a bag or plastic sheath. For reasons of coronial integrity of evidence, all scanning is undertaken without the removal of metallic or other clinically placed objects such as catheters. If required, a later additional scan is performed with these objects removed, and both datasets are archived together. Separate body parts or comingled remains are scanned only after careful arrangement on the CT couch by appropriately trained staff.

CT scans performed routinely at the VIFM involve three separate components:

1. *Full-body scout in both antero-posterior (AP) and lateral views for planning of the two helical acquisitions.*
2. *0.5mm contiguous helical acquisition of the head and neck, which are then converted to 1mm at 0.6 overlapping slices using both a soft-tissue and bone algorithm for archival and forensic evaluation on the workstations of the Institute. These scans were not applicable to this study.*
3. *1mm contiguous helical acquisition of the full torso including lower limbs, which are then converted to 2mm at 1.6mm overlapping slices on a body soft-tissue algorithm for archival and forensic evaluation on the workstations.*

Approximately 2000 individual DICOM files are produced for each body scanned, with approximately 900 produced from the torso and limb acquisition. Each case generates approximately 1.2GB of DICOM data, with around 700MB being from the torso and lower limb.

3.3.4 Case Selection

The primary objective of this study was to describe the morphology and QCT characteristics of the femur and to compare morphology of the proximal femora bilaterally. Broadly, femurs that displayed signs of pathology or trauma unrelated to a normal or expected pattern of ageing were not included in the study. Images where gross distortions due to positioning or artifact effects were evident were also excluded from the study. Cases where homicide was the cause of death, or where some other ethical reason was identified (i.e. involved a person well known to the public) were also excluded from the study.

Whilst it was important to ensure that the entire femur was included in the scan FOV for the anthropological evaluation, the QCT analysis required a more stringent evaluation in terms of what cases could be included for analysis. A full outline of the problems encountered in using mortuary-based data placed into a clinically-based software package is explained in detail in chapter 4. Generally, errors from body placement outside the centre of the FOV (i.e. data clipping), hands placed over the hips (especially in the very slim) and gross external rotation of the lower limb were by far the most common reasons for assessing the scans as unsuitable for QCT analysis. The paucity of female numbers, especially in the younger age groups was also a hurdle in gaining enough data to present statistically significant findings.

The data collection protocol involved first checking that the case was permitted to be downloaded with consideration of both the ethics approval and any legal impediment. As mentioned previously, cases where there was a note of likely homicide, death in custody or where a high level of media interest was likely. Identification of these cases was done with the assistance of mortuary staff.

The initial aim was to collect approximately 20 of each sex in each decade cohort, and to include age-related fracture cases where possible, for a further 20 in each. It quickly became apparent that obtaining these numbers for the females in all but the oldest group was going to be challenging.

The first group to fill the required 20 cases was the males 21 – 30 years, followed by the males 51 – 60 years. Of the females the 71 – 80 years and 31 – 40 years were the fastest filling. Cases under 20 years of age were not collected until later in the collection period when it was noticed that full fusion of the epiphysial plates of the femur was evident radiologically in those in late puberty. Full information relating to the age ranges used and numbers in each category may be found in chapters four and five.

3.3.5 Personal Details & Anonymity

Anonymity provided a limitation. The lack of knowledge regarding ethnicity may be a confounding factor in the measurement of specific anthropological features especially as one may logically assume a predominantly white population in this type of study (212). Background information on socioeconomic status would also been of use in determining overall risk factors present in the group (213). The lack of patient specific background information such as the use of bisphosphonates and/or hormone-based therapy, and nutritional and exercise routines are also a recognised limitation in directly comparing individuals within each of the archetypes.

3.3.6 Data Downloads

CT datasets from 337 individuals covering the superior pelvic border to the inferior lower limb (depending on how tall the subject was, the feet may not have been included in the scan), were downloaded from the VIFM principally over the period 13/12/2007 to 16/06/2008.

- 17 of those 337 were the retrospective downloads matching the **MFC** femoral specimens. No bone calibration phantom was used in scanning these

cases which were performed on the same MDCT unit as were the other cases. The QA slope and intercept values obtained were applied to these 17 cases as with all others to obtain QCT results.

- 272 cases represent ***normal*** (i.e. fulfilling the selection criteria) bilateral examinations, deemed not to be exhibiting signs of bone-related pathology or trauma unrelated to ageing.
- 14 cases represent recent unilateral femoral neck **fractures** used in the observational work of chapter six.
- 19 cases remain unused as they were later found to contain either image **artifact**, bone pathology, or had one hip that was unable to be evaluated using the QCT program, usually due to extreme rotation.
- 15 cases of unilateral **prosthesis** or fracture pinning have also not been used as originally planned, as artifact from the beam hardening effect caused by the prosthesis prevented a QCT analysis of the contra lateral hip as planned.

Figure 41 describes the collection of the MDCT data. The use of the QCT software was not applied until midway into the data collection period. As the candidates processing skills were enhanced by practice and DICOM trim and editing was employed, more of the problematic presentations (i.e. hands over the pelvis and significant external rotation), were able to be evaluated. The cases that failed QCT were re-attempted at least 5 times over the course of the evaluation period. Only data clipping effected cases where not re-attempted because these were recognised as likely producing erroneous quantitative readings.

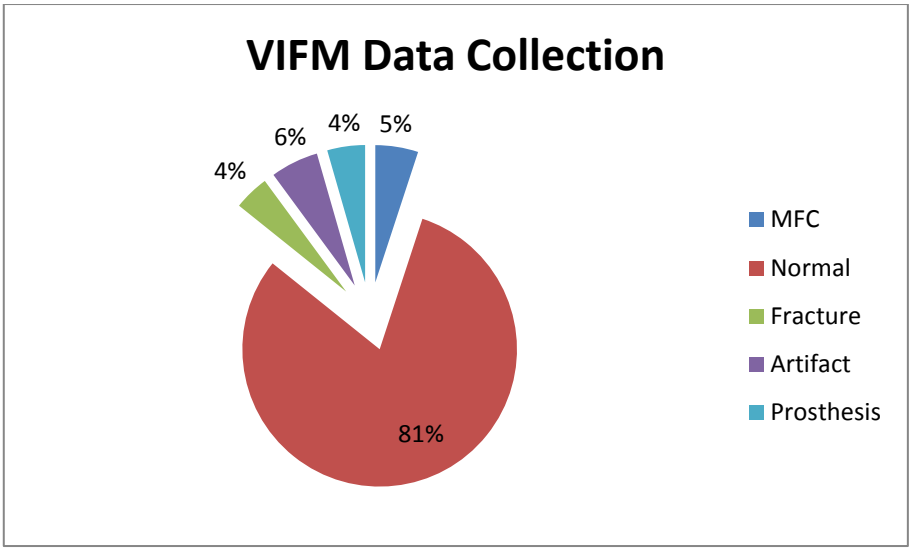

Figure 41 VIFM Data Downloads by type

Of the 289 *normal* bilateral examinations which have been used for the reference study, both female (n = 134) and male (n = 155) datasets were collected, with an age-range of 15-95 years. The weight of each individual was available at download. The height data was collected manually as a batch with the assistance of VIFM staff at the completion of the download period.

3.3.7 Data Management and Storage

Data was collected directly from the VIFM server approximately twice a week to ensure access to a suitable breadth of cases. Rewritable CDs were used to download individual cases as initial experience using other forms of media such as a USB drive and DVD resulted in the random loss of data due to overwriting. Advantageously, the *one-case-one-media* system conveniently provided a checking point to ensure that the anonymous data related to a specific notebook entry.

CT files are routinely transferred at the VIFM from the scanning unit to the Picture Archive Communication System (PACS) via a Vitrea™ Workstation arrangement, with the primary scanning system only able to hold cases for up to three days. Older data were able to be retrieved from the PACS, though it was

very slow and restricted any access to the system by the pathologists while retrieving the files, and so was rarely used.

Files were converted from proprietary Toshiba™ format to Digital Imaging and Communications in Medicine (DICOM) standard, anonymised, and then downloaded to CD. The process of creating an anonymous DICOM header for all data files was essential in ensuring compliance with the ethics approval. A download of each individual case took 15-30 minutes depending on network traffic.

Disc data was then transferred to a PC which was then backed up to a 1TB network attached storage (NAS) device as data volume was large, and both PC and Mac operating systems were deployed for this study. The NAS was RAID (redundant array of independent discs) configured to further ensure against unexpected loss of data.

Data were initially tabulated using Microsoft™ Excel Office 2007, and download identification entries with physical measurements were made on the day the data were downloaded. QCT and anthropological data was later entered into this spread sheet as the measurements were completed. The Excel spread sheet was converted into to an SPSS™ 17 file for statistical evaluation.

3.3.8 Limitations Overview

While every effort was made to minimise and control sources of error, there remain factors that almost certainly contributed negatively to the results obtained. The fact many of the measurements and differences found were on average smaller than the slice thickness (i.e. 1mm scanned and 2mm reconstructed) or resolution is one such example. The population used as the source of these findings is also acknowledged as a source of potential bias in terms of their representation of the Australian urban population generally.

The sample selection and sampling framework used to acquire these data has an acknowledged aspect of bias. Though regionally well grouped (all from the state of Victoria and predominantly from the greater Melbourne metropolitan area) the sample contains a large number of those who have died unexpectedly from suicide and accident which are atypical manners of death in the general population, and therefore may represent a bias toward a particular social grouping (214). The effects of this type of sampling bias however are almost impossible to determine. An overview of the problems encountered in using a cadaveric sample with clinical imaging is available as appendix 4I.

3.3.9 Statistical Analysis Overview

This thesis does not contain traditional *"tests of hypotheses"* type statistics. What it does include is a combination of equivalence testing and various forms of descriptive and observational statistics. This means that care must be taken in the interpretation of the various statistical tests contained in the work. When a t-test performed between groups detects no statistically significant difference, it does not mean that a conclusion may be made that there are no differences. The only thing that may be concluded from an insignificant t-test for these biological data is that there is not enough evidence available to support a finding of significant difference between groups. What this means is that should there have been the opportunity to observe more cases, it is entirely possible (and in extremely large numbers, entirely likely) that there would be observed differences eventually, in almost all of the variables tested.

As mentioned previously, much of the studies contained in this work involve descriptive and observational analyses. The statistical analyses were performed using SPSS statistical software (version 17.0.2, SPSS, Chicago Ill, USA). Kolmogorov-Smirnov tests were used to determine if all anthropological variables examined were normally distributed (215). As all variables tested in this work were normally distributed ($p>0.05$), paired and independent samples t-tests were used to evaluate significance between males and females. Comparisons between age groups used analysis of variance (ANOVA) and

multivariate analysis of variance (MANOVA) analysis. The level of significance chosen for all procedures was 0.05 or 5%.

Linear regression analysis was used to predict age and physical characteristics from QCT and anthropological parameters. The significance for testing was set to $p < 0.05$. Variations between conditions were evaluated using a multivariate one way ANOVA Wilks' Lamda (Samuel Stanley Wilks 1906 - 1964) evaluation (216).

3.3.10 CT Equipment List

- Toshiba Aquilion16™ CT scanning unit
- Agfa IMPAX™ miniPACS
- TeraRecon AquariusNet™ Server
- Mindways™ solid bone calibration phantom SN2805
- Mindways™ solid QA calibration phantom SN2888
- Catphan 600 CT Calibration Phantom SN600219

3.3.11 Computer Equipment and Software List

- MacBook Pro 15inch 2.5GHz 2GB RAM running Mac OS X 10.5.5
    - OsiriX™ Version 3.2.1
- PC 3.0GHz 4 GB RAM 24inch DELL monitor running Windows XP SP3
    - Microsoft Office 2007
    - Photoshop Extended CS3
    - CT-Expo v1.6E
- Buffalo 1TB NAS in RAID 5 array
- Mindways™ QCT Pro 32bit v1.0.2.6
- Mindways™ QCTPro Version 4.2.82 software
    - QCT Slice Picker v1.2.15.100
    - QCT Pro Database Dump Utility v4.2.7.70
    - QCT Pro Server Manager v1.0.9.8
    - AW CD Reader and DICOM Send Utility v1.0.0.1
    - CTXA Hip Exam Module v4.3.86.3

CHAPTER 4

THE EVALUATION OF QCT CHARACTERISTICS OF THE HIP IN A MODERN AUSTRALIAN POPULATION

"Failure is the opportunity to begin again more intelligently."

~ Henry Ford ~

Chapter four describes the quantitative computed tomography (QCT) examination of 289 pairs of human proximal femurs using cross-sectional data from a mortuary population. The primary aim was to describe the QCT characteristics of the proximal femur. The overall objectives were to establish a valid evaluation tool, compare differences of male and female results, and to also evaluate differences of symmetry. The hypothesis was that clinical software may be used effectively on mortuary-based MDCT data to derive population-based assessments of quantitative bone characteristics.

The chapter produces descriptive and quantitative modelling of the age-related differences of bone mineralisation characteristics of the proximal femur for both men and women across a contemporary adult lifespan in a predominantly urban population. In doing this, the work also provides a comprehensive investigation into the applicability of a routine mortuary-based MDCT scanning protocol to supplement the limited QCT data available from living individuals.

The investigation uses commercial QCT software to establish the population-based variation of the proximal femur. The software is US Federal Drug Authority (FDA) and Australian Therapeutic Goods Administration (TGA) approved for use in establishing volumetric bone mineral density (vBMD) in the living. The point in performing the QCT evaluation in the living is to determine fracture risk due to age-related bone deterioration. The software has not previously been used for a large scale mortuary-based application to assist in the determination of population-based age characterisations.

Given that this investigation utilises clinical software, and the methods discussed may one day be used in the living, the chapter also contains an evaluation of the ionising radiation dose used to obtain the QCT evaluation images. This is designed to place the mortuary-based examination into a clinical context, as a feature of this work is its aim to produce foundation data with broad utility across both clinical and anthropological disciplines.

4.1 Introduction

Mineralisation is the material property of bone examined radiographically (217). Generally the more mineralised the bone matrix, the stiffer the structure. A compromise between stiffness and flexibility exists in healthy bones. Through the process of normal ageing however, this balance is not always maintained, and bones become more brittle, and hence more prone to fracture with increasing age.

Factors such as mineral mass and content, bone size, porosity, cortical thickness, trabecular pattern connectivity and number, micro-damage status, remodelling rate and osteocyte density are all known factors in determining the resistance to failure with increasing age in bone (218). Very little however is known about the interrelatedness of all of these factors. Even less is known about how these factors are *normally* expressed across the adult lifespan and between genders in a contemporary predominantly urban population, such as exists in Australia.

Histological examination of bone tissue reveals a structure comprised of hierarchical building blocks. Bone may be explained from the smallest hydroxyapatite crystals measured in nanometers, to osteocytes measured at the micrometer scale; to bone vasculature measured by the 10s of microns; and finally to the organ-based structures which are usually measured in centimeters. The femur is the largest bone in the human body, but importantly it is also one of the main weight-bearing bones, supporting locomotion from early childhood.

Bone is comprised of a network of collagen fibres impregnated with mineral salts. As mentioned, it is the presence of the radio-opaque mineralised structure that is utilised in the radiological evaluation of bone. Mammalian bone is generally classified as being either trabecular or cortical, based on micro-structural properties and porosity. In the human skeleton 80% by mass is comprised of cortical bone, with the trabecular component making up the remaining 20%. Figure 42 demonstrates a CT-based 3D reconstruction of the femoral head in coronal orientation. Note the dense outer cortical bone encapsulating the matrix of rod and strut trabecular bone, and the complex patterning of the trabecular struts along the femoral head. The image demonstrates the utility of 3D imaging in evaluating the complex structure of bone.

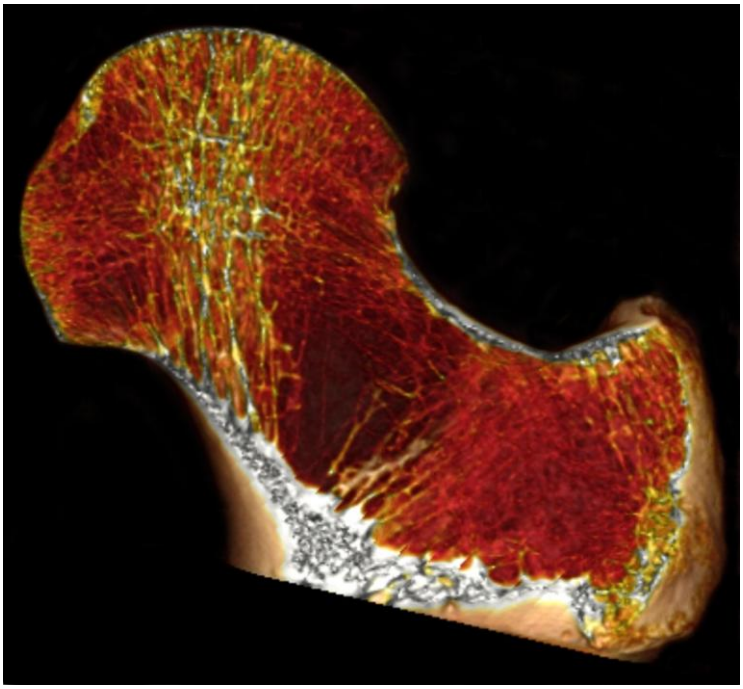

Figure 42 CT reconstruction midway through the femoral head

Scan performed on a dry femur using an iCat™ dental cone beam CT unit (0.25mm pixel size)

4.1.1 Bone Mineral Density

Bone mineral density in the context of quantitative computed tomography (QCT) refers to the apparent volumetric mineral density of bone. It is termed *apparent bone mineral density* as any one voxel will contain elements of both mineralised

and non-mineralised bone structure. Bone mineral density (BMD) has generally been used as a clinical measure of bone strength, but there are other important factors in determining strength, including bone geometry (64, 219, 220).

4.1.2 QCT and DXA

Quantitative Computed Tomography (QCT) is a non-invasive three-dimensional (3D) radiological technique designed to provide an estimate of the ash weight of bone. A typical piece of wet bone (remembering that there are both trabecular and cortical contributions,) has a physical density of approximately 2.2g/cm^3, and a mineral or ash weight of approximately 1.6g/cm^3. This assertion is derived from the approximation that 0.6g/cm^3 of wet bone is composed of organic matter and water. The density of bone as expressed by QCT is therefore an expression of the *mineral density* of the bone. The accuracy of QCT is typically between +/- 10-15% (221).

Because the neck of the femur is a complicated structure, a robust 3D imaging technique is an attractive means of engaging engineering based assessment such as buckling ratio and section modulus. The Mindways™ software used for this study contained a bone investigation tool (BIT) component which provided some biomechanical calculations. Primarily however the computed tomography x-ray absorptiometry (CTXA™) which evaluates densitometry was the primary evaluation tool. The reason for a separation of parts in the software is that the CTXA™ has FDA and TGA approval for clinical applications, the BIT does not. The classification of approval determines the funding arrangements in clinical evaluations.

Dual energy x-ray absorptiometry (DXA) is a planar technique used to assess areal bone mineral density (aBMD) which is expressed as g/cm^2. DXA is a 2D application and does not measure volumetric mineral content, but rather an *apparent density* of mineral deposition (BMAD) extrapolated across an area of the bone surface. Importantly, the DXA approximation is made without an indication of the spatial distribution of mineral across the sampled area (222).

The appeal of the DXA technique for serial BMD analysis is its relatively low radiation dose and widespread geographical access (223).

The aBMD is expressed clinically via the production of a t-score which is referenced to a population specific dataset, when reference data is available. The t-score is a term used by the World Health Organization (WHO) to define the osteoporotic state of an individual (98). Osteoporosis is defined as an individual having a t-score 2.5 standard deviations below the mean for young adults in their specific reference population.

4.1.3 Cortical Bone Differentiation

Separating the cortical component of bone from trabecular using radiologically-based technology is challenging. The differentiation achieved using the CT technique is an arbitrary one based on the setting of a threshold set by Hounsfield number. The Hounsfield number (or more specifically the range of numbers) selected for the threshold value equates to the linear attenuation coefficient of bone tissue, and the threshold selected results in material above the threshold considered cortical, and that below, trabecular. From a technical perspective, this means that the separation of the two bone components will be heavily influenced by the selection of various scanning parameters, particularly the slice thickness and slice reconstruction algorithm.

The cortex in the femoral neck is a very thin structure that forms the outermost shell existing at varying depths. The cortex has also been shown to decrease in thickness as a person ages, though the process is not uniform across the femoral neck structure (224). The imaging voxel used in clinical MDCT acquisitions is finite, and its size is often an order of magnitude or larger than that of the cortical thickness under measurement. The consequence of this finite size is referred to as the *partial volume effect* and has been explained in detail in chapter three. It represents a significant problem in imaging ageing bone in-vivo where decreasing cortical thickness has been associated with an increased risk of

fracture (225). An example of the difficulty in extracting or segmenting cortical bone from the cross-sectional reconstruction of the hip is shown in figure 43.

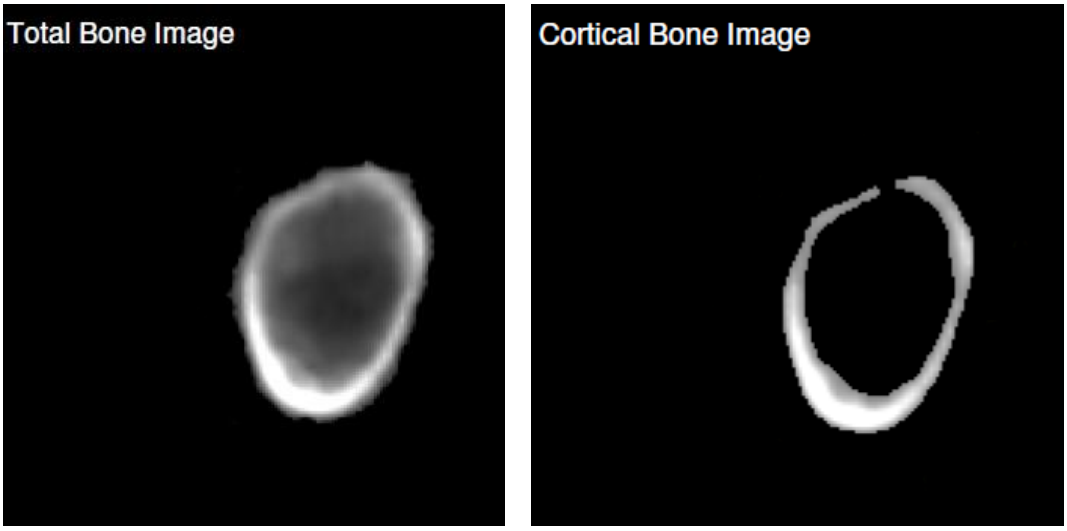

Figure 43 Total and cortical bone images from MFC597

The images in figure 42 were segmented using the Mindways™ QCT software on the scans of a 58 year old male, representing a *normal adult*. The images clearly show the difficulty in extracting the cortical bone margin using a segmented cross-sectional reconstruction of the femoral neck. Note in the cortical bone image the inclusion of some trabecular component in the inferior segment where the cortical bone is at its thickest, and the apparent loss of cortical border entirely in the superior femoral neck where the cortical bone is significantly thinner. The later finding does not represent the true anatomy, as the cortex is actually intact.

The anatomical position of the femoral neck also complicates an evaluation of cortical and trabecular components of bone. This is because the anatomical plane of the long axis of the hip is different to the axial reconstruction plane of the MDCT interpolation. This is termed *out-of-plane resolution*.

In the mortuary context the segmentation of the hip for QCT was further complicated because of the various contorted states of the bodies. Software that was designed for clinical use is presented under the condition of guidelines

related to the positioning of the patient for image acquisition. Unfortunately these guidelines cannot be applied in the case of imaging the deceased. Therefore an additional degree of error relating to the determination of bone borders through radiological segmentation was introduced. Hands placed over the hips were also difficult to separate from the hips in the segmentation process, especially in the very slim. Appendix 4D provides an explanation of the extraction of QCT data using the Mindways™ program.

4.1.4 Radiation

One of the primary concerns clinically in the routine application of QCT techniques relates to the necessity to use a greater ionising radiation dose compared to that of the DXA. There have also been reports of inherent inefficiencies of geometry associated with x-ray beam width and the detectors in MDCT technology (226). The latter phenomenon is due to the impact of the cone-beam effect in what is a volumetric rather than sliced acquisition imaging technique. While the instrumentation-based limitations of the MDCT detector bank remains outside the scope of this thesis, the analysis of ionising radiation burden will be explored.

The ability to perform off-axis reconstructions and increased access to machines has led to a proliferation in the use of CT technologies. The result is an increased burden of radiation dose to the overall community (142). Whilst it is not the intention of the author to promote the use in the living of full-body CT imaging as conducted at the VIFM; there is a need to fully explore MDCT for the purpose of *clinical* bone mineral evaluation, and hence a need to discuss ionising radiation dose.

There are few examples in the literature of an evaluation of effective dose in the application of QCT for bone mineral assessment after the early 1990s (227). The lack of information is likely as a result of a reliance on the National Radiation Protection Board (NRPB) in the UK providing information on normalised organ doses for CT using Monte Carlo analysis techniques (228). These estimations

however do not take into account dose modulation as a function of the automated exposure facility on commercial CT scanners. These estimations therefore provide only a worst-case scenario in terms of the total dose for any given procedure. It is an objective of this dose study to assess the effective dose of QCT both for the techniques used on the dead and the living.

4.1.5 Overall Study Aim and Objectives

The overall aim of this study was to describe the QCT differences of the proximal femur related to gender, age and symmetry. Specific objectives were as follows:

- establish the ability to use MDCT data from a mortuary environment for bone mineral investigation using a clinical QCT software package,
- test the reproducibility of the QCT method,
- describe a valid protocol for the QCT evaluation of the human femora from the VIFM MDCT data,
- describe the differences of QCT characteristics related to symmetry, gender difference and age-related change,
- predict biological age from QCT characteristics of the femoral neck,
- compare QCT evaluations across age and gender groups,
- calculate and compare dose calculations for clinical and VIFM effective radiation dose,
- describe sources of error generated by the unorthodox *patient* positioning.

4.2 Materials and Methods

4.2.1 Sample Description

Chapters 4 and 5 use evaluations made from the analysis of the bilateral femora of 289 individuals ranging between 15-95 years of age from both sexes, n = 155 males and n = 134 females. The 289 subjects consist of a cross-sectional heterogeneous sample derived from the high-resolution CT scans from bodies routinely admitted to the VIFM. The VIFM population represents individuals who die unexpectedly in the state of Victoria in Australia. To facilitate analysis of the

data the group was divided into male and female and each gender was divided into five age categories (15-29 years, 30-44 years, 45-59 years, 60-74 years and 75-95 years) in a manner that created similar group size, and was cognisant of the relatively long peri-menopausal period in females (229). The distribution of females demonstrates a slight bias in terms of a greater number being in the oldest group when compared to the males. Age and gender distributions are shown in figures 44 and 45 respectively.

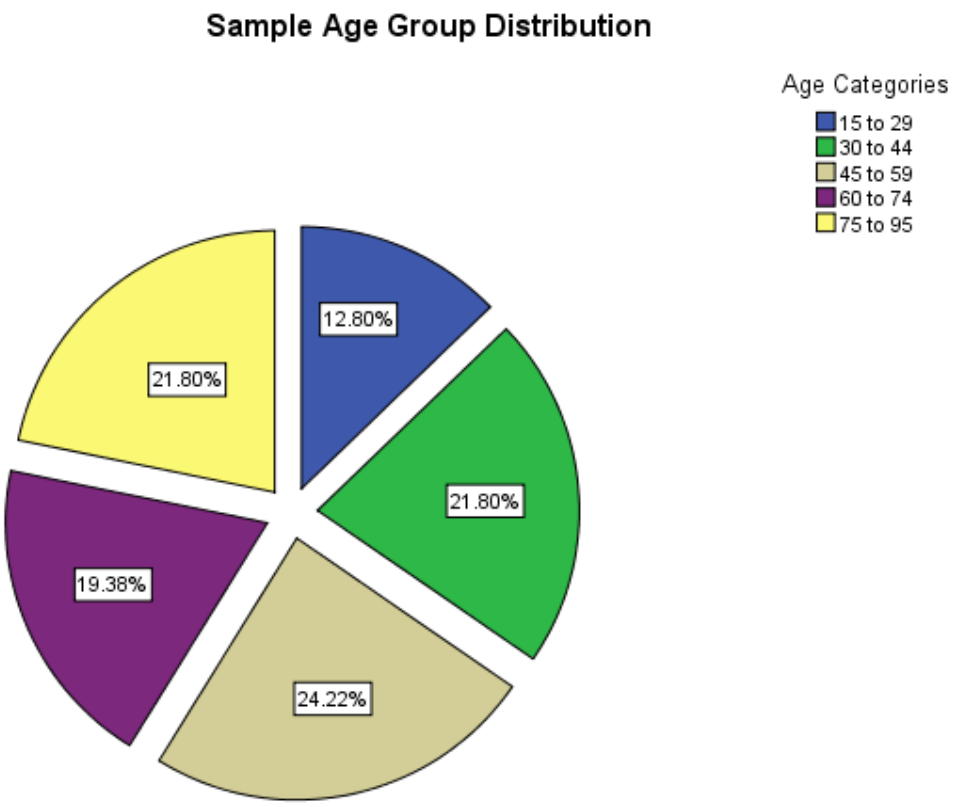

Figure 44 Age distribution - five groups

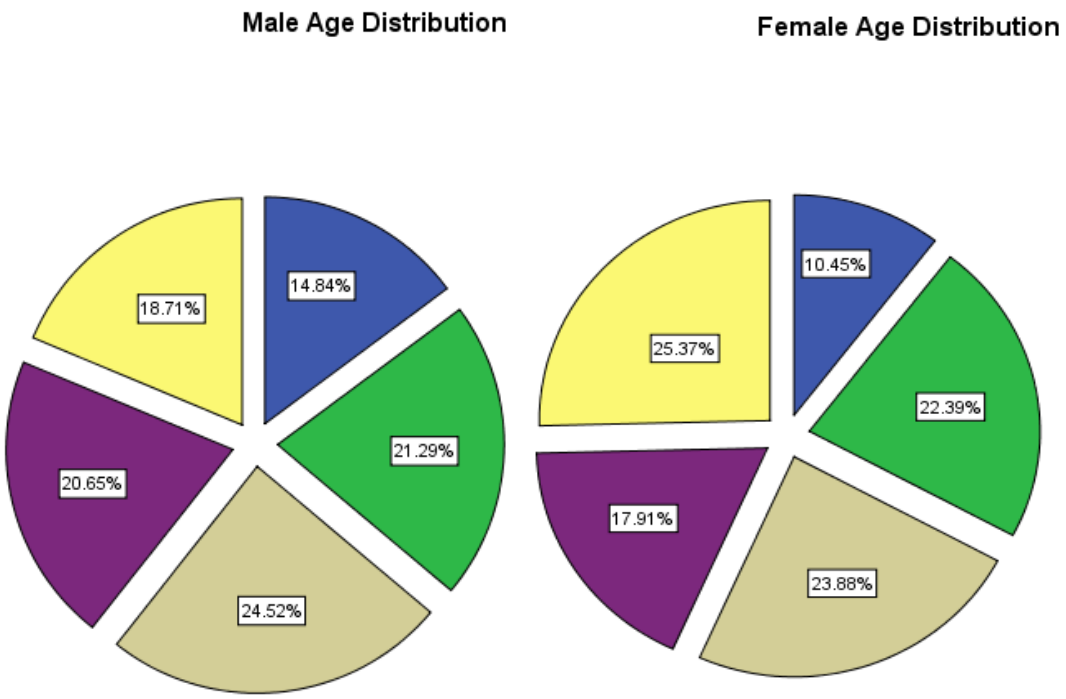

Figure 45 Age and gender distributions of VIFM groups

The age of the deceased was taken from their VIFM admission record, which uses their last birthday age. All individuals under the age of 25 years were evaluated radiographically to ensure skeletal maturity. This was done by searching for evidence of a radiolucent line representing the immature or unfused growth plate. Figure 46 provides an example of the evaluation of the degree of femoral fusion.

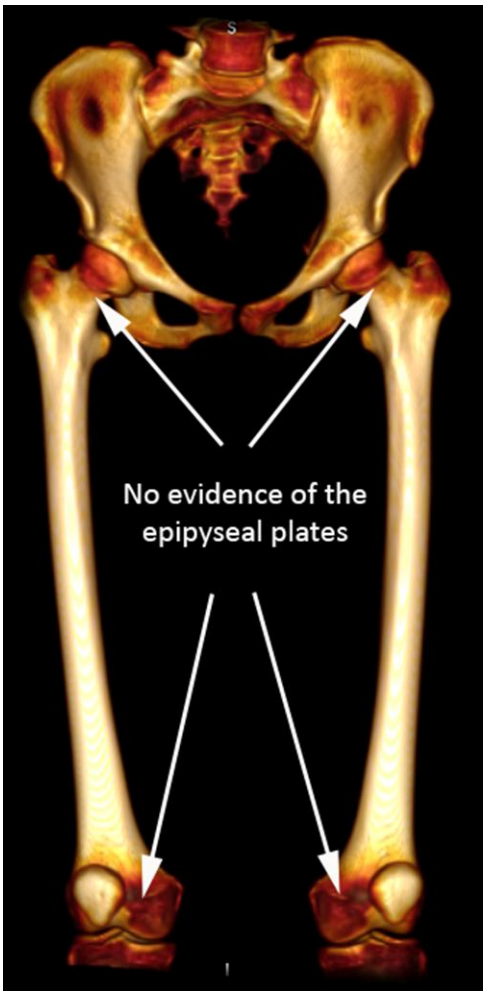

Figure 46 Radiological epiphysis fusion check

Female 17 years of age for which a check for the skeletal maturity was conducted.

Height, weight and BMI were also recorded at admission, and those results are evaluated with the gross morphological evaluations undertaken in chapter five.

4.2.2 Statistical Methods

Statistical analyses were performed using SPSS statistical software (version 17.0.2, SPSS, Chicago Ill, USA). The level of significance chosen for all procedures was 0.05 or 5%. More information on the statistical methods used for this study may be found in **section 3.3.9.**

4.2.3 CT Calibration Materials and Methods

Despite the fact that ethics approval allowed for the full download of the lower limb DICOM image files, it did not provide an opportunity to re-evaluate the raw CT sinograms. This would have been desirable as it would have enabled the selection of a reconstruction algorithm suited to the separation of cortical and trabecular bone as discussed in chapter three. A comparative evaluation of the slice reconstruction algorithm used or any other technically-based analysis was therefore impossible.

Though the slice thickness and spacing for the reconstructed images used at the VIFM were of a smaller voxel size than suggested by the manufacturer (136), there was concern that these data may not be suited to QCT Pro™ analysis. The concerns related to the VIFM's application of a reconstruction algorithm weighted towards soft-tissue differentiation, and the fact that the QCT technique relies on the ability of the software to differentiate bony components. The physical positioning of the bodies for scanning was also of concern. Three quality assurance (QA) and calibration tests were therefore performed:

- QA of MDCT unit
- Bone calibration phantom QA
- Proof of concept evaluation

QA of MDCT Unit

A Catphan 600™ CT testing phantom was borrowed from a local teaching hospital, and a full evaluation on both the CT unit at the VIFM, and an identical CT unit located at the hospital was undertaken. The testing phantom was used as

per the instructions in the manual (194), and the conduct of the examination was supervised by the physicist from the hospital from which the phantom was borrowed. A discussion of the relevant results from the testing is contained in chapter three. Results from the Catphan600™ QA test results are labeled as appendix 3C for the clinical comparison and as 3D for the VIFM results.

Bone Calibration QA

The calibration of the Mindways™ QCT tool was undertaken to establish precision estimates for BMD. The bone calibration QA procedure provides inputs into the analysis software supporting the bone calibration phantom functionality. The Mindways™ QA calibration phantom was also borrowed from the local teaching hospital. The testing was conducted according to the recommendations in the user manual (136), using the routine acquisition parameters of the VIFM. In performing the QA examination, the testing phantom is combined with the bone calibration phantom and scans performed. The scans are then processed using the QCT software. The testing establishes slope and intercept values for Hounsfield number and apparent density for the five hydroxyapatite rods for the particular MDCT system used. The values and precision estimates obtained in a subsequent QCT analysis relate only to the CT unit used. The bone and QA phantoms are shown in figure 47.

Figure 47 Mindways™ QA and bone calibration phantoms

The Mindways™ solid bone calibration phantom uses a K_2HPO_4 or calcium hydroxyapatite mineral equivalent standard for all calculations, which has been used an appropriate analogous for bone (136).

The results of the QA conducted indicated an estimated precision of 0.73 mg/cc for BMD of 100 mg/cc for the results on the VIFM unit. The QA testing audit result is shown as figure 48. The full report is in appendix 4C.

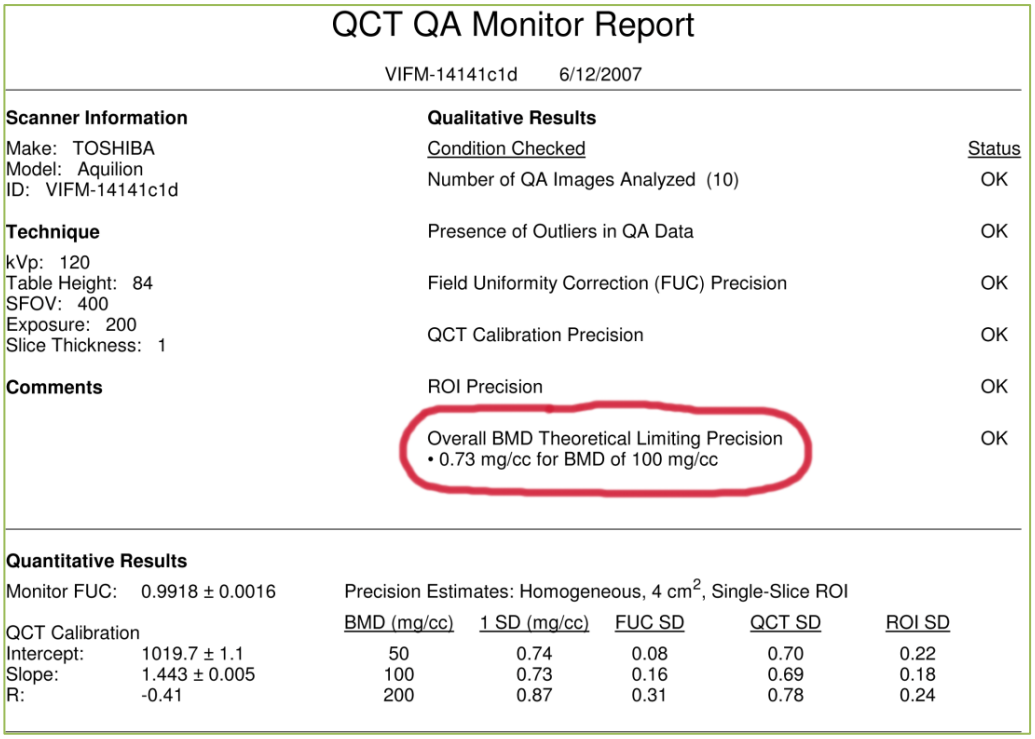

QCT QA Monitor Report

VIFM-14141c1d 6/12/2007

Scanner Information

Make: TOSHIBA
Model: Aquilion
ID: VIFM-14141c1d

Technique

kVp: 120
Table Height: 84
SFOV: 400
Exposure: 200
Slice Thickness: 1

Comments

Qualitative Results

Condition Checked	Status
Number of QA Images Analyzed (10)	OK
Presence of Outliers in QA Data	OK
Field Uniformity Correction (FUC) Precision	OK
QCT Calibration Precision	OK
ROI Precision	OK
Overall BMD Theoretical Limiting Precision • 0.73 mg/cc for BMD of 100 mg/cc	OK

Quantitative Results

Monitor FUC: 0.9918 ± 0.0016

QCT Calibration
Intercept: 1019.7 ± 1.1
Slope: 1.443 ± 0.005
R: -0.41

Precision Estimates: Homogeneous, 4 cm^2, Single-Slice ROI

BMD (mg/cc)	1 SD (mg/cc)	FUC SD	QCT SD	ROI SD
50	0.74	0.08	0.70	0.22
100	0.73	0.16	0.69	0.18
200	0.87	0.31	0.78	0.24

Figure 48 Mindways™ QA report for the VIFM unit

An estimate of the precision for 100mg/cc (circled in red) is provided in testing. The value will alter depending on the selection of reconstruction algorithm and slice thickness.

All QC and calibration testing procedures were well within range of the clinical thresholds set out in the Mindways™ (136) and Catphan™ 600 manuals (194).

Proof of Concept

Two test cases (full DICOM series) were also sent to research collaborators in the United Kingdom (UK) in a test for practicality and to asses body positioning. The UK bone research group has experience using the Mindways™ software, and has a collaborative relationship with the research group to which the author belongs.

The cases selected for the proof of concept study were a 77 year old female with a BMI of 19.15 and an 80 year old male whose BMI was 22.34. The cases were selected to represent the potentially more challenging groups to evaluate, as the hip position for both cases was externally rotated. The external rotation was as previously described, a common presentation for the VIFM cases. An internal rotation of the lower limbs is used in clinical examinations to move the femoral

neck into profile away from the pelvis. The QA scan (slope and intercept values) performed on the VIFM unit was sent to Cambridge for them to use for their evaluation. Full results of the proof of concept study may be found as appendix 4F.

4.2.4 Software Materials and Methods

The BMD evaluation component of this study used two tools from the Mindways™ QCT Pro™ software package. The clinical bone mineral analysis software which is referred to as the CT X-ray Absorptiometry (CTXA™), and the research-based Bone Investigation Tool (BIT). The distinction between clinical (CTXA™) and research (BIT) tools is made on the basis of FDA and TGA approval which is applicable to the clinical software only. A copy of the conformity Australian documentation may be found in appendix 4B. An example of the output from the application of both tools is presented as appendix 4C. Generically these combined software apparatus will be referred to as the QCT tools.

QCT software was provided free of charge by the manufacturer Mindways™ USA. Updates were also provided free of charge by online download. Seven variables from the QCT output were selected for measurement. The limited selection was based on the ability of the software to deal with the unusual physical presentation of the VIFM population, notably the marked external rotation of the lower limbs. The variables chosen were femoral neck volumetric bone mineral density (vBMD), areal bone mineral density (aBMD), bone mass, bone area, bone volume, buckling ration and finally the cortical depth. All variables evaluated are related to the findings from a 10mm cross-section in the middle of the femoral neck.

The calculation of radiation dose required another commercial software package known as CT-Expo™. The radiation dose delivered for a CT study depends on many of the factors selected by the operator (e.g. tube current and voltage, slice thickness, thickness of body part and helical pitch), but it is also related to the

design of CT scanner (230). The decision was therefore made to source a dose calculation program that had manufacturer specific functionality, and that specifically included the Toshiba unit used at the VIFM. The CT-Expo™ program was therefore selected after discussion with a medical physicist and a representative from the CT equipment manufacturer. The program was purchased from the vendor in Germany and downloaded online. The clinical protocols used for the VIFM dose comparison were provided by a local major teaching hospital that performs QCT examinations for a large multi-national clinical drug trial.

4.2.5 QCT Methods

In standard clinical practice the two main reasons for performing a bone densitometry examination are to firstly to identify those who have a lower than expected bone mineral density for their age, and secondly to monitor the effects of therapy for a deficiency in bone mineral density (98).

Serial application of QCT examinations may be used to establish a rate of change in an individual, but the sensitivity of QCT overall depends largely on the technique applied. This is the same for the DXA evaluation. Therefore data from one CT site may not necessarily be able to be translated for use with data from another site. This particular aspect of QCT will be discussed further in chapter six, and is mentioned here in the context of the work being a large cross-sectional study of adults, where all measurements were performed by the same individual, using data collected from the same MDCT unit.

The bone calibration phantom was installed onto the MDCT unit at the VIFM underneath the couch mattress so that it would not interfere with day-to-day operational activities. The device was attached via Velcro™ strips to enable cleaning of the couch underneath, and for its removal if required at the completion of data collection. A full explanation of the technique used to extract the CT slices, translate the files (converting to a format usable for the QCT program) and input the analysis values is contained in appendix 4D.

The 10mm cross-section (CS) region of interest (ROI) analysis option of the femoral neck (FN) was used in preference to the 15mm which is also available in the software. The choice was made based on the external rotation present in most of the femoral necks evaluated. Using the 15mm ROI for evaluating these cases would have resulted in including a large section of the pelvis in the segmentation phase of the analysis.

A list of the variables investigated is shown in table 3 indicating the depth to which this study evaluates age-related change in the femoral neck in comparison to that conducted routinely.

Evaluations	Clinical DXA study	VIFM QCT study
aBMD	√	√
vBMD		√
Bone Mass Density		√
Bone Area Density		√
Bone Volume Density		√
Average Cortical Bone Depth		√
Buckling Ratio Femoral Neck		√

Table 3 Clinical DXA v VIFM QCT overview

Each variable expresses a quantitative characteristic of the femoral neck and was performed as bilaterally on each case. Detailed descriptions of each of the variables are as follows.

Bone Mineral Density Components

Volumetric bone mineral density **(vBMD)** describes the calculation of apparent volumetric bone mineral density located within the 10mm mid-femoral neck cross-section. The calculation is expressed in units of in mg/cm^3. The value is referenced to the bone calibration phantom scanned at image acquisition, for which precision estimates were established as discussed previously.

Areal bone mineral density **(aBMD)** describes the calculation of apparent areal bone mineral density located within the 10mm mid-femoral neck cross-section. The calculation is expressed as g/cm^2.

The QCT software calculates apparent vBMD, but also includes an algorithm for a calculation of the expected aBMD value, or DXA equivalent. A recent study has demonstrated high-quality correlation of aBMD results as determined using the Mindways™ software and DXA studies (231). A comparative test using one wet proximal femoral specimen was performed at a local clinical centre using saline bags as soft-tissue equivalent. The results of the comparison, which were almost exactly equivalent, are contained in appendix 4E.

Bone Mass, Area and Volume

Bone **mass** describes the apparent mass of bone located within the 10mm mid-femoral neck cross-section and is a function of the vBMD. The calculation is expressed in grams (g). The calculation refers to an estimate of mass relative to the aqueous K_2HPO_4 standard in the calibration phantom.

Bone **area** describes the area of bone tissue located within the 10mm mid-femoral neck cross-section. The calculation is expressed in cm^2. The measurement reflects the apparent area of bone and therefore the accuracy is affected by the threshold of attenuation values which may be set in the QCT software, and which are also affected by the choice of reconstruction algorithm.

Bone **volume** describes the apparent volume of bone located within the 10mm mid-femoral neck cross-section. The calculation is expressed in cubic cm (cc) or cm^3.

Cortical Depth

Cortical depth refers to an amalgam of the apparent cortical volume and the apparent cortical area for the 10mm volumetric field in the centre of the femoral neck. The variable represents the concept of an average cortical bone depth in

that it is the volume of bone of a certain threshold divided by its projected area (232). The thickness of the cortex is not consistent around the femoral neck. A thick inferior shell is coupled with a thinner superior shell. The cortical depth measurement therefore provides an *averaged* amount of regional cortex.

As our bones continually expand with age (by surface apposition) then likely the average depth of bone (the volume of the bone divided by the area that it takes up) will also expand to maintain the bones' shape. With age however, it is likely that while the shape is maintained, the cortical thickness decreases, though not uniformly over the entire surface (224). If we say a bone has a volume (V) and a projected area (A), then area density is (BMC/A), and volume density is (BMC/V). Volume density divided by area density (V/A) is therefore average depth. Hence the naming of the variable, which is the volume of the cortical bone (Vc) divided by the area of the cortical bone (Ac).

The Mindways™ K_2HPO_4 standard has been verified against ash weight, and presents a calculation predicated on a specific CT number matching that of an ash-weight-equivalent with an accuracy of +/- 10% (233). This arrangement of association with biological tissue becomes slightly less useful when analysing trabecular bone as each pixel will contain a degree of hematopoietic marrow (apparent density relative to aqueous K_2HPO_4 of approximately 0mg/cm3) and fatty marrow (apparent density relative to aqueous K_2HPO_4 of approximately -50mg/cm3). The reported accuracy of mineral mass relative to the K_2HPO_4 standard therefore is more accurate for areas of higher mineral density like cortical bone.

Also, given the high soft-tissue weighting of the slice reconstruction algorithm used at the VIFM, it was decided to concentrate on cortical rather than trabecular calculations using the VIFM MDCT data. The partial volume effect using the very fine cortical bone structure in cross-section is however recognised as likely decreasing the accuracy of cortical bone measurements, especially in the elderly. The reason for using the cortical depth variable is an attempt to capture

any trend in the radiological expression of ageing femoral neck that is not captured in a routine BMD analysis. The cortical depth represents a variable which theoretically is less sensitive to differences of geometry.

There are therefore four recognised factors that have adversely affected the ability to separate cortical from trabecular bone.

- The ability of the QCT software to establish an appropriate threshold for cortical and trabecular separation
- The finite size of the imaging voxel coupled with a very thin cortex known to be thinning with increased age
- The out of plane nature of the femoral neck in relation to the axial scan plane of the MDCT slice reconstructions
- The contorted state of the bodies in a mortuary setting

Buckling Ratio

Buckling ratio is an engineering term used by Mindways™ to describe the average bone radius at the femoral neck divided by the average cortical depth. Early application of the buckling ratio concept in animals (234) and in humans (235), demonstrated a use for bone strength-based studies to establish fracture risk. Evaluation of buckling strength in the femoral neck however represents a crude approximation of the engineering concept of buckling ratio.

Though using buckling ratio in the femoral neck is somewhat controversial, thinning cortical bone is none the less a major expression of ageing in the region and therefore most likely a risk factor for fracture (224). Buckling ratio simplistically provides an analysis of risk of fracture by buckling in response to injury rather than torsion, bending and/or compression; in an assumption that a thin walled object (such as the ageing femoral neck) may well fracture in this way. The term buckling ratio is therefore an expression of the thinning cortex in the femoral neck and the qualitative relationship that this likely forms with a susceptibility to failure.

QCT Reproducibility

Although there are obvious advantages to using a 3D techniques to evaluate subtle age-related changes in bone, poor patient positioning impacts negatively on the results of a QCT examination (236). For this reason a limited test of reproducibility on the application of technique was performed. This test was in addition to the proof of concept test.

To assess error due to the application of a slightly modified QCT technique ten cases were randomly selected and sent to the research collaborators at Cambridge for evaluation. The Cambridge group has experience in investigating age related changes in the proximal femur, (61, 224, 237, 238) and experience with the Mindways™ product. Results from the Cambridge evaluation were emailed back as PDF documents. The researchers performed the re-evaluation as a blind study. Results from the comparison of the Melbourne and Cambridge techniques are included as graphed and tabled comparisons as part of appendix 4F.

4.2.6 QCT Radiation Dose Analysis Methods

The CT-Expo v1.6 software provides functionality for the calculation of weighted CTDI, volume or effective CTDI, dose-length product, organ specific doses and effective dose (E). A comprehensive description of these terms and their derivation is available in chapter three.

Though ionising radiation dose is of little concern in the production of MDCT scans from the dead, a primary contention of this work centers around the ability to use clinical data to support forensic and anthropological data and *vice versa*. An investigation into effective dose was therefore undertaken. The relative paucity of dose-related data for MDCT examinations was also a prime motivator in performing the investigation.

CT procedures report radiation dose as an effective dose unit depending on the organ/s included in the exposure field. Procedures such as plain x-ray and DXA

report dose as skin entrance exposures. It is difficult to approximate the relationship between the skin entrance doses and the effective dose, even when a dose area product (DAP) meter is installed on the x-ray device (239).

Doses were estimated using the parameters from a routine MDCT exposure series used at the VIFM, and then compared to a routine clinical QCT series. The clinical routine contained a choice for the operator on either a 170mA or 270mA technique depending on the size of the patient, and so estimations were made using both factors. The clinical protocol also included the option of either a 10cm or 20cm scan length, and both of these protocols were also evaluated.

The software used to analyse the results was CT-Expo v1.6, which is a commercial product designed to evaluate CT dose across a range of commercial CT instrumentations. The program in its licensed form allows the user to a select from a list of clinical brands and types of machines from which the estimations of dose are then based. The freeware application does not provide equipment specific calculations.

CTExpo™ is designed to calculate doses delivered under various CT and MDCT parameters. It is not designed specifically for individualised patient study, but rather it presents a series of calculations or estimations based on four body presentations, male, female, child and baby. No estimation of dose was made for either of the child or baby, as adult age-related expression were the focus of this work. Table 4 presents all CTExpo™ body type assumptions taken into account in delivering the dose calculation.

	Adam	Eve	Child	Baby
Length (cm)	170	160	115	57
AP Size (cm)	20	18.8	17.6	12.2
Weight (kg)	70	60	22	4.2

Table 4 CT-Expo patient assumptions

Within the program user interface there are a series of white boxes that require the entry of data taken from the CT acquisition used. There are also grey shaded cells that display guiding information pertinent to the entry or interpretation of the calculations to enhance accuracy.

The *"calculate"* mode provides the utility for the calculation of dose for all body types, and also provides for the selection of the scan range. The scan range can either be entered as a length (z- to z+ in cm) or set as limits between two user defined z-values. When entered, these z-values are applied to a diagrammatical representation of the body type which visually demonstrates any association with the vital organs for which a specific scatter, or primary dose may then be calculated. Figure 49 documents the application of the CT-Expo software on a 20cm long (z-axis length) segment centred on the male adult pelvis.

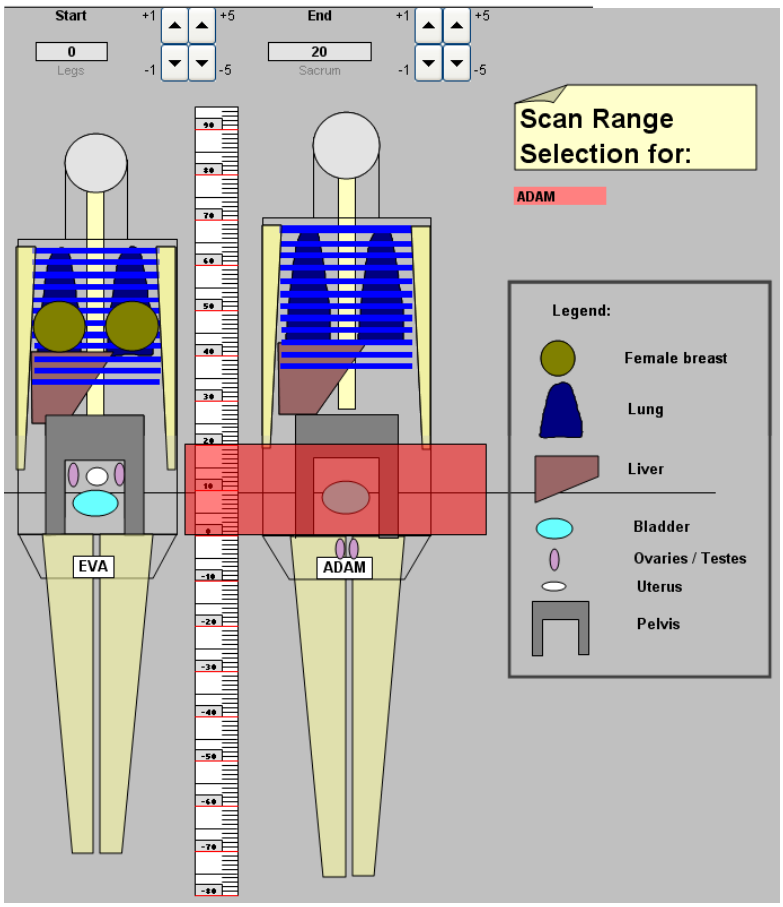

Figure 49 CT-Expo™ scan range selection

Screen capture. Red box denotes the dose calculation region.

The selection of z-reference points (scan position and length) was performed with input from the clinical and VIFM protocols. After using the software and reviewing some of the VIFM images it is the contention of the author that the 10cm scan length as indicated as an option in the clinical protocol would rarely be applicable to adult Australians. The inclusion of the entire femoral head and lesser trochanter is vital for the QCT software to establish anatomical planes for the calculation of densitometric and morphometric values. None of the Australian cases used in this study would fit easily along a 10cm scan. Table 5 documents the three techniques evaluated for dose.

VIFM Protocol	170mA Clinical Protocol	270mA Clinical Protocol
10cm scan	10cm scan	10cm scan
20cm scan	20cm scan	20cm scan

Table 5 Dose estimation and comparison groups

4.3 Results

4.3.1 QCT Results

QCT Reproducibility

All but one result (case 2008 1712) of the 10 cases sent for re-evaluation at Cambridge were in close agreement (within 2-5%) with the local results for both aBMD and vBMD determinations. Bone mass, area and volume evaluations were also well within a 5% tolerance except one case (case 2008 0723) which demonstrated over 8% variation. A full table of results including the two initial proof-of-principle test cases discussed in chapter three, and graphed comparisons are included as appendix 4F.

Bone Densitometry

Comparisons of the vBMD and aBMD variables to determine any significant difference between left and right values for each individual were performed. Both the vBMD (p<0.001) and aBMD (p=0.035) demonstrated significant difference between left and right values.

Results for vBMD symmetry are included as figure 50. Right mean values have been subtracted from left mean values, and so a positive value denotes a larger right-sided measurement, and a negative value, a larger left-sided measurement. A zero value indicates left-right symmetry.

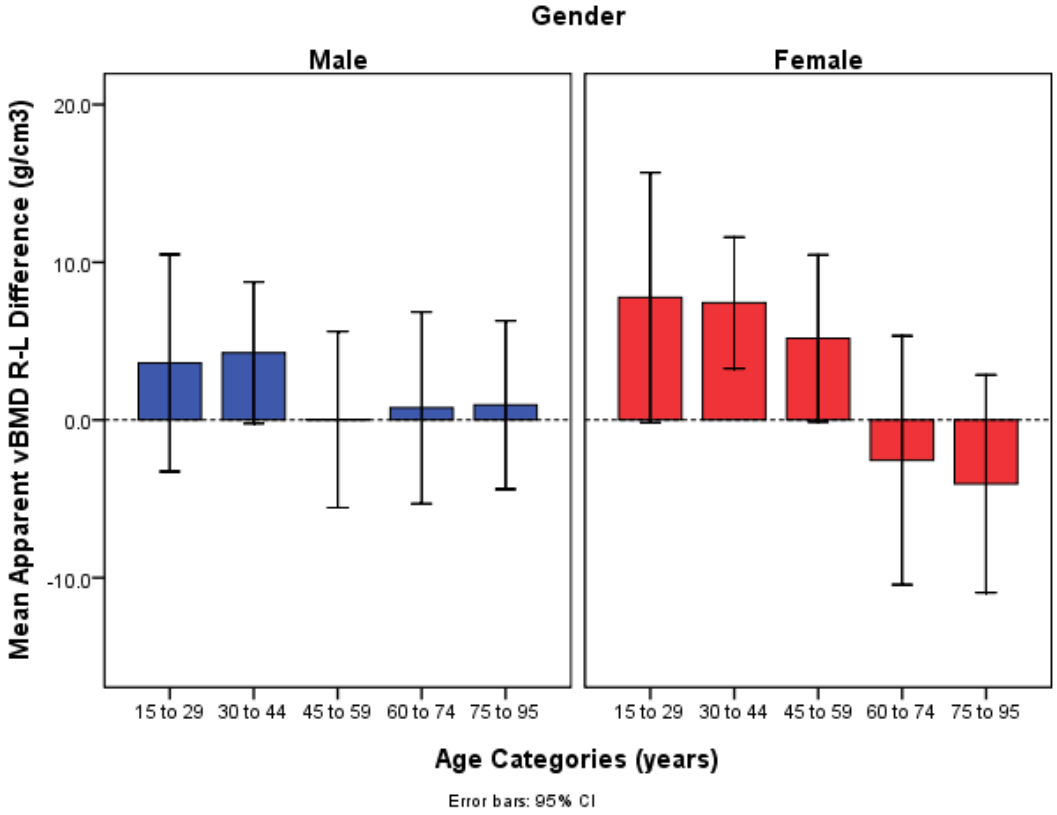

Figure 50 Apparent mean vBMD difference (right – left)

Significant differences were observed for mean asymmetries between age groups overall (p=0.038). Separated into gender groups, significant differences were not established between age categories for the male groups (p=0.755). Though not significant, males generally presented with a higher right-sided vBMD for all age categories.

The females however did demonstrate significant right-left differences (p=0.014) between age groups overall, with the 30-44 years and 75-95 years demonstrating the most significant asymmetry (p=0.042). Females generally were observed to have a higher right-sided vBMD than the males, but were observed to have reversed this trend to demonstrate higher left-sided mean values in the oldest

two age categories. Results for the evaluation of aBMD symmetry are included as figure 51.

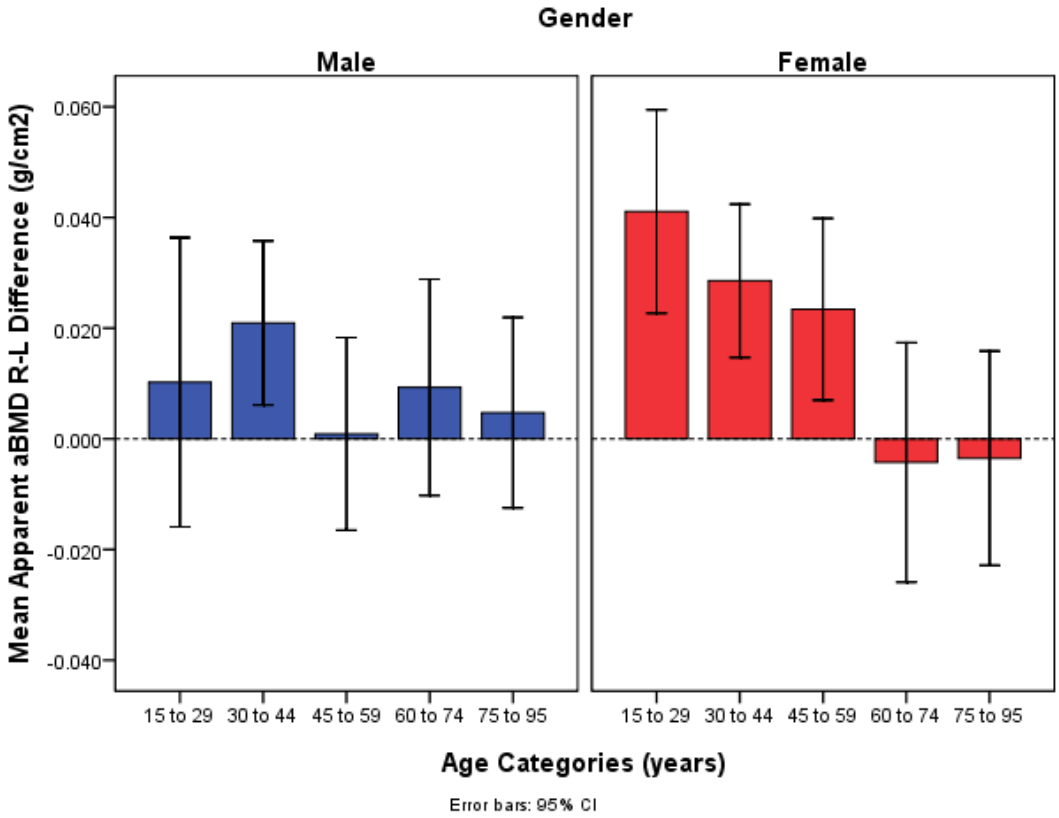

Figure 51 Apparent mean aBMD difference (right – left)

An evaluation of the mean differences between left and right values of aBMD demonstrated a small but consistently higher right-sided mean value for the males, except in the middle age-range where there is a symmetrical presentation. The general pattern for aBMD is similar to that of the vBMD which likely reflects that the aBMD estimate is a function of the calculated vBMD for the QCT software used.

Again significant differences were observed for the mean asymmetries between age groups overall (p=0.031). Significant differences were not established for the male groups (p=0.559). The females did demonstrate significant differences (p=0.002) between age groups overall, with the 30-44 years group demonstrating significant difference to the 75-95 years group (p=0.035) and the 75-95 years group (p=0.025).

Mean results of apparent vBMD and aBMD from each of the right and left sides for all age groups and both genders are included in table 6 and table 7 respectively.

		Right 3D apparent vBMD (g/cm2)			Left 3D apparent vBMD (mg/cm3)		
		Mean	Std Dev	Std Err	Mean	Std Dev	Std Err
Male	15 to 29y	314.8	43.7	9.1	311.1	41.6	8.7
	30 to 44y	291.9	46.0	8.0	287.7	42.9	7.5
	45 to 59y	274.9	44.4	7.2	274.9	40.7	6.6
	60 to 74y	266.7	47.8	8.4	266.0	46.9	8.3
	75 to 95y	229.9	42.8	8.0	228.9	45.7	8.5
Female	15 to 29y	321.3	40.1	10.7	313.6	41.9	11.2
	30 to 44y	295.5	60.8	11.1	288.1	60.7	11.1
	45 to 59y	288.2	44.8	7.9	283.0	45.0	8.0
	60 to 74y	236.7	44.6	9.1	239.3	47.3	9.7
	75 to 95y	197.1	43.0	7.4	201.2	42.2	7.2

Table 6 vBMD right and left mean values for age groups and genders

		Right 2D apparent aBMD (g/cm2)			Left 2D apparent aBMD (mg/cm3)		
		Mean	Std Dev	Std Err	Mean	Std Dev	Std Err
Male	15 to 29y	0.96	.14	.03	0.95	0.14	0.03
	30 to 44y	0.93	.14	.02	0.91	0.13	0.02
	45 to 59y	0.87	.14	.02	0.87	0.13	0.02
	60 to 74y	0.86	.15	.03	0.85	0.15	0.03
	75 to 95y	0.76	.13	.02	0.75	0.15	0.03
Female	15 to 29y	0.91	.10	.03	0.87	0.10	0.03
	30 to 44y	0.86	.17	.03	0.83	0.17	0.03
	45 to 59y	0.83	.15	.03	0.80	0.15	0.03
	60 to 74y	0.70	.13	.03	0.70	0.14	0.03
	75 to 95y	0.57	.12	.02	0.58	0.11	0.02

Table 7 aBMD right and left mean values for age groups and genders

Females were observed to have higher vBMD mean values than the males until after the age grouping correlating to the period following female menopause (60-74 years). In comparison the aBMD is higher at all times in the male groups.

Significant differences between age groups overall for the right (p<0.001) and left (p<0.001) **apparent vBMD** were observed. Between groups, the 15-29 years group demonstrates no significant difference with the 30-44 years group for right (p=0.116) and left (p=0.537) mean values, and equally the 30-44 years group demonstrates no significant difference with the 45-59 years groups for either of the right (p=0.09) or left (p=0.780) mean values.

For the male age groups, no significant difference was demonstrated between mean values for the 15-29 years and 30-44 years right (p=0.341) and left (p=0.280), the 30-44 years and 45-59 years right (p=0.509) and left (p=0.733), 45-59 years and 60-74 years right (p=0.942) and left (p=0.913)and 60-74 years and 30-44 years groups right (p=0.166) and left (p=0.268).

For the female groups, no significant difference was demonstrated between the mean values for the 15-29 years and 30-44 years right (p=0.462) and left (p=0.485), the 30-44 years and 45-59 years right (p=0.975) and left (p=0.994), and 45-59 years and 15-29 years groups right (p=0.204) and left (p=0.288).

Significant differences were observed between groups overall for the right (p<0.001) and left (p<0.001) **apparent aBMD**. Between groups the 15-29 years group demonstrates no significant difference with the 30-44 years group for right (p=0.502) and left (p=0.439), the 30-44 years group demonstrates no significant difference with the 45-59 years groups for either of the right (p=0.502) or left (p=0.808) and the 45-59 years group demonstrates no significant difference with the 60-74 years mean values for right (p=0.121) or left (p=0.212).

For the male groups no significant difference was observed between mean values for the 15-29 years and 30-44 years right (p=0.899) and left (p=0.756), the

15-29 years and 45-59 years right (p=0.114) and left (p=0.183) the 30-44 years and 45-59 years right (p=0.454) and left (p=0.812), 45-59 years and 60-74 years right (p=0.986) and left (p=0.938)and 60-74 years and 30-44 years groups right (p=0.056) and left (p=0.070).

For the female groups no significant difference was only observed between mean values for the 15-29 years and 30-44 years right (p=0.715) and left (p=0.859), the 30-44 years and 45-59 years right (p=0.929) and left (p=0.964), and 45-59 years and 15-29 years groups right (p=0.316) and left (p=0.547).

The differences in the mean vBMD and aBMD values in both males and females were also evaluated by averaging the left and right values and results are included as figure 52.

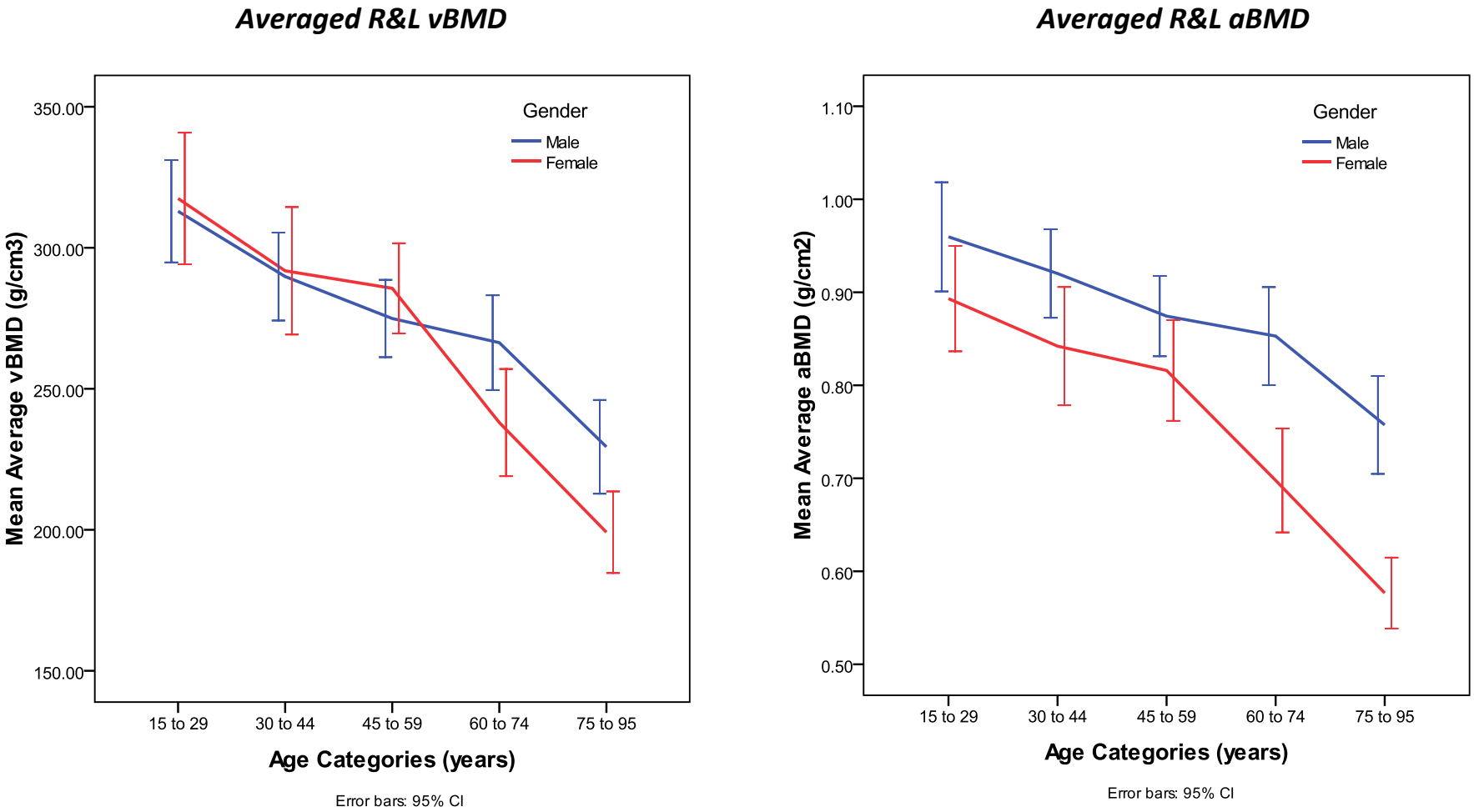

Figure 52 Averaged vBMD and aBMD male and female for all age groups

There is a pattern of steady decline of averaged (right and left) bone mineral density over increasing age which is apparent in both genders, and by both areal (DXA equivalent) and volumetric analysis methods. Significant differences were observed between male and female grouping for both the vBMD (p=0.04) and aBMD (p=<0.001) averaged results with the vBMD value shown to be a more sensitive indicator for age-related bone difference.

Results of the evaluation of percentage differences between subsequent age groups for males and females are included as table 8 and 9 respectively. Assessments of the apparent vBMD percentage differences demonstrate significant divergence between subsequent age groups when compared by gender.

Males	Average vBMD (mg/cm^3)	% Difference to next age group	Overall Change
15 – 29 years	312.95		
30 – 44 years	289.80	↓7%	
45 – 59 years	274.90	↓5%	↓27%
60 – 74 years	266.35	↓3%	
75 – 95 years	229.35	↓14%	

Table 8 Average vBMD decline for age groups – males

Females	Average vBMD (mg/cm^3)	% Difference to next age group	Overall Change
15 – 29 years	317.45		
30 – 44 years	291.80	↓8%	
45 – 59 years	285.60	↓2%	↓37%
60 – 74 years	238.00	↓17%	
75 – 95 years	199.15	↓16%	

Table 9 Average vBMD decline for age groups – females

Males demonstrate a consistent downward mean apparent vBMD transition until the 60-74 years and 75-95 years where the drop is almost 5 times that of the average difference between previous transitions. For females the downward trend commences with the 45-59 years to the 60-74 years groups which correspond to the peri-menopausal through postmenopausal clinical age groupings (105).

Females in the youngest group (15-29 years) have an apparent mean vBMD approximately 1.5% higher than those in the young male group, and this higher mean value continues through the 30-44 years group (1%) and 45-59 years groups (5%). By the next age bracket (60-74 years) however, the mean difference in vBMD between the sexes is shown to have moved significantly to a point where the males now have a 10% advantage over the females in terms of skeletal mineralisation in the femoral neck. For the final age group (75-95 years) the average difference between the mean apparent vBMD between males and females is 13% higher for the males.

Linear regression modelling was conducted using the averaged apparent vBMD to model to establish a relationship with age from QCT data. As sample numbers in each of the five age groups were small, (especially in the younger age groups), the modelling used a dichotomous grouping of 50-years and under and those over 50-years. More information on the dichotomous grouping of these data is found in chapter five. Full results of the regression are contained as appendix 4G and the regression equations are presented as table 10.

Category	Age Equation
All	111.264-(0.213 x vBMD in gm/cm^3)
All Males	110.048-(0.209 x vBMD in gm/cm^3)
Males ≤ 50 years	48.601-(0.047 x vBMD in gm/cm^3) p=0.055
Males > 50 years	97.344-(0.110 x vBMD in gm/cm^3)
All Females	112.046-(0.215 x vBMD in gm/cm^3)
Females ≤ 50 years	45.361-(0.031 x vBMD in gm/cm^3) p=0.169
Females > 50 years	106.392-(0.153 x vBMD in gm/cm^3)

Table 10 Linear regression models for age using average apparent vBMD

Note that for the males and females less than 50 years of age the *p* values are insignificant, where all other results have *p* values less than 0.001.

Bone Mass, Area and Volume

Evaluation of bone mass (males p=0.597 and females p=0.434), area (males p=0.322 and females p=0.153) and volume (males p=0.871 and females p=0.814) showed no significant difference between right and left values.

Figure 53 graphs the mean differences for right and left mean values in males and females for each of the clinical age groupings. Left values again have been subtracted from the right so a positive value represents a higher right-sided measurement and a negative a higher left-sided measurement.

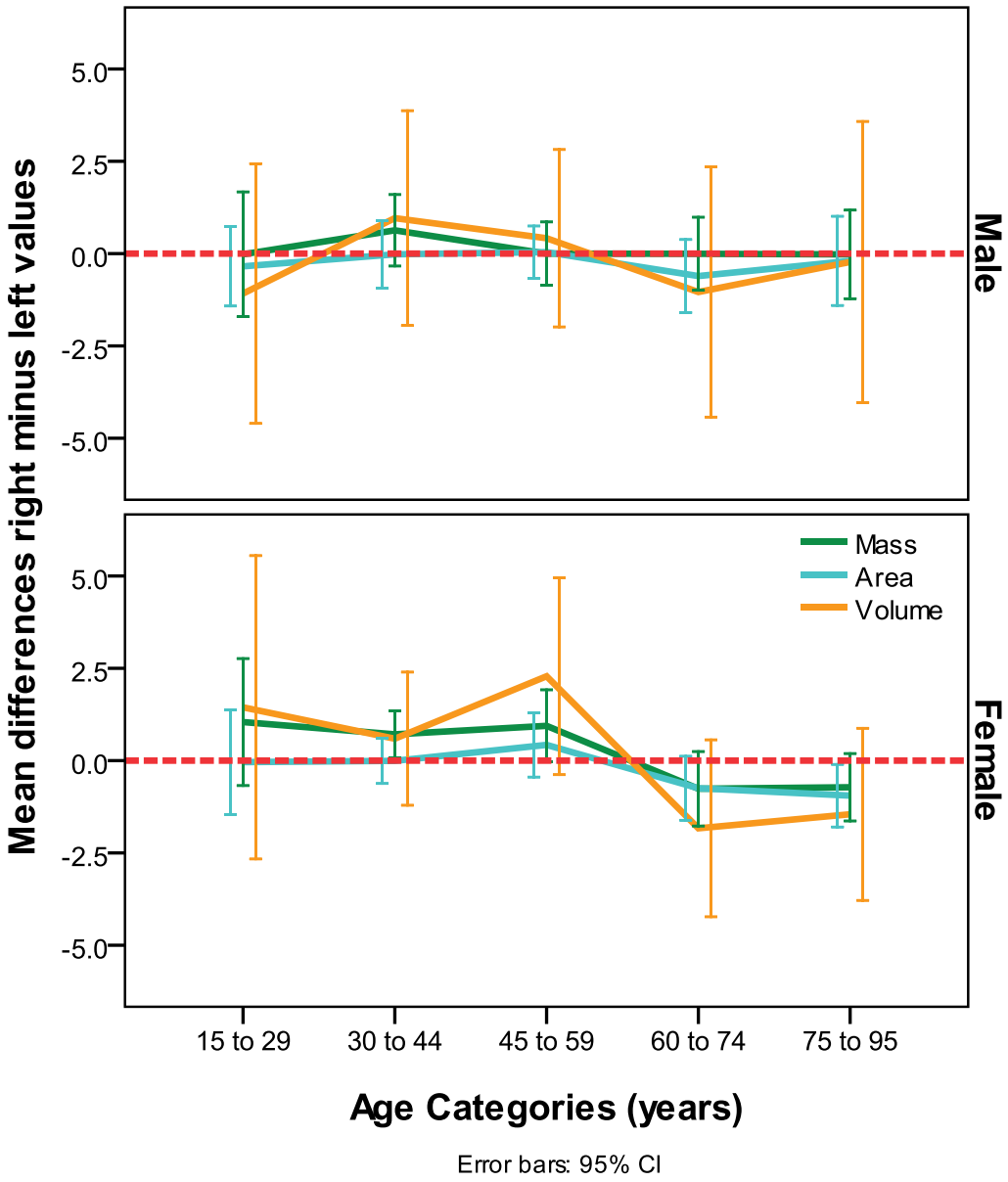

Figure 53 Mean differences for mass, area and volume

No consistent left or right variation of symmetry has been observed. There are however wide variations of mean symmetry seen especially in the bone volume measurement in both genders and across all age groupings. The smallest degree of asymmetry is observed in the bone mass measurement for males and older females, and bone area for the young females. Similar patterns of asymmetry across age groups are observed for males and females, with the females generally demonstrating more variability than the males in all age categories.

Averaged mean values for each of bone mass, area and volume for males and females are presented in table 11.

Averaged R&L		Mass (g)		Area (cm^2)		Volume (cc)	
		Mean	Std Dev	Mean	Std Dev	Mean	Std Dev
Male	15 to 29 years	31.74	5.8	32.97	2.9	101.56	14.0
	30 to 44 years	31.33	5.9	34.02	3.7	108.64	16.5
	45 to 59 years	30.83	5.8	35.21	3.6	112.68	16.6
	60 to 74 years	30.98	7.4	36.00	4.1	116.02	19.0
	75 to 95 years	27.72	5.9	36.52	3.7	121.03	15.5
Female	15 to 29 years	24.46	2.6	27.41	1.8	77.58	7.8
	30 to 44 years	22.81	5.4	27.05	2.9	78.67	11.9
	45 to 59 years	23.14	5.6	28.13	3.3	80.80	14.8
	60 to 74 years	20.00	4.3	28.64	2.7	84.23	10.2
	75 to 95 years	17.03	3.6	29.56	3.2	86.36	13.1

Table 11 Bone mass, area and volume

For males significant differences were established between age groups for bone area (p=0.003) and volume (p<0.001), but not for bone mass (p=0.112). For the females significant differences were established between age groups for bone mass (p<0.001) and area (p=0.012), but not for bone volume (p=0.061).

The average mean vales for bone mass, area and volume variables comparisons between males and females are presented in figure 54.

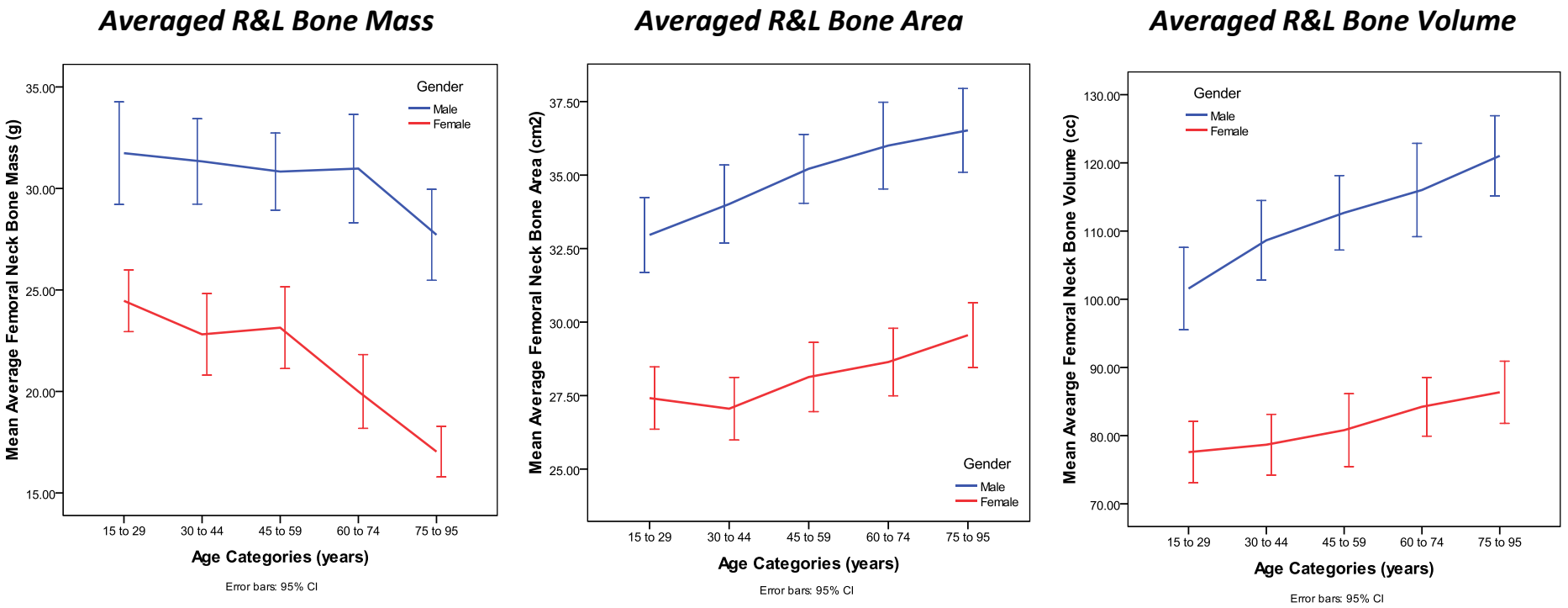

Figure 54 Bone mass, area and volume comparison – clinical groups

Significant differences (p<0.001) between males and females were observed for bone mass (M=30.52 and 21.09), area (M=35.03 and 28.27), and volume (M=112.42 and 82.01), indicating that all three variables may be confidently used for discrimination between male and female bone samples in the adult human.

Bone mass was observed to decrease slightly with increasing age, and both bone area and volume increase as age increases for both genders. The percentage differences between the youngest and oldest groups are included as table 12.

Overall Differences - Youngest group compared to Oldest group		
CS Bone Mass (g)	Male	↓ 13%
	Female	↓ 19%
CS Bone Area (cm^2)	Male	↑10%
	Female	↑6%
CS Bone Volume (cm^3)	Male	↑16%
	Female	↑9%

Table 12 Bone mass, area and volume % differences

Cortical Depth

The cortical depth measurement as previously mentioned represents the volume (cm^3) of cortex within the 10cm ROI in the middle of the femoral neck divided by the area (cm^2). Significant differences (p<0.001) between left and right values for cortical depth were observed. Separate right, left and averaged means for each gender and age grouping are included as table 13.

	(mm)	Left Cortical Depth		Right Cortical Depth		Avg. Cortical Depth	
		Mean	Std Dev	Mean	Std Dev	Mean	Std Dev
Male	15 to 29 years	**.90**	0.2	**.99**	0.2	**.94**	0.2
	30 to 44 years	**.80**	0.2	**.96**	0.2	**.88**	0.2
	45 to 59 years	**.76**	0.2	**.90**	0.2	**.83**	0.2
	60 to 74 years	**.72**	0.2	**.83**	0.2	**.78**	0.2
	75 to 95 years	**.61**	0.2	**.68**	0.2	**.64**	0.2
Female	15 to 29 years	**.86**	0.2	**1.01**	0.2	**.93**	0.2
	30 to 44 years	**.73**	0.2	**.88**	0.2	**.80**	0.2
	45 to 59 years	**.71**	0.2	**.85**	0.2	**.78**	0.2
	60 to 74 years	**.59**	0.2	**.65**	0.2	**.62**	0.2
	75 to 95 years	**.45**	0.1	**.47**	0.1	**.46**	0.1

Table 13 Mean right and left cortical depth

For both males and females the mean right cortical depth measurement was approximately 14% larger than the left mean value, though differences of symmetry were observed to be slightly less as age increased. Line graphs of left and right cortical depth average for all five age groups for both genders is included as figure 55.

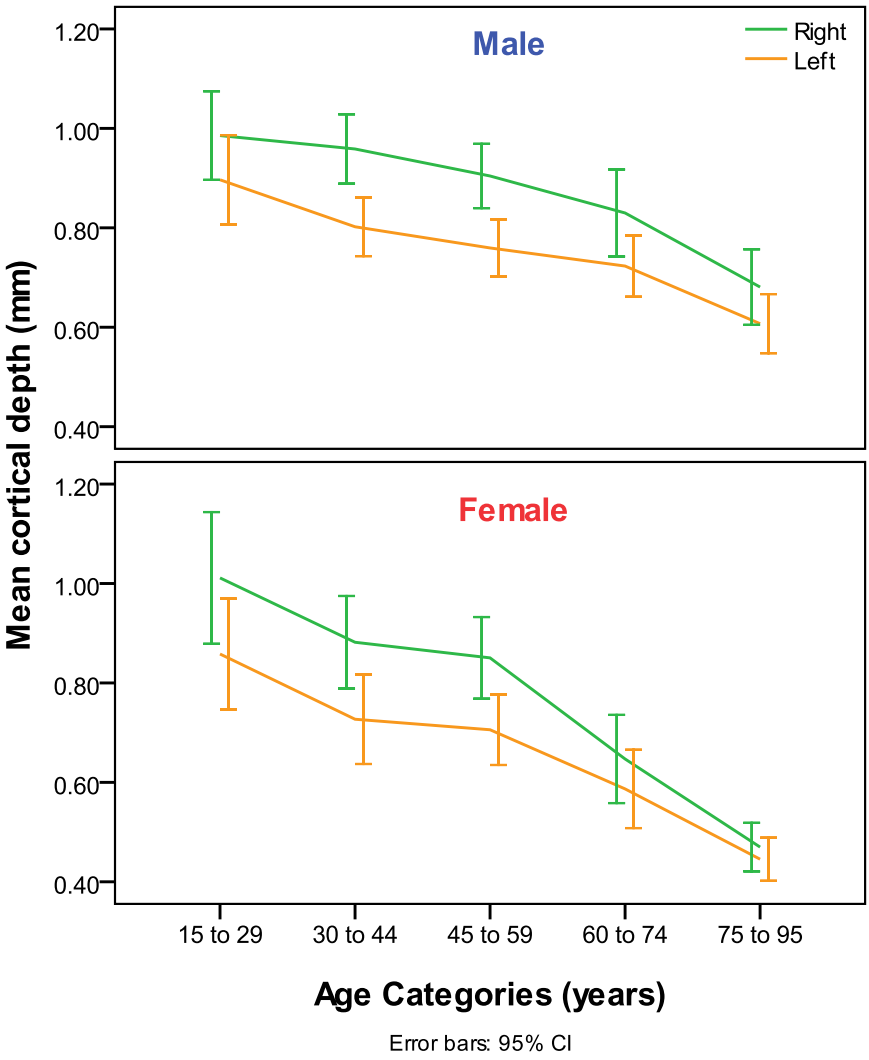

Figure 55 Right and left cortical depth, males – females

The right-left asymmetry is observed to be less significant as age increases for both genders, most obviously for the oldest two age categories in the females.

As the measured cortical depth values were very small relative to the size of the imaging voxel, a graph demonstrating the mean of the averaged values of left and right cortical depth for each of the gender and age groups is also presented as figure 56.

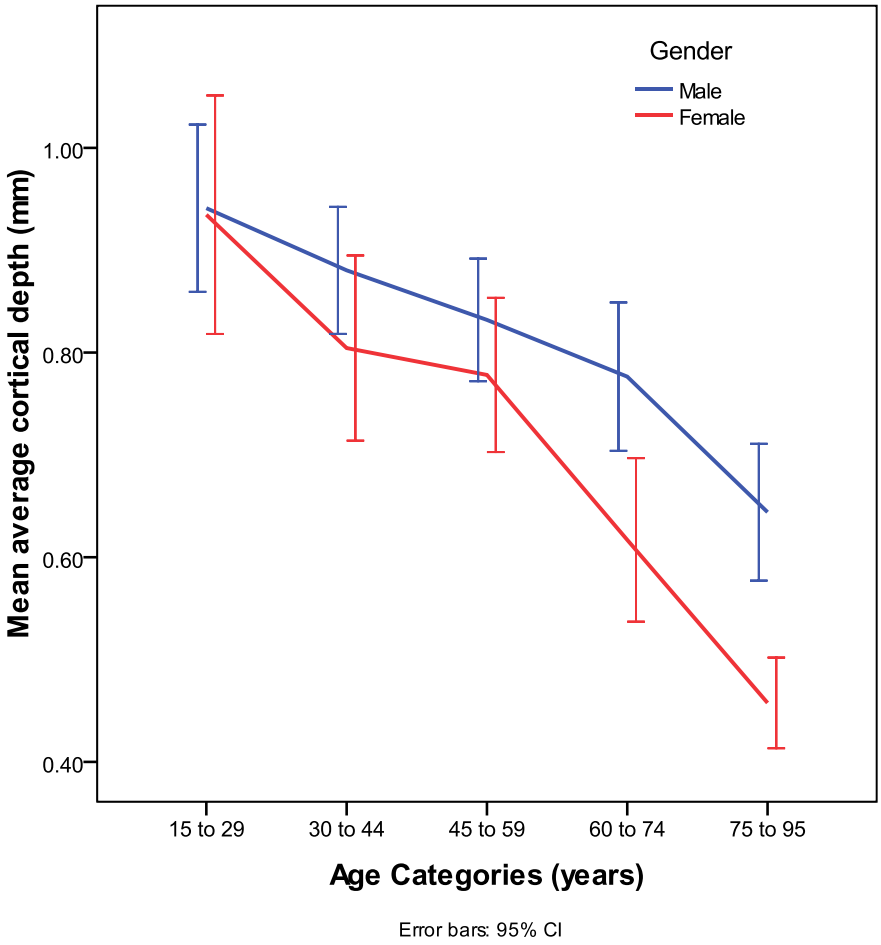

Figure 56 Average cortical depth for all age groups and both genders

Average cortical depth measurements are shown to decrease with increasing age in both genders with males and females having similar cortical depth measurements only in the youngest age grouping. Gender differences of cortical depth however are not significant until the oldest two age groups.

Averaged cortical depth comparisons demonstrate significant differences (p<0.001) between the mean cortical depth in males (M=0.81, SD=0.21) and females (M=0.69, SD=0.25). For males, significant differences were observed between the 15-29 years and both the 60-74 years (p=0.012) and the 75-95 years (p<0.001) groups, the 30-44 years and 75-95 years (p<0.001) groups, the 45-74 years and 75-95 years (p=0.01) groups and the 60-74 years and 75-95 years (p=0.045) groups.

Significant differences (p<0.001) were also observed between almost all female age groups, with only the 15-29 years and 30-44 years (p=0.215), the 15-29 years and 45-59 years (p=0.098) and the 30-44 years and 45-59 years (p=0.984) demonstrating no significant difference.

Table 14 outlines the percentage differences in average femoral neck cortical depth for males and females in the transition between the five age groupings. The differences reflect differences in the averaged (left and right) value. Transitions where significant differences (p<0.05) have not been established are marked *.

Percentage Differences of the Average Cortical Depth in the Mid Femoral Neck by Age		
30 to 44 Years	Male	↓6%*
	Female	↓14%*
45 to 59 Years	Male	↓6%*
	Female	↓3%*
60 to 74 Years	Male	↓6%
	Female	↓21%
75 to 95 Years	Male	↓18%
	Female	↓26%

Table 14 Average cortical depth % differences

The differences of cortical depth for age in males are shown to reduce consistently by 6% at each age group transition. The females however demonstrate a pattern similar to that seen in the vBMD, in that the cortical depth loss decreases, but that loss accelerates dramatically for the last two age groups. The loss of 14% from the youngest to the next age category does stand out in comparison to all other results for this variable though the difference was not statistically significant.

Table 15 demonstrates the average mean loss by percentage of cortical bone depth for males and females.

Mean percentage difference of mean cortical depth between youngest and oldest groups	
Males	32% less
Females	50.5% less

Table 15 Cortical depth difference between oldest and youngest groups

Older females therefore had less than 1/2 of the cortical bone depth of their young counterparts, while older males had around 1/3rd less cortical depth than their younger group.

Linear regression modelling of the average cortical depth for age and gender produce the equations documented in table 16.

Category	Age Equation
All	90.199 – (47.278 x cortical depth in mm)
Males	89.987 – (45.529 x cortical depth in mm)
Females	91.616 – (51.355 x cortical depth in mm)

Table 16 Linear regression equations for age using average cortical depth

The equations demonstrate that although young females commence with a similar cortical depth measurement to that of males, they decline more rapidly as a function of age. The equations therefore demonstrate significant (p<0.001) interaction between cortical depth and gender for age prediction.

Buckling Ratio

There were no significant differences (p<0.05) observed between the left and right values for buckling ratio. The results for both left and right mean values

from the analysis of buckling ratio obtained using the BIT software tool are included as table 17.

		Right buckling ratio		Left buckling ratio	
		Mean	Std Dev	Mean	Std Dev
15 to 29 years	Male	**4.3**	1.6	**4.3**	1.6
	Female	**3.6**	1.1	**3.6**	1.0
30 to 44 years	Male	**5.6**	1.8	**5.6**	1.6
	Female	**5.0**	1.9	**5.0**	1.9
45 to 59 years	Male	**6.2**	1.8	**6.5**	1.9
	Female	**5.7**	1.4	**5.8**	1.7
60 to 74 years	Male	**7.4**	2.3	**7.8**	2.6
	Female	**7.3**	1.9	**7.2**	1.8
75 to 95 years	Male	**8.9**	3.1	**8.7**	3.4
	Female	**9.2**	2.5	**9.3**	3.1

Table 17 Mean cross-sectional femoral neck buckling ratio - age and gender

No significant difference (p=0.162) was observed between the buckling ratios of males and females as a function of age. Averaged (left and right) mean of buckling ratio is shown as figure 57.

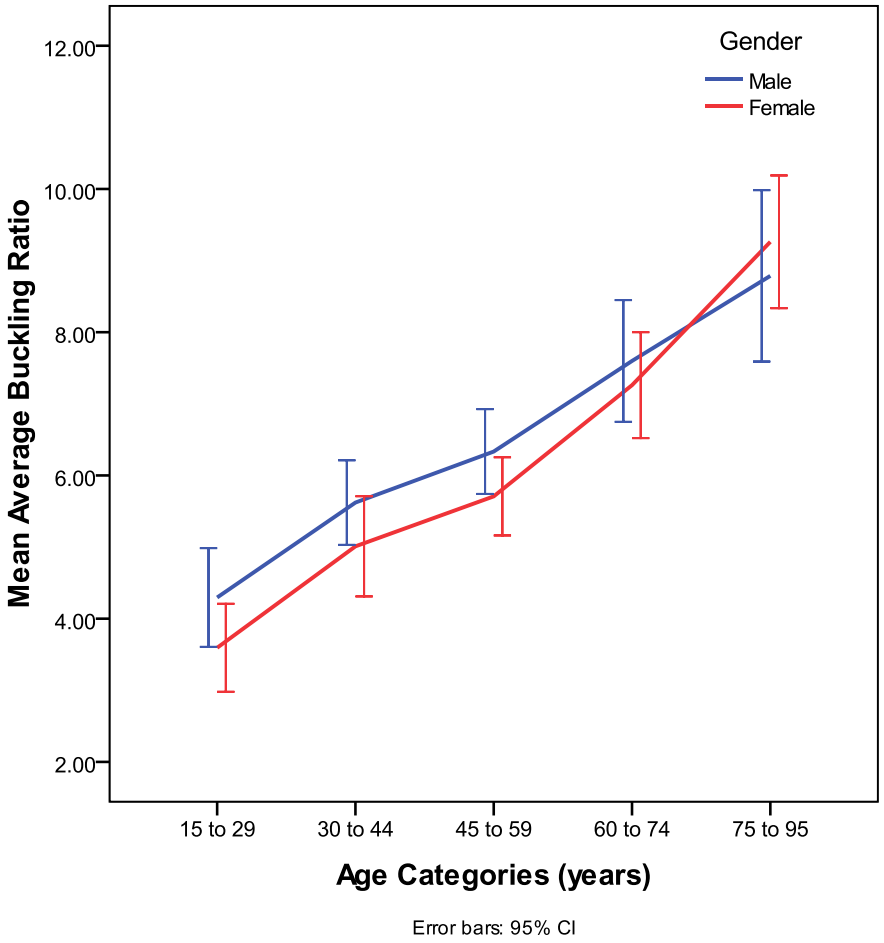

Figure 57 Average buckling ratio male- females

A similar pattern of difference through all age categories between males and females is observed with a gradual increase in buckling ratio with age for both genders. In the elderly grouping however the buckling ratio transition to a point where the shorter female femoral neck advantage is lost to their more rapidly thinning cortical thickness, leading theoretically to a greater likelihood of a buckling type fracture in failure.

4.3.2 QCT Dose Results

Because the pitch factor used for both the VIFM and clinical acquisitions was one, the CT dose indices, $CTDI_W$ and $CTDI_{VOL}$ obtained for this test are identical. The value for the VIFM scan for $CTDI_W$ and $CTDI_{VOL}$ was 19.1mGy. The 270mA clinical scan had $CTDI_W$ and $CTDI_{VOL}$ values of 17.1mGy, and the 170mA clinical scan delivered 10.8mGy for both the $CTDI_W$ and $CTDI_{VOL}$. A detailed description of these dose related terms is contained in chapter three.

Because dose length product (DLP) is a weighted result of the CTDI and the scan length, these values are the same for both male and female dose reports for each scan length. However the 10cm scan length, if ever used clinically, is likely to be exclusively applied on female patients as the males have a larger femoral head (remembering that the lesser trochanter must be included for the QCT software to provide a region specific output from the segmentation). Again the point being made is that the 10cm length scan would rarely be indicated on an adult of normal stature in an Australian population, though for completeness these results have been included.

The DLP_W for the 20cm length scan was 448mGy/cm for the VIFM, 403mGy/cm at the clinical 270mA, and 254mGy/cm for the 170mA clinical scan. At 10cm scan length the values were 257mGy/cm for the VIFM scan, 231mGy/cm for the clinical 270mA and 146mGy/cm for the clinical 170mA scan.

Table 18 records the calculations of effective dose for a **full-body scan** performed on a male and female using the VIFM scanning parameters. The maximum scan length for a full-body scan using the CT-Expo program has been used in each case. The maximum scan length for the Toshiba MDCT unit is 180cm, though a practical maximum scan length is more likely to resemble the CT-Expo maximums (males 170cm and females 160cm). Dose to the uterus or testes, as well as the surface bone dose for the femoral head has also been included for completeness. Doses are recorded as effective dose (E).

Full-Body VIFM	$CTDI_W$ (mGy)	DLP_W (mGy/cm)	E (mSv)	Uterus/Testes (mSv)	Bone (mSv)
Male 170cm scan	19.1	3241	26.9	28.8	63.1
Female 160cm scan	19.1	3051	28.2	32.0	63.8

†Australian Background Radiation Dose 3.0mSv per year (Source ARPASA)

Table 18 Dose report full-body VIFM scans - male and female

The full-body scans conducted at the VIFM therefore deliver approximately 9.6 years of background equivalent effective dose for males and approximately 10.7 years for females. Bone surface dose is similar for both genders. As mentioned previously, it is not a contention that this scan series ever be used for an evaluation of bone in a living individual. What is of note in this estimation is that the female uterine dose is greater than the male testicular dose.

Figure 58 from a study in the UK demonstrates the life-time risk of developing cancer associated with abdominal CT scans (201). These UK data show a significantly increased risk of developing cancer as a result of a CT scan before the age of 35 years, but that the risk become significantly less with exposures at increasing age.

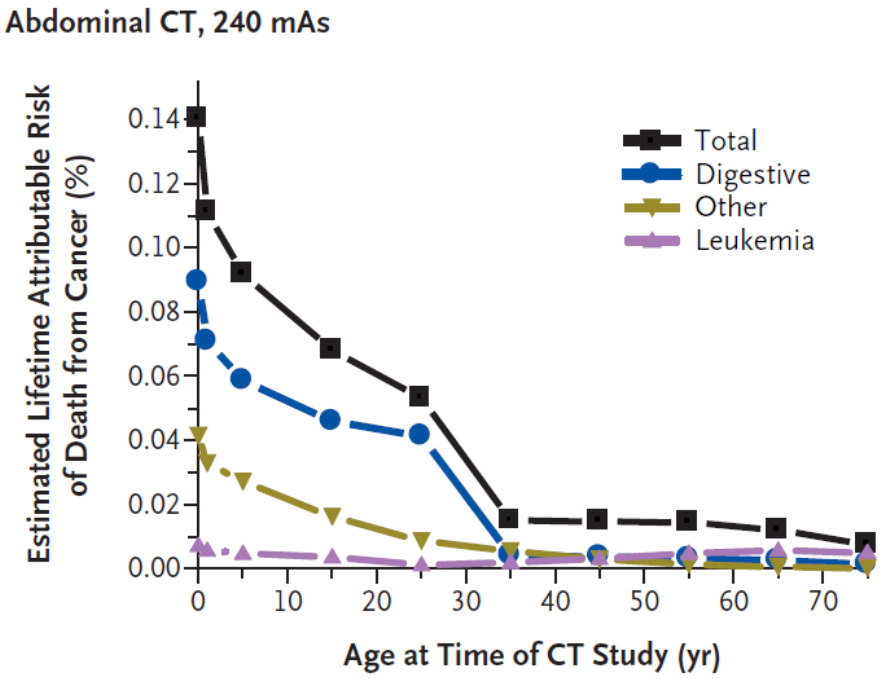

Figure 58 Estimated lifetime attributable risk of death from cancer after a CT scan (201).

Data downloaded directly from NEJM source with permission.

The VIFM protocol is not however performed on the living, so the results for both the 10cm and 20 cm scans using the specifications from the VIFM MDCT acquisition are presented with clinical dose comparisons. Table 19 documents the calculation of the effective dose (E) per examination, and includes either the uterine dose or testicular doses as appropriate.

		20cm Scan Length			10cm Scan Length		
		E (mSv)	Uterus (mSv)	Testes (mSv)	E (mSv)	Uterus (mSv)	Testes (mSv)
VIFM	Male	8.6	0	27.1	6.5	0	25.3
	Female	4.7	10.2	0	2.7	4.1	0
270mA	Male	7.8	0	24.4	5.8	0	22.8
	Female	4.3	9.2	0	2.4	3.7	0
170mA	Male	4.9	0	15.4	3.7	0	14.3
	Female	2.7	5.8	0	1.5	2.3	0

Table 19 Dose results 20cm and 10cm scan lengths – male and female

The results record scatter dose (0.1 mSv) estimations for each of the liver, spleen, stomach and pancreas when using the 20cm length scans, for both males and females. No organ specific scatter dose outside the scan field was registered for the 10cm scans. Direct doses were modeled for bone marrow and surface, bladder, colon, small intestine, skin and either of testes or ovaries and uterus for both genders. A full output of each of the dose models is contained as appendix 4H.

Because of the superficial location of the testes, and their location within the FOV, the male effective dose for the QCT scans modeled significantly higher than the females. The position of the uterus within the pelvis and the slightly higher orientation within the FOV resulted in a lower effective dose (E) overall being modeled for all of the female scan series.

While only very small calculated differences were shown between both male and female VIFM and 270mA clinical series, there was significant dose reduction by limiting scans to 10cm and using a lower tube current of 170mA. The larger reduction in Effective dose calculated for the male 10cm series compared to the female is likely the result of the primary field not including the entire testes, but again it should be noted that the entire femoral head would not be expected to be captured in almost all Australian adult men.

The Radiological Society of North America (RSNA) has a comprehensive website (http://www.rsna.org/) with a page devoted to radiation safety indicating the average effective doses for routine radiological procedures (240). Using the RSNA recommendations as a guide, the following table has been produced to provide a comparative overview of the effective doses delivered for all of the QCT series examined. The table also provides a context for these doses using DXA and abdominal and pelvic CT scan estimations. The **20cm scan length** has been used for the comparisons table 20, as it best represents what is used in the clinical setting.

Procedure	Effective Dose (mSv)	Background† Equivalent
CT Abdomen and Pelvis	10	3 years
DXA Evaluation	0.001*	< 1 day
Male VIFM Series (20cm scan)	8.6	2.8 years
Female VIFM Series (20cm scan)	4.7	1.6 years
Male 270mA Series (20cm scan)	7.8	2.6 years
Female 270mA Series (20cm scan)	4.3	1.4 years
Male 170mA Series (20cm scan)	4.9	1.6 years
Female 170mA Series (20cm scan)	2.7	11 months

* No mention was made of the anatomical site/s examined
† Normal background 3mSv annually

Table 20 QCT dose comparison – 20cm scan length

4.4 Discussion

4.4.1 QCT Reproducibility

As a result of the initial QCT examinations performed by the investigator and the UK proof of principle study, modifications to the analysis technique were made. Alterations were also necessary to the case selection criteria for the study.

The small variation across all of the variables recorded in the reproducibility study were within reasonable expectation (2-5%) in terms of a different operator, especially given the complexity of the physical presentation of many of the cases. Appendix 4I contains an analysis of the impediments to reproducibility caused by using the mortuary-based images.

The differences observed in the bone mass, volume and area results from Cambridge review relate to the choice of a slightly steeper sampling plane as demonstrated in figure 59.

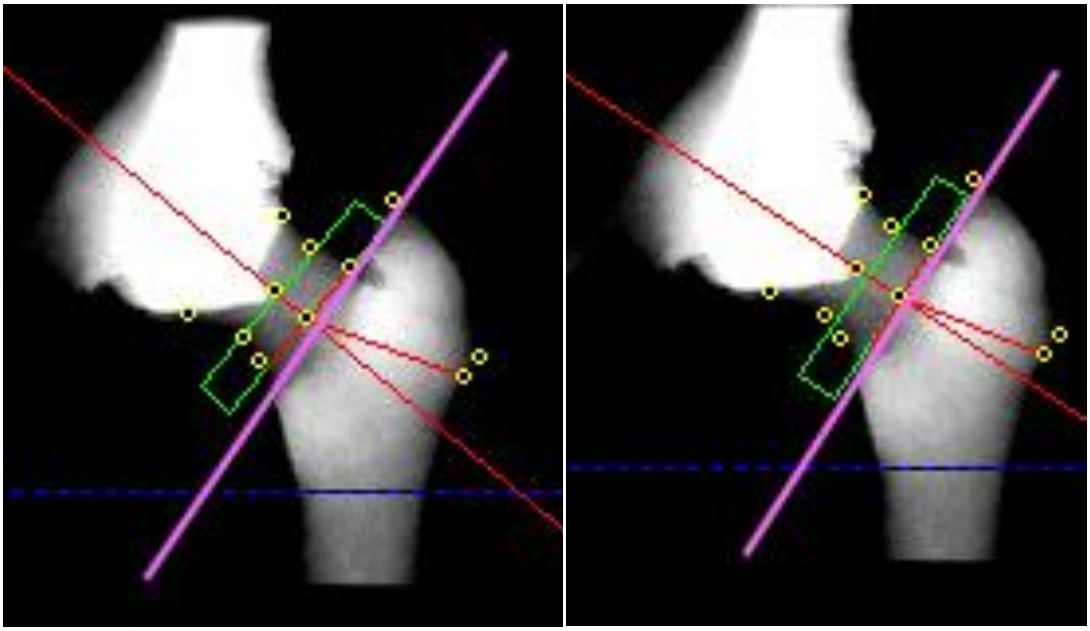

A B

Figure 59 QCT reference plane comparison

Note the difference in reference plane (pink line) as used as a default option (A) and by the investigator (B) mapped on the ROI evaluation box (green) and femoral neck axis (long red line)

The sampling plane B (using the inter-trochanteric line as a guide) was engaged for measurements as it was more able to be accurately reproduced for the VIFM sample given the marked external rotation exhibited by most of the cases. The degree of external rotation frequently caused a failure of the automated rotation element in the QCT application, which is supposed to assist in accurately positioning and repositioning the evaluation box to the mid femoral neck.

The ROI (green box) is positioned by the software according to the estimate of the long axis of the femoral neck (long red line). With marked external rotation the obscuring of the femoral neck by the pelvis (dense white area over the head of femur) in the segmentation process makes estimation problematic. It was therefore decided that as long as the rotational component of the hip was set consistently, (set manually by the operator) the inter-trochanteric line would be a more reproducible positioning guide for the setting of the ROI.

4.4.2 QCT

Notwithstanding the challenges associated with limited information on the MDCT technology, access to raw CT data and the physical presentation of many of the deceased; this study has demonstrated that routine mortuary-based MDCT data may be used for a population-based QCT study of bone in the proximal femur. Using clinical software for this study has demonstrated that the production of population-based data related to age-based densitometric characteristics of the proximal femur is possible, even though an orthodox clinical positioning routine is not able to be employed. It is however recognised that the accuracy of the technique would be further enhanced should a routine approach be able to be applied at a later date.

Symmetry

The age-related bone mineral model of the femoral necks for this population showed significant differences related to symmetry for both males and females, which has not previously been established anywhere else in the literature. Left-right asymmetry were apparent using both aBMD and vBMD analysis. The right-sided bias (i.e. the right side having a higher BMD value than the left) was shown to be more pronounced for the youngest age categories than their older counterparts for both genders. The difference is partly explained by the presumption that like the general population, around 80% of this sample are right footed (241). Though anthropologists might argue that the population used for this study may be biased by a physiological factor such as left-handedness, acting to select those associated with earlier mortality (242).

The temporal pattern of symmetry for the middle age to older males is likely and expression of the lower amount of high-intensity activity expected in those age ranges (243). The reason that the older two groups of females demonstrated a small but significant left bias in total contradiction to all other groups is less obvious, though the 95% confidence intervals (CI) of the results are indicative of a higher than average variability in these age groups generally. The degree of asymmetry demonstrated generally, especially in the young, indicates a need for

careful clinical consideration when selecting a unilateral approach for serial BMD analysis using either DXA or QCT methods.

Evaluation of the apparent vBMD data demonstrate that adult females of child-bearing age are conferred a small advantage of vBMD compared to males, which is not reflected in observations of the aBMD data. After the period of menopause however, the vBMD benefit for females falls significantly faster than it does for males. A similar pattern was also shown for aBMD, though vBMD was more sensitive to age-related differences.

BMD, Mass, Area and Volume

The observed decrease in averaged, apparent vBMD for both males and females from the youngest adult (15-29 years) group to the next age category (30-44 years) shows one of the largest percentage differences between subsequent age groupings. The larger than expected decrease observed is demonstrated by both male and female groups. Factors such as dietary and lifestyle influences likely go some way to explaining the differences (244), but this study finding is not able to be definitively explained as no lifestyle and dietary information is available for this population.

The linear regression modelling performed however establishes significant relationships for both gender and vBMD for age. The equation's robustness in terms of significance for the youngest male and female groups is not as convincing as for all other older groups. This finding is likely due to the small sample size in this younger age group, and the high variability of the measurement biologically as the skeleton matures.

In terms of bone mass, area and volume at the femoral neck, females present overall as significantly smaller in size but more variable than males across all three aspects and all age categories. Evaluations of symmetry reflect the findings from the vBMD and aBMD results in terms of there being a slight but consistent right-sided bias in the earlier years which progresses to a more symmetrical

presentation with increasing age, or in the case of the oldest females, a slightly left-sided bias. Observed increases in cross-sectional bone area and volume with increasing age supports a finding of periosteal apposition in the femoral neck, which has been reported previously (245, 246). These data however showed a more obvious increase in size (i.e. greater degree of apposition) for males than in females, most likely due to the differences in size generally, and the impact of partial volume effect in using MDCT technology. The finding of decreasing femoral neck bone mass for both genders were found to correlate with vBMD differences as would be expected with ageing.

The results for femoral neck bone mass, area and volume are positive in terms of the ability to use each of the measurements as a discriminator of male and female, as gender has a significant effect on the size of each of these variables. This particular finding also supports a multivariate approach to fracture risk determination (247) in terms of giving sufficient weighting to the gender-based morphometric differences in the femoral neck, leading into the results from cortical depth analysis.

Cortical Depth

The results of the analysis of cortical depth differences of age and gender for the VIFM population produced a number of significant findings. Significant mean asymmetry was observed for both genders, with the right femoral neck cortical depth measurement consistently higher than that of the left, with the magnitude of difference almost identical for both genders especially in the younger age categories. The larger right-sided mean measurement was however shown to shift towards symmetry with increasing age; again in both genders but was more significantly asymmetrical as a function of age in females than in males.

A percentage difference in females of 50.5% was observed when comparing the mean cortical depth of the youngest group to the oldest group. This result compares to a 32% difference observed between the oldest and youngest male groups. These results contrast to a 37% difference expressed in vBMD for the

females and 27% for the males across the oldest and youngest groups. This finding indicates a significantly higher sensitivity for age-related bone loss for the cortical depth variable in comparison to the apparent vBMD, variable using this QCT technology.

The difference in cortical depth measurement for males across all age groups except the oldest, demonstrated a consistent 6% loss between a younger category to the next older age transition. Females however demonstrate an increasing age-related difference expressed as a percentage loss between transition age groups, with only the 30-44years to 45-59 years transition period demonstrating a similar transition to that of the males. This finding is particularly important as unlike vBMD, the females have been shown to begin adulthood with less cortical depth than the males, and so have less to lose to begin with.

The acceleration of cortical depth loss observed after the menopausal-age period in females is significant and not unexpected, given the higher rate of fracture in females as compared to males, which has been linked to estrogen deficiency (248). These observations however indicate a definite role for the cortical depth measurement in assessing fracture risk, especially as its determination may be directly taken from values from the TGA and FDA approved outputs from the QCT clinical software. That is these data are not outside the routine in terms of what is collected clinically.

Buckling Ratio

Of most interest in the evaluation of the buckling ratio data is the fact that for females, it is not until the oldest age grouping that the ratio is greater than that of the males. This occurs even though the difference in cortical thickness (and cortical depth) at the femoral neck is significantly less than that of the males at all but the youngest age groups. This finding likely reflects the protective effect of a smaller cross-sectional size in relation to buckling for the females. Sub-periosteal expansion combined with cortical thinning therefore likely increases the likelihood of buckling type injury beyond that which would be expected from

the reduction in section modulus or bone mass alone. That is the woman's somewhat shorter neck in comparison to the man; counter the effect of their more quickly thinning cortex until the oldest group where the cortex is so thin that the neck length is no longer the dominant effect in determining the buckling ratio. This observation therefore supports the opinion that the buckling ratio is a rather crude geometric parameter in assessing fracture risk in either men or women (249), though a longer hip-axis length has recently been related to an increased risk of hip fracture (250). Buckling ratio may therefore still be of some use in determining an age or gender estimation for a femoral neck age characteristics if used in conjunction with other morphological or quantitative features.

4.4.3 QCT Radiation Dose

The dose calculations for the proximal femur QCT study has demonstrated that the radiation doses delivered for the purposes of the VIFM *virtual autopsy* are similar to those used in the clinical environment when the length of the scan range is taken into consideration, (i.e. the proximal femora). The significance of the finding is that it has demonstrated that it is technically feasible to integrate data from this mortuary-based study into those of clinical practice. This finding both broadens the potential to use this method clinically, and provides impetus for the further integration of the MDCT technology into mortuary environments.

The effective radiation dose (E) delivered during one **full-body VIFM MDCT scan** compared to the background Australian dose of 3mSv per year, results in the delivery of approximately 10-years of background dose equivalent for each admission. This result was presented for interest, and the VIFM protocol is not proposed as a general screening tool for bone assessments in the clinical setting.

Australian data from 2007 estimates that 40 fatal cancers every year may be attributed to unnecessary CT scans (251). The objective of a clinical CT examination is therefore to provide diagnostic information at the lowest possible dose, to reduce deleterious risk. The problem is that though low-dose QCT

examinations are easily performed, the resultant reduced signal to noise ratio does not produce enough spatial information required for bone geometry assessments such as the cortical depth. Therefore a thorough evaluation of the balance of risk and clinical effect are therefore recommended.

For the 20cm scan length evaluations, the differences in effective dose between the clinical procedure and that delivered at the VIFM are small (less than 10%) for both males and females. This study also demonstrated convincingly, but not surprisingly, that a shorter scan length combined with a lower tube current will produce the lowest effective dose for a QCT scan. As mentioned previously however this may not be appropriate from a diagnostic viewpoint and it is unfortunate that this technical aspect has not been able to be tested in this study. The largest contributing factor to an increased effective dose for males using a QCT technique is the proximity of the testes to the scan field, as they are usually located within the primary radiation beam. Therefore the overall effective dose for QCT is larger for males than for females.

Ionising radiation dose burden in the context of routine screening for BMD seems superficially well favored toward DXA in comparison to QCT. One day's normal background as delivered by DXA compared to approximately two year's background equivalent for a QCT examination. The unlikely but possible deleterious effects of an ionising radiation dose however would rarely be the first question asked clinically to establish a pathological or disease status or indeed *accurate* fracture risk. The radiation concern is also less likely a consideration as a person moves beyond child-bearing years, which is where BMD screening occurs most frequently. The additional complexity however in discussing human reproductive age, is the fact that men may remain fertile well into what is considered old age.

The position of the hips in relation to the pelvis and consequently the reproductive organs, obviously result in a larger impact on the determination of equivalent dose than if they were just about anywhere else in the body. The

biological position is something that cannot be altered, but measures such as those discussed in this work, including keeping tube current as low as possible, can be utilised clinically to minimise the radiation burden. The question of how much additional radiation is warranted, or should be considered acceptable, will therefore likely to be determined by how much the specificity in terms of fracture risk can be improved in using the QCT technique.

To assess the health impact of radiation exposure, one needs to evaluate the lifetime risk for all cancers, and make an estimate on the risk of mortality and on increased incidence associated with exposure (252). The age at which cancer occurs is also of concern in evaluating the overall impact, and there have been suggestion that further monitoring studies be conducted with children who have had radiation-based treatment as part of their care (253). A discussion of the exact nature of the expected impact of wide-scale implementation of QCT in place of DXA is not within the scope of the thesis; nevertheless this investigation has highlighted a need for further discussion, especially as there appears to have been little until now.

4.5 Conclusion

Overall the results from the QCT analysis of the VIFM group clearly demonstrate that the Mindways™ QCT clinical software may be confidently used as a tool for the evaluation of age-related densitometric and geometric differences. This capability provides enormous potential for developing a more accurate archetypal model for femoral fracture, and for establishing biological age in anthropology.

The age-related bone mineral density characteristics of the modern, urban Australian population examined demonstrate significant differences and large variability across gender and age. The temporal pattern of BMD loss observed was found to be significantly different for males and females. The study has also observed evidence of significant differences of symmetry, most notably in the

younger age categories, and in females generally that have not previously been identified. The investigation has also revealed that in general, younger individuals of both genders demonstrate a higher BMD of the right hip in comparison to their left. The result likely reflects the higher levels of activity in the young, and the prevalence of right footedness in the population generally, but this does need to be tested conclusively using more individual health documentation.

Volumetric BMD was shown in this study to be greater in females than in males in all age categories up to menopause, after which the vBMD is shown to decrease at a rate significantly more rapid than males. The males in the VIFM population demonstrate a slow and steady declining vBMD up until the most elderly grouping where the rate of decline was observed to be similar to that of the females. Areal BMD measurements demonstrate similar trends in relation to the relative declines of density for both males and females, though aBMD does not capture the higher volumetric loading of mineralisation for females of child-bearing age. The finding of higher vBMD in younger females is likely an important factor in future research involving the hormonal influences on BMD levels generally, especially in light of the results of the analysis of cortical depth.

The variable introduced as *cortical depth* was revealed to be a more sensitive indicator of femoral neck bone ageing than that of either the vBMD or aBMD. Right cortical depth was shown to be significantly greater than that of the left for both males and females in all age groups. The differences of symmetry were however less as age increased, and presented as almost symmetrical for the oldest female group. The average cortical depth measurement was similar in both males and females only at the youngest age category; though at no age grouping did females have a greater mean cortical depth than males. Further investigation of fracture rates in the left and right femoral necks of aged males and females will provide insight into the significance of the finding.

The buckling ratio as both a discriminator of male and female femoral specimen and for fracture risk determination was shown to be of little practical value. The evaluation did however demonstrate that the shorter femoral neck of the females has a protective effect in terms of a buckling type injury well into old age. A future study investigating the various types of fractures and their prevalence in either gender may be supported using this variable.

The results generally from the evaluation of spatial QCT properties of the proximal femur demonstrate clear discrimination between male and female specimens using any of the bone mass, area or volume variables. Females were observed to have more variability in all three measurements in terms of symmetry, though the differences overall were small. These results may be of significance in a general anthropological evaluation of physical and lifestyle characteristics of a population.

An investigation into the distribution of lean and fat mass overall would be a useful addition to further work, especially as there have been findings suggestive of a variety of effects from lean mass positively affecting bone (254). Normal lean mass is suggested as a mediator for fracture prevention in men (255), and may explain some of the differences in cortical depth seen as there was significant variability in the BMI, height and weight of each of the male groups generally.

Results from the estimation of ionising radiation dose delivered during QCT show that substantially higher doses are delivered for both males and females in comparison to the DXA examination (2 years against 1 day respectively). The result is however presented in the light of results delivered by the QCT examination generally, which indicate superior sensitivity for the quantification of age-related change, and potentially fracture risk. So, why is it that the current literature appears more in favor of over medicating to treat osteoporosis rather than over exposing radiologically speaking to test for the condition? This is especially perplexing as so little specific dose-related modelling exists from which to make an informed decision either way.

CHAPTER 5

HUMAN VARIATION OF FEMORAL MORPHOLOGY USING 3D MDCT EVALUATIONS

"There will come a time when you believe everything is finished. That will be the beginning."

~ Louise L'Amour ~

Chapter five describes the development and application of novel 3D MDCT techniques for the evaluation of femoral osteological differences across an adult population. The primary aim was to describe the morphological characteristics of the human femur. The overall objectives were to describe a valid protocol for femoral morphological evaluation, to compare differences of male and female results, and to also evaluate differences of symmetry. The hypothesis is that there is predictable morphologic age, gender and symmetry related differences within a contemporary predominantly urban adult population spanning 80 years.

The work is presented from the perspective of the anthropologist, and presents an evaluation of the bilateral femora of those between 15 – 95 years of age from a current predominantly urban Australian population, which has never previously been done.

The chapter includes the following;

- an introduction to the field of forensic anthropology,
- an analysis of reproducibility and error for the measurements undertaken,
- a quantitative radiological evaluation of morphological variation related to symmetry, gender, generation and age.

5.1 Introduction

The four main components for establishing a biological-identity are age, sex, stature and ethnicity (256). The forensic anthropologist aims to use known biometrical relationships between a body part and the whole to build an estimate of features which is then used to determine the identity of remains. The determination of sex and age at death are especially important assessments for medico-legal or coronial investigations, and in narrowing the search for an identity from remains (257). However, the ability to determine either or both of these components from only isolated bones and skeletal fragments, as in the event of a disaster victim identification (DVI), armed conflict investigations or other mass fatality incidents (MFI) is hugely challenging.

Skeletal identification of sexual dimorphism in adults is based mainly on size differences where the male specimen is significantly larger than the female (258), and on functional differences expressed morphologically in regions such as the pelvis. Some of those size differences have been explored in the previous chapter. Examination of sexual dimorphism and population variation of symmetry has generally however been extremely limited (259), and accurate age determination of the skeleton or of skeletal fragments is consequently profoundly more difficult than if comprehensive referenced data were available. The accuracy of morphological assessments is related to the availability of appropriate reference data relating specifically to the growth and development, ethnicity and culture of the population to which the remains are connected.

Body proportions differ between populations due to variation in the genetics of the individuals and the environment in which the population lives. Therefore temporal skeletal changes that occur over time in populations, require that information be periodically updated (258). Well-documented secular or generational data from relevant populations is imperative if an accurate determination of age and sex is to be made from skeletal remains. At present there is a serious lack of osteological developmental information from any

current adult contemporary population (260). The use of inappropriate reference data may be a source of serious error in estimating such variables as height, sex, ethnicity and age.

The most widely used individual long bone for the establishment of stature or height is the femur. Recognised techniques for the evaluation of age using the proximal femur lack precision, with estimates of +/- 5 years representing best practice. Evaluation of the femur to determine biological-age has previously shown a consistent underestimation in those over 50 years (261). It is well accepted that large populations result in more DNA variation than smaller groups, and that genetic diversity is therefore related to population size (262). As the Australian population grows genetically, there is an imperative to also grow (or perhaps more accurately begin to construct) our osteological reference database to account for the morphometric variation.

Forensic osteology is a sub-branch of forensic anthropology that deals with identity determination from skeletal remains for medico-legal reasons (4). The comingling of body parts in DVI and MFI events often hamper efforts to identify remains for repatriation to the appropriate family for burial, and for prosecutorial purposes. The quest to repatriate the remains of family members and to produce appropriate evidentiary material, after such catastrophic events requires the combined efforts of social and scientific disciplines, and it is vitally important to establish validated robust scientific methods to ensure appropriate justice in legal proceedings.

5.1.1 Height and Weight

Before building a contemporary database of femoral osteological variation for anthropological purposes, it is first important to review the most current data available from the living equivalent group. It is also important to evaluate some of the challenges in establishing routine biological measurements such as height and weight from deceased persons.

In 1995 the Australian Bureau of Statistics (ABS) reported that people tended to overestimate their height and under estimate their weight, and as such BMI was found to be a useful tool when self-reporting techniques are used (243). Over four successive self-report surveys conducted during 1990-2005 the weight of Australian men increased from 77.4 kg in 1990 to 83.6 kg in 2005 (an overall increase of 6.2 kg) (263). Broken into age groupings, the increases ranged from 3.5 kg (for 18-24 year olds) to 7.5 kg (for 35-44 year olds). The average height of men increased slightly over the same period to 178.4cm, with the greatest increase (1.6 cm) occurring in the 25-34 years and 35-44 years age groups.

The average weight of females also increased over the period, from 62.6 kg in 1990 to 67.7 kg in 2005 (a total increase of 5.1 kg). An average weight rise was observed across all age groups, ranging from 3.0 kg in the 75 years and over age group to 6.2 kg in the 25-34 years age group. The average height of females also increased marginally during this period to 163.9cm, with the greatest increase (1.8 cm) occurring in the 25-34 years age group (263). Specific Victorian state data available indicate a population ratio of 97.9 men for every 100 women in 2007, slightly up from 97.2 in 2002, and a median age of 36.9 years, slightly up on 2002 level of 36 years (1). A formal enquiry by the author revealed that the ABS has no specific statistics on femoral assessments of any type.

The reconstruction of height from body length has been discussed since the 1800s, with Rollet in 1888 establishing that living height could be estimated from a formula using the length of the femur (264). Various methods have since been used to evaluate height from long bone measurements, with varying degrees of error (265). Changes in height after skeletal maturity is slow and minimal, though there are no longitudinal adult studies to establish a definitive rate, or indeed an evaluation of any of the factors contributing to the changes (266).

There are reports in the literature of an increase of approximately 2cm in supine height in cadavers as opposed to vertical height in the living, which may occur as a result of the lessening of the curvature of the spine (267) but the degree to

which lengthening occurs will certainly depend on the level of rigor present at the time of measurement. Severing of the Achilles tendon (260) has also been discussed as a method of further reducing error from supine measurements, though such invasiveness is difficult to justify given that most height and weight statistics in the living are, as mentioned, based on self-reporting.

5.1.2 Anthropological Bone Evaluation

The gold standard for the morphological investigation of bones has conventionally involved the process of excision and then defleshing prior to examination. Typically, non-destructive imaging methods such as plain x-ray have been used for forensic osteological evaluations, and though bone mineral analysis techniques such as DXA have only occasionally been used for archeology investigations, they are almost never used in forensic anthropology (268). Recently however MDCT techniques have been used for 3D multi-planar reconstructions, removing the need for defleshing (269).

The gold-standard for determining biological-identity from bone tissue is DNA matching. The extraction of DNA able to be used for matching from bone tissue involves pulverisation of a sizeable piece of tissue. Specific DNA investigations of bone and teeth such as nuclear short tandem repeat typing presently require the destruction of a minimum of five grams of bone material from each skeletal fragment tested, and are reported to be more accurate when used on weight-bearing bones (270). Femoral samples however taken for a recent randomised study using International Commission for Missing Persons (ICMP) methods required between 12-22 grams of tissue (271). A specific and accurate reference anthropological dataset will therefore provide useful information for selected and targeted DNA testing of skeletal remains; limiting any unnecessary destruction of biological material. This is also of use in situations where cultural sensitivities preclude the dismemberment of the dead, as in Australian aboriginal communities (262).

It is useful to note that DNA testing is not always able to confer identity. DNA testing reports are issued from the ICMP only if they are within a statistical significance of 99.95% or greater, as part of the kinship-based identification (272). This means that DNA analysis may not be adequate in determining the identity of the deceased, especially if the familial link or reference source is not a biological parent or identical twin. Efforts to use clothing and other physical clues to form an identity or triage destructive testing have also been applied with limited success (273). Various histological techniques have been historically used to evaluate the age of bone specimens with varying degrees of confidence (274-277). No one testing method, including DNA analysis, exists supporting the identification of human remains from skeletal fragments.

The strength in using an MDCT dataset for bone evaluation, apart from the fact that it is non-invasive, is that the morphometry of the femur from surface observation may be enhanced by looking inside the bone architecture. Multi-planar reconstructions improve the utility of CT data. The fine-detail reconstruction methods used have created the opportunity to unearth new ways of examining the external and internal architecture to better understand the changes that are taking place over time.

5.1.3 Overall Study Aim and Objectives

The overall aim of this study was to describe the morphological differences of the human femur related to gender, age and symmetry. Specific objectives were as follows:

- establish the ability to use MDCT data from a mortuary environment for surface and internal morphological investigation using DICOM evaluation software,
- describe sources of measurement error using digital technology and morphological landmarks using a repeated measurement analysis,
- describe a valid protocol for the morphological evaluation of the human femora from the VIFM MDCT data,

- describe expressions of directional asymmetry of morphology for gender and age groups,
- describe morphological differences across age and gender groups,
- calculate and compare the effective doses delivered for clinical and VIFM MDCT procedures,
- predict age, stature and height characteristics from morphological assessments of the femora.

The novel 3D radiological method developed was applied to MDCT 3D reconstructions of the bilateral femora from a current predominantly urban Australian adult population. Changes of a generational nature were evaluated where possible, but were limited due to the relatively short 80-year adult age-range. Where appropriate, data are correlated with findings from chapter four. To assess reproducibility and error, a repeated measurements analysis of variance was conducted.

5.2 Materials and Methods

5.2.1 Sample Description

This study utilised the DICOM datasets (*n*=289) generated in chapter four. Cross-sectional DICOM images of the pelvis and lower limb data were used to generate full 3D reconstructions for each of the bilateral femora. The reconstructed CT slices used to create the 3D images were not isotropic but were overlapped to minimise data file size whilst maximising the signal to noise ratio (183).

The age groupings used for the clinical evaluation in the previous chapter were designed to evaluate small, predominantly age-related changes, and hence an interval age grouping variable was required. This study, designed to evaluate gross 3D adult femoral morphology was predicated on the assumption that the morphological differences of the femora both symmetrically and across the sample, would be small. It was also expected that some of the measurements would communicate generational and gender-based differences that would be

difficult to extract from age-related variation. For this anthropological evaluation therefore, the sample was divided into male and female, and then into those 50 years and under, and those 51 years and over. Figure 60 demonstrates the frequency of those age and gender distributions.

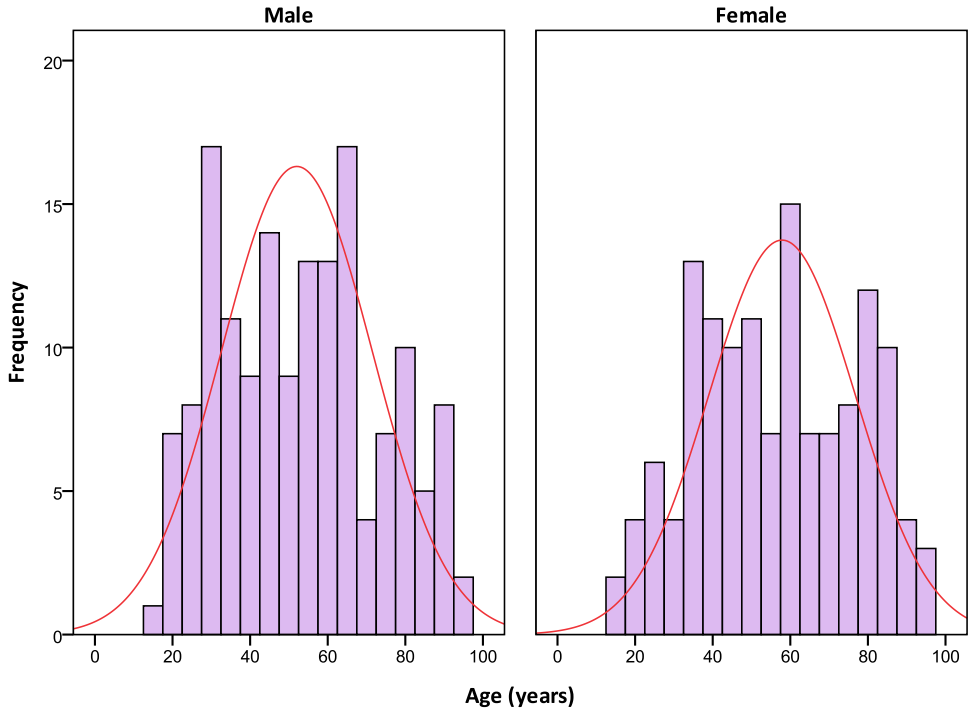

Figure 60 Age histogram males and females in VIFM cohort

When the body was admitted to the VIFM, mortuary staff measured supine length. This value represents the maximal length from the vertex of the skull to the inferior calcaneus of the foot. Those admissions that were too contorted for staff to record a height were not included, based on the impact that the contortion had on the presentation of the hip for QCT analysis. Figure 61 presents a CT representation of the height measurement provided by the VIFM staff.

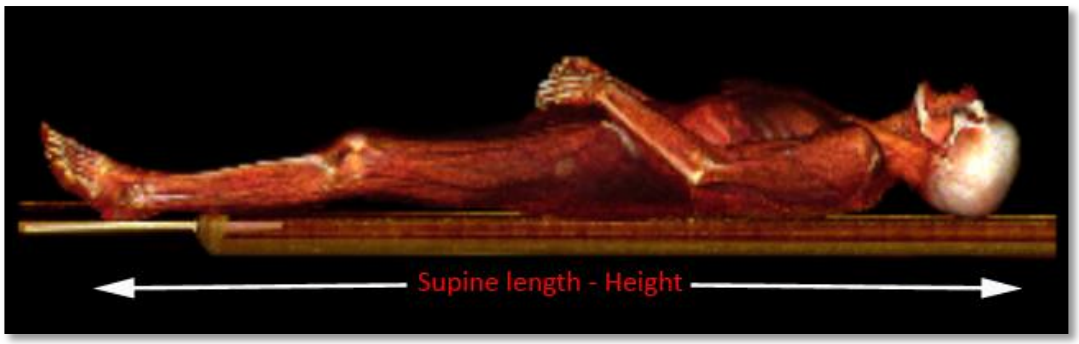

Figure 61 Supine body length or height

During admittance, mortuary staff also recorded the weight of each individual. The bodies were weighed according to a protocol, which includes weighing them with whatever clothing, and other attachments they were wearing or connected to (i.e. shoes, catheters, IV bags etc.) at the time of death. The height and weight for each subject was processed to deliver the body mass index (BMI). Evaluations of individual BMI were made in accordance with WHO guidelines (278, 279). Table 21 reports the WHO classifications of body mass index according to the weight of an individual (kg) divided by the square of their height (metres).

Classification	BMI Range (kg/m^2)
Underweight	**<18.5**
Normal	**18.5-25**
Overweight/Pre-obese	**25-30**
Obese	**>30**
Morbidly Obese	**>40**

Source: Adapted from WHO 1995

Table 21 World Health Organization BMI classifications

5.2.2 Study Design

A cross-sectional study of *n*=289 DICOM datasets of bilateral femora (as per chapter 4) was undertaken. Axial datasets were reconstructed into surface renders using the OsiriX software tool. The program OsiriX (version 3.2.1) is a Macintosh-based DICOM viewing and measurement program available free in 16bit format (http://www.osirix-viewer.com/). OsiriX was used both to convert the DICOM files into 3D volume renders, as well as for the measurements.

The morphometric measurements undertaken were adapted from methods performed using traditional caliper measurements (280). The femur is one of the most commonly measured bones in the body, and the application of 3D imaging methods meant there was a wide range of possibilities for creating a novel 3D reporting template.

Using obvious and reproducible bone landmarks to minimise observer variability was the primary goal in implementing the novel method. Estimates for long and short femur length measurements were made in cases where a total knee replacement device or distal femoral fractures were identified (*n*=4) and epicondylar widths for these cases were entered as missing variables. The same investigator measured all variables. All measurements were performed bilaterally.

Table 22 names the variables and assigns the category for which analysis has been made. A full description of each of the variables is located in section 5.2.4. The structure of the *Results* and *Discussions* sections will broadly follow the headings of the table 22 (percentage directional asymmetry, symmetry, generational and gender and age), and will also include a comprehensive analysis of the physical characteristics of the population used, and the reproducibility evaluation.

Variables	%DA	Symmetry	Generational	Gender & Age
Long Femoral Length	√	√	√	
Short Femoral Length	√	√	√	
Sub-trochanter Width	√	√		√
Mid-femoral Width	√	√		√
Epicondylar Width	√	√		√
Femoral Axis Length	√			√
Femoral Angle	√			√
Avg. Femoral Head Area	√			√
Avg. Hounsfield Units	√			√
Trabecular Margin Length	√			√
Femoral Neck Width (1:4)	√			√

Table 22 Anthropology measurement headings and variables

A particular focus of this research is an analysis of femoral symmetry across both genders and age groupings. As has been the convention in recent anthropological asymmetry evaluations (259, 281), directional asymmetry percentage (DA%) data was generated for comparisons of symmetry between left and right femoral structures.

$$\frac{Right - Left}{Average\ of\ Right\ and\ Left}\ X\ 100$$

Equation 9 Directional asymmetry percentage equation

DA% standardises the raw asymmetric differences from elements measured, and provides a means for directly comparing changes in magnitude for both small and large structures such as femoral length and mid femoral width. The DA% method provides positive values for larger right-sided values and negative values for larger left-right-sided values.

5.2.3 Statistical Methods

Statistical analyses were performed using SPSS statistical software (version 17.0.2, SPSS, Chicago Ill, USA). The subjects have, for the purposes of this work, been separated into age groups as appropriate for the expected magnitude of differences across age and gender groupings. As previously mentioned, this means that for this chapter age has been treated as a gender-based dichotomous variable with the grouping of males and females separated into a group ≤ 50 years and the other representing those > 50 years. Where a linear or quasi-linear relationship has been identified, or is likely between groups, regression modelling techniques have been applied to explore differences in relation to their effect on age prediction. More information on the statistics methods used in these evaluations may be found in **section 3.3.9.**

5.2.4 Morphometric Methods

A total of eleven quantitative measurements were made bilaterally on all cases as previously tabled. External assessments were adapted from conventional caliper-based methods (280). Novel radiological evaluations such as the trabecular margin length were created in an effort to establish an age-based correlation with height and gender data. All measurements were performed on a 3D reconstruction to ensure no variation due to rotation or flexion influences or error from the hip and knee. Some data from chapter four has also been included in the overall evaluation where appropriate.

The long femoral length shown in figure 62 describes the longest vertical measurement of the femur from the proximal femoral head to the inferior border of the medial femoral condyle. The short femoral length, also shown in figure 62, describes the longest vertical measurement of the femur from the superior tip of the greater trochanter to the inferior border of the lateral femoral condyle. The short femoral measurement is of use in a forensic anthropological setting in cases where the femoral neck has been fractured or is missing.

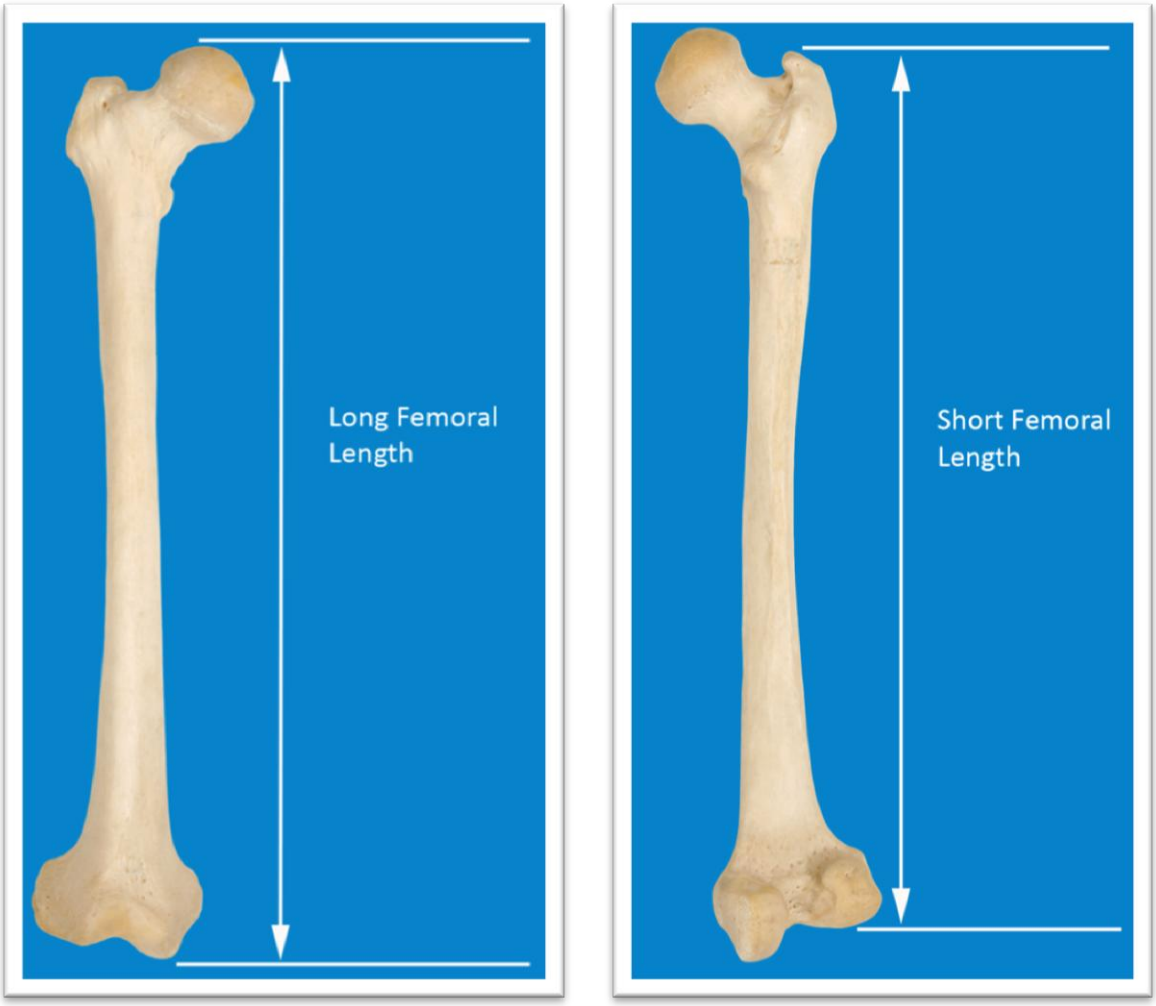

Figure 62 Long and Short Femoral Lengths

The long femoral length is measured from the antero-posterior surface femoral view and the short femoral length is measured using the postero-anterior surface femoral view. (Photography by Chris Owen Melbourne Dental School)

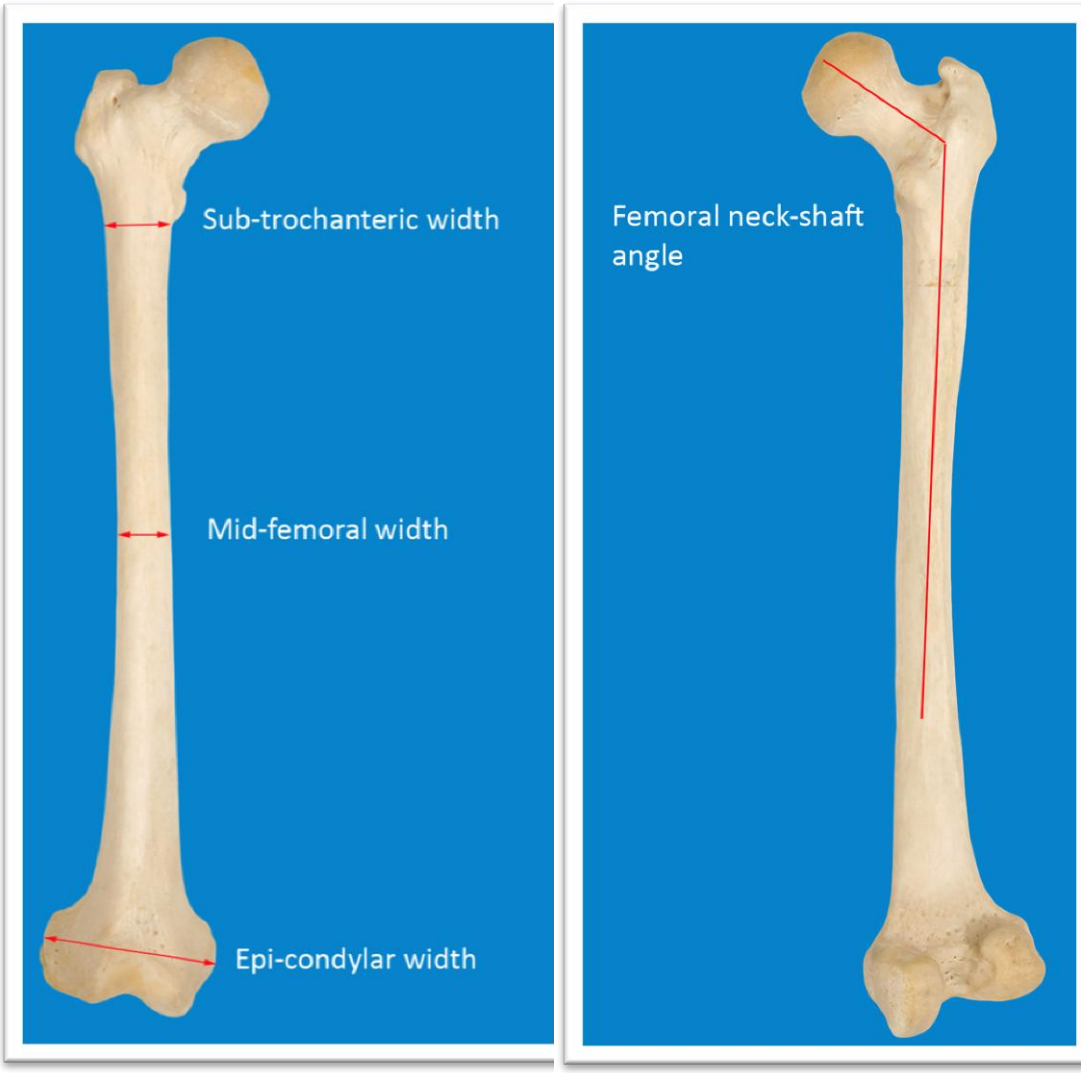

Figure 63 Femoral Width Measurements and Femoral Head Angle

The maximal width measurements taken from each femur are indicated above. They are represented by the three arrowed locations. The other image represents the technique used to derive the femoral neck-shaft angle from the 3D femoral reconstruction. (Photography by Chris Owen Melbourne Dental School)

There were three measurements of maximal width taken from the axial reconstructions and these are identified in figure 63. The epicondylar-width represents the maximum medial to lateral distance immediately below the lesser trochanter. The mid-femoral width measurement represents the maximal medial to lateral distance at a point midway along the long femoral measurement. Lateral width for the measurement was chosen rather than the antero-posterior (AP) diameter, because at this region of the femur, the *linea aspera* is nearly always present on its posterior surface, and it was thought that the variable size of this structure would interfere with a repeatable measurement. The epicondylar-width represents the maximal distance between the medial and lateral epicondyles of the femur. All measurements were chosen using readily identifiable anatomical landmarks.

The femoral neck-shaft angle also shown in figure 62 represents the angle between a line drawn along the AP proximal long axis of the femur, and its intersection with one drawn along the midline of the femoral neck.

The femoral head area measurement shown in figure 63 represents the largest circular/oval region of interest (ROI) that could be fit into the sagittal reconstruction of the hip and acetabulum. The area measurement displayed by the analysis software was recorded as a number rounded to the first decimal place. The Hounsfield units mean provided was also recorded for comparison with the vBMD data from the previous chapter.

The femoral-hip-axis length also in figure 64 represents a midline measurement of the longest distance from the proximal border of the femoral head to the lateral border of the femoral shaft along the line of the femoral neck.

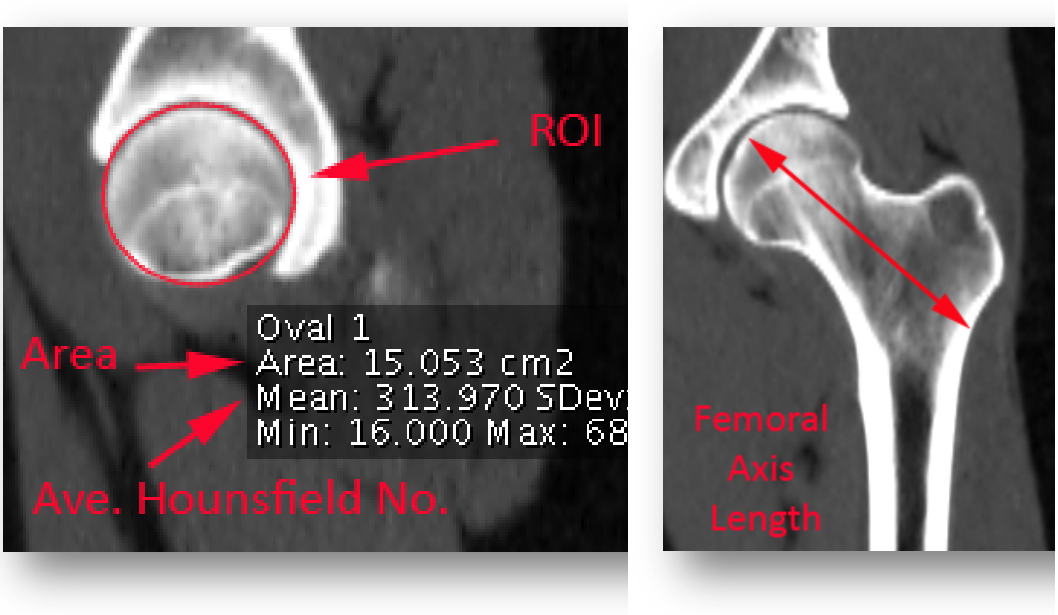

Figure 64 Femoral head area and femoral axis length

The femoral head area represents the largest circular region of interest that was able to be fitted over the sagittal reconstruction of the hip as shown in the red circle. The arrows on the para-sagittal hip reconstruction on the right demonstrate the landmarks used for the determination of the femoral axis length.

The trabecular-margin length of the proximal hip was also measured from a midline para-coronal reconstruction, as shown in figure 65. An axial reconstructed slice through the hip was identified, and then a para-coronal line was drawn along the long axis of the hip. The resultant reconstruction as shown in figure 64, demonstrates the midline of the proximal 1/3rd of the femur. The process was repeated for each individual hip.

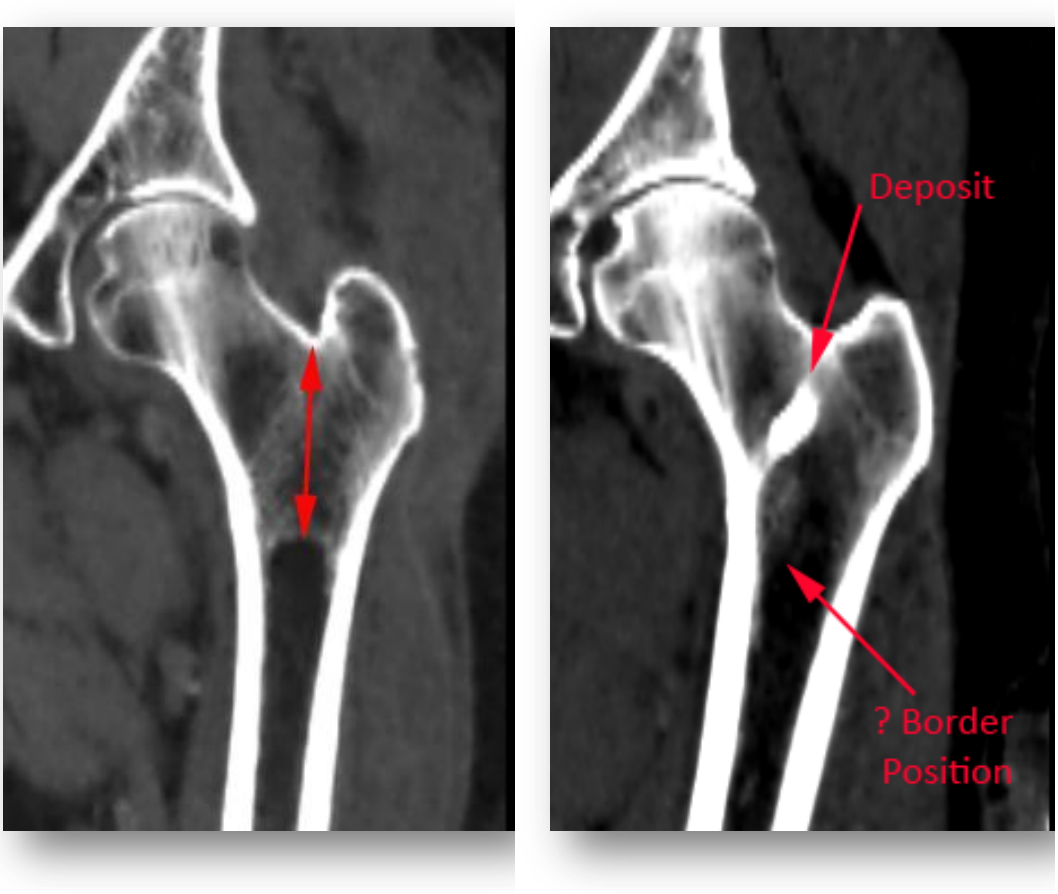

Figure 65 Trabecular margin length

The red arrows on the first image denote the points from which the trabecular margin length measurement was obtained. The second image presents a common challenge in finding the inferior border in some younger people. The image also demonstrates the presence of a heavy metal deposit in the hip.

The trabecular margin was variable in terms of the contour and shape of the inferior border. The upper border of the margin measurement represented the most proximal point of the junction between the greater trochanter and the femoral neck. The lower border represented the most inferior point midline to the inner bone cortex.

The criteria used to determine the trabecular margin length measurement was based on an observational study by Schanz in 1956 that observed a receding of the trabecular border in the humerus (282). Schanz's observations were followed by Ascádi and Nemeskéri in 1970 where they described six-phases of migration of the trabecular margin of the proximal femur (283).

Femoral neck geometry in elderly females has been associated with femoral neck fracture (284). The femoral neck width was measured using the QCT software (discussed in chapter four), which automatically locates a reproducible point along the neck relating to the area with the smallest cross-section. The reference point has a ratio of 1.4 in relation to the height as measured from superior to inferior periosteal surfaces, divided by the width (285). Figure 66 documents the femoral neck width.

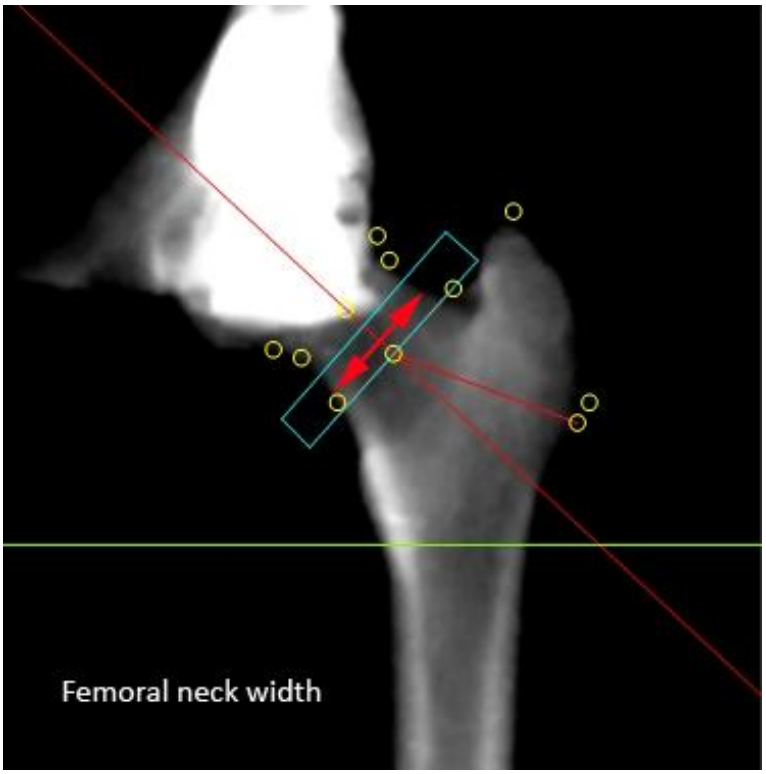

Figure 66 Femoral neck width (FNW)

The red arrows demonstrate the measured distance.

5.2.5 Reproducibility Methods

An evaluation of morphometric variations of the human femur requires easily identifiable landmarks that are also mirrored for a study of bilateral symmetry. The 3D MDCT reconstructions also provide the opportunity to explore measurements deep within the surface structure of the bone which introduces potential error. Poor identification of landmarks is a recognised issue in performing both manual and computational assessments from images (286), and

a significant challenge in using gross morphometric measurements for gender and age determination are the random and systematic errors induced by the subjective identification of reference points and bone orientation generally (287). Precision was calculated using an inter-observer study.

The test was performed as blind study 8-months after completing the first evaluation. Thirty individuals (or approximately 10% of the total cases) were randomly chosen. Two from each male and female decade cohort were selected, though only one female and one male were selected from the youngest decade cohort, as their contribution to the overall sample was small (males *n*=6, females *n*=5). Nine of the measurements were re-evaluated bilaterally (total of 18 measurements per individual) using the same OsiriX™ version software and computer as used in the original evaluation. Automated measurements obtained using the QCT package were not included in the re-evaluation.

5.3 Results

5.3.1 Physical Features

Age, Height, Weight and BMI

The average age of the population was 54.48 years. The average age of the males (53.03 years) was slightly less than the average for the females (56.17 years). The mean age of the ≤50 year group was 34.8 years for the males and 36.1 years for the females. The mean age of the >50 years group was 69.3 for the males and 71.0 years for the females. On average therefore, the males were 16-months younger than the females between younger groups, and between older groups the males were 20-months younger than the females.

Table 23 describes the mean height, weight and BMI for all cases, separated by age and gender categories.

		Height (cm)		Weight (kg)		BMI	
		Mean	Std Dev	Mean	Std Dev	Mean	Std Dev
Male	≤50 years	176	7.50	82.6	17.75	26.66	5.00
	>50 years	171	6.93	77.0	15.38	26.36	5.12
Female	≤50 years	164	6.10	66.2	14.74	24.58	5.14
	>50 years	158	6.25	69.8	16.89	27.75	5.53

Table 23 Height, weight and BMI mean values

On average the males from the younger group (176cm) were 3% taller than those from the older group (171cm), and for females, the younger group (164cm) had a mean height 4% taller than the older group (158cm). The difference in mean height between genders was a 7% male height advantage (12cm taller) for the young groups and an 8% height advantage (13cm taller) to the older males. Mean heights using the clinical groups from chapter 5 have also been produced for comparative purposes and is presented as figure 67.

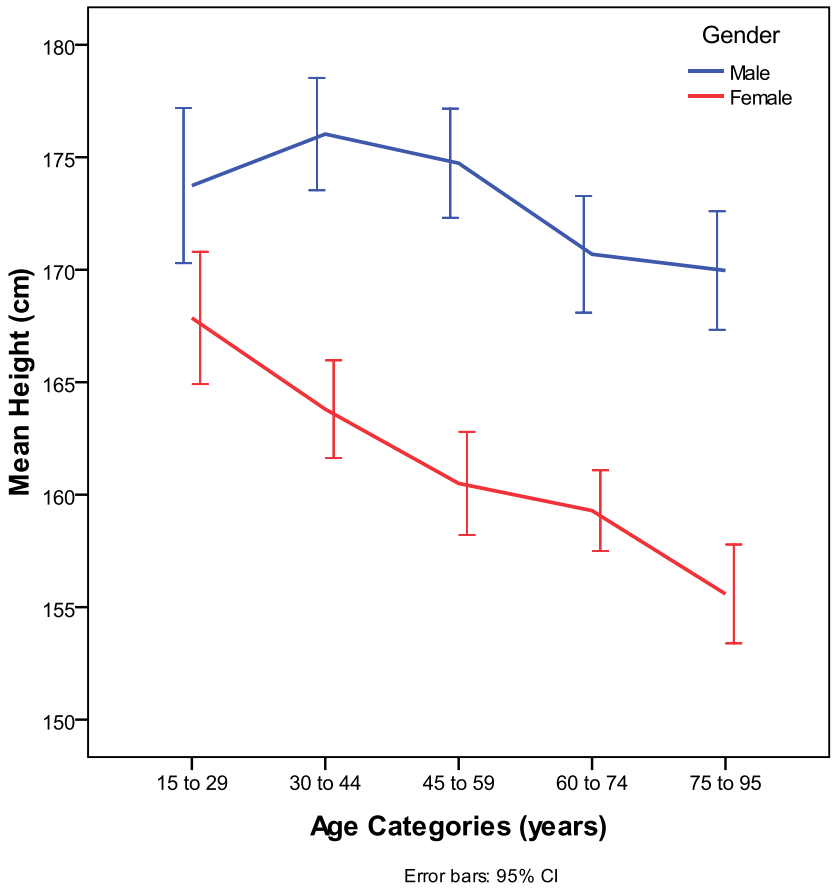

Figure 67 Height against age - clinical age groups

Significant (p<0.001) differences were observed for the clinical age groupings between the mean heights for males and females in all age categories except the youngest age category.

Using the dichotomous age groupings (≤50 years and >50 years), the mean weight for the older male group (77kg) was 7% less than that of the younger group (82.6kg). For the females however, the mean weight for the older group (69.8kg) increased by 5% when compared to the mean of the younger group (66.2kg). The difference in mean weight between genders showed a 20% (16.4kg) heavier male between younger groups, and a 16% (12.8kg) heavier male between older groups.

A logical theory would present that the taller the individual, the larger the expected weight, but no significant association between weight and height was observed for either age group or for either gender.

The mean BMI of both male groups was similar with only a 1% higher mean recorded for the younger male group (26.66 kg/m^2) compared to that of the older group (26.36kg/m^2). The females however differed markedly between age groups, with an 11% higher mean BMI recorded for the older group (27.75 kg/$m^{2)}$ in comparison to that of the younger group (24.58 kg/m^2). The mean BMI of young female group was the only BMI within the WHO normal range. All other age groups occupied the obese category.

BMI averaged by gender demonstrated small gender differences with the males recording an average of 26.51 kg/m^2 and the females 26.17 kg/m^2, both of which are classified as overweight. Recent studies of the living Australian population record that currently 50% of those over the age of 25 have body mass indices above the healthy range (288).

5.3.2 Reproducibility

The following results relate to the repeated measurements conducted on nine bilateral measures manually obtained using OsiriX™. Table 24 describes the mean values from each of the original and repeated measurements of the left and right sides. The suffix (2) denotes mean results from the second analysis.

Right Side	Mean	Std Dev	Left Side	Mean	Std Dev
long femur length (mm)	445.56	29.39	long femur length (mm)	446.46	29.03
long femur length2 (mm)	445.67	29.88	long femur length2 (mm)	446.17	29.56
short femur length (mm)	421.29	28.65	short femur length (mm)	421.08	28.50
short femur length2 (mm)	422.80	29.26	short femur length2 (mm)	423.07	28.79
sub-trochanter width (mm)	30.97	2.73	sub-trochanter width (mm)	30.47	2.76
sub-trochanter width2 (mm)	31.15	2.69	sub-trochanter width2 (mm)	30.83	2.51
mid-femoral width (mm)	27.38	3.50	mid-femoral width (mm)	27.65	3.23
mid-femoral width2 (mm)	27.59	2.86	mid-femoral width2 (mm)	27.84	2.86
epicondylar width (mm)	79.63	7.15	epicondylar width (mm)	79.62	6.89
epicondylar width2 (mm)	79.76	6.90	epicondylar width2 (mm)	79.45	6.64
femoral axis length (mm)	95.57	8.13	femoral axis length (mm)	95.00	7.40
femoral axis length2 (mm)	95.44	7.37	femoral axis length2 (mm)	95.38	6.81
femoral head area (cm^2)	16.04	2.67	femoral head area (cm^2)	15.69	2.62
femoral head area2 (cm^2)	15.85	2.75	femoral head area2 (cm^2)	15.73	2.56
femoral head Hounsfield avg.	339.83	68.24	femoral head Hounsfield avg.	339.83	69.96
FH Hounsfield avg2	340.87	74.77	FH Hounsfield avg2	346.30	69.57
AP trab. margin length (mm)	52.07	9.62	AP trab. margin length (mm)	54.40	8.56
AP trab. margin length2 (mm)	52.39	8.98	AP trab. margin length2 (mm)	52.77	8.11

Table 24 Reproducibility mean results - left and right

Although the mean and standard deviation between the two separate investigations demonstrate good correlation, there is a possibility that results are misleading due to the power of averaging in using a significant sample size as large as 30. For example, if there was a +2mm difference in one measurement, and a -4mm variation in another, together they produce a net difference of zero which does not give a true indication of the degree of variability. The repeated measures analysis was performed to evaluate these individual variations. Bilateral evaluations are included as table 25.

Multivariate Test **Right Side**	F	*p*	Partial Eta Squared
Right long femur	.671[a]	.420	.023
Right short femur	13.494[a]	<0.01	.318
Right sub-trochanter width	.754[a]	.392	.025
Right mid-femoral width	.721[a]	.403	.024
Right epicondylar width	.336[a]	.566	.011
Right axis length	.127[a]	.725	.004
Right femoral head volume	2.748[a]	.108	.087
Right head Hounsfield average	.042[a]	.839	.001
Right trabecular margin	.278[a]	.602	.009

Multivariate Test **Left Side**	F	*p*	Partial Eta Squared
Left long femur	.180[a]	.674	.006
Left short femur	19.087[a]	<0.01	.397
Left sub-trochanter width	2.305[a]	.140	.074
Left mid-femoral width	.631[a]	.433	.021
Left epicondylar width	.372[a]	.546	.013
Left axis length	1.377[a]	.250	.045
Left femoral head volume	.092[a]	.764	.003
Left head Hounsfield average	1.749[a]	.196	.057
Left trabecular margin	10.697[a]	.003	.269

Table 25 Multivariate test results – right and left

Significance is indicated in the table (*p*) as is the effect size (partial eta squared). Areas where the results indicate significant variance are highlighted in yellow.

Significant variation ($p<0.05$) was observed for both left ($F=13.494$, $p<0.001$) and right ($F=19.087$, $p<0.0001$) short femoral length, and for the left trabecular margin length ($F=10.697$, $p<0.003$). The size of the difference indicated by the partial Eta Squared is small for all other variables where no significant variation

has been found. For the right short femur (32%), the left short femur (40%) and the left trabecular margin (27%) the differences are however large.

5.3.3 Symmetry Evaluation

The symmetry results are presented in two parts. Firstly as a %DA to ascertain a general morphometric pattern, and then as a detailed symmetrical evaluation of only those variables indicated in the %DA findings.

% Directional Symmetry

Two tables have been produced from the analysis and are presented as table 26 and 27. The first highlights all percentage differences where the left side is the largest value (i.e. is dominant). The second table highlights which of the groups %DA express the highest and lowest (i.e. the extremes) values for each of the variables.

	% Directional Asymmetry Mean Values - Dominance							
	Male				Female			
	Age Category				Age Category			
	50 and under		51 and over		50 and under		51 and over	
	Mean	Std Dev	Mean	Std Dev	Mean	Std Dev	Mean	Std Dev
% DA long femur length	-.27	1.0	-.18	1.0	-.21	1.1	-.23	1.2
% DA short femur length	-.08	0.6	-.11	0.7	.01	0.7	-.13	0.7
% DA sub-trochanter width	1.23	4.4	.21	3.8	.89	3.5	.42	3.3
% DA mid-femoral width	-1.21	5.3	-1.58	4.0	-2.49	5.6	-.95	5.6
% DA epicondylar width	.07	2.2	-.18	1.8	-.33	2.1	-.34	1.9
% DA femoral axis length	.47	2.0	.10	1.6	-.29	1.7	-.19	1.7
% DA trabecular margin length	.21	11.8	-.11	12.0	1.02	15.6	-1.29	16.0
% DA femoral angle	.01	1.5	.40	1.2	.41	1.6	-.09	1.2
% DA femoral neck width	-.57	4.2	.33	3.4	.53	4.5	.38	4.7
% DA femoral head area	.39	4.7	.53	4.5	.62	5.3	.15	6.3
% DA femoral head HU average	.66	9.2	.06	13.6	2.34	9.5	-1.77	15.4

Table 26 Percentage Directional Asymmetry Mean Values – Dominance

Left Dominance (RED) and Right Dominance (BLUE)

	% Directional Asymmetry Mean Values - Extremes							
	Male				Female			
	Age Category				Age Category			
	50 and under		51 and over		50 and under		51 and over	
	Mean	Std Dev	Mean	Std Dev	Mean	Std Dev	Mean	Std Dev
% DA long femur length	-.27	1.0	-.18	1.0	-.21	1.1	-.23	1.2
% DA short femur length	-.08	0.6	-.11	0.7	.01	0.7	-.13	0.7
% DA sub-trochanter width	1.23	4.4	.21	3.8	.89	3.5	.42	3.3
% DA mid-femoral width	-1.21	5.3	-1.58	4.0	-2.49	5.6	-.95	5.6
% DA epicondylar width	.07	2.2	-.18	1.8	-.33	2.1	-.34	1.9
% DA femoral axis length	.47	2.0	.10	1.6	-.29	1.7	-.19	1.7
% DA trabecular margin length	.21	11.8	-.11	12.0	1.02	15.6	-1.29	16.0
% DA femoral angle	.01	1.5	.40	1.2	.41	1.6	-.09	1.2
% DA femoral neck width	-.57	4.2	.33	3.4	.53	4.5	.38	4.7
% DA femoral head area	.39	4.7	.53	4.5	.62	5.3	.15	6.3
% DA femoral head HU average	.66	9.2	.06	13.6	2.34	9.5	-1.77	15.4

Table 27 Percentage Directional Asymmetry Mean Values – Extremes

Extremes of high difference **(PINK)** and low difference **(GREEN)** of symmetry

Comparisons using Table 26 results demonstrate that the older female group express a strongly left-sided dominant tendency (i.e. the left values are greater than the right values) in all but the sub-trochanteric-width, femoral-neck-width and femoral-head-area. Both male groups and the younger females do not show the same degree of left-sided dominance, though all groups share larger left-sided mean values for the long femoral length and mid-femoral-width. The sub-trochanteric-width and the femoral-head-area are the only two variables where the right-sided values are higher than the left for all groups. Overall, of the eleven variables tested, both the younger males and females had only four variables observed to be left dominant, while for the older males the total was five. The older females however were observed to have eight out of eleven variables with left-sided values larger than those of the right.

Table 27 results demonstrate that, there are only 4 of the 11 variables where the extreme values (i.e. highest and lowest % differences) are not shared by the one gender. They are the epicondylar-width, trabecular-margin-length, femoral-angle and femoral head Hounsfield unit average. The females have seven of the values of highest difference, while the males have eight of the lowest differences.

Of those variables where the percentage difference of the mean values is above 1%, the young male group has two variables (sub-trochanter and mid-femoral widths), and the older males have only one (mid-femoral width). The older females have two variables with a greater than 1% variation (trabecular margin and Hounsfield unit average) while the younger females have the largest number of variables, at three (mid-femoral width, trabecular margin length and Hounsfield unit average). The mid-femoral width is the most asymmetric variable in percentage difference terms, while the femoral angle is the most symmetrical feature measured.

Assuming that the femur does not increase perceptibly in length over the period of adult life, and taking into account evidence of femoral periosteal apposition

established in chapter 4, a further evaluation of symmetry was performed. The sub-trochanteric, mid-femoral and epicondylar widths were evaluated for symmetry seeking trends for both age groups and genders.

Long Femoral Length Symmetry

Symmetry between left and right long femoral lengths was measured. Significant *(p*<0.01) difference between the mean values of long femoral length were found, with the left measurement on average longer (0.98mm) than the right and which is documented in figure 68.

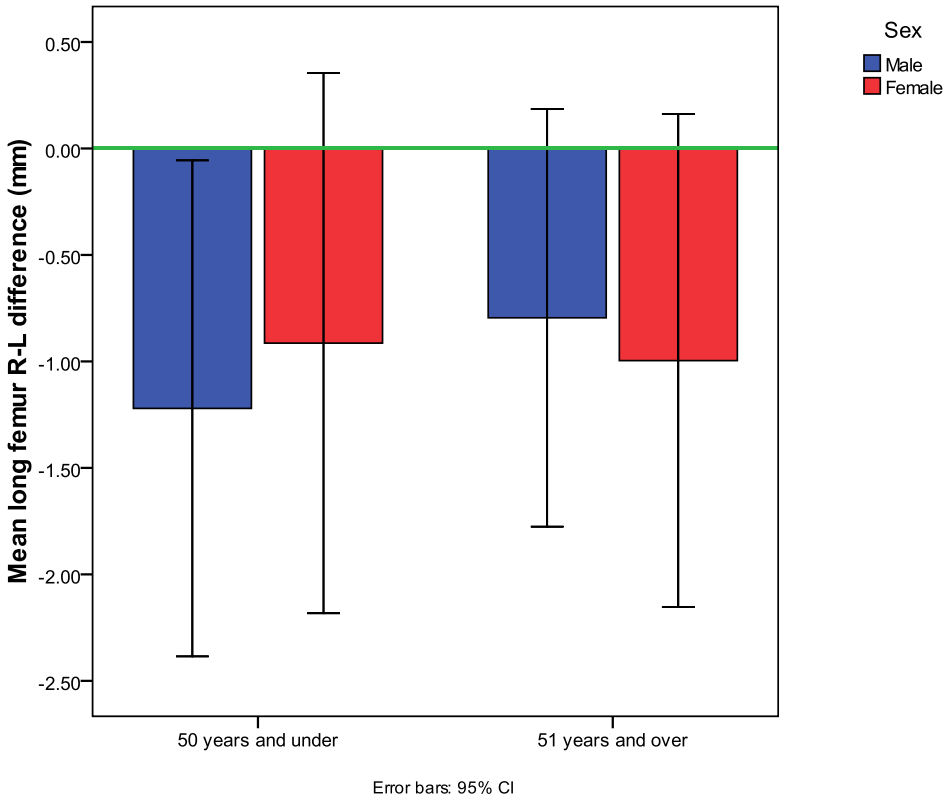

Figure 68 Mean long femoral length difference

The asymmetry observed is likely associated to a leg dominance in humans which is similar to right handedness that accounts for approximately 80-90% of the world's population (289). No information relating to handedness for this population was available.

The study population (*n*=289) was filtered to select only those cases where the left long femur measured longer than the right. 56% of males (*n*=87) and 52% (*n*=70) of females had left long femoral measurements longer than their right, representing an average of only 54%.

Short Femoral Length Symmetry

An evaluation of symmetry between left and right short femoral lengths showed significant *(p*=0.027) differences between the mean values of maximal length, with the left measurement on average slightly longer (0.56mm) than that of the right, expressing a similar trend to that exhibited in the long measurement. Findings are documented in figure 69.

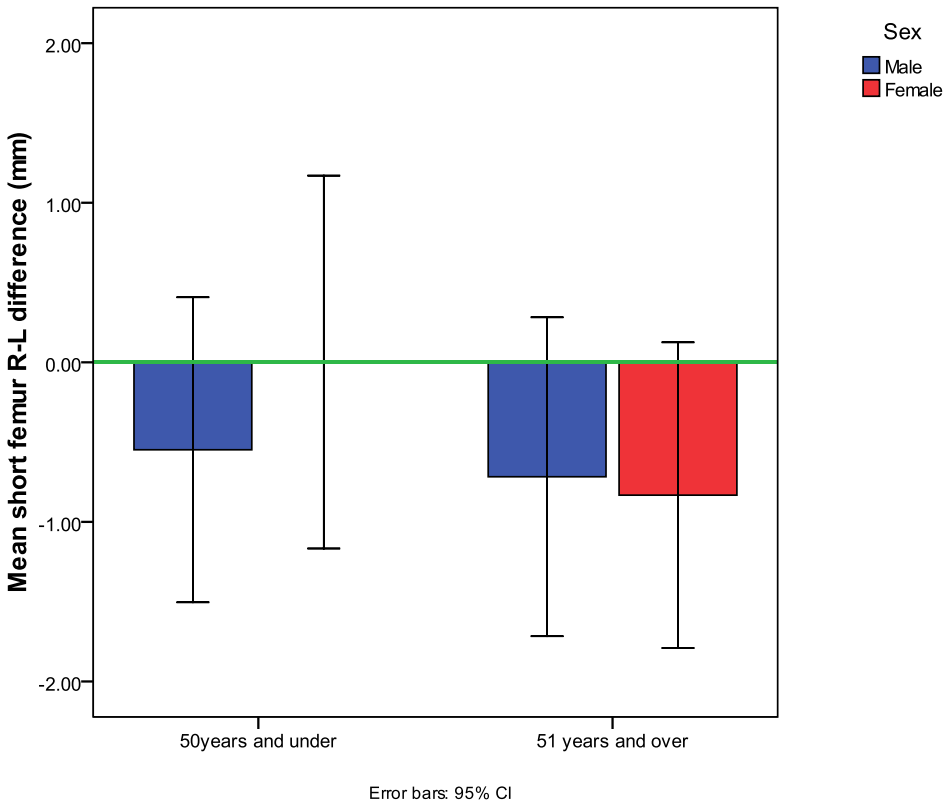

Figure 69 Mean short femoral length difference

A longer left-sided mean value was not observed in the female 50 and under group, where the mean values of the short femoral lengths are identical. The error bars for the group are also slightly greater than for the other three age groupings indicating a higher variability in the measurement,

Sub-Trochanter Width

No significant difference (p=0.005) between the sub-trochanter measurements for left and right were shown.

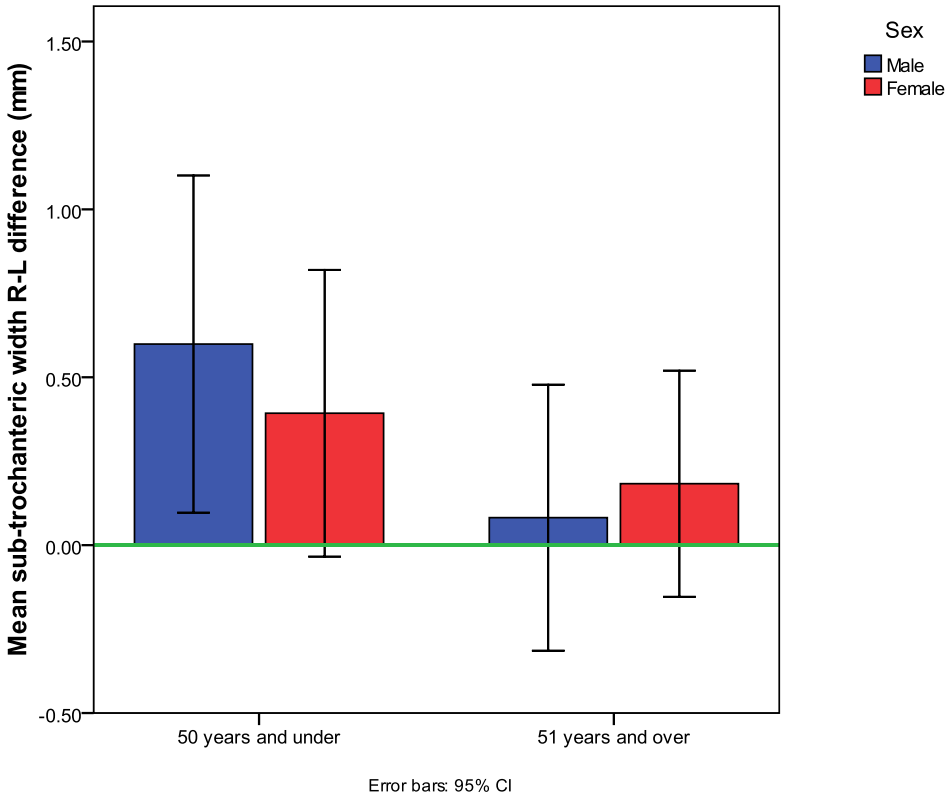

Figure 70 Mean sub-trochanter width difference

Figure 70 documents a slightly wider measurement for the right side as compared to the left on average, though results show no consistency for gender or age group, and weak association for the bias for the older males and females.

Mid- Femoral Width Symmetry

Symmetry assessment between left and right mid-femoral widths found a significant (p<0.01) difference between the mean values of maximal width within the group. Results are documented as figure 71.

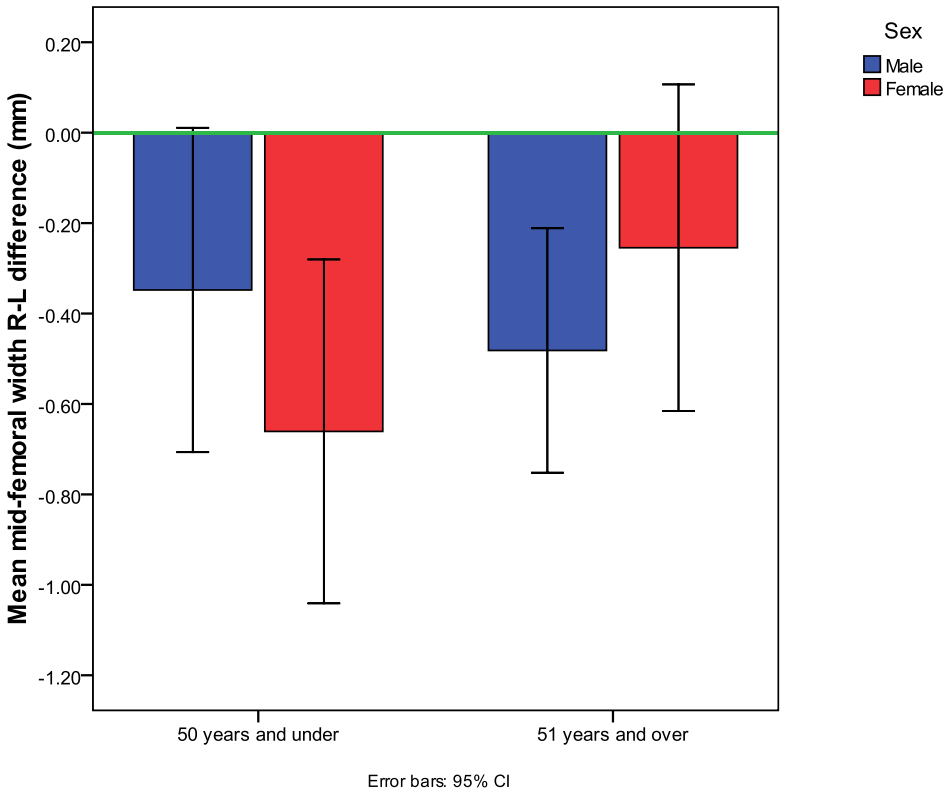

Figure 71 Mean mid-femoral width difference

The left-sided mean measured slightly wider (average of 0.4mm) than the right. Similar to all other significant symmetrical differences, the difference does not demonstrate any consistent trend when comparing the younger with the older groups, or between males and females, though is less obvious in the older groups.

Epicondylar Width Symmetry

No significant difference (p=0.104) was established between the epicondylar width measurements for left and right sides.

5.3.4 Generational Differences

The primary source of evidence for a secular or generational change for the investigation was derived from the long femoral length and its relationship to height. Therefore an evaluation of the differences in height as a function of femoral length, age and gender were conducted.

Height, Gender and Age Regression Equations

Results from linear regression modelling to predict height using age and gender are presented in table 28.

Category	Height (cm) Equation
Males	178.58 – (0.029 x age in years)
Females	170.62 – (0.179 x age in years)

Table 28 Height as a function of age regression equations

Results according to the model demonstrate that while females are generally shorter than males, they decline in height more quickly as a function of age. The model also demonstrates that there is a statistically significant interaction between age and gender as a predictor for height (p = 0.047).

Long Femoral Length

An evaluation of the contribution of the femur to the overall height of the subjects was then undertaken to establish generational variation over the two age categories for each gender.

The relationship between height and maximal femoral length was calculated for both males and females by dividing the height measurement (mm) by the long femoral length average (mm). The percentage contribution of the femur to overall height for each of the groups was calculated by dividing the mean height (mm) into the mean long femoral length (mm) and multiplying by 100. Table 29 documents the mean values for these four variables for each gender and age group.

	Relationship of Height to Long Femoral Length			
	≤ 50 years		> 50 years	
	Male	Female	Male	Female
	Mean	Mean	Mean	Mean
Height (mm)	1756.58	1640.00	1708.90	1579.87
Left long femur length (mm)	470.9	434.6	463.8	427.0
Height to Long Femur Ratio	3.74	3.78	3.69	3.71
% Long femur to height	26.82	26.51	27.14	27.02

Table 29 Height and long femoral values

Height assessments demonstrated significant differences (p<0.001) between the mean heights of males and female in the younger and older age categories. The larger mean height of the younger males compared to that of the older male group (2.71% taller younger males) was smaller than the mean height difference comparing the older females with their taller and younger female counterparts (3.67% taller younger females). These data demonstrate that females in this group gained a generational height advantage at a quicker rate than did the males.

The length of the femur will alter very little throughout the adult lifespan, especially in this VIFM population as these data do not include those with degenerative bone conditions such as severe osteoarthritis that would affect the long measurement. As other weight-bearing supports such as the spinal column are known to deteriorate with increasing age (290), the long femoral length may then be used as calibration standard for evaluating height-based changes occurring as a result of increased age. Evaluating the differences in percentage contribution to height from the long femoral length (see table 29) is therefore a practical means by which the mean ageing effects may be examined.

The effect of age on height from these data is observed to be more pronounced in females (decrease of 0.51%) than in males (decrease of 0.32%) using the

percentage contribution of the long femoral length to height differences between the two age groupings. Females are therefore shown to lose slightly more height from age-related sources than do males.

Long Femoral Length and Height Regression Equations

Linear regression modelling was performed for each category of data, all, males, females and then both age groups of each of the male and female groups. A full series of calculations is labelled appendix 5B, and a table of the equations are included as table 30.

Category	Height Equation
All	(2.77 x length of long femur in cm) + 43.082
All Males	(2.23 x length of long femur in cm) + 65.910
Males ≤ 50 years	(2.39 x length of long femur in cm) + 63.616
Males > 50 years	(2.08 x length of long femur in cm) + 74.792
All Females	(2.41 x length of long femur in cm) + 57.070
Females ≤ 50 years	(2.09 x length of long femur in cm) + 73.545
Females > 50 years	(2.31 x length of long femur in cm) + 59.630

Table 30 Long femoral length regression equations for height

The model demonstrates a significant interaction between age and gender as a predictor for height.

Short Femoral Length

The relationship between the long femoral measurement and the short femoral measurement was evaluated to establish the usefulness of the short measure as an appropriate substitute for the long measurement when the femoral head region is damaged or missing. Mean values for the right and left short femoral length

including an average percentage contribution to the long femoral measurement is included as table 31.

	≤ 50 years		> 50 years	
	Male	Female	Male	Female
	Mean	Mean	Mean	Mean
Right short femur length	443.0	409.3	438.1	404.1
Left short femur length	443.5	409.3	438.8	405.0
% Short femur to long	**94.19**	**94.17**	**94.62**	**94.85**

Table 31 Short femur mean values and percentage contribution to long femur

For both males and females in the younger groups, the short femur length mean represents just over 94% of the long mean value. For males and females in the older groups, the short length average represents closer to 95% of the long value.

Short Femoral Length and Height Regression Equations

Regression modelling was performed for the short femoral length as a function of gender and age. The equations are included as table 32, and a full series of calculations may be found as appendix 5C.

Category	Height Equation
All	(2.94 x length of short femur in cm) + 42.654
Males	(2.45 x length of short femur in cm) + 65.346
Males 50 and under	(2.63 x length of short femur in cm) + 59.038
Males 51 and over	(2.16 x length of short femur in cm) + 76.282
Females	(2.47 x length of short femur in cm) + 60.184
Females 50 and under	(2.25 x length of short femur in cm) + 71.933
Females 51 and over	(2.36 x length of short femur in cm) + 62.798

Table 32 Short femoral length regression equations for height

The differences between age and gender groups modelled similarly to the long femoral results.

5.3.5 Gender and Age Differences

All measurements except for long and short femoral lengths (evaluated as generational) have been included in an evaluation of gender and age influences. Comparisons of the various width measurements of males and females were significantly different (p<0.05).

Femoral Widths and Ratios

Three maximal width measurements of the femur at points immediately inferior to the lesser trochanter (sub-trochanter), mid femur and at the epicondyles of the knees were analysed. The purpose of the three evaluations was to establish quantitative evidence for femoral apposition with increasing age. Mean values for each of the variables as well as their averaged results for each age group and gender is included as table 33.

All variables measured in mm	Femoral Widths							
	≤ 50 years				> 50 years			
	Male		Female		Male		Female	
	Mean	Std Dev	Mean	Std Dev	Mean	Std Dev	Mean	Std Dev
Right sub-trochanter width	32.5	3.0	30.0	2.6	32.7	2.5	30.3	2.3
Left sub-trochanter width	31.9	2.5	29.6	2.4	32.6	2.6	30.1	2.2
Avg. sub-trochanter width	32.2	2.5	29.8	2.3	32.6	2.4	30.2	2.1
Right mid-femoral width	29.4	2.8	25.2	2.9	30.6	2.4	27.7	2.4
Left mid-femoral width	29.7	2.7	25.8	3.2	31.1	2.3	27.9	2.3
Avg. mid-femoral width	29.5	2.6	25.5	3.0	30.8	2.3	27.8	2.2
Right epicondylar width	83.3	4.9	73.9	3.8	84.7	4.7	74.2	4.0
Left epicondylar width	83.2	4.8	74.3	4.1	84.9	4.6	74.6	4.1
Average epicondylar width	83.2	4.7	74.1	3.8	84.8	4.5	74.4	3.9

Table 33 Femoral width mean values

In an effort to separate the effects of age-related surface apposition and those associated with individual differences in femoral length, the three width

measurements were divided into the long femoral length measure. This created a ratio of width as a proportion of length, and the results are included as table 34.

	Long Femoral Length - Femoral Width Ratios							
	Male				Female			
	≤ 50 years		> 50 years		≤ 50 years		> 50 years	
	Mean	Std Dev	Mean	Std Dev	Mean	Std Dev	Mean	Std Dev
R long femur to sub-trochanter ratio	14.54	1.23	14.23	1.01	14.52	1.20	14.12	1.05
L long femur to sub-trochanter ratio	14.83	1.17	14.29	.97	14.74	1.19	14.23	1.01
R long femur to mid-femur width ratio	16.09	1.33	15.19	1.05	17.45	2.24	15.49	1.23
L long femur to mid-femur width ratio	15.95	1.43	14.98	.99	17.06	2.26	15.38	1.16
R long femur to epi-condyle ratio	5.65	.33	5.48	.31	5.88	.34	5.75	.29
L long femur to epi-condyle ratio	5.67	.31	5.47	.32	5.86	.35	5.73	.28

Table 34 Long femur to femoral widths mean ratios

Results from the length-width ratio analysis demonstrate a lower ratio of mean width for each of the right and left values in the older groups compared to the younger ones. This finding establishes evidence for surface apposition changes for both genders, assuming again that the length of the femur remains constant throughout adult life.

Older males and females demonstrate a 3% wider sub-trochanter and epicondylar-width ratio compared to that of the younger groups. Analysis of the mid-femoral width ratio demonstrates a 6% wider ratio for the males and 10% wider ratio for the females. Results therefore indicate a slightly larger effect of periosteal apposition in females than for males for the mid-femoral measurement.

Sub-Trochanter Width

Overall, the widest sub-trochanter mean was demonstrated by the older males, though it was only 1% more than the young males. The young females were observed to have the narrowest mean sub-trochanter width, but again this was only about 1% less than the older females. For the younger age group, the males had a mean width 8% wider than the young females, and the older males had a mean width that was also 8% greater than the older females. A summary table of the percentage differences of the averaged sub-trochanter widths between age groups and gender is provided in table 35.

Sub-trochanter	M ≤ 50 years	M > 50 years	F ≤ 50 years	F >50 years
M ≤ 50 years	NA	↓ 1%	↑ 8%	↑ 6.5%
M > 50 years	↑ 1 %	NA	↑ 9%	↑ 8%
F ≤ 50 years	↓ 8%	↓ 9%	NA	↓ 1%
F >50 years	↓ 6.5%	↓ 8%	↑ 1%	NA

Table 35 Sub-trochanter % differences

Overall, the sub-trochanter width demonstrates clear differentiation between male and female samples which is shown in figure 72. Using the broad dichotomous age categories, no significant difference of sub-trochanter width between age groups of the males (p=0.299) or females (p=0.349) was observed.

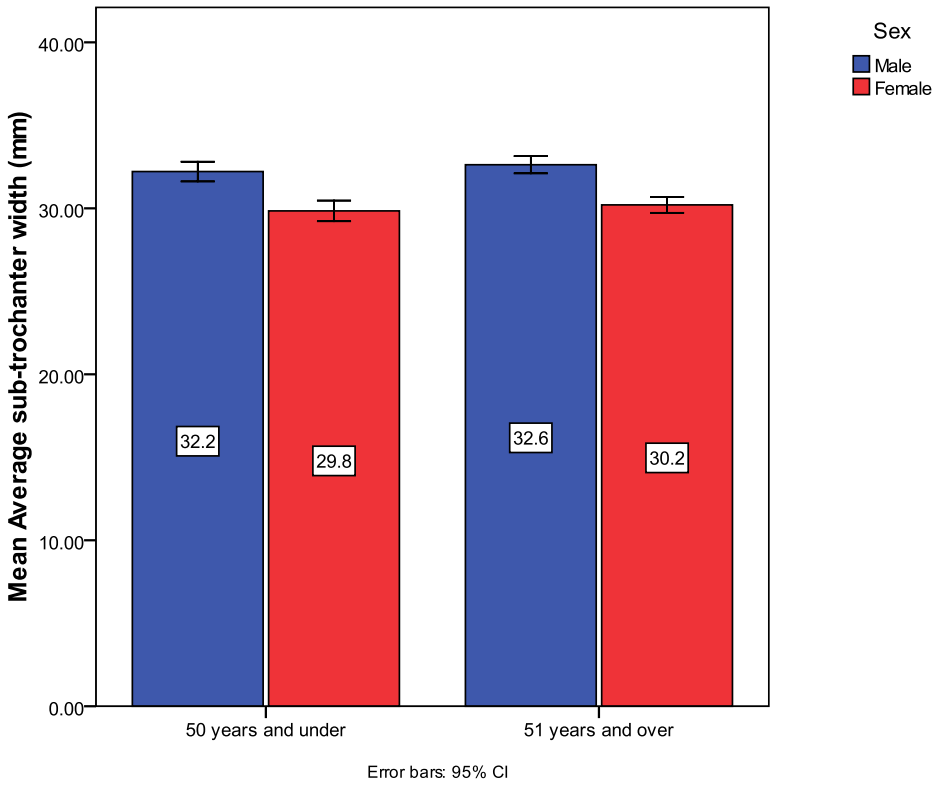

Figure 72 Averaged mean sub-trochanter width

Mid-Femoral Width

When the right and left mid-femoral widths were averaged, again the narrowest mean width was exhibited by the young females and the widest by the older males. Comparing genders between age groups, the older females had a mean mid-femoral width 8% wider than their younger group. The older males however had only a 4% greater average mean width when compared with their younger group.

When comparing between the sexes, the young males had a 13.5% wider average mean mid-femoral width measurement compared to the young females, though only a 10% wider measurement is observed for the older males in comparison the older females. A summary table of the % differences of the mid-femoral widths between age groups and gender is provided in table 36.

Mid-femoral	M ≤ 50 years	M > 50 years	F ≤ 50 years	F >50 years
M ≤ 50 years	NA	↓ 4 %	↑ 13.5%	↑6 %
M > 50 years	↑ 4 %	NA	↑ 13%	↑ 10%
F ≤ 50 years	↓ 13.5%	↓ 13%	NA	↓ 8 %
F >50 years	↓ 6%	↓ 10%	↑ 8 %	NA

Table 36 Mid-femoral % differences

Overall, the mid-femoral width demonstrates clear differentiation between male and female bone samples as shown in figure 73. Using the broad age categories, significant differences between the mid-femoral width between age groups for the males (p=0.001) and females (p≤0.001) were observed. In this observation, apposition appears more rapid in females than in males.

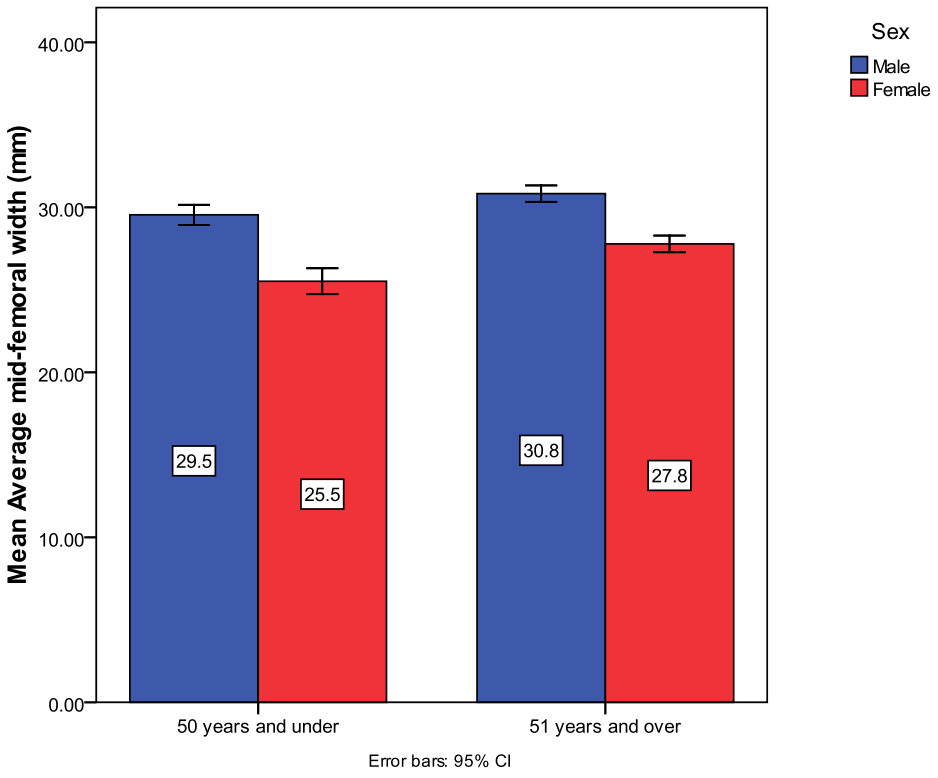

Figure 73 Averaged mean mid-femoral width

Epicondylar Width

When averaged values were compared within gender groups, the young females had the most narrow epicondylar width, though the older females had a mean

width only 0.5% wider. For the males, the older group had a mean width 2% wider than the younger males. The young males had mean epicondylar widths 11% wider than did the young females, while the older males had a 12% width advantage over the older females. A summary table of the % differences of the averaged epicondylar widths between age groups and gender is provided in table 37.

Epicondylar	M ≤ 50 years	M > 50 years	F ≤ 50 years	F >50 years
M ≤ 50 years	NA	↓ 2%	↑ 11%	↑ 11%
M > 50 years	↑ 2%	NA	↑ 12.5%	↑ 12%
F ≤ 50 years	↓ 11%	↓ 12.5%	NA	↓0.5 %
F >50 years	↓ 11%	↓ 12%	↑ 0.5%	NA

Table 37 Epicondylar % differences

Overall, the epicondylar width variable is observed to show clear differentiation between male and female bone samples as demonstrated in figure 74. Using the broad age categories, significant differences between age groupings for epicondylar width of the males (p=0.038) were observed but differences were not significant for the females (p=0.711).

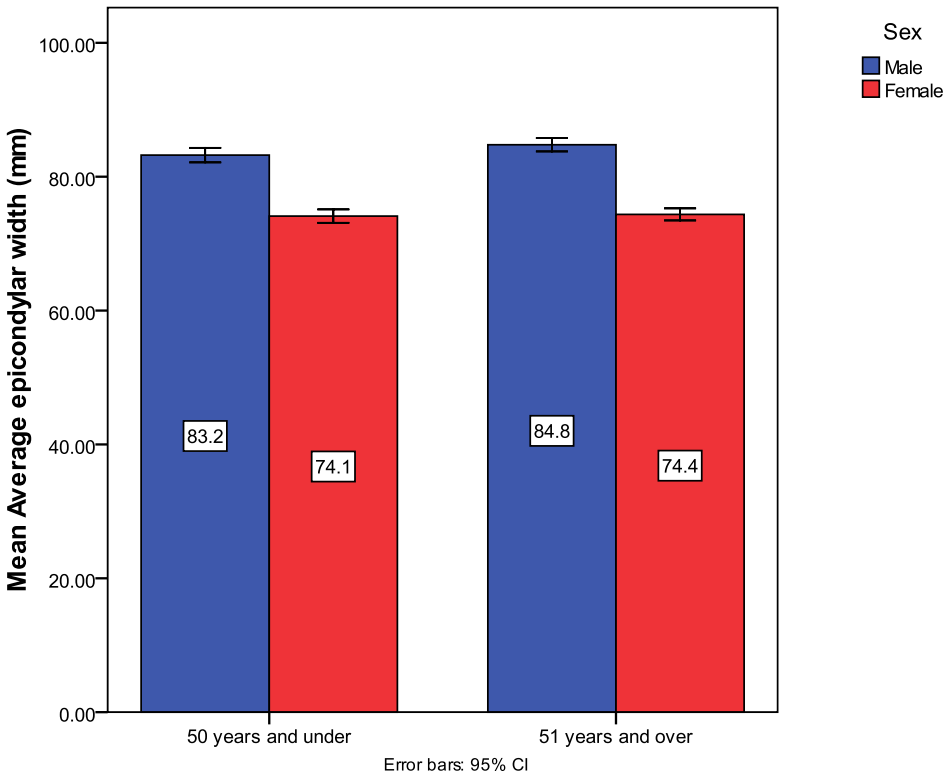

Figure 74 Averaged mean epicondylar width

Femoral Axis Length

The mean of the femoral axis length was evaluated bilaterally for both genders and age groupings, and included as table 38.

	(Hip) Femoral Neck Axis Length							
	Male				Female			
	≤ 50 years		> 50 years		≤ 50 years		> 50 years	
	Mean	Std Dev	Mean	Std Dev	Mean	Std Dev	Mean	Std Dev
R FN axis (mm)	101	6	104	7	90	5	91	6
L FN axis (mm)	100	6	104	7	90	6	91	6

Table 38 Femoral axis length mean values

No significant differences between right and left values for femoral neck axis length (p=0.684) were observed. An independent samples t-test was performed to establish the significance of the differences in mean axis length for males and

females across the two age groups. While for females there was no significant difference (p=0.262) between the older and younger mean values, the males did demonstrate statistically significant variation (p=0.005) between the mean of the younger group compared to that of the older group, though the difference was just 3mm.

Overall, the femoral axis length demonstrates clear differentiation between male and female bone samples. Using the broad age categories, significant differences between the older and younger age groups for femoral-axis length of the males (p=0.05) were observed, though not for females (p=0.262). The clinical age categories were applied to the average value in an effort to better describe the differences, and are included as figure 75.

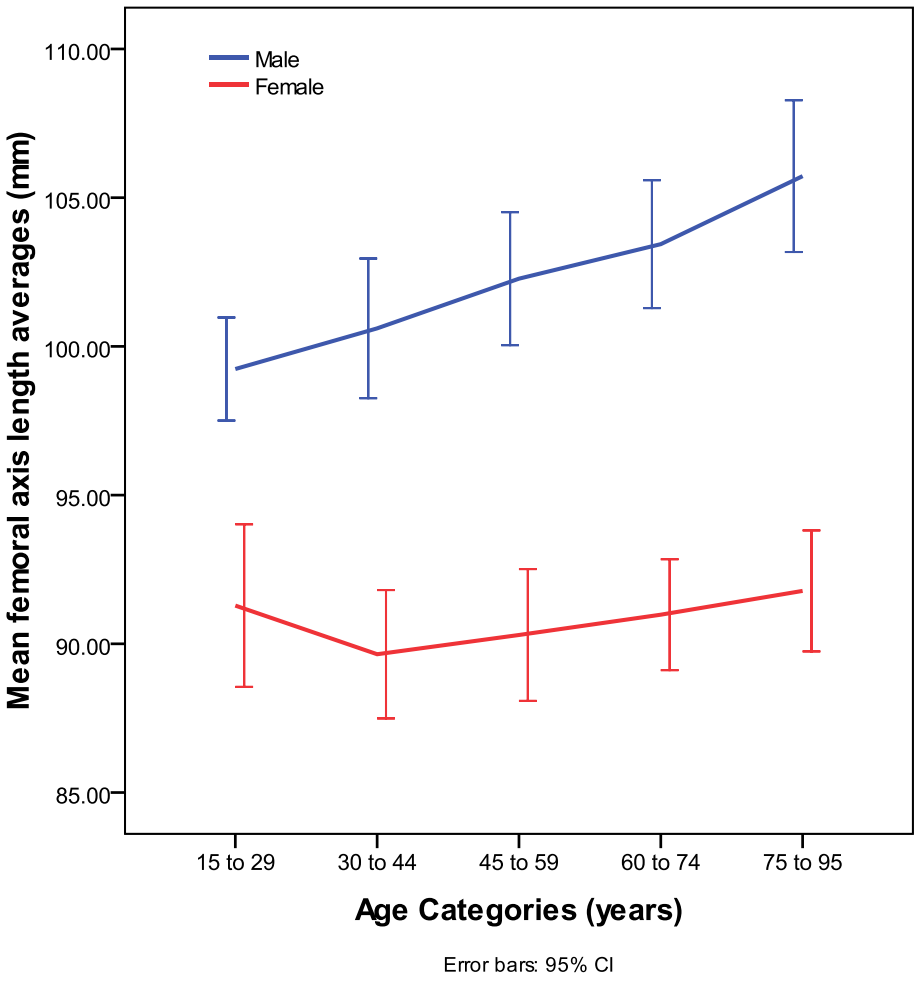

Figure 75 Femoral axis length – clinical age categories

Figure 74 demonstrates a gradually increasing axis length with age for males, but not for females where differences related to age are much less.

Femoral Head Area

The mean values for each gender and age grouping for femoral head (FH) area are included as table 39.

(cm^2)	Femoral Head Area							
	Male				Female			
	≤ 50 years		> 50 years		≤ 50 years		> 50 years	
	Mean	Std Dev	Mean	Std Dev	Mean	Std Dev	Mean	Std Dev
R FH area	18	2	18	2	14	2	14	2
L FH area	18	2	18	2	14	1	14	2

Table 39 Femoral head area mean values

The FH area measurement demonstrated no significant difference (p=0.154) between right and left values. No significant difference was observed between the FH area of the young groups and that of the older groups for either gender. The male femoral head area mean measurement was however significantly and consistently 22% larger than that of the female.

Femoral Neck Width (FNW)

No significant difference (p=0.516) between the right and left values of the FNW was shown. Average FNW demonstrated assessment showed no significant difference (p=0.083) between the femoral neck widths of either of the age groups for the males, and was also insignificant (p=0.395) for difference for the young and older females. Left and right FNW mean measurements for each of the gender and age groupings are described in table 40.

(mm)	Femoral Neck Width							
	Male				Female			
	≤ 50 years		> 50 years		≤ 50 years		> 50 years	
	Mean	Std Dev	Mean	Std Dev	Mean	Std Dev	Mean	Std Dev
R FNW	33.5	3.1	34.3	2.9	30.4	3.2	30.9	3.5
L FNW	33.8	2.6	34.2	2.7	30.2	2.5	30.8	3.3

Table 40 FNW mean values

Though statistically insignificant, the trend in table 40 suggests a slightly wider femoral neck for both the older males and females. The clinical age categories were therefore applied in an effort to better describe these observed differences and are included as figure 76.

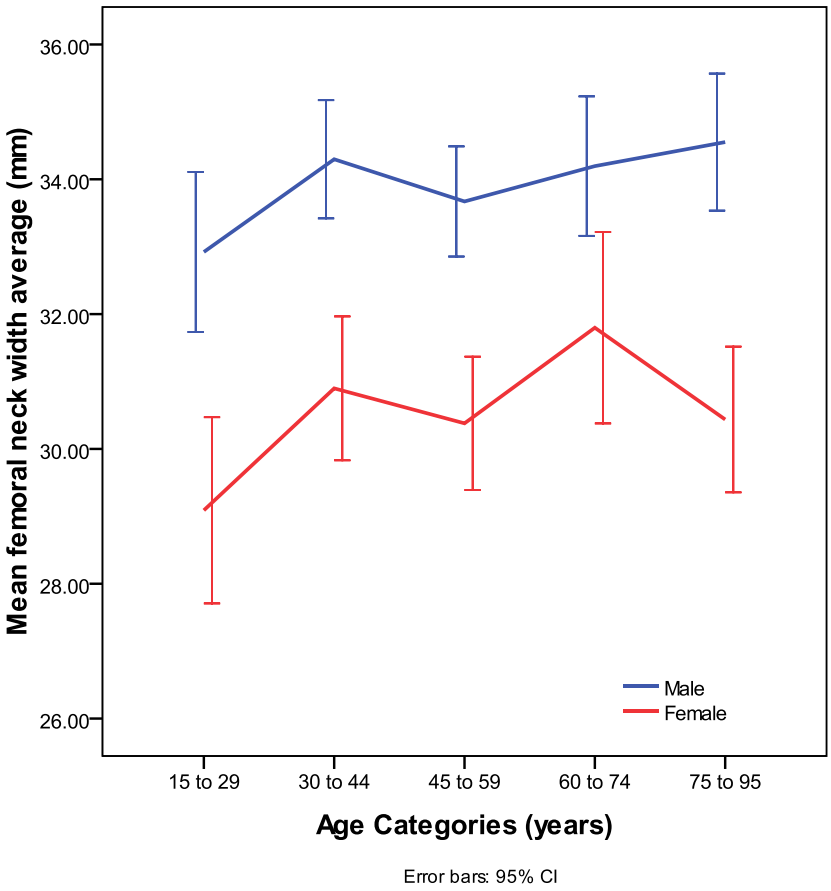

Figure 76 Femoral neck widths - clinical age categories

Figure 75 indicates large variation across age categories for both genders is observed, especially in the female data. The trend biologically however is toward an increasing femoral neck width with increasing age. Table 41 documents the percentage differences of the age groups and genders for FNW.

FNW	M ≤ 50 years	M > 50 years	F ≤ 50 years	F >50 years
M ≤ 50 years	NA	↓3%	↑10 %	↑8 %
M > 50 years	↑ 3%	NA	↑ 12%	↑ 10%
F ≤ 50 years	↓ 10%	↓12%	NA	↓ 2 %
F >50 years	↓ 8%	↓10%	↑ 2%	NA

Table 41 FNW % differences

The young females were observed to have the lowest mean femoral neck width, with the older females having a 2% wider neck than their younger counterparts. The older males had a mean width 3% higher than the young males. The young males had a mean width 10% wider than the young females, and the older males also had mean widths 10% greater than the older females. The greatest difference was between the older males who had a mean width 12% higher than the young females. The biological pattern therefore is similar to that of the other femoral width measurements.

Evaluation of the right and left femoral angles were observed to have no significant differences of symmetry. Mean values are described in table 42.

Degrees	Male		Female		Male		Female	
	≤ 50 years		> 50 years		≤ 50 years		> 50 years	
	Mean	Std Dev	Mean	Std Dev	Mean	Std Dev	Mean	Std Dev
Right FNSA (°)	127	3	128	4	126	3	126	4
Left FNSA (°)	127	3	128	3	126	3	126	4

Table 42 Femoral head angle mean values

Little variation was measured across the mean values for gender and age group. The young males and older females recorded a mean femoral angle of 126 degrees, and the young males recorded a mean femoral neck angle between the young females and older groups at 127 degrees.

Trabecular Margin Length

The inferior border of the trabecular margin was variable in terms of both position and shape as shown in figure 77.

Figure 77 Trabecular margin differences

The three images above represent the differing shapes and contours found in the examination of the trabecular margin length. All represent those in the 51 years and over category.

In older individuals it was usually easier to identify a clear trabecular margin in the femoral shaft. For the younger cases where there was more hematopoietic marrow, it was often much more difficult to identify the inferior margin.

Symmetry of right and left values for the trabecular margin length were evaluated. There was no statistically significant difference between the right and left mean values for trabecular margin length (p=0.950). A graph of the right and left mean values for each of the gender and age groups is included as figure 78. Mean values are also indicated.

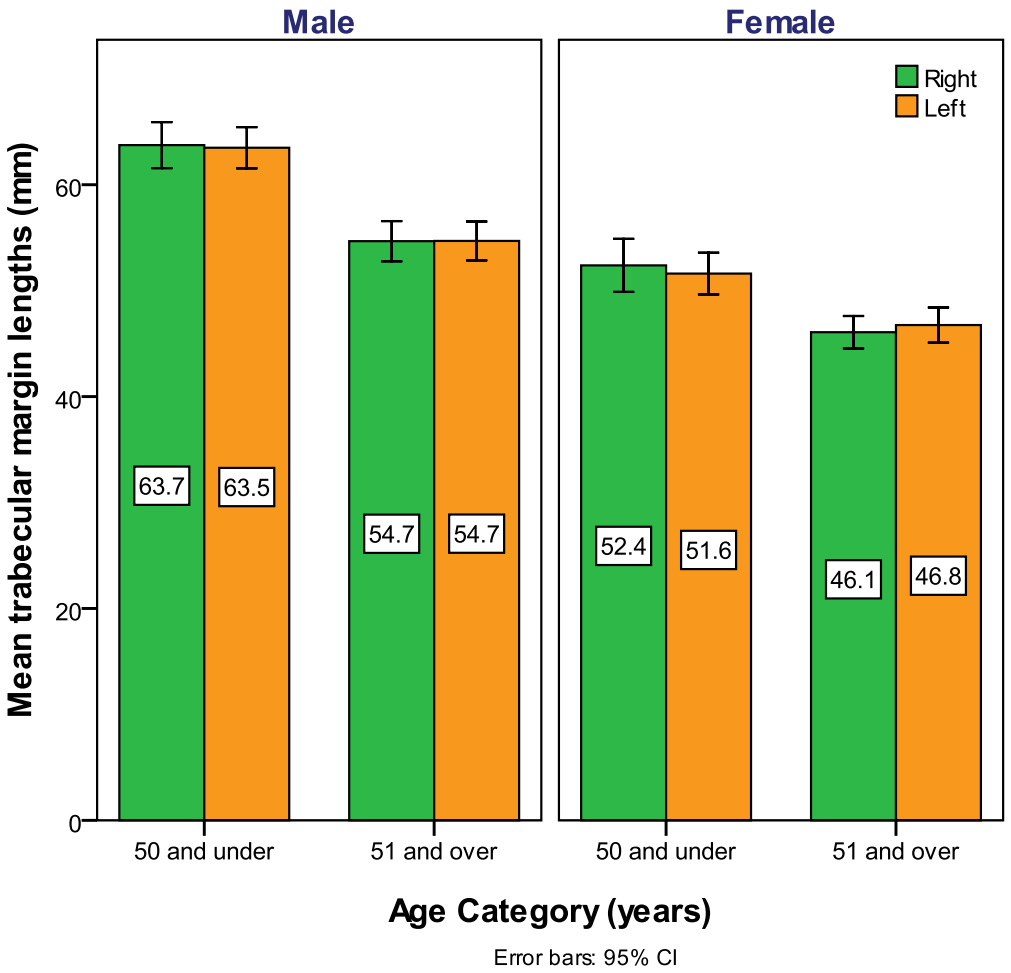

Figure 78 Right and left trabecular margin lengths – male and female

Averaged right and left vales showed statistically significant differences (p<0.001) between the two age groups generally, and between male and female groups. Table 43 demonstrates the %percentage differences between gender and age groups.

Trabecular Margin	M ≤ 50 years	M > 50 years	F ≤ 50 years	F >50 years
M ≤ 50 years	NA	↑15 %	↑ 19%	↑29%
M > 50 years	↓ 15%	NA	↑ 4%	↑ 16%
F ≤ 50 years	↓19%	↓4%	NA	↑ 12%
F >50 years	↓ 29%	↓16%	↓ 12%	NA

Table 43 Trabecular margin length % differences

The older females had the smallest mean trabecular margin length, which represented a 12% decrease when compared to the young females. The older males had measurements 15% less than those of the young males.

When compared by gender, the older males had trabecular margin lengths 16% more than the older females, and the young males had a mean measurement 29% more than the older females. The greatest difference was observed between the young males and the older females, with a 29% greater mean length for these males. All values were uncorrected for height or femoral length.

As the differences in the trabecular margin length were large using the dichotomous grouping, a comparison using the clinical age groups was also performed and figure 79 documents that comparison.

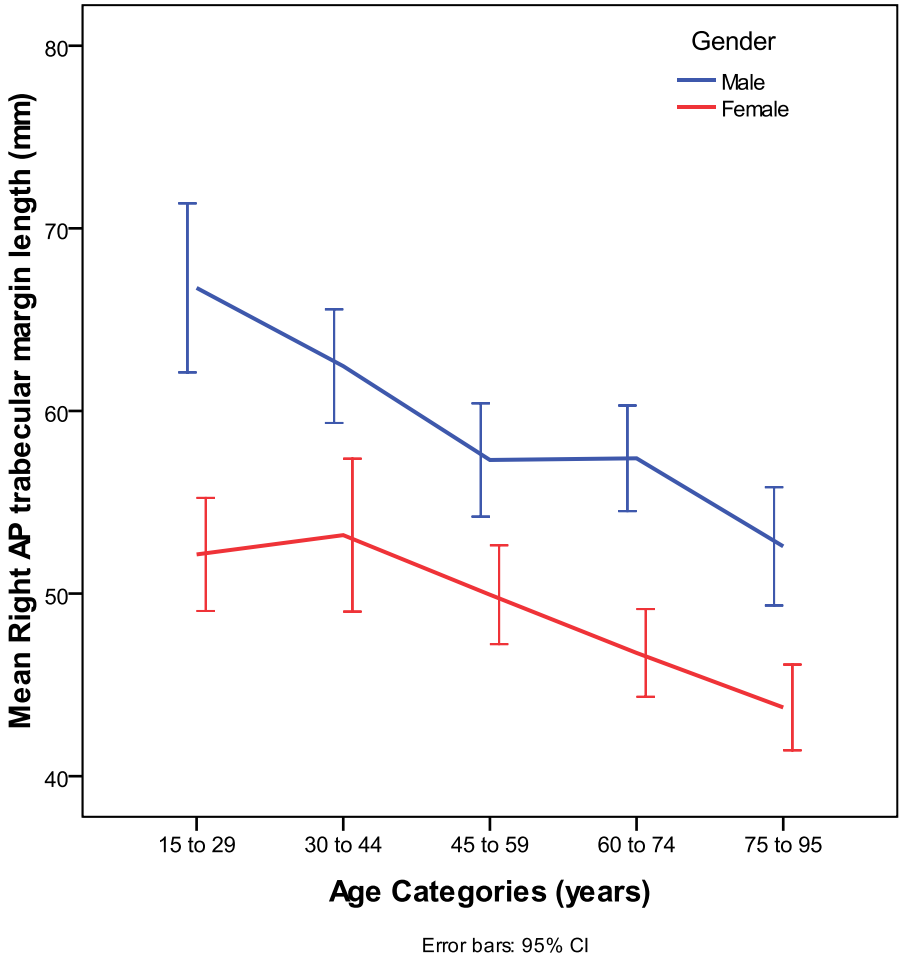

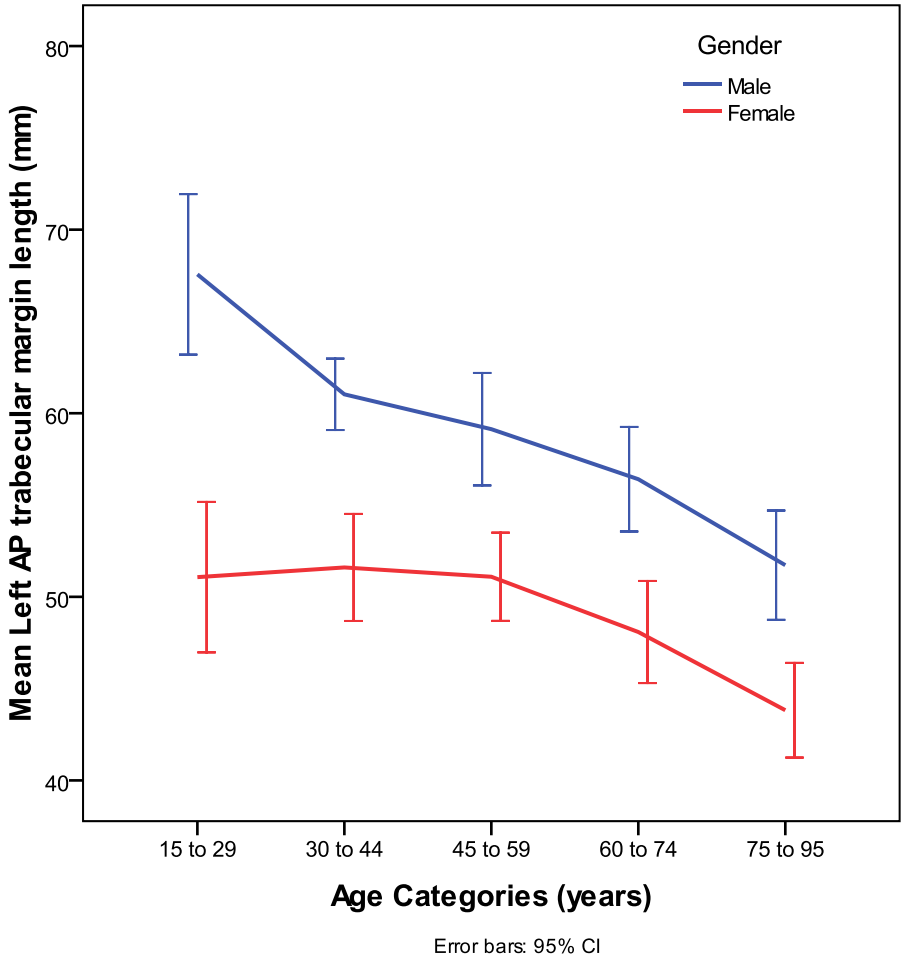

Figure 79 Trabecular margin lengths - clinical age groups, male and female

Figure 78 demonstrates that trabecular margin length decreases in length with increasing age. The significant difference (p<0.001) between the male and female data at all age groups, indicates a possible utility for the differentiation of gender using this variable.

Trabecular Margin Lengths Regression Equations

Regression modelling was performed for the trabecular margin length as a function of both age and gender, and results are included as table 44.

	Age Equation (years)
Male	122.719 – (1.183 x right trabecular margin length in mm)
Female	120.503 – (1.319 x right trabecular margin length in mm)

Table 44 Trabecular margin length linear regressions for age

The modelling demonstrates significant (p≤0.001) correlation of the trabecular margin length with age and gender.

Hounsfield Average Femoral Head

The Hounsfield number used in CT is an expression of the linear attenuation co-efficient of the material under investigation. The unit is energy dependent and as such for the purposes of quantitative CT measurements there may be errors in its representation (291), and so the value is usually calibrated against a substance or series of substances of known density (bone calibration phantom), as was performed in chapter 4.

The purpose in evaluating the un-calibrated measurement of Hounsfield units in the femoral-head was to ascertain the relationship with the calibrated apparent vBMD results obtained in the femoral-neck and reported in the previous chapter. That is, can the Hounsfield unit measurement of the femoral-head provide an indication of the vBMD of the femoral-neck? The Hounsfield average represents an easily reproduced variable that requires no additional software to acquire.

No significant difference (p=0.593) between the right and left values for the Hounsfield unit average in the femoral head was observed. As there were significant differences between the right and left vBMD findings, a comparison between the apparent vBMD calculations was made for both left and right sides. Figures 80 and 81 document each of the comparisons.

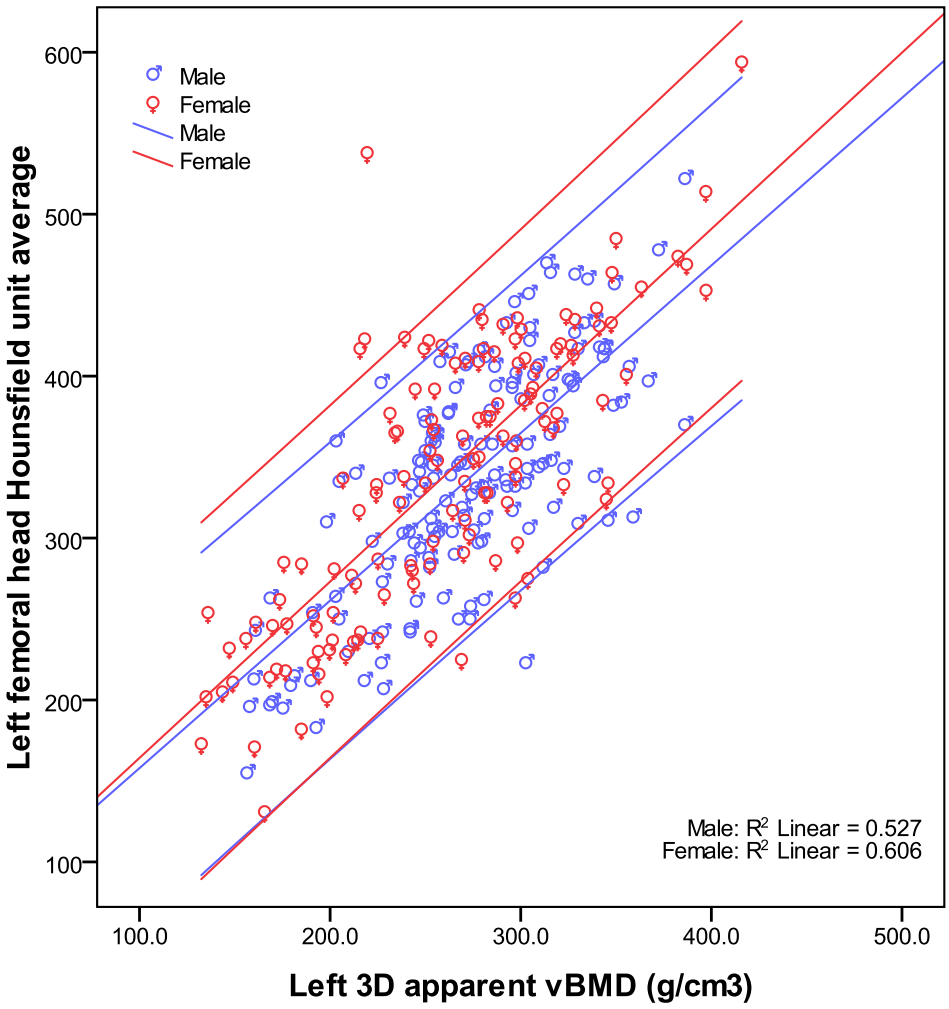

Figure 80 Left apparent vBMD against femoral head Hounsfield unit average

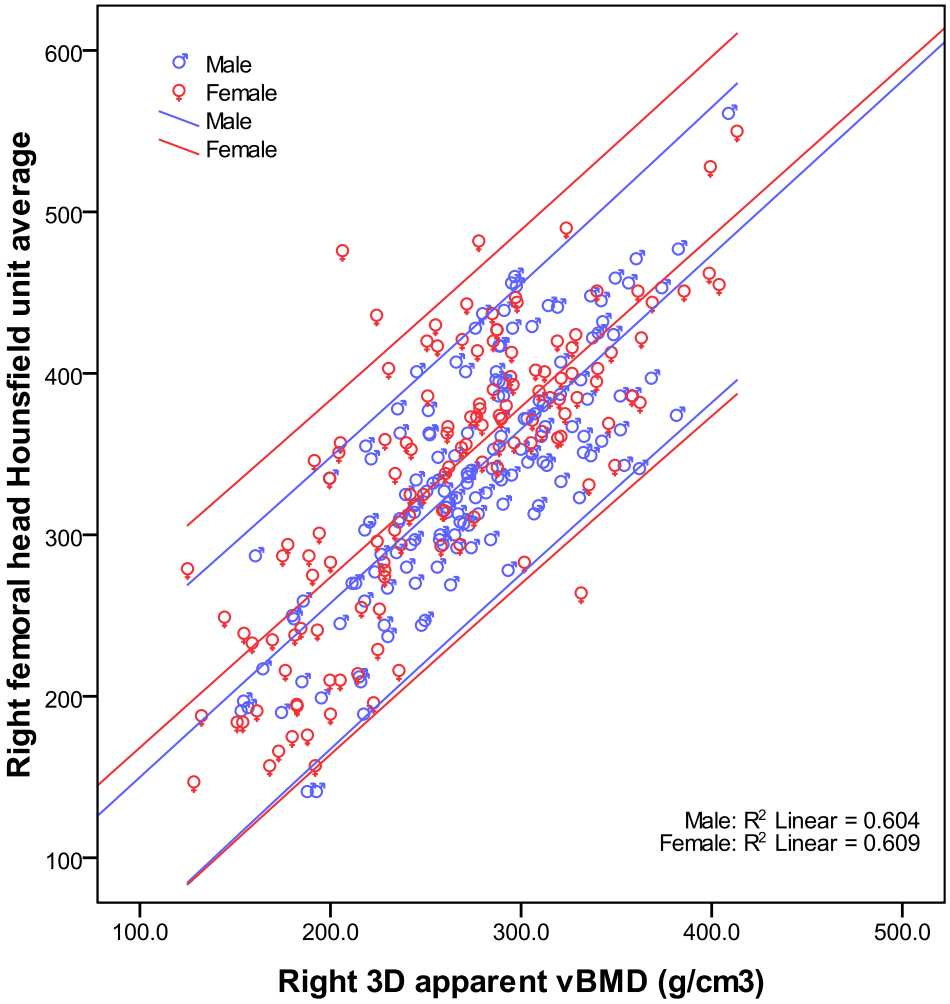

Figure 81 Right apparent vBMD against femoral head Hounsfield unit average

Strong correlation was observed between the un-calibrated femoral-head results and the calibrated femoral-neck assessments, for both the left and right-sided measurements, and in both males and females. Figure 82 documents the application of the clinical age groupings to further assess the right and left correlation.

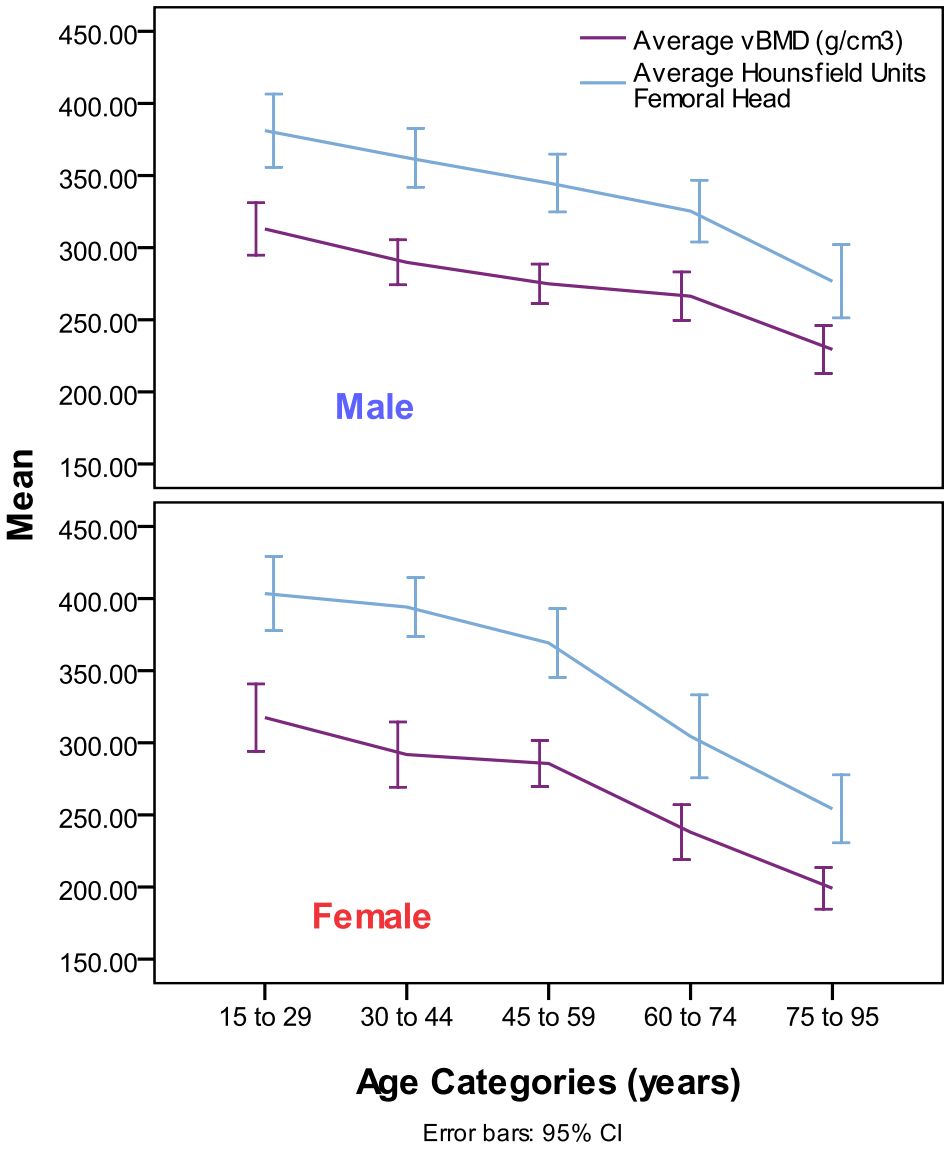

Figure 82 Apparent vBMD vs. femoral head Hounsfield unit average - clinical age groups

The correlation between the Hounsfield average in the femoral-head and the vBMD in the femoral-neck is generally closer for the males than for the females, with correlation in the younger females being the most variable. The finding of the assessment indicates an association of bone changes in the femoral neck and the femoral head.

Hounsfield Average and Age Regression Equations

Regression modelling to predict femoral-head Hounsfield unit average as a function of both age and gender is presented in table 45.

Category	Age Equation
Male	101.836 – (0.145 x Hounsfield unit average)
Female	112.547 – (0.167 x Hounsfield unit average)

Table 45 Hounsfield unit (HU) linear regression equations for age

Regression modelling demonstrates significant ($p \leq 0.001$) correlation of the femoral-head Hounsfield unit average with age and gender. The significance of the modelling is that that this evaluation of age has been achieved using CT images independent of ancillary hardware or software.

5.4 Discussion

The main goals of this study were to assess the ability to use the MDCT data to produce 3D volume rendered images from which both novel and conventional anthropological measurements could be undertaken, and to establish a normative bilateral MDCT femoral database. Both goals have been achieved. The hypothesis was that there is predictable morphologic age, gender and symmetry related differences within a contemporary predominantly urban adult population spanning 80 years. This anthropologically based study has demonstrated that the routine collection of mortuary-based MDCT data may be used for a population-based study of the morphometric features of the adult human femur, and a robust foundation model has been established.

5.4.1 Physical Features

The average age of the females in the VIFM population was slightly older than the males, and the population overall was obese. These findings reflect current Australian population data demonstrating a slightly longer life-expectancy for

females, and a growing trend towards obesity in the population generally (8). The VIFM mortuary sample used for this study is therefore found to be representative of the current Australian population in terms of general physical characteristics.

5.4.2 Reproducibility

The assessment, and consequently the reproducibility for the short femoral length, and to a lesser extent the trabecular margin length, was problematical. The reason for the difficulty in evaluating the short femoral measurement related to the tendency of older individuals to show degenerative changes around the tendon insertions of the greater trochanter. The insertion of *gluteus medius* and *minimus,* which are major hip abductors, are located at the greater trochanter. The muscle and bone complex is necessary to hold the pelvis level during walking, and gross weakness in these muscles in old age is not uncommon (292). Ligamentous attachments associated with lower limb mobility are put under repetitive and complicated forces during locomotion, all of which impact on the tendency for the development of osteoarthritic conditions. If average BMI increases in the population, as it is currently, then these forces are likely to exacerbate the radiological changes seen at the sites of tendon insertion.

Figure 83 presents an example of the degenerative changes encountered when analysing some of the elderly VIFM cases. The arrows represent the areas of degenerative change, while the single hip image is a *normal* elderly case. Almost all elderly cases from the population exhibited some degree of arthritic change in the ligamentous insertion at the greater trochanter.

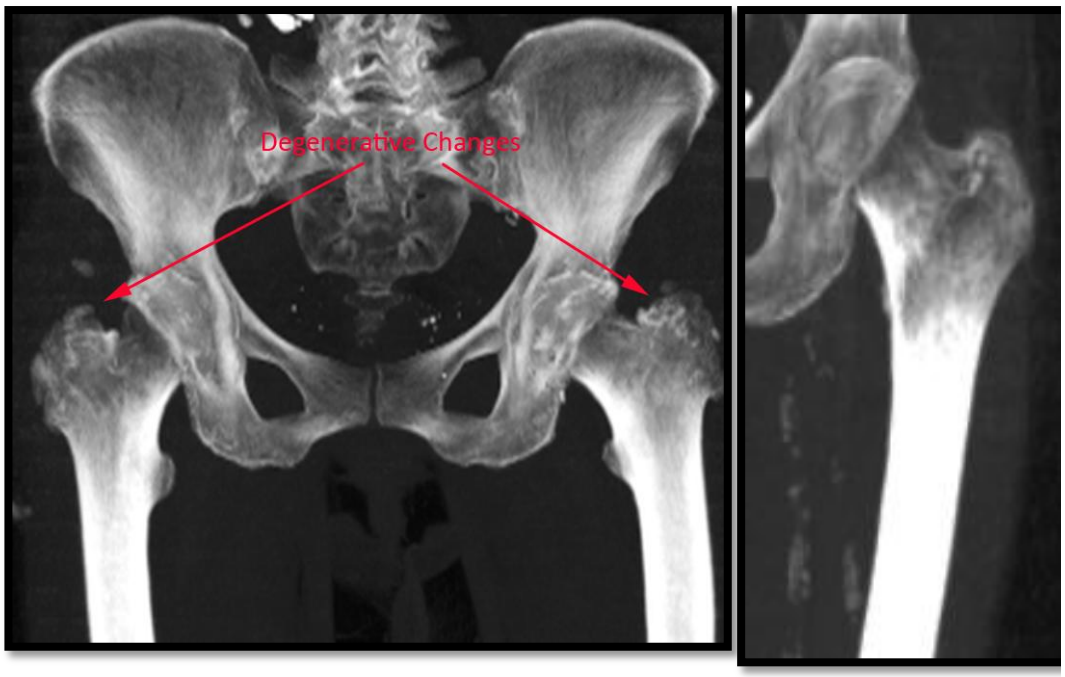

Figure 83 Greater trochanter *gluteus medius* insertion point changes

The reason for the poorer reproducibility of the left trabecular margin measurement is less straight forward, only because this was not a finding for the right-sided evaluation. Unlike the quantitative measurements undertaken in chapter 4, these linear morphometric assessments were not subjected to potential error from unorthodox positioning. The likely reason for the reduced reproducibility is therefore either biological (i.e. as a function the processes of the bone itself in relation to footedness or some other factor) or in the way the midline reconstructions were formed. A further independent observer analysis may provide clarity on this matter.

5.4.3 Symmetry

The study of symmetry demonstrated evidence of significant morphometric asymmetry of the femora. The percentage directional asymmetry (%DA) evaluation, demonstrated a significant left bias, or larger left-sided measurements generally, which was especially evident in the older females. The right sub-trochanter width and femoral-head area were the only morphometric variables to show larger mean right-sided measurements across age group and

gender, perhaps indicating a positive response to bone building from right footedness.

The study of symmetry demonstrated a consistently longer measurement for the left long and short femoral lengths (approx. 1mm and 0.6mm respectively), and the left mid-femoral width (0.4mm). Females presented with more variable femoral symmetry generally, with the younger group having more extreme degrees of asymmetry overall. It is noted however that the mean differences between right and left measurements were substantially smaller than the slice thickness (1mm) used for the reconstructed images, which may be a potential cause of error. There are previous reports however in the anthropology literature of slightly longer left femoral lengths using data collected on defleshed human specimens, (259, 293); supporting the findings of asymmetry in this study using an MDCT technique. No correlation with handed or footedness was able to be performed on these data, but would nonetheless be a useful part of any future study.

5.4.4 Generational

The secular increase in height (and associated long femur length) shown in this study is reflected in other research studies conducted all over the world, most notably after WW2 (294). The generational or secular observations of this study show a consistent relationship between height and both the long and short femoral length for both genders and for both age groups. The long femoral length contributes approximately 27% of an individual's height, and the short femoral length was shown to represent approximately 94% of the long femoral measurement for the young age groups and closer to 95% of the long femoral length in the older age categories. The difference in the short femoral length compared to the long in terms of the overall height contribution likely represents either age or generational influences in the femoral head. The relatively short 80-year adult lifespan used for this study makes it difficult to make a definitive case for either influence, but may be a useful avenue to explore over a longer time period in the context of femoral neck fracture.

The repeated measurement analysis indicated a potential for error in the short femoral measurement as mentioned previously. The error however would result in the older groups having a lesser percentage contribution to the long measurement, and not the larger measurement that they have demonstrated. A further long-term longitudinal study of males and females is a reasonable method of evaluating the difference conclusively.

Young females in this VIFM population have shown to increase mean height at a slightly greater rate than the males (females=3.67% and males=2.71%). The older females however were shown to have lost more height with ageing from sites other than the femur than the males (females=0.51% and males=0.32%). The long femoral length was used as a calibration standard for each individual in these findings. Regression modelling of the data supported these findings, and a series of equations for the determination of both height and age from femoral length were produced. Given that in some DVI and mass casualty events the femoral head is missing, a series of regression equations was also established for the short femoral length. All provide a robust establishment of height from either long or short femoral length.

The male femur was found to be significantly longer (8% on average) than the female. The degree of gender difference was seen in both the young and older groups, though as mentioned previously, the young females were shown to be increasing their femoral length slightly faster than were the males when compared across age groupings overall.

All cases used for this study were checked for fusion of the epiphysial plates prior to them being included. This resulted in the inclusion of a small number of adolescents (15 to 19 years). The suitable inclusion of persons so young into this study given this criteria puts into question the presently recognised age at which the epiphysial plates fuse in the femur (295). Further investigation of the mean age of fusion of these growth plates with statistical power is therefore recommended.

5.4.5 Gender and Age

Results of the gender and age comparisons demonstrate that all three cross-sectional bone width measurements may be used as discriminators between male and female femoral bone samples. The most definitive distinction may be made using the epicondylar width measurement.

Analysis of the mid-femoral width measurement produces evidence of femoral periosteal apposition by way of comparing the ratio of mean widths to length of the younger groups to those in the older groups. For the mid-femoral width measurement, the females also demonstrated larger significant differences between age categories than those between the male age groups. The finding indicates that the increase in mid-femoral width due to apposition likely occurs more rapidly in females than in the males. Again statistical power would be enhanced in any further study by increasing population numbers in all groups, and 80 years is a short time span anthropologically speaking.

Previous findings of significant increases in the hip axis length (HAL) with age (296) have not been reproduced in this MDCT-based study for females. Small differences with age have however been observed in the males. The lack of significant findings in this study related to HAL are likely as a result of the very small changes occurring biologically, combined with the relatively large size of the reconstruction pixels used to generate the image and determine the measurement.

The maximal femoral head area was shown not to be affected by age in either males or females. The variable as a discriminator between males and females however was proven with a 22% difference on average between male and female measurements at all age groupings.

Femoral neck width data was collected using the QCT software outlined in chapter four. An analysis of the male and female data using the clinical age categories demonstrates wide variation in the mean values for each of the age

groupings. The female data especially demonstrates wide variation when measured over different ages. The variability was due to the difficulties encountered in obtaining a consistent hip rotation for measurement using the QCT program which has been explained previously. A repeat study using a 3D volume render for measurement may enhance accuracy for this variable.

Very little variation was observed for femoral neck-shaft angle between age and gender groups, and as it was manually measured. It is therefore difficult to see this variable as a standalone discriminator for either age or gender. It would however be useful to study femoral neck angle further in a longitudinal-study to establish any variability during an individual's ageing as has been observed in other skeletal areas, such as the sacrum (297).

Results from the investigation of the trabecular margin length demonstrate it to be a significant indicator of age for males and females. The distance-based measurement decreases with age at a similar rate in both genders. Modelling in the form of regression analysis was performed and produced robust equations for the evaluation of age using these data.

Results from the comparison between femoral-neck vBMD evaluation and femoral-head average Hounsfield unit evaluation, demonstrate that they correlate well, though become more strongly correlated as age increases. This study has therefore demonstrated that there are similar age-related bone mineralisation changes occur in the femoral-head to those occurring in the femoral-neck.

5.5 Conclusions

The results from the 3D morphometric analysis of the VIFM group clearly demonstrate that the MDCT data may be used as a tool for the evaluation of age-related change, and for the formation of a *virtual* adult human femur population database from which to build. Robust prediction models for age, stature and height have been presented. This morphological 3D study was cross-sectional,

and so it presents findings of differences throughout a current population rather than changes in individuals over time. Great care therefore needs to be taken in extrapolating these results forward for the younger categories in the process of modelling age.

The aim of this study was to establish a 3D MDCT-based radiologically based method for the evaluation of the femurs to establish age, gender and secular differences in the population, which it has done. In doing this, the work also provides the first 3D morphological assessment of human femora from a contemporary, urban Australian population. The study demonstrates that this novel assessment method is an effective tool for the evaluation of 3D radiological morphology of the femur for documenting age characteristics, and establishes the model for further population data entry.

The repeated measurement analysis conducted confirmed the suitability of the selected landmarks for evaluation points of reference. All variables however demonstrated patterns of dependency on image resolution and anatomical recognition, indicating that the resolution of the CT image or dataset is a non-trivial factor in determining the overall quality of measurements undertaken.

Based on the variables evaluated, the non-invasive MDCT assessment alone may be used to determine sex and stature, and general age characteristics of the femur. The work has also presented findings relating to the relative asymmetry of femoral morphometry in humans, especially in females, which has not previously been reported in a contemporary adult population. This work is also the first study to identify a possible link between the lengths of the trabecular margins in the proximal femora to age as determined by CT assessment.

CHAPTER 6

A COMPARISON OF THREE MDCT SCANNING SITUATIONS FOR DETERMINING AGE-RELATED CHANGE IN BONE

"Physics concerns only what we can say about nature."

~ Neils Bohr ~

Chapter six describes a study that extends key technical findings recorded in the previous two research chapters. The primary aim was to establish the quantitative and spatial differences in data obtained under differing CT environments. The overall objective was to quantify those differences if possible in order that a prediction of the effects of the environmental changes is produced. The hypothesis is that alterations in the CT scanning conditions and environment will produce little change in the spatial assessments, and consistent variation for the quantitative evaluations. The study uses the reconstructed CT slice data from three different scanning conditions applied to 17 proximal right femora from the Melbourne Femur Collection (MFC).

6.1 Introduction

As discussed in chapter four, BMD studies are used clinically to diagnose osteopenia or osteoporosis. DXA-based studies have also been applied in anthropology to establish aspects of bio-cultural history such as diet (2).

BMD testing is commonly used in the living a number of times over a long period to evaluate age-related changes, or to assess treatment efficacy (298). Medicare in Australia will pay for a BMD evaluation every 12 or 24 months depending on the item number used. The serial nature of clinical BMD evaluations means that there is a strong need for the testing to be highly reproducible. That is, successive measurements performed on a bone (i.e. femur, spine etc.) must produce the same

quantification every time, all other factors being equal. The precision of this type of testing is expressed as a coefficient of variation, which is not the same as accuracy. That is, the expected value may not necessarily be the true or *ashed* equivalent value. What it does mean is that repeated measurements are shown to lie within a "precise" range of values. It is this precision or reproducibility over a long period of time that confers the usefulness of a BMD evaluation. The precision of the Mindways™ QCT testing methods discussed in chapter 3, was found to be +/- 5% though the manufacturer has set +/- 10% limits in the user documentation (136).

Mathematically a method with a 2% coefficient of variation requires a change of at least 5-7% between two assessments to be within a 95% confidence levels (221). Therefore for any two or more measurements, where there is an expectation that less than a 5.7% biological variation has occurred; the test is not clinically warranted. That is if the expected change in the tissue is not significantly large enough to account for the error in the precision of the testing method, then the test result is meaningless. This consequently means that if various types of testing methods are available, the choice between those two tests should be based on at least three things:

1. availability of a previous test for comparison,
2. the magnitude of the change expected, (i.e. a parathyroidectomy will show a significant change in DXA-based BMD six months postoperatively, whereas other drug or therapy-based interventions may not have such a striking short term effect) (136),
3. the risk profile of the patient in relation to such aspects as radiation sensitivity (age).

Given the slow rate of bone turnover generally, the *better* test for the serial evaluation of BMD is the one best able to demonstrate subtle biological change. That is of course if BMD is the *correct* and/or only variable to test for both cortical and trabecular bone.

The proximal femur is composed of trabecular or spongy internal bone with a thin cortical shell-like outer, the proportions of which are based around the function and purpose of the bone. Trabecular and cortical bone however do not have the same cellular turnover rates, with the cortex turning over at around 1/20th the rate of the trabecular bone. The high-risk fracture areas of the spine and femoral neck, which are evaluated clinically to establish osteoporotic status, also vary considerably with regard to the quantities of cortical and trabecular bone. The difference in the distribution of bone category, and the time taken to measure any significant status change, will therefore impact on the choice of clinical evaluation method.

Being able to accurately discriminate between trabecular and cortical bone mineral density is a desirable feature in an evaluation of fracture risk. Being able to do so with a high degree of reproducibility and accuracy is obviously even better. 3D CT-based assessment techniques therefore has the advantage over 2D techniques in evaluating ageing bone, especially given the complicated 3D structure of most of weight-bearing bone. As discussed in chapter four however, the arbitrary threshold-based separation of the trabecular and cortical components of bone using CT does not necessarily deliver the same finding as histological examination. The technical challenges in separating trabecular and cortical contributions are however non-trivial using even micro CT techniques, where over 30% variation has been described (125).

Other studies have also observed differences in BMD results using the DXA and QCT methods on the same samples (299). Some doubt has therefore been cast on the accuracy of the DXA method in general for accurately expressing mineral density values and fracture risk (129). Doubt which may be considered reasonable when over 50% of women with a hip fracture have DXA derived BMD values that do not reflect an osteoporotic condition as determined by the WHO classification, while many of those who do fracture are not considered osteoporotic (101).

The aBMD value changes observed as a result of osteoporotic drug therapy, also give no real indication for the success of these treatments in preventing fracture (167). The lack of sensitivity and specificity in using BMD as an analogue to bone strength, bone age and bone *quality* (whatever that may mean), is likely because it describes only one part of the multiple components that combine to determine the resistivity of bone to fracture.

The mineral density of bone in the hip has been also been used extensively as a measure of bone strength, and as a tool for the selection of various therapies (299). QCT has also been used to derive structural expressions of strength such as cross-sectional moment of inertia (CSMI), section modulus (Z), cross-sectional area (CSA) and buckling ratio (BR), in what is broadly termed hip structural analysis (HSA) (300). These derivations of strength however are based on a model hip, the creation of which, necessarily involves simplifications of form and structure. Structural analysis therefore remains a particularly controversial part of the description of ageing bone.

6.1.1 Overall Study Aim and Objectives

The overall aim of this QCT-based study is to establish the effect of a small number of technical and environmental alterations to the MDCT acquisition, to the clinical QCT output. Specific objectives were to:

- describe the quantitative and qualitative differences affected by changes in the MCCT scanning environment,
- describe and predict the relationship, if any, to each of the evaluations,

The purpose in performing this testing was to establish a sense of the expected precision in using clinical QCT data from one study, and mixing it with data from another. The reciprocity of QCT data is key to building and maintaining an MDCT population database, and for establishing a degree of consistency in serial measurements.

6.2 Materials and Methods

6.2.1 Sample Description

The study sample consisted of the MDCT scans of 17 proximal femoral specimens from the Melbourne Femur Collection (MFC), which is one of the largest and best documented collections of human femoral tissue in the world. The collection is supervised by Professor John Clement of the University of Melbourne, in the School of Dental Science. The 17 cases selected for study represented the only MFC specimens for which an MDCT scan was performed upon the bodies' admission to the VIFM. All other current MFC samples were collected before the introduction of the MDCT scanner in 2005, and hence were not considered.

Of the cases available, there were 11 males and 6 females represented in the group of 17 which will be referred to as the MFC17 hereafter. The MFC17 group has an average age of 58.88 years (range 20 – 84 years). The average weight of the bodies from which the sample were obtained was 83.76 kg (range 51 – 116 kg), with an average height of 169.47 cm (range 152 – 192 cm), which provides an average BMI value of 28.82 kg/m^2 (range 18.73 – 39.63 kg/m^2), which resides in the overweight WHO category. Details for each of the MFC17 cases are included as table 46.

		Age (Years)	Weight (kg)	Height (cm)
Females	MFC579	59	104	162
	MFC580	20	51	165
	MFC586	81	51	156
	MFC588	84	52	157
	MFC589	51	75	159
	MFC591	76	58	152
Males	MFC576	31	95	192
	MFC577	24	84	176
	MFC584	64	99	178
	MFC585	74	74	161
	MFC587	64	105	185
	MFC590	45	116	182
	MFC592	79	77	168
	MFC593	60	76	166
	MFC594	52	109	175
	MFC595	79	99	179
	MFC597	58	99	168

Table 46 MFC17 physical overview

6.2.2 Statistical Methods

Statistical analyses were performed using SPSS statistical software (version 17.0.2, SPSS, Chicago Ill, USA). Differences between scanning conditions were tested using a simultaneous comparison technique. More information on the statistical analysis used for this work may be found in **section 3.3.9.**

6.2.3 MDCT Methods

As previously mentioned, the MFC17 cases were identified from all other MFC specimens as being those which had MDCT scans performed on admission to the VIFM. The bone specimens were identified by direct inspection as intact (i.e. not previously used for interventional or destructive bone research investigations) and additionally labeled. The MFC17 samples are stored in a freezer at -70°C at the University of Melbourne Dental School.

The case numbers taken from the MFC17 were tracked back to the VIFM CT number via a tissue bank enquiry. The CT body numbers were then given to the information technology (IT) support personnel at the VIFM for retrieval from the archived PACS. Once loaded onto the PACS, the CT cases were downloaded on to CD media as per the procedure outlined in chapter 3, including the de-identification process.

The MFC17 specimens were then taken to the VIFM and scanned once using the same technical factors (i.e. kV, mA etc.) to those used for the original body scan except that the FOV used was 180mm or 240mm rather than the usual 500mm for a full-body. Slices were then reconstructed from the data as 1mm contiguous slices using the same algorithm as used on their admission at the VIFM (FC03 or FC01). The data was also reconstructed to produce 0.5mm contiguous slices using the bone algorithm (FC81). A summary table of the three scanning conditions is included as table 47.

Study Name	Bone Status	Slice Thickness	FOV	Algorithm
Body	in-situ	2mm/2mm	500mm	FC03
Bone	specimen	0.5mm/0.5mm	180 or 240mm	FC81
Soft	specimen	1mm/1mm	180 or 240mm	FC03

Table 47 Scanning conditions for the environments

The QCT analysis of these data used the “no phantom” functionality of the Mindways™ program, where an analysis is undertaken using only the QA slope and intercept values collected at the initial calibration phase described in chapter three. The calibration phantom was included in the images collected for the specimen scan but was unable to be used for the QCT evaluation as the FOV was too small for the analysis program. The bone investigation tool (BIT) part of the program can process images with a small FOV, but using this type of analysis did not fit with the clinical model of this validation method. The original scans from the bodies were

also analysed without the phantom as the scans were performed prior to the introduction of the bone calibration phantom at the VIFM.

The full QCT clinical testing procedure was performed on all three groups of slice reconstructions, on all 17 cases; the right hip in the body, and both a bone and soft-tissue algorithm applied to specimen scans of the right hip specimens.

An analysis of both the spatial (i.e. bone area and volume) and bone mineral density (i.e. vBMD and bone mass) characteristics was undertaken. The six variables chosen for evaluation represent routine clinical usage of the software and match those measured in chapter four for the 289 person sample. The cortical depth and buckling ratio were also included as these were thought to provide a means of observing the effect of the application of the algorithm relating to strength characteristics. The aBMD was not evaluated as it is derived via the application of an algorithm on the vBMD data.

6.3 Results

Each of the six variables tested on the MFC17 cases were plotted on line graphs which represent individual cases along the x-axis, and the three measurements results for that variable in the y axis, and results are included as appendix 6A.

The individual results for all variables were then assigned a weighting according to their fractional contribution to the sum for each of the cases. The value for the *body, bone* and *soft* scanning conditions were converted to a percentage of the 100% whole. The expectation therefore, if there was no difference between the applications of the various scan environments on the result from each variable, is that each of the % results would provide a 33.33% contribution to the value for each variable. Table 48 documents the actual contributions measured, and includes the highest contribution value for each variable highlighted red, and the lowest a blue.

Variable	% Body	% Bone	% Soft
Bone Mass % Contribution	29.9	39.7	30.4
Bone Area % Contribution	34.9	32.4	32.7
Bone Volume % Contribution	36.7	31.2	32.1
vBMD % Contribution	27.0	42.1	30.9
Cortical Depth % Contribution	35.7	36.9	27.4
Buckling Ratio % Contribution	35.7	28.3	36.0

Table 48 Total (%) distribution of three scan conditions

The distribution of values in the table indicates that the bone area (34.88%, 32.40% and 32.37%) delivers the most consistent result independent of the algorithm, slice thickness, FOV or surrounding tissue environment. The most variable factor of the three environments was the volumetric bone mineral density value (27.03%, 42.06% and 30.92%).

The application of the *bone* algorithm and conditions resulted in a highest estimation for three of the six variables, (bone mass, vBMD and cortical depth) while the in-situ *body* scans results in the lowest estimation of those same three variables. The *soft*-tissue fine slice series provides the middle estimation in all categories, except in the area of buckling ratio where it provides a slightly higher estimation than the *body* scanning condition. A series of individual multivariate analyses was then undertaken to compare these results statistically.

6.3.1 Multivariate Analysis

Comparisons were made for results of bone area, bone volume, bone mass, vBMD, cortical bone depth and buckling ratio measurements for *body*, *bone* and *soft* MDCT scanning conditions. The Wilk's Lamda, *p* value and eta squared are included in the table 49. For all variables, there were highly significant effects for the scan condition. A comprehensive table of the ANOVA analyses for these data is included as appendix 6B.

Variable	Wilk's Lamda	*p*	eta squared
Bone area	0.476	*p*=0.004	0.524
Bone volume	0.241	*p*<0.005	0.759
Bone Mass	0.107	*p*<0.005	0.893
vBMD	0.023	*p*<0.005	0.977
Cortical bone depth	0.079	*p*<0.005	0.921
Buckling Ratio	0.518	*p*<0.005	0.482

Table 49 Comparison of measurement results

The eta squared result reveals exceptionally large effects (>0.1) from the condition for all variables, and is most profound for the vBMD, and less so for the buckling ratio and bone area.

To assess any correlation of the effect of the bone scanning condition on the spatial and quantitative aspects of the QCT analysis, the bone area (spatial) and the vBMD (quantitative) were selected for further analysis.

6.3.2 Correlation and Regression (Spatial)

A comparison of the *body* scan condition with the *soft* scan condition was made and a scatter plot of that comparison is presented in figure 83. The *body* and *soft* scan conditions represent images acquired in different environments, (in-situ and specimen), but use the same image reconstruction algorithm. Other differences between the two conditions are the FOV (500mm in the *body* and 180-240mm in the *soft*) and the reconstructed slice thickness (2mm in the *body* and 1mm for the *soft*). The R^2 value (intercept suppressed) for these scan conditions that used same slice reconstruction algorithm but different biological conditions was 0.826.

A comparison of the *soft* scan condition is included as a comparison in figure 84. Both conditions represent scans of the specimens and therefore any difference will reflect influences from a different reconstruction algorithm. Other differences between the two scanning conditions are the reconstruction slice thickness (1mm for the *soft* and 0.5mm for the *bone*). The R^2 value for the scan conditions using the

same scanned information but processed using different slice reconstruction algorithms was 0.924.

Stepwise regression analysis indicated no influence from the age of the tissue donor on the bone area measurements. The following linear regression summaries were therefore created:

Soft Condition Bone area = (0.791 x *Body* Bone Area) + 4.95

(Constant *p* value = 0.105)

Soft Condition Bone area = (0.932 x *Bone* Bone Area) + 2.43

(Constant *p* value = 0.261)

The regression residuals were normally distributed for both equations. Results indicate a strong and consistent relationship between the two reconstruction algorithms representing *soft* and *bone* conditions. Results also indicate a small effect on the spatial result from the biological environment (i.e. in the *body* or as a specimen) from which the QCT analysis is made.

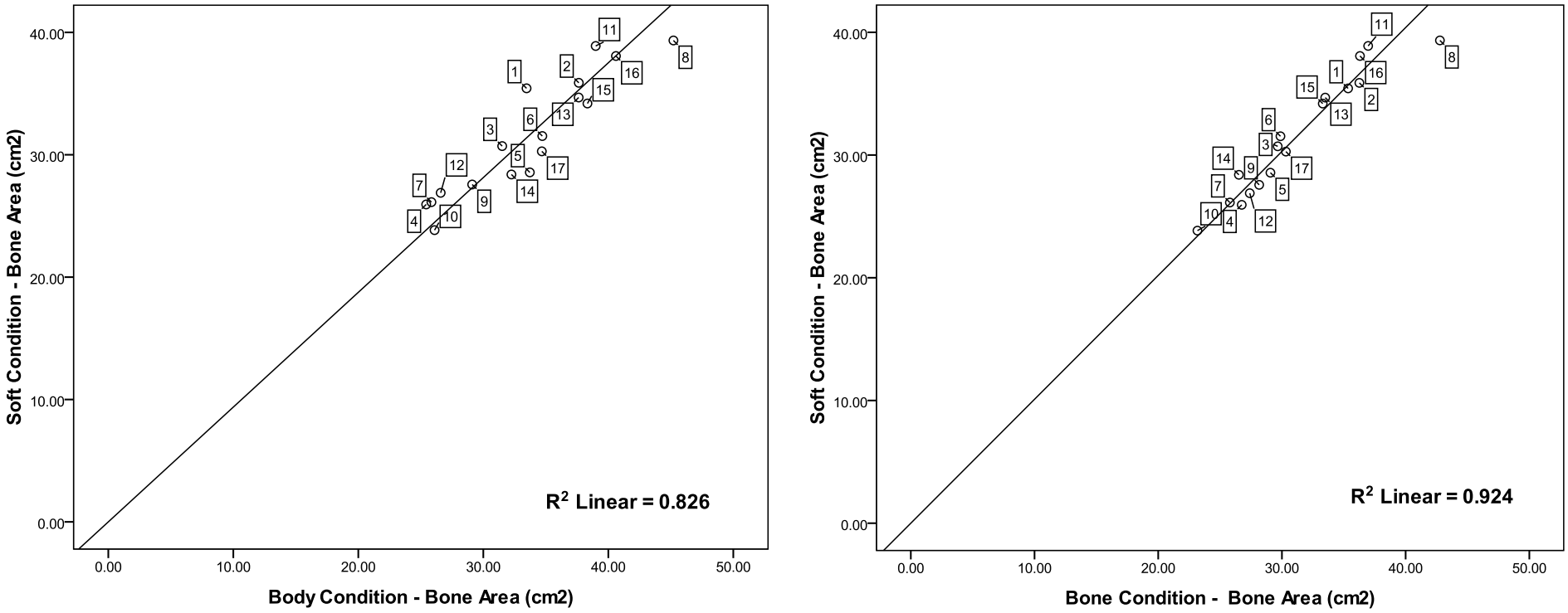

Figure 84 *Body*, *Soft* and *Bone* scan conditions scatters for bone area QCT evaluation

6.3.3 Correlation and Regression (Quantitative)

All conditions were maintained for the evaluation of quantitative QCT effects as for the spatial analysis in the section above.

A comparison of the *body* scan condition with the *soft* scan condition is presented in figure 84. The R^2 value (intercept suppressed) for the scan conditions using that used the same slice reconstruction algorithm but a different biological environment was 0.783.

A comparison of the soft scan condition is included in figure 85 for comparison. The R^2 value for the scan conditions using the same scanned information but processed using two different slice reconstruction algorithms was 0.937.

Stepwise regression analysis indicated no influence from the age of the tissue donor on the bone area measurements (p=0.723). The following regression summaries were created:

Soft Condition vBmD = (0.945 x *Body* vBMD) + 50.20

(Constant p value = 0.114)

Soft Condition vBMD = (0.866 x *Bone* vBMD) – 51.57

(Constant p value = 0.014)

The regression residuals were normally distributed for both equations. Results indicate a strong and consistent relationship between the two reconstruction algorithms representing the *soft* and *bone* conditions, which is similar to that of the spatial comparison. Results also indicate a small effect on the quantitative result from the biological environment (i.e. in-situ or specimen) from which the QCT analysis is made, which is slightly larger than that demonstrated in the spatial analysis.

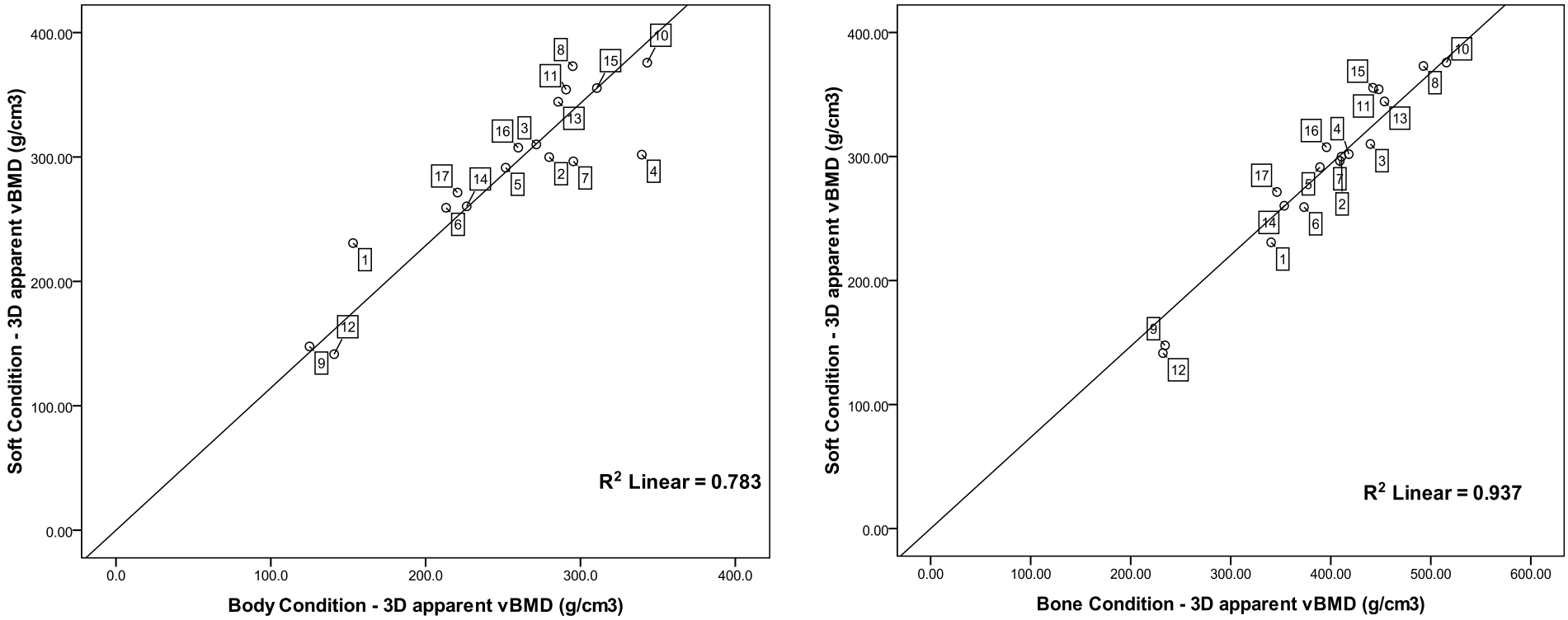

Figure 85 *Body*, *Soft* and *Bone* scan conditions scatters for vBMD QCT evaluation

6.3.4 Image Inspection

The case labeled MFC580 was observed to have the most variability of those tested throughout the three scanning conditions. The original body condition scans were therefore reconstructed for 3D scrutiny. Inspection of the DICOM data from this case demonstrated that the right hand was positioned over the right hip during the admission VIFM scan, and an AP and lateral radiograph generated from those data are included as figure 86. There were however no notes in the research records to indicate that the QCT analysis was anything other than straightforward for this case. The unexpected variation in results for this case therefore remains unexplained. Issues known to have affected QCT analysis due to hand position have been previously explained in appendix 4I.

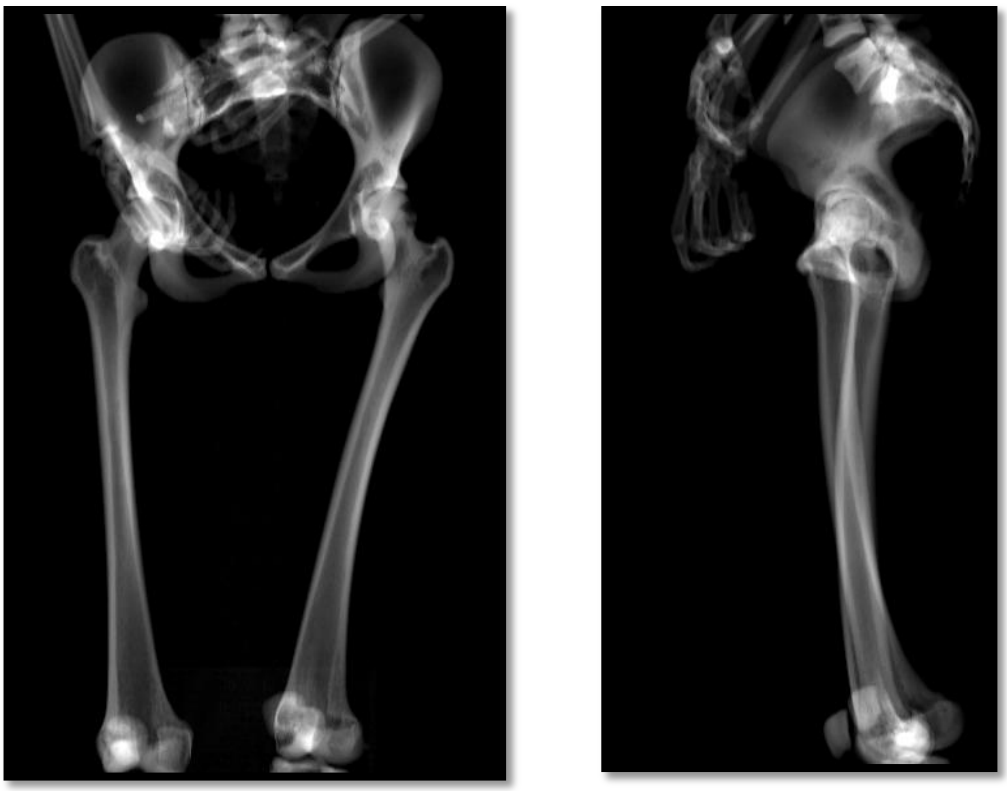

Figure 86 AP and lateral radiographs of MFC580

Note the left hip while being in some degree of rotation and adduction, does not have the hand positioned over it. The right hip however is in good position from a rotational perspective, but has the hand right over the hip area.

6.4 Discussion

The evaluation of three varied MDCT scanning conditions clearly demonstrates that the biological environment (i.e. within the body or as a bone specimen), and choice of reconstruction algorithm, slice thickness and FOV, either separately or in combination, has a predictable effect on QCT spatial and quantitative measurements. The differences in measurements obtained were shown to be less in terms of spatial evaluation than for the quantitative assessment for all conditions, though all differences in measurement were consistent and thus predictable. There were however significant limitations in this study.

In retrospect the scanning condition for the specimens may have been better managed by limiting the number of different technical aspects to only the algorithm and biological state, i.e. does the fact that the bone is scanned as a specimen (no soft-tissue surrounds) alter the results, or is it the algorithm alone affecting the measurement obtained? The calibration of the images by using the bone calibration phantom may also have improved the reproducibility of the results. The investigation may also have been more effective if each DICOM series or scan condition represented only one change in the scanning environment instead of the two or three which were included.

The opportunity to rescan the specimens was time limited, and access to the VIFM PACS server for raw data storage was also problematic for any period longer than one week. Also the *body* condition scans were performed in 2005, and hence only the slice reconstruction data were available. The opportunity to store raw sinogram CT data for later reanalysis would have been of significant benefit to this study. Unfortunately, this functionality is currently not possible at the VIFM.

Generally however, the effects on the calculation of QCT spatial and quantitative measurements were demonstrated for these seventeen samples to be consistent and predictable. A higher degree of correlation was demonstrated in scan

conditions where the biological environment was the same (in or out of the body) irrespective of the slice reconstruction algorithm. Their precision in terms of direct spatial measurement, and qualitative CT assessment against bone ash weight were not part of the experiment, as there was no permission for the destruction of the samples.

The results obtained in this study confirm that careful consideration needs to be given to using "*accurate*" or indeed "*true*" density in a quantitative imaging context. The conflation of the terms *true* and bone density as it relates to the radiological expression should be avoided. A*pparent* most certainly needs to be reinstated in most of the bone mineral-based clinical literature both in the expression of 2D and 3D assessments. The detail that the value expressed by BMD analysis is analogous to a hydroxyapatite bone equivalent and not the actual ash weight cannot just be assumed even with the use of a calibrating device. The partial volume effect in measuring bone is too great.

The QCT observations demonstrate that there also needs to be close consideration given when comparing one set of data to another or an individual's data to that of anyone else. This is especially so if there is a change to the scanning parameters used between series. There is a need to provide with any comparison, some sense of exactly what effect may be expected from the different imaging protocols used, or how those differences have been addressed in the analysis. Unless the same machine using the same algorithm and the same slice interval and reconstruction method is employed, the data is not necessarily comparable on its own. It could also be argued that if it is not the same technologist or researcher doing the analysis, then there needs to be some establishment of the effort made to reduce any effects of reproducibility errors. The magnitude of expected change in serial BMD measurements is usually too small.

The findings from the image inspection procedure conducted for one case demonstrated that the results of the *body* imaging condition is likely affected by

the positioning of the hands over the hip region. The variation of results may also be indicative of the slight degree of rotation of the hip that was also evident. The finding emphasises the need for careful positioning in the living, and the potential for an additional source of error in using the clinical software for *"off label"* mortuary analysis.

The consistency of CT number as a result of detector and photon regulation, as well as the ability of the MDCT system to negate the effects of body habitus changes that may accompany ageing, likely has a positive effect on QCT reproducibility. Likely to be less positive are the effects of various artifact reduction algorithms on producing aesthetically pleasing but somewhat *manufactured* images in terms of their quantitative attenuation effects. It would therefore be highly constructive to repeat a similar study on data where image correction algorithms have been employed in an effort to either confirm or negate their effect on the QCT assessment. These data would be extremely useful for the QCT examination of an individual who has had one hip replaced with a prosthetic device, as these people at present are unable to be assessed using QCT because of beam hardening artifact. The application of a correction for the beam hardening artifact would likely affect the QCT measurement.

Though well correlated, the findings of the study strongly indicate that quantitative CT analysis is sensitive to very small changes in the imaging protocol in terms of the precision, though spatial measurements are less sensitive to the same changes. The application of the "bone" algorithm to the MDCT data for example resulted in an image-weighting that enhanced spatial characteristics visually (i.e. the trabeculae were crisp and well defined, and hence spatially well represented) at the expense of quantitative integrity (i.e. the BMD estimations were well inflated compared those of the other scan conditions). Ionising radiation dose clinically is also a consideration when attempting to maximize the signal to noise ratio.

The application of a bone algorithm clinically attempts to improve fine spatial resolution, but this comes at the expense of higher image noise (191), and hence requires additional dose to maintain an appropriate signal to noise ratio. Every scanning adjustment on the CT unit is balanced by an offset in some other factor, and therefore a fine balance between image quality and dose is required.

6.5 Conclusion

Great care is required in attributing the words *true* or *absolute* to a clinical assessment of quantitative radiological measures such as vBMD made using QCT techniques. The MDCT scanning parameters used to produce the reconstructed slice information have a significant effect on qualitative, and to a lesser extent, spatial assessments made, and thus affect precision.

The limited number of specimens used for this study has necessarily limited the scope of the investigation. The study has however highlighted a need for further investigation into methods that may be used to link data and findings from one clinical site or unit to another. The need is especially clear for those individuals requiring serial bone investigations for fracture risk assessments that are conducted years apart and where testing equipment and personnel have most likely changed.

CHAPTER 7

HIP FRACTURE, DEATH AND HOW MDCT DATA CAN IMPROVE FRACTURE RISK EVALUATION IN THE LIVING

"Uncertainty in the presence of vivid hopes and fears, is painful, but must be endured if we wish to live without the support of comforting fairy tales….To teach how to live without certainty, and yet without being paralyzed by hesitation, is perhaps the chief thing."

~ David Malone ~

Previous chapters have presented self-contained empirical studies that have been linked by the overarching goal of providing a radiological model of age dependent change in the human femur. The chapters have contained detailed discussion sections that relate to CT technology and to the scientific population-based findings, and those will not be repeated in this chapter. Rather those data will be used as a reference from which a comparison will be made with the data from a small number of individuals with femoral neck fracture. The hypothesis is that the fracture cases will present with similar QCT and morphometric assessments as the normal or control group from the first two research chapters.

In line with that hypothesis, chapter 7 presents the following:

- An evaluation of the prevalence of hip fracture resulting in death using a statistical analysis of data from the VIFM.
- An analysis from a limited number of hip fracture cases which are then related to the previous *normal* population-based studies conducted in chapters 4 and 5.

7.1 Introduction

The central aim of this thesis has been to define a series of reproducible radiological expressions of ageing, both clinical and morphological, in the human femur. In doing this, the goal is to produce a model of what is occurring now in an ageing Australian predominantly urban population. The prevailing clinical use of

these data lay in methods to better determine the fracture risk in living individuals. Hence an epidemiologically-based examination of hip fracture among those who have died and been admitted to the VIFM has been interwoven with an evaluation of a small number of unilateral fracture cases.

Diseases of the muscles, bones and tendons were attributed to 1076 registered deaths in Australia in 2006 (301). This represents 0.8% of all deaths registered in Australia for that year, though one expects that hip fracture was a contributing factor to the deaths of many more individuals. This epidemiological data demonstrates a rise from 0.6% of all reported deaths in 1997. The 2006 results reveal that females had over twice the number of deaths (*n*=747) than males (*n*=329) attributable either directly or indirectly from diseases of muscle bone and tendon, which is consistent with data from the previous decade. The median age at death generally in Australia increased slightly over the decade. The median age at death for men rose from 75.8 years in 1997 to 80.8 years in 2006. The median age at death for females increased from 80.2 years in 1997 to 84.4 years in 2006.

Osteoporosis was stated as the registered cause of death for 250 Australians in 2006 (301). More than four times the number of females (*n*=211) were registered to have died from osteoporosis than males (*n*=39), with recorded median ages at death of 89.3 years for the females and 87.9 years for the males.

ABS data from 2001 estimates that 32% of the population (approximately 6 million people) have a disease of the musculoskeletal or connective tissues as a long-term health condition (302). These data record that 1.6% of the population had osteoporosis, with almost all being over the age of 25-years. The prevalence of osteoporosis increases with age, particularly for women, with 10% of women between 65 and 74 years reporting having the condition, and 15% of those 75 years and over. These ABS data however represent those with diagnosed conditions and one expects that far more Australians live with undiagnosed bone and or connective tissue conditions.

Health expenditure for osteoporosis in Australia in 2004-2005 was more than $304 million, which represents almost 8% of the total direct health expenditure on arthritis and musculoskeletal conditions for that year (303). Pharmacy dispenses accounted for 71% or $215 million of the total osteoporosis-related expenditure.

Australian health status data shows Medicare claims per person in Australia in 1998 were on average 10.8 per person, and in 2008 they had risen to an average of 13 per person (304). Men averaged 8.8 medical services in 1998 and 10.9 in 2008, while women averaged 12.8 medical services in 1998 and rose to 15.2 in 2008. Medical services provided to those 65-years and over averaged 24.2 visits in 1998 and 29.8 in 2008. These data demonstrate that increases in average life-expectancy will impact significantly on the ability to service the healthcare needs of the nation both financially and through workforce requirements generally.

7.1.1 Overall Study Aim and Objectives

The overall aims of this chapter are to describe the prevalence of hip fracture at the VIFM, and to compare data from a limited number of fracture cases with the reference data created in chapters 4 and 5. Specifically

1. The VIFM hip fracture evaluation provides an epidemiological review of the prevalence and causes of hip fracture-related deaths for the population admitted to the VIFM during the 2008 calendar year. The purpose of the evaluation is to establish a context for the quantitative hip fracture evaluation to follow.
2. The MDCT hip fracture evaluation compares quantitative QCT data from fourteen individuals, who sustained a unilateral fracture of the hip and died, with the overall data from the clinical chapter four, and the anthropological data from chapter five. The purpose is to identify any factor or combination thereof, which may indicate a tendency to hip fracture. Two-dimensional BMD studies have previously been shown to be sensitive in terms of

identifying age-related change but are not particularly specific in terms of identifying those that will fracture (102).

7.2 Materials and Methods

7.2.1 Sample Description

The VIFM hip fracture review data was sourced with assistance from research staff at the VIFM. The data represents admissions at the VIFM in 2008 where a hip fracture was either directly or indirectly related to the cause of death (COD).

The MDCT fracture group data is derived from 14 unilateral MDCT examinations that were conducted and collected in accordance with the QCT and anthropological outlines previously described. The measurements made for the group are from the contra-lateral or ***non-fractured hip***. No assessment of the fractured hip has been undertaken. The fracture group consisted of seven left (male *n*=5, female *n*=3) and seven right (male *n*=2, female *n*=4) investigations of the contra-lateral or normal hip. The average age was 85.6 years (range of 71 – 98 years), the average weight was 52.9kg (range of 28 – 75kg), and the average height was 156.4cm (range of 137 – 171cm), with an average BMI of 21.38 (range of 14.92 – 27.83).

7.2.2 Statistical Methods

Statistical analyses were performed using SPSS statistical software (version 17.0.2, SPSS, Chicago Ill, USA). Only data from those 70- years and over have been used for the un-fractured comparison group. Further information regarding the statistical methods used in this study may be found in **section 3.3.9.**

7.2.3 VIFM Hip Fracture Epidemiology Methods

In 2008 there were 4062 admissions to the VIFM. In April of 2009 a request was made to statistics support staff for the number of admissions that included a pathology report that indicated a recent hip fracture as being causal to death. A request for age, height and weight for each subject was also made as per the ethics approval for this project.

The investigator provided a key word list as well as Boolean expressions, to the statistics support member who conducted the searches, deleted multiple entries and then de-identified the information for transmission. The cause of death (COD) statement that was included in that information was then coded by the investigator. Those admissions where the COD was clearly and primarily associated with an age-related fracture of the hip were coded as **[1].** Those cases where it was evident that a low velocity fall and not the hip fracture itself was likely the primary COD were coded as **[2].** Hip fractures caused by high velocity impact fractures such as road trauma and falling from a height were coded as **[3],** and finally in cases where the pathologist's report indicated a recent hip fracture causal to death but an unstated COD, a code of **[4]** was used. The sample was also separated into male and female groups to establish gender influences on COD categories of hip fracture.

7.2.4 MDCT Hip Fracture Methods

The MDCT hip fracture data used was collected along with the non-fracture data and hence during the same time period. Fracture data was collected from individuals that could be identified radiologically as having a unilateral fracture of the hip, and that fulfilled all other study-related requirements (as outlined in the common materials and methods data collection section in chapter three) for the non-fractured hip. The collection of these fracture cases was limited to those with an age-related cause.

Radiological evaluations from the contra-lateral side to that of the fracture were used. Findings described in chapters four and five show an almost symmetrical presentation of age-related characteristics such as vBMD, aBMD, cortical depth and Hounsfield unit average in those over the age of 70 years. The assumption of symmetry would be problematic in a study evaluating the non-fractured side in younger individuals if handedness, or more importantly, footedness was not known (241).

Those cases where a unilateral total hip replacement (THR) was used to treat a fracture were not collected, as ethics approval did not provide access to records to assess if the THR was used to treat an age-related osteoporotic fracture or another pathological condition. It was also difficult to establish an effective image segmentation of the hip using the QCT software in cases where a THR was placed, as beam-saturation and hardening effects usually affected the non-fractured side significantly enough to render either automatic or manual hip processing impossible. Image quality for these cases in terms of the signal to noise ratio may be improved with the application of a noise suppression or beam hardening correction algorithm (305) though as previously discussed, this will impact the radiation burden. The application of *mathematical corrections* would also likely affect the quantitative features of the data from which the determination of BMD is subsequently made as described in chapter 6.

Figure 87 documents images from one of the fracture cases where a Zimmer™ hip screw has been inserted into the fractured hip. The case presents an example of a new or recent fracture. Several fracture cases presented with these types of fixation devices. A fracture line was distinguishable in the femoral neck or trochanteric line, and the beam hardening effect was significantly less than for the THR, and so these cases were able to be analysed using the QCT software.

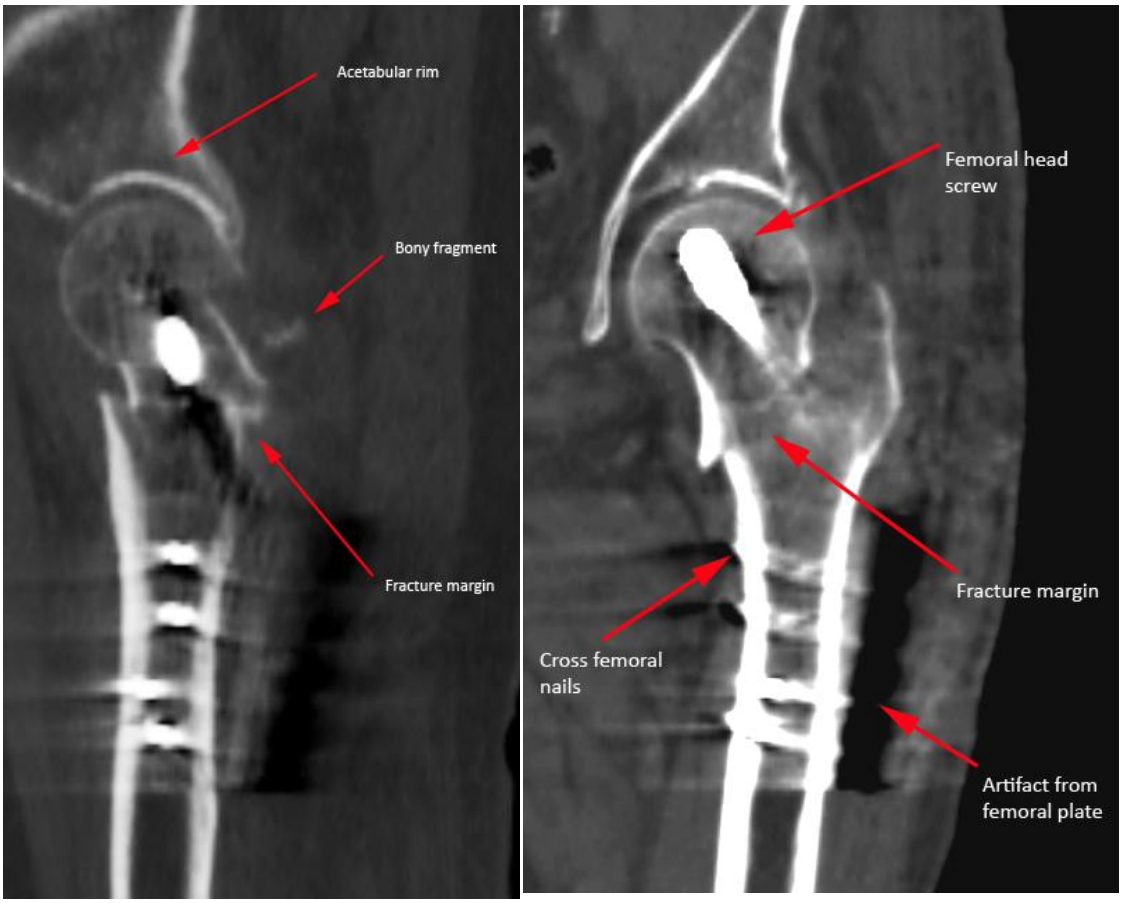

Figure 87 Sagittal and coronal examples of a recent fracture

Note the presence of bone fragments (labeled) indicative of a new fracture.

7.3 Results

7.3.1 VIFM Hip Fracture Epidemiology Results

Database searches from 2008 cause of death entries identified a total of 87 admissions (males *n*=54 or 59.7%, females *n*=33 or 40.3%) that were attributed by the pathologist as being associated with a recent fracture of the hip. The hip fracture sample therefore represents 2% of the total number of admissions for the 2008 calendar year at the VIFM, though there were likely more cases that fit the study criteria, but they lacked the classification of the pathology report to adequately identify them. The 87 cases broken into COD categories for each gender are included as table 50.

	2008 VIFM Hip Fracture Admissions			
	Male		Female	
	n	%	n	%
Age-Related Fracture	11	12.6%	18	20.7%
Fall-Related	3	3.4%	3	3.4%
High Velocity Impact	38	43.7%	10	11.5%
Unstated	2	2.3%	2	2.3%

Table 50 COD breakdown of numbers

The prevalent COD associated with a hip fracture was represented by males (*n*=38 or 43.7% of the sample) and involved in a high velocity impact incident. The second largest number of deaths associated with a hip fracture was represented by females (*n*=18 or 20.7% of the sample) and involved an age-related fracture of the hip. Ignoring the contribution from the unstated category, for the VIFM hip-fracture groups, males are 37 times more likely to experience a hip-related fracture linked to their death by a high-velocity impact than they are an age-related hip fracture. For females however the results are amplified and reversed, in that they are 48 times more likely to experience an age-related hip fracture linked to their death, compared to that of a high-velocity impact hip fracture incident. A low-velocity falling incident linked to death with an associated hip fracture is represented identically for both males and females (3 cases or 3.4% of the sample). Because of the low subject number in the unstated COD category (2 in each or 2.3% of the population), a comprehensive analysis of these results has not been included.

An examination of the mean age for each of the COD categories was also conducted and is included as table 51. The average age of the high-velocity impact category is substantially lower (males, 40 years and females, 30 years) than that of the age-related hip fracture and fall-related deaths (males, 77 years for both and females, 83 and 82 years respectively).

	Fracture Types and Age							
	Age-Related		Fall-Related		High Velocity Impact		Unstated	
	Age (y)		Age (y)		Age (y)		Age (y)	
	Mean	Std Dev	Mean	Std Dev	Mean	Std Dev	Mean	Std Dev
Male	**77**	10	**77**	11	**40**	19	**34**	48
Female	**83**	8	**82**	9	**30**	16	**49**	4

Table 51 COD code and mean ages

For the VIFM hip-fractured groups, the average age of males who died as a direct result of an age-related hip fracture is 8% (approximately 5 years) younger than those females who died as a consequence of the same event. An evaluation of the mean height of the individuals in relation to the COD code was also made and is included as table 52.

		Height (cm)		Weight (kg)		BMI	
		Mean	Std Dev	**Mean**	Std Dev	**Mean**	Std Dev
Male	Age-Related	**170**	8	**71**	17	**24.41**	4.96
	Fall-Related	**167**	6	**52**	8	**22.98**	5.97
	High Velocity Impact	**172**	6	**81**	18	**27.22**	5.14
	Unstated	**170**	1	**70**	9	**24.20**	3.40
Female	Age-Related	**153**	5	**51**	14	**21.69**	5.37
	Fall-Related	**152**	5	**52**	10	**22.23**	3.77
	High Velocity Impact	**157**	7	**59**	11	**23.73**	4.06
	Unstated	**148**	15	**67**	23	**30.21**	4.30

Table 52 Height, weight and BMI of hip fracture death victims

High-velocity impact victims of hip fracture were found more likely to be taller on average than the other groups for males and females. Both male and female fall-related groups were slightly shorter than their age-related fracture comparative groups. For males, the age-related fracture group was around 2% taller than the fall group, and the fall group where on average 3% shorter than the high-velocity

impact group. For females there were less difference (1cm or less than 1%) in mean height between the fall and age-related fracture groups. The mean difference between the shorter fall-related group and the taller high-velocity impact group was slightly greater at 3% which is the same difference as seen in the males.

In relation to weight, the fall-related males were significantly (p<0.05) lighter than the age-related group (27%) though the standard deviation in age for each category indicates large variation across the groups generally. For the females, as with the height mean values, these COD groups were of similar mean weights. The heaviest group for both males and females was the high-velocity impact group if the unstated group is again disregarded. For the males the high-velocity impact group was 36% heavier than the fall-related group and 12% heavier than the age-related fracture group. For the females, the high-velocity impact group was 12% heavier than both of the other age-related fracture groups. BMI for each group was analysed and is presented as figure 88.

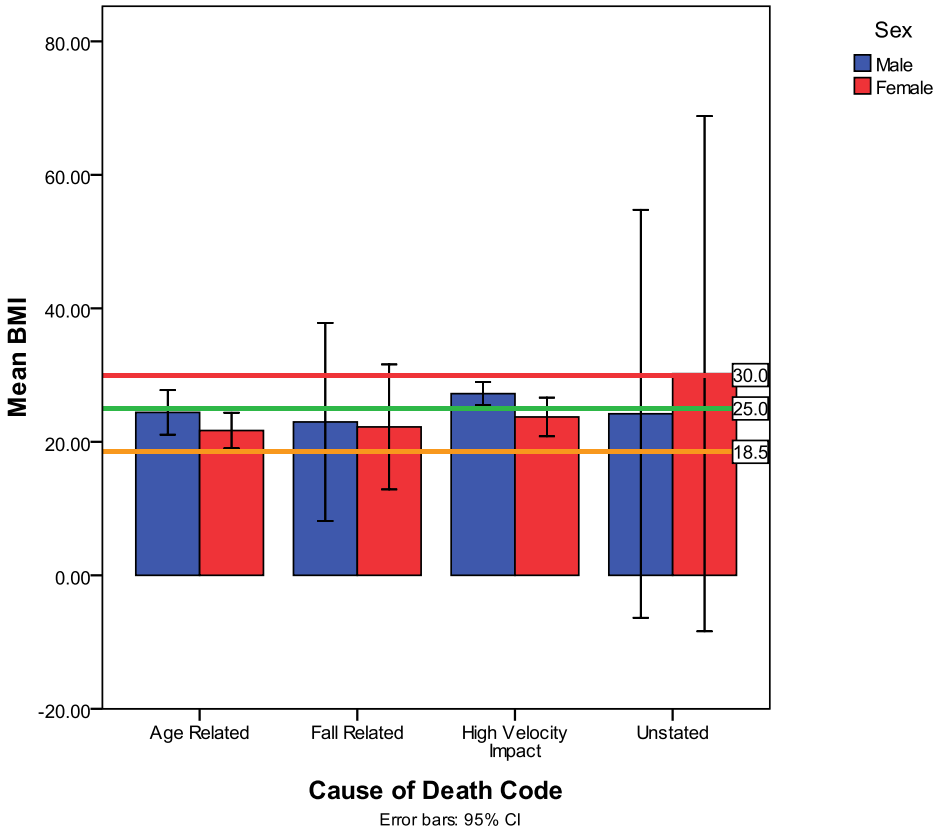

Figure 88 COD code and mean BMI for gender

Results from the comparison of mean BMI, show the male high-velocity impact group (25-30 kg/m^2) as having a substantially higher mean BMI than the age, fall and unstated categories. The fall and age-related fracture categories for both males and females were in the *healthy* BMI range (18.5-25), though the 95% confidence intervals for the fall-related group indicate substantial variation across BMI ranges generally. For the females, all except the unstated category were in the healthy BMI range.

If BMI levels for males and females are combined, the high-velocity impact and unstated categories both appear in the overweight range as demonstrated in figure 89. The age-related hip fracture category demonstrates 95% confidence levels inside the healthy range, while the fall-related category occupies the underweight (under 18.5), normal and overweight categories.

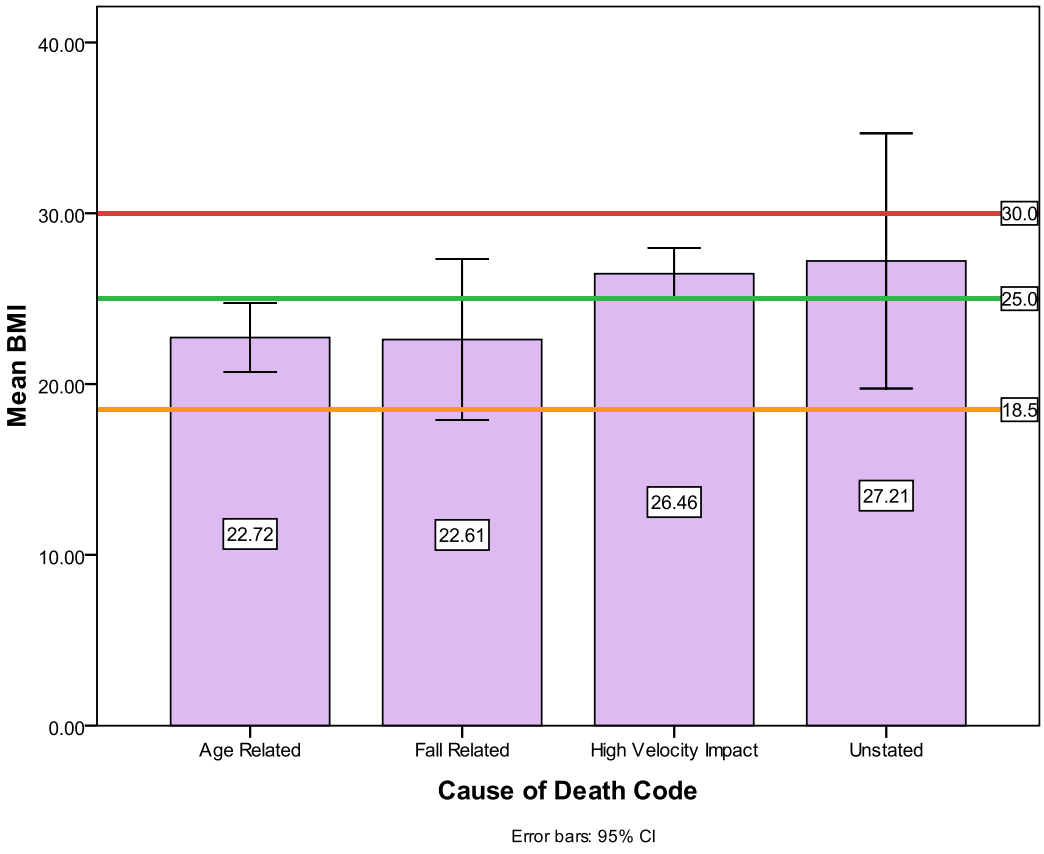

Figure 89 COD vs. mean body mass index: combined genders

Normal range (orange and above), overweight range (green to red).

7.3.2 MDCT Hip Fracture Results

All results from the fracture analysis were compared to those obtained from the non-fractured cases previously described. Full tabled evaluations of the non-fractured anthropological and clinical studies are available in appendix 5A. Results in the appendix are presented as both dichotomous and clinical age groupings.

The youngest fracture case was represented by a 71 year old female, and as such results from the non-fractured groups for which comparisons are made, have been limited to those ≥70 years. Definitions of the variables used for the fracture and non-fracture comparison may be found in chapters four and five under the *Materials and Methods* sections. Tables of the clinical and anthropological result comparisons of the fracture and non-fracture groups for each side are included as tables 53 and 54. It should be again noted that the values represented for the fractured group are from their non-fractured hip, and that there are only 14 fracture cases.

≥ 70 Years Data Only	**Hip fractue**		**≥70 Years Data Only**	**Hip fracture**	
	No	Yes		No	es
	Mean	Mean		Mean	Mean
Right long femur length (mm)	**441.2**	**440.0**	Left long femur length (mm)	**442.1**	**444.0**
Right short femur length (mm)	**418.2**	**414.6**	Left short femur length (mm)	**418.9**	**417.5**
Right sub-trochanter width (mm)	**31.4**	**31.1**	Left sub-trochanter width (mm)	**31.0**	**30.8**
Right mid-femoral width (mm)	**28.9**	**27.2**	Left mid-femoral width (mm)	**29.6**	**28.3**
Right epicondylar width (mm)	**7.6**	**79.0**	Left epicondylar width (mm)	**79.2**	**803**
Right femoral head length (mm)	**97.7**	**96.3**	Left femoral head length (mm)	**97.9**	**98.6**
Right femoral head area (cm2)	**16.1**	**15.9**	Left femoral head area (cm2)	**16.2**	**17.0**
Right Hounsfield average	**261.0**	**204.7**	Left Hounsfield average	**266.7**	**211.1**
Right AP trabecular margin (mm)	**48.0**	**51.2**	Left AP trabecular margin (mm)	**47.6**	**46.9**
Right femoral neck width (mm)	**32.5**	**31.1**	Left femoral neck width (mm)	**32.4**	**33.5**

Table 53 Mean morphometric measurements - fracture and non-fracture

≥ 70 Years Data Only	Hip fracture		≥ 70 Years Data Only	Hip fracture	
	No	Yes		No	Yes
	Mean	Mean		Mean	Mean
Right 2D BMD (g/cm2)	.664	.527	Left 2D BMD (g/cm2)	.664	.493
Right 3D BMD (g/cm3)	214.193	178.650	Left 3D BMD (g/cm3)	216.108	158.675
Right Bone Mass (g)	21.565	16.115	Left Bone Mass (g)	22.003	16.578
Right Bone Area (cm2)	32.076	30.473	Left Bone Area (cm2)	32.697	33.910
Right Bone Volume (cc)	100.216	91.117	Left one Volume (cc)	101.311	105.888
Right cort. depth(mm)	0.890	0.290	Left cort. depth (mm)	0.760	0.300
Right buckling ratio	8.970	11.000	Left buckling ratio	8.988	14.238

Table 54 Mean QCT measurements - fracture and non-fracture

No significant differences (p>0.05) for any of the morphological measurements such as femoral length (p=0.839), mid femoral width (p=0.363), femoral neck area (p=0.612), femoral axis length (p=0.444), or trabecular margin length (p=0.072) were observed. No significant difference was observed for the aBMD (p=0.644) or femoral head Hounsfield unit average (p=0.382) which were demonstrated as indicators of age-related difference in chapters 3 and 4.

Significant differences between the fracture and un-fractured groups were however observed for **vBMD** (p=0.037), femoral neck bone mass (p=0.027) and **cortical depth** (p=0.017).

Figure 90 documents apparent vBMD for fractured and non-fractured cases (averaged value of left and right for the non-fractured group) against age for those 70 years and over. The blue dots represent the non-fractured cases and the red dots the fracture cases. A line of best fit including 95% confidence intervals has been included to compare groups.

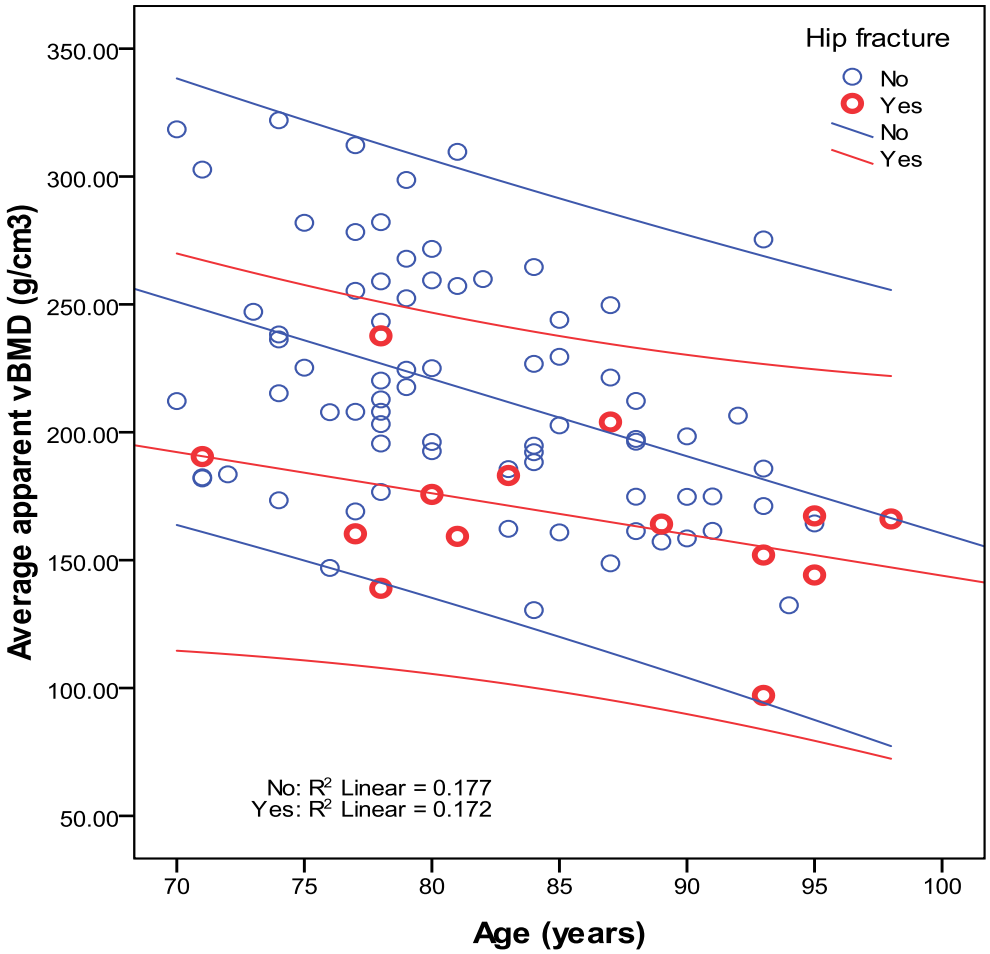

Figure 90 Apparent vBMD of fracture and non-fracture groups

At least four of the 14 fracture cases display an apparent vBMD value of their non-fractured hip that would be considered normal for their age, (i.e. the value sits close to the line of best fit for the non-fractured cases). The result likely reflects clinical findings indicating that approximately 50% of hip fractures are found in people with *normal* BMD levels (102). The other aspect to note regarding this graph is that the slope of both the fracture and non-fracture groups is similar, even with the small numbers in the fracture group, though the line is significantly below that of the non-fracture group in terms of the vBMD for each age category.

Figure 91 documents results for fractured and non-fractured cases of the apparent aBMD (average value of left and right for the non-fractured group) against age for those 70 years and over.

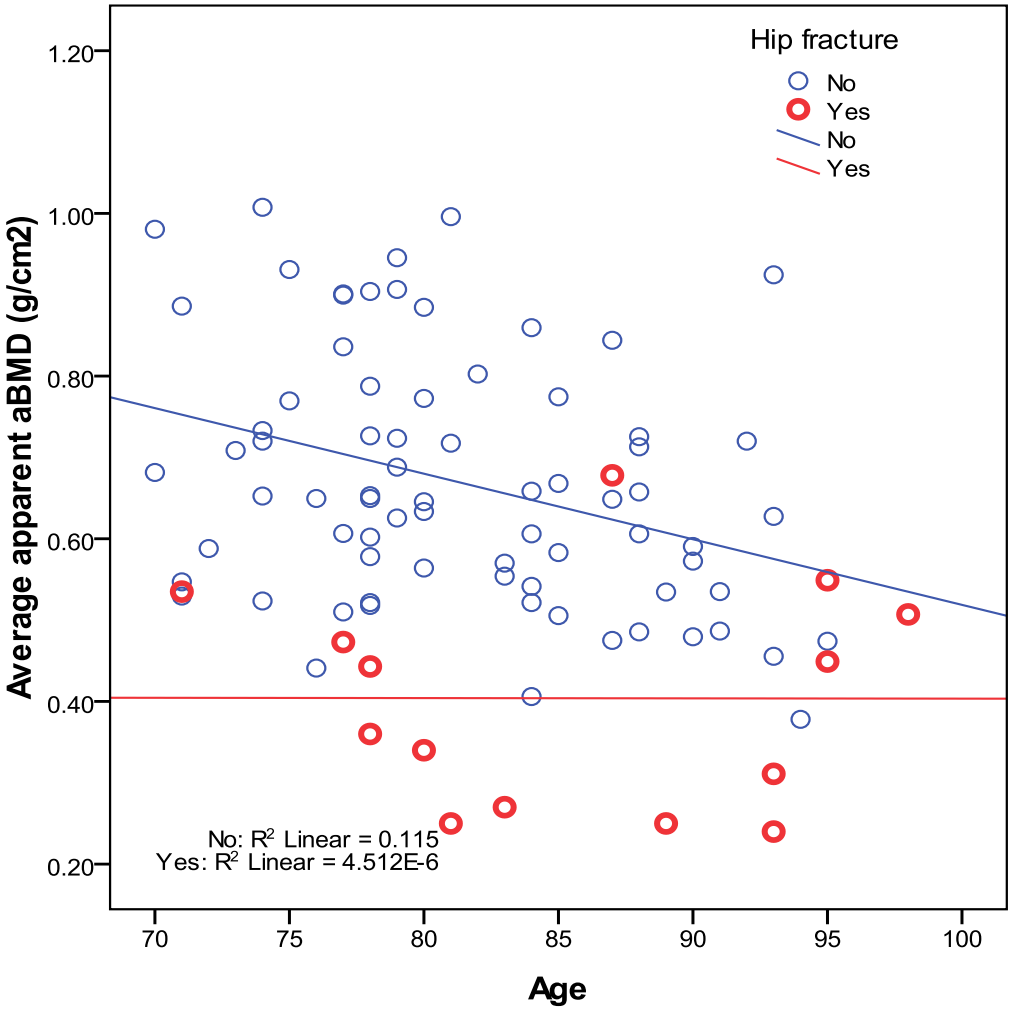

Figure 91 Apparent aBMD of fracture and non-fracture groups

The result indicates a difficulty given the subject number (*n*=14), in producing a line of best fit for the non-fractured cases. The inability to detect a lack of relationship is likely a result of the relatively small scale of differences that are available in the DXA-based equivalent technique.

The variable of cortical depth is described in detail in chapter four and represents the volume of the cortical bone (Vc) divided by the area of cortical bone (Ac) in the femoral neck. The cortical depth was shown in chapter four to be more sensitive to age-related changes in mineralisation properties of the femur than either of the aBMD or vBMD. The apparent cortical depth against age for those 70 years and over is presented as figure 92.

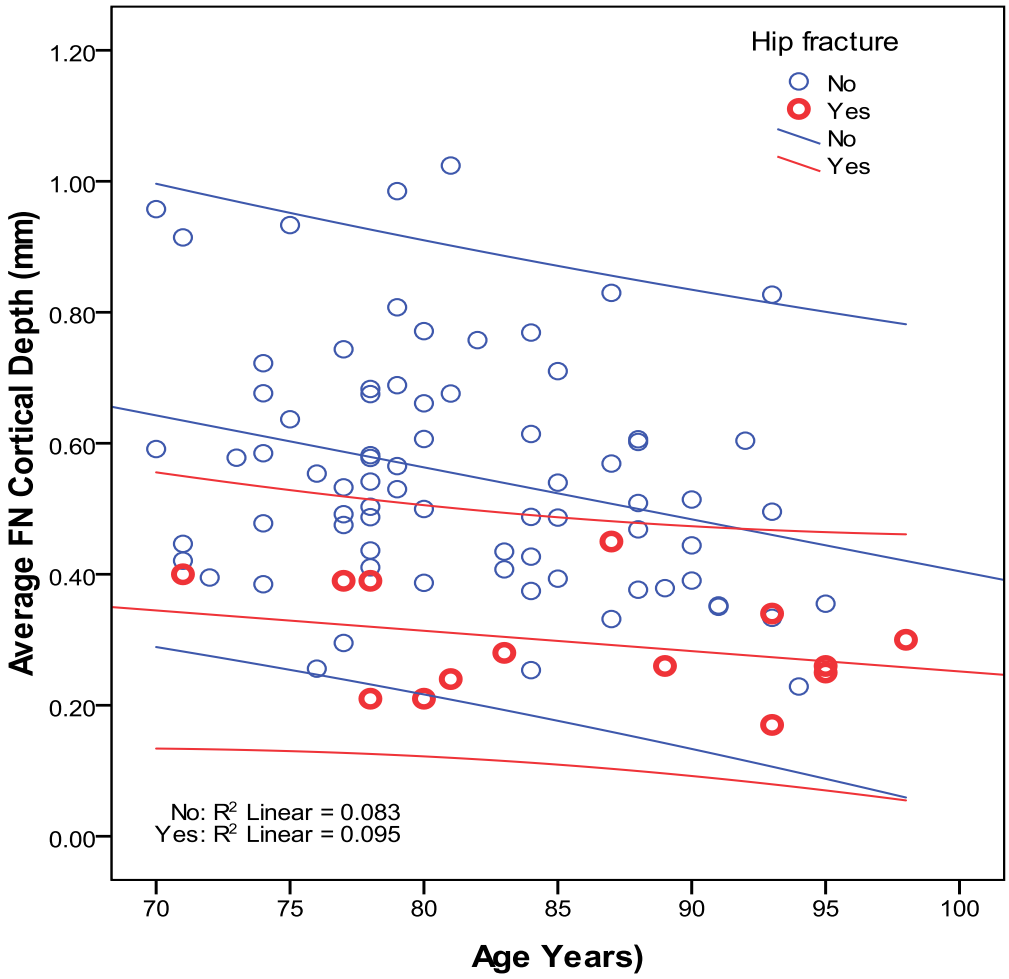

Figure 92 Apparent cortical depth of fracture and non-fracture groups

Results demonstrate that though there is one fracture case that sits more closely to the line of best fit for the non-fracture cases, there **are no fracture cases** above the mean un-fractured line, unlike the aBMD and vBMD age comparisons. The cortical depth is therefore more discriminating for fracture in these data. There are also five elderly hip measurements where the apparent cortical depth for age are below or close to the line of best fit for the fracture cases which likely represents those at the greatest fracture risk. Figure 93 compares apparent vBMD and cortical depth for males and females with and without FN fractures, including only those ≥ 70 years.

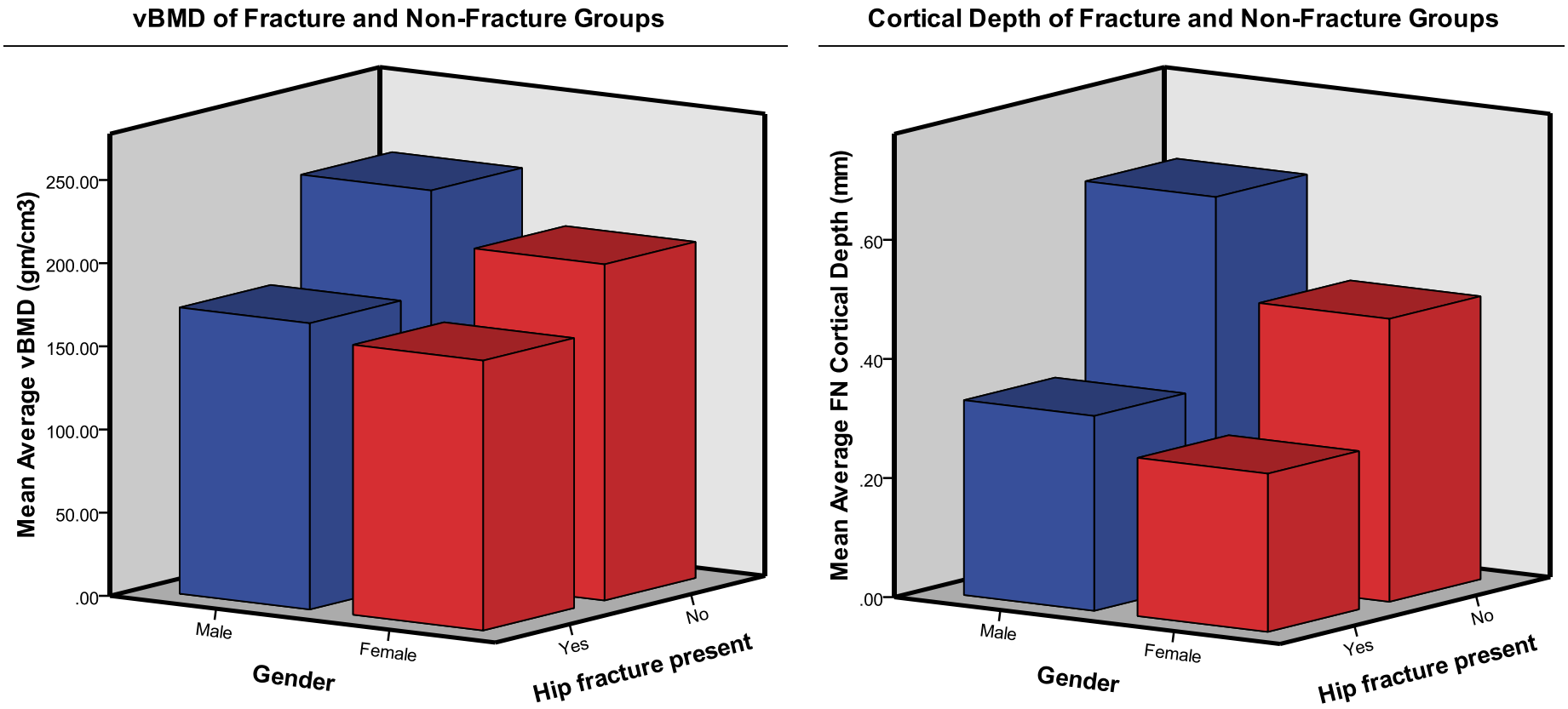

Figure 93 Apparent vBMD and cortical depth in fracture and non-fracture groups

Note the magnitude of difference evident between the fracture and non-fracture groups, i.e. the normal and fracture groups have more similar values in terms of vBMD than they do in relation to their average cortical bone depth.

Figure 93 present two observational results; firstly the magnitude of difference between the fracture and non-fracture groups using the apparent cortical depth and vBMD. Secondly it presents the male vBMD measurement relative to the female, in relation to fracture.

To ascertain any influence of BMI on fracture status, Figure 94 documents the differences in the male and female mean BMI for the fracture and non-fracture groups.

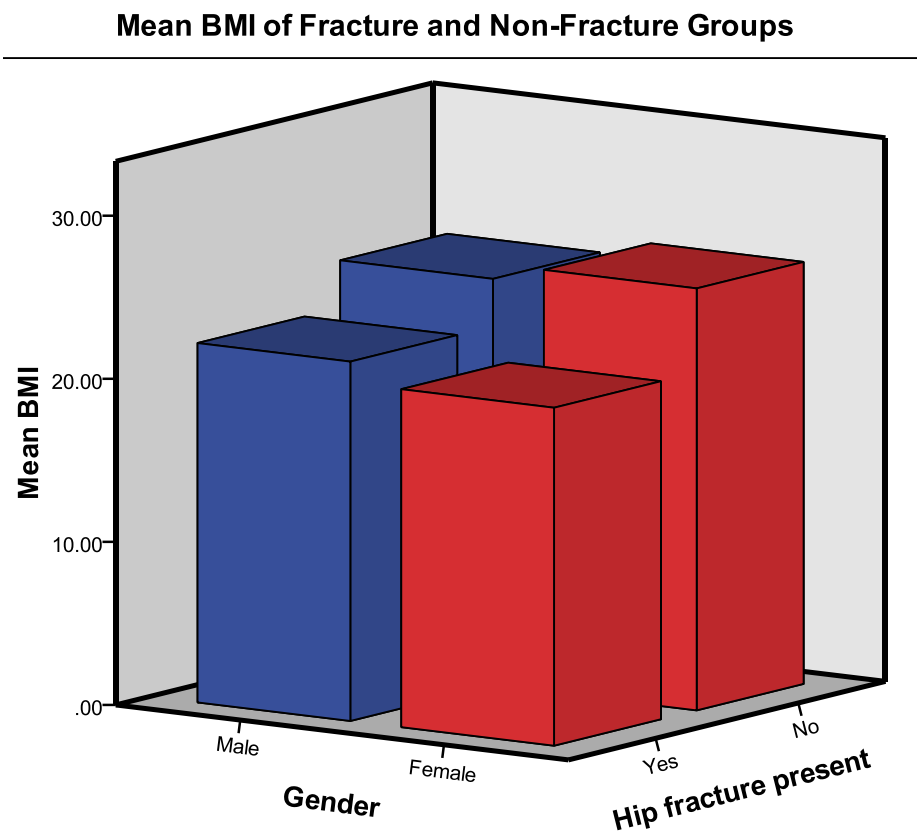

Figure 94 Mean BMI fracture non-fracture comparison

Results demonstrate a slightly lower mean BMI for the fracture groups as compared to those without a fracture.

To establish any gender bias in the cortical depth results, the data was separated for female and male contribution, and results are presented as figure 95.

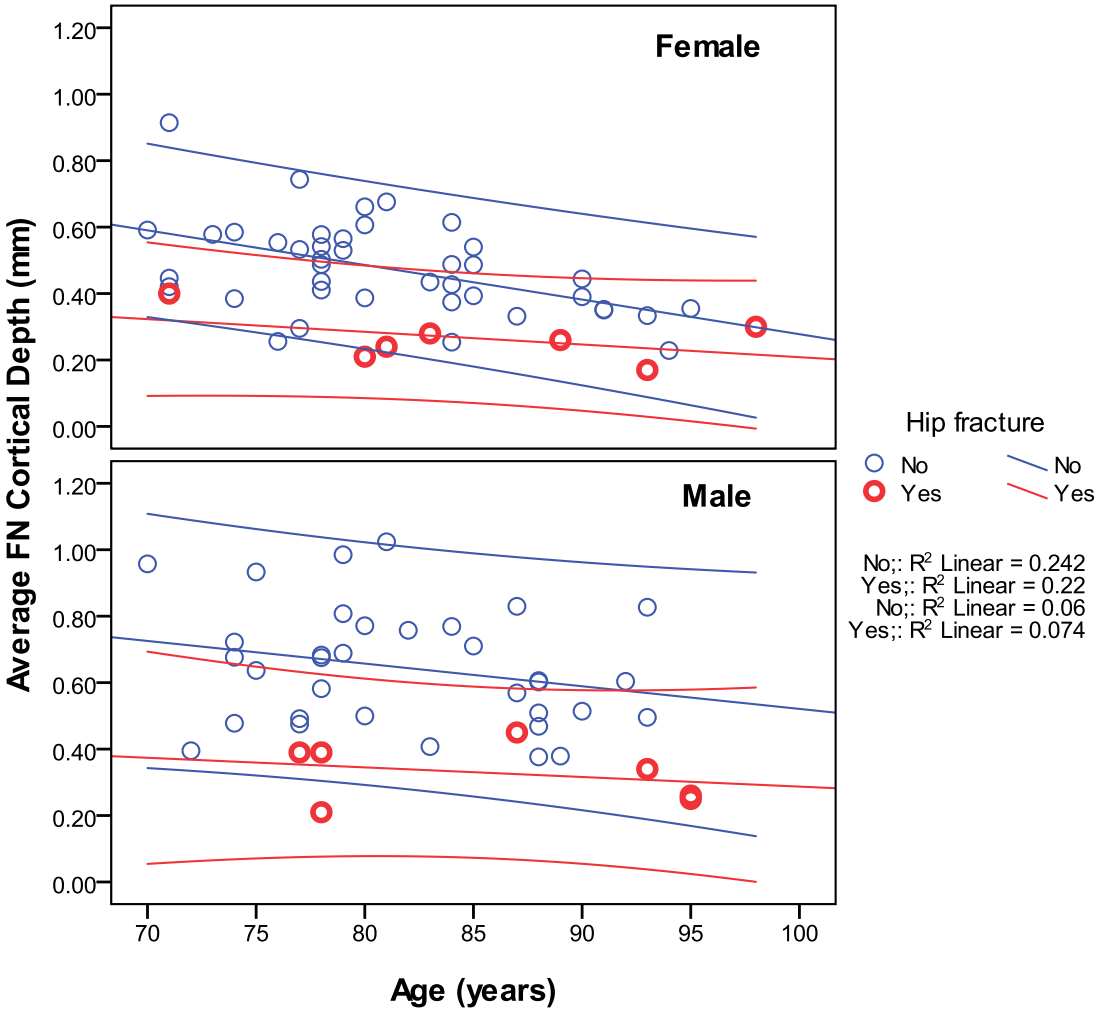

Figure 95 Cortical depths vs. age separated by gender

Figure 95 demonstrates a consistent result in terms of the fractured reference line of best fit for both males and females being almost identical; again noting that there are only seven cases in each gender category.

Fracture cases were then assessed as either inter-trochanteric (IT) or neck of femur (NOF) and comparison made of the cortical depth mean values. Eight NOF cases (males *n*=3, females *n*=5) and six IT cases (males *n*=4, females *n*=2) were identified. Results are included as table 55.

Average Cortical Depth			
Hip fracture present	Mean	N	Std. Deviation
None	.5518	75	.17918
IT	.3117	6	.07360
NOF	.2850	8	.09517
Total	.5116	89	.19182

Table 55 Average cortical depth and fracture type

No significant differences (p<0.05) between the cortical depths of each of the two fracture types were identified for the sample. Observation indicate there to be a possibility of a lower cortical depth resulting in a NOF fracture compared to the inter-trochanteric, though statistically results have been negatively impacted by the small sample size.

7.4 Discussion

7.4.1 VIFM Hip Fracture Epidemiology Discussion

The epidemiological component of this study has observed that of the four VIFM fracture groups; hip fracture-related deaths are more commonly associated with high-velocity impact incidents in young adult males, and age-related bone deteriorations in elderly females. Those males that do however die as a result of age-related hip fracture, have been shown on average to be five-years younger than their female counterparts, which may be explained in part by the increased longevity of females in comparison to males generally (1), and has been reported in the literature previously. This finding of age disparity between the sexes for hip fracture is however an indication of the need to accelerate research into the male osteoporotic condition, especially as life-expectancy differences between genders are reducing (1). The higher mean age of the males involved in a high-velocity impact incident as compared to the females, is likely due to the contribution of work-related deaths as more men are involved in farming and transport industries.

In evaluating the physical characteristics of height weight and BMI of the VIFM hip-fracture sample, it is clear that the high-velocity impact-related hip fractures are taller, heavier and hence have a higher BMI than the old age and fall-related deaths. This fits with current Australian population trend data indicative of a taller and heavier population generally (263). The fall and age-related categories however for both males and females occupy a *healthy* WHO BMI category which counters the frail and malnourished elderly hip fracture stereotype, and therefore requires further investigation (175). It is also possible that their *"healthy"* status triggered their admission to the VIFM rather than a routine death certification.

The inclusion of pathological fractures of the hip was not part of the evaluation, and indeed effort was made to ensure none of these types of fractures were included. There is however epidemiological evidence supporting the inclusion of pathological fractures in any evaluation of osteoporotic fracture, as excluding them is likely causing a substantial underestimation of the burden of osteoporosis (306). Further investigation is therefore warranted. Statistical significance for the entire evaluation might also be enhanced by performing the same search parameters over a 3 or 5 year period, assuming that pathologists' reporting methods had not altered over this period.

7.4.2 MDCT Hip Fracture Discussion

The results from the study of 14 unilateral fracture cases indicate a significant correlation of a lower than expected vBMD for age, with an increased likelihood of hip fracture. Approximately one third of those that had fractured their hip however had vBMD levels that were considered *normal* for their age when compared with their un-fractured peers. Significantly however, the results comparing cortical depth and the presence fracture demonstrated that this variable is likely a more sensitive indicator of hip fracture, as none of those that fractured had a *normal* cortical depth when compared to age matched non-fractured cases. Significant correlation for fracture was not however demonstrated for the aBMD variable even though the measurement is calculated

in the QCT program from the vBMD value. The cortical depth evaluation of the fracture cases also showed potential in correlating the age-related reduction in this measurement with fracture type. Care however needs to be taken with regard to the significance of these particular results as the sample numbers in the fractured group are small and the type of fracture sub-groups smaller again.

The selection of only recent fracture cases assumed a normal level of activity prior to that fracture. The lower than expected vBMD and cortical depth recorded for the fracture cases may also have been as a result of the sedentary nature of the individuals (307), as VIFM case information relating to the activity levels of the individuals was not known.

This fracture study has also demonstrated that in terms of gender differences in femoral neck fracture, the cortical depth may also provide some insight into the empirical distribution of fracture. Cortical depth was shown in chapter four to be significantly higher in the right femoral neck than the left in the young, but that degree of asymmetry was shown to reduce as age increased. There are currently no known data that establishes the prevalence of femoral neck fracture in Australia as a result of osteoporotic cause. The finding of asymmetry in chapter 4 therefore presents a future pathway into understanding the epidemiology of hip fracture in the population generally if hip fracture statistics and cortical depth can be matched in statistically significant numbers. A further study evaluating cortical depth measurements from the high speed-impact-related fracture deaths is also required to determine if there is an association for those with a low cortical depth at any age which predisposes them to a fracture given the high-impact condition.

These fracture data demonstrate that for males and females in this VIFM group, an apparent cortical depth of approximately 0.4mm in the femoral neck at the age of 70 years is a sign of a strong indicator of immanent hip fracture. Obviously the finding is presented with the knowledge that only seven cases existed in each category from which the conclusion is made, and that osteoporotic fractures can

occur in those much younger than 70 years. This finding however is also suggestive of a nominally *"safe"* or *"minimal risk of fracture"* cortical depth value existing for both males and females under a given set of scan conditions. The *"healthy"* value is represented by the values above the line of best fit for the un-fractured group. This sort of differentiation does not currently exist clinically for the vBMD or aBMD variables as mentioned previously. The finding represents the possibility of limiting osteoporotic medications for those unlikely to fracture using the cortical depth as a "*true"* indicator of fracture risk in the femoral neck.

The analysis of BMI and fracture indicated no significant link between BMI and fracture exists for the small population. There is however a requirement for more work to be done in establishing the effects, if any, on the vBMD and cortical depth measurements and BMI. This is important as the Australian population presently has a mean BMI much higher than at any other time in our history.

There was no observed association between trabecular margin length and fracture in these data. The trabecular margin length measurement was established in chapter five to be strongly associated with increasing age, especially in men. It has not however been shown to be indicator of fracture risk in this study. Indeed no femoral morphometric variables tested were shown to be strongly associated with hip fracture.

7.5 Conclusion

QCT and anthropological evaluations have been performed on the un-fractured side of a small number of males and females who had recently sustained a fracture of the proximal femur. These results have then been compared to those from age-matched peers of males and females that have been described in chapters 4 and 5. An epidemiological review of proximal femur fracture in the VIFM population for 2008 has also been included to provide a context for the

population from whom QCT and morphometry evaluations subsequently undertaken.

The unilateral age-related hip fracture study has presented further evidence for using mortuary MDCT data for the refinement of hip fracture risk indicators in the living. Mouse and rat models will not provide useful data in a fragility study, as they bear only a very small amount of weight across four rather than two legs, and thus human investigations such as those discussed throughout this thesis are important. QCT findings have presented the cortical bone depth measurement as a potentially more sensitive indicator of hip fracture risk than either vBMD or aBMD. The aim clinically in comparing fracture and normative data is to determine a range for which treatment and therapy is warranted to minimise or decrease fracture risk, and monitor therapy. Therefore it is a recommendation that further significant studies are performed to further assess the use of the cortical depth variable to identify fracture risk from *imminent* through to *possible* and *unlikely*. The results presented show sufficient practical potential for the use clinical of this variable, and are further suggestive of assisting in predicting the type of fracture, which will also assist in creating targeted or individualised preventative therapy.

Though broad morphometric features of the femora did not appear to correlate with hip fracture in the small fracture sample evaluated, there is however a clear need to continually monitor the generational and age-related changes occurring in the Australian population. The gross morphometry of the femur was shown in chapter 5 to be changing, as are the racial, nutritional and environmental factors that are hallmarks of 21st century urban lifestyles. These fracture data from the VIFM therefore have provided an opportunity to use the novel methods developed in previous chapters to work backwards to identify those most at risk of a femoral neck fracture. The data used is from those for whom the fracture was eventually fatal, and hence these individuals might have had the most benefit from early intervention in lowering their fracture risk if that were possible.

CHAPTER 8

CONCLUSIONS, RECOMENDATIONS AND FUTURE RESEARCH

"There is pleasure in recognising old things from a new point of view."

~ ***Richard Feynman*** ~

8.1 Summary

The major goal of this thesis was to contribute to a greater understanding of the three-dimensional radiological expressions of age-dependent change in the human femur. The practical aim was to design empirically reliable and valid radiological methods to measure age-related differences, and then apply them in the analysis of data from a representative Australian urban population. The final outcome was to construct a theoretical model of age-based difference that can be used to improve prediction of age-related change, and determine biological age characteristics of the human femur generally. The research undertaken used a series of independent empirical studies linking clinical and anthropological disciplines, applied to high-resolution MDCT scans of the femur from a large cross-sectional heterogeneous mortuary population.

A population-based model of the densitometric and morphometric characteristics of bilateral femora did not exist previously, either for a contemporary or past population. The motivation for this work therefore was based in the improved assessment of femoral fracture risk and biological characterisation for disaster victim identification. Current clinical technology provides a basis for the development of a non-invasive 3D technique that has the potential to be used to model age-related changes. This study provides a background into the age-related changes occurring in the femoral bone as our urban population ages, and experiences an increased life-expectancy generally.

Due to the novel application of multiple detector-row computed tomography (MDCT) technology, and its application to medical and anthropologic disciplines, the dissertation has included detailed descriptions of technical features and scientific backgrounds. This has been done because of the wide ranging audience for which this thesis may have interest, and the various levels of familiarity with the equipment and processes used on the part of the reader. Again, due to the novel nature of both the source of MDCT images and the protocols developed, significant effort has also been made throughout to identify potential issues relating to the application of these techniques on the living as demonstrated through the analysis of effective radiation dose in chapter four.

As mentioned throughout, the availability of high-resolution MDCT data and the time constraints on the project have limited the size and scope of the undertaking. These limitations apply in particular to forecasting future changes in the femoral-ageing model or archetype. Nonetheless, the findings are extremely important in highlighting the current status of femoral radiological age characteristics, as well as for identifying potential future trends.

- The first study described in **chapter four**, analysed and compared both spatial and bone mineral density measurements of the bilateral proximal femurs of the 289 adults. The study used commercial clinical QCT software supported by the placement of a bone calibration phantom in the mortuary scanner. In producing the image data, the study established that QCT studies in the dead, conducted without orthodox clinical *patient* positioning can be used to produce bone densitometric assessments. The study also created a reference data base of densitometric differences of the femoral neck in the cross-sectional urban population examined, with particular attention to expressions of gender, symmetry and age. Furthermore the study established the ionising radiation dose delivered by the VIFM MDCT scan and placed it into the context of a clinical investigation for the living.

- The second study described in **chapter five** analysed and compared both the surface and internal gross morphometric measurements of the bilateral femora of the 289 adult population. The study presented a novel, reproducible and importantly, non-invasive method of assessing gender, symmetry, secular and age-related femoral morphology. This study established a practical physical anthropological method, as well as providing supporting evidence for the further application of digital methods for morphological bone assessment.
- The third research study described in **chapter six** analysed the effects of three different MDCT scanning conditions on the spatial and quantitative CT measurements obtained using the clinical software discussed in chapter four.
- The final research study described in **chapter seven** compared the QCT and anthropological findings from a small number of unilateral femoral neck fracture cases to those from the reference data base built in chapters four and five. These comparisons and the epidemiological analysis of the VIFM hip fracture statistics provided observations into the factors important in the analysis of fracture risk for the Australian population generally using 3D imaging.

8.2 Key Findings

The quantitative radiological expressions of age-related differences in the modern urban adult Australian human femur were found to be extremely variable. Nonetheless, given that this work represents the first of its kind, the results are sufficiently encouraging for the author to advocate for further exploration in the development of a radiological-based human archetypal model of femoral age-related change. While it was hoped that the research would produce a simple model of age-related change that may be characterised on a few morphological and/or densitometric variables, this was found not to be the

case. Therefore, this thesis is further evidence to the complex nature of the individual and population-based ageing process generally.

The thesis has also provided evidence to the effects of the application of different algorithms using CT-based technology to assess bone-ageing characteristics. This finding is made especially important as most bone femoral assessments made clinically are based on 2D methods applied to the complex 3D architecture of bone. While it was not the direct intention of this work to dismantle the clinical application of 2D techniques to characterise ageing bone; this work has clearly shown considerable advantages to using the 3D clinical CT based technique.

Results have demonstrated an advantage inherent in the QCT method compared to DXA in determining femoral fracture risk in the living. This advantage is particularly apparent in the study of fracture and cortical bone depth in the femoral neck, as results are presented with a significant number of normal age and gender matched cases. Results have also presented evidence of densitometric and morphological variations of symmetry of the femora as a normal part of the ageing process not previously identified. Young females have been shown to have the most asymmetrical femora, while variations of symmetry in men were shown as less remarkable over the adult lifespan.

Results from studies conducted through the course of the thesis have also produced results supporting the active deployment of non-invasive CT methods for triaging human femoral remains the purposes of mass disaster victim identification, and associated biological identity related requirements. The triaging process using densitometric and morphometric characterisation to select specimens for invasive testing, will prevent or limit the destruction of human tissue necessary for DNA matching. This non-destructive process is of special significance for people such as the Australian aboriginal committee, whose culture does not support the destruction of human tissue.

Results are presented describing the previously unreported age-related changes in the femoral trabecular margin length as visualised using CT. This is an important finding for further isolating the age characteristics of the femoral bone as the derivation of this assessment is possible using tools commonly available in DICOM reading software. The changes observed in the trabecular margin length over age however were not able to be linked to an increase or decrease in any fracture risk of the femoral neck. This aspect may have been due to the relatively small sample size.

Modelling in the form of regression equations and observational assessments for age and physical characteristics such as height has been produced from the densitometric and morphological data. Variables that have been modelled provide robust approximations for height and stature characteristics from the femur, as well as a definitive classification for the sex. It is noted that no single variable assessed provides clear and definitive classification of all of these physical characteristics, though one would expect that this would be the case using only a single long bone.

A key feature in establishing the ongoing flow of information regarding skeletal health and development of the Australian population is the future availability of data. The data will preferably be from non-invasive sources. This thesis has conclusively demonstrated that a mortuary based MDCT scanning facility is able to deliver data that is of sufficient quality for both anthropological and clinical application. This supply of high quality detailed radiological images is of vital importance in understanding the expressions of ageing, but access is limited in the living due to concerns over ionising radiation hazards.

The conclusions from observations contained in this thesis indicate the possibility of a CT-based screening system for the risk of osteoporotic fracture of the femoral neck; however this would require delivering a substantially higher radiation dose than that of current DXA technology. The findings support further investigation into the risk of the higher radiation dose, and the benefit in terms

of a potentially more accurate diagnosis of fracture risk, especially in the context of population based screening. Vigorous informed debate is required before the issue of what is and what is not appropriate in terms of ionising radiation doses delivered for the purposes of diagnosis; especially in age-related conditions, as deleterious effects from radiation exposure often take decades to emerge. Fear and ignorance cannot be allowed to prevail over valid scientific discussion. Interestingly the same *radiation dose debate* is currently being engaged by cardiac specialists who are often reluctant to use MDCT-based cardiac screening because of concerns over dose (305, 308). Perhaps these experiences may inform those yet to come in the fields of QCT analysis and osteoporosis investigation.

Though clinical decision making in this regard is well outside the scope of the thesis, it was useful to establish QCT effective dose estimates for both male and female subjects. Dose estimations showed that while doses are significantly larger than would be delivered during DXA, the advantages of the QCT in terms of a more accurate determination of fracture risk in the elderly will likely be deemed clinically appropriate in a risk-benefit analysis.

If more MDCT units are to be installed in mortuaries where they are used to augment the routine autopsy, the data collected needs to provide pertinent information about ageing, as well being able to be integrated with other information gathered previously. Optimised and standardised protocols need to be developed, with a view to integrating them with clinical investigative methods, so that full utilisation of all data is made. The methods developed in this thesis have sought to combine anthropological and clinical findings for a more complete radiological evaluation of bone, and to more broadly describe the age-related changes. This was a unique perspective from which to investigate the population, and exigent in terms of potentially merging data. Key in this work though, is the finding that though challenging, the amalgamation of methods has provided data with a broader utility than either of one method alone would have created.

8.3 Methodological Advances and Limitations

The advances of technology since the commencement of this project have been moderate in terms of the evolution of the clinical MDCT scanner. Incremental advances in the detector component design and cone-beam algorithm have occurred across all major manufacturers. Few MDCT units however have been collocated in mortuary facilities; hence the VIFM still stands out as an example of foresight in establishing *"best practice"* in the context of the coronial investigation.

The potential for efficiently evaluating the massive amounts of data generated by procedures such as MDCT, pQCT and synchrotron microCT is however advancing rapidly as general advances in computational speed continue. It is expected that file sizes involved in implementing these types of technology will become decreasingly problematic as a direct result of computational advances and cheaper data storage options. It is however of note that dealing with the relatively small files involved in this work (700MB) provided a number of difficulties in obtaining appropriate hardware and software to manage the undertaking.

The study presented is cross-sectional, and so it present findings of differences within a current population rather than changes in individuals over time. Great care therefore needs to be taken in extrapolating the results for the younger categories in the process of modelling for increased age. However it is noted that statistical significance in biology is often difficult to establish, especially when limited access to personal information is available.

It is acknowledged that some of the cases used to produce data in this study may have been subjected to physical therapies and medications such as antiepileptic drugs (AED's), bisphosphonates or corticosteroids, prior to death, which would likely affect the measurements obtained. It is however posited by the author that

this status is representative of the usual circumstance in identifying bones from mass disaster events, but is none the less a limitation of this study.

8.4 Future Research Directions

Future research recommendations are suggested based on further enhancing the modelling of human femoral-ageing within the Australian population. The consequential health issues associated with an increasing average life-expectancy will likely frame future policy and action by governments generally. Future research in the field of age-related changes in bone will increase the ability to determine biological identity using bones or skeletal fragments from events such as the 2009 bushfires that occurred in Victoria killing 173 people (211).

For the living, femoral age models that have the ability to be calibrated for such things as previous and current medications, genetic or racial background, physical activity levels and other lifestyle factors would present new opportunities to more closely examine individual factors influencing age-related expressions. Related to this is the need for new research that explores the extent to which these factors will be affected by a further increase in average life-expectancy, and the impact that this will have on the economic and health policies of the country generally.

As mentioned previously, the data collection and post processing methods developed for this research can be extended by supplementary investigation and additional data, with a view to further enhancing estimation of biological age and archetypal modelling. Cross-cultural and geographical comparisons will also provide further insight into ageing, as continuously updated sets of archetypes are produced.

Finally the variable described as *cortical depth* has been demonstrated as a sensitive indicator of age-related change and fracture risk. The findings

presented in relation to this variable are particularly encouraging given the findings on the stability of quantitative and spatial CT measurements also provided. Further testing that includes greater subject numbers will bring further clarity to the association of this variable with fracture risk. The work would also be enhanced by a better understanding of the radiological differentiation of cortical and trabecular bone. Correlating bone histology with CT images may involve synchrotron microCT methods, and would greatly assist in setting a more accurate or consistent threshold for bone tissue, further enhancing the portability of results from one CT unit to another.

8.5 Conclusion

QCT and CT-based morphological expressions of human femoral ageing have been shown to be extremely variable, further demonstrating that the processes involved as an individual's bone ages are complicated. To say that the inter-individual variability expressed as age-related differences in bone may be defined by the degree to which an individual is afflicted by *osteoporosis*, is overly simplistic.

Novel and adapted MDCT methods for bone QCT and morphometry have been demonstrated throughout this thesis to be efficient and effective methods for 3D quantification of age-related change in human femora using a mortuary-based population. While the use of higher resolution images are desirable to mitigate error associated with the partial volume effect, current clinical MDCT resolution (1-2mm) images have been shown to be effective for documenting age-related densitometric and morphometric differences. The radiological expressions of age-related differentiation at the femoral neck, and in the femur are consistent in terms of increasing age being inversely related to bone mineral density, though young adults and females were shown to be more variable generally, especially in terms of femoral symmetry. Females were also shown to lose volumetric mineral density and cortical depth more quickly with age than males, especially after the period of menopause; even though they commence

adulthood with similar or greater levels than males. The pattern of bone mineral loss however in elderly men was shown to be similar to that of the females, which indicates a need for the further investigation of the male osteoporotic condition.

This thesis has provided evidence of the relationship between the radiological attributes of the human femur and age. Human biological variation has therefore limited the precision of regression modelling in not accounting for the extrinsic effects of genetics, behavior and environment in the ageing process. The further refinement of MDCT techniques that include both intrinsic and extrinsic ageing aspects will likely provide success in terms of enhancing the precision of age estimation and biological identity. The most important contribution of the thesis has been the development of novel and adapted MDCT methods that have furthered the understanding of age-related femoral change in terms of fracture risk determination. A clearer determination of hip fracture risk is vitally important as populations generally increase average life-expectancy, and governments struggle under the cost of an increasingly complex and expensive set of diagnostic tests.

REFERENCES

1. ABS. Population by Age and Sex, Australian States and Territories, Jun 2002 to Jun 2007. Canberra: Australian Bureau of Statistics; 2007.
2. Stini WA. Osteoporosis in Biocultural Perspective. Annual Review of Anthropology. 1995;24:397-421.
3. Abrahamsen B, Van Staa T, Ariely R, Olson M, Cooper C. Excess mortality following hip fracture: a systematic epidemiological review. Osteoporosis International. 2009 Oct;20(10):1633-50.
4. White TD, Folkens PA. The human bone manual. Amsterdam; Boston: Elsevier Academic; 2005.
5. Harada S, Rodan GA. Control of osteoblast function and regulation of bone mass. Nature. 2003 May;423(6937):349.
6. Sievanen H, Kannus P, Jarvinen TL. Bone quality: an empty term. PLoS Med. 2007 Mar;4(3):e27.
7. ABS. Population Projections Australia, 2004 to 2101. Canberra: Australian Bureau of Statistics; 2005.
8. ABS. Australian Historical Population Statistics. Canberra: Australian Bureau of Statistics; 2006.
9. Treasury. Intergenerational Report 2007. Canberra: Australian Government; 2007.
10. Currey JD. Bones : structure and mechanics. 2nd ed. Princeton, N.J.; Woodstock: Princeton University Press; 2006.
11. Wilson EE, Awonusi A, Morris MD, Kohn DH, Tecklenburg MM, Beck LW. Three structural roles for water in bone observed by solid-state NMR. Biophysical journal. 2006 May 15;90(10):3722-31.
12. Duda GN, Schneider E, Chao EY. Internal forces and moments in the femur during walking. Journal of biomechanics. 1997 Sep;30(9):933-41.
13. Wang X, Bank RA, TeKoppele JM, Agrawal CM. The role of collagen in determining bone mechanical properties. Journal of Orthopaedic Research. 2001 Nov;19(6):1021-6.
14. Viguet-Carrin S, Follet H, Gineyts E, Roux JP, Munoz F, Chapurlat R, et al. Association between collagen cross-links and trabecular microarchitecture properties of human vertebral bone. Bone.46(2):342-7.
15. Gorski JP. Is all bone the same? Distinctive distributions and properties of non-collagenous matrix proteins in lamellar vs. woven bone imply the existence of different underlying osteogenic mechanisms. Critical Reviews in Oral Biology and Medicine. 1998 Sep;9(2):201-23.
16. Nyman JS, Roy A, Shen X, Acuna RL, Tyler JH, Wang X. The influence of water removal on the strength and toughness of cortical bone. Journal of biomechanics. 2006;39(5):931-8.
17. Garn SM. Human Growth. Annual Review of Anthropology. 1980;9(1):275-92.
18. Brookes M. The blood supply of bone : an approach to bone biology. London: Butterworths; 1971.
19. Cowin SC, Doty SB. Tissue mechanics. New York: Springer; 2007.

20. Moore SG, Dawson KL. Red and yellow marrow in the femur: age-related changes in appearance at MR imaging. Radiology. 1990 Apr;175(1):219-23.
21. Shen W, Chen J, Punyanitya M, Shapses S, Heshka S, Heymsfield SB. MRI-measured bone marrow adipose tissue is inversely related to DXA-measured bone mineral in Caucasian women. Osteoporosis International. 2007 May;18(5):641-7.
22. Feik SA, Ellender G, Crowe DM, Ramm-Anderson SM. Periosteal response in translation-induced bone remodelling. Journal of anatomy. 1990 Aug;171:69-84.
23. Kolodny A. The Periosteal Blood Supply and Healing of Fractures: Experimental Study. The Journal of Bone and Joint Sugery. 1923 Oct;5(4):698-711.
24. Frost HM. Bone biodynamics. 1st ed. Boston, USA: Little; 1964.
25. Parfitt AM. Quantum concept of bone remodeling and turnover: implications for the pathogenesis of osteoporosis. Calcified tissue international. 1979 Aug;28(1):1-5.
26. Roodman GD. Mechanisms of bone metastasis. New England Journal of Medicine. 2004 Apr;350(16):1655-64.
27. Lieberman DE, Pearson OM, Polk JD, Demes B, Crompton AW. Optimization of bone growth and remodeling in response to loading in tapered mammalian limbs. The Journal of experimental biology. 2003 Sep;206(Pt 18):3125-38.
28. Thompson DD. Age changes in bone mineralization, cortical thickness, and haversian canal area. Calcified tissue international. 1980;31(1):5-11.
29. Wolff J. Concerning the interrelationship between form and function of the individual parts of the organism. By Julius Wolff, 1900. Clinical orthopaedics and related research. 1988 Mar(228):2-11.
30. Pearson OM, Lieberman DE. The aging of Wolff's "law": Ontogeny and responses to mechanical loading in cortical bone. American journal of physical anthropology. 2004;Suppl 39:63-99.
31. Huiskes R. If bone is the answer, then what is the question? Journal of anatomy. 2000 Aug;197 (Pt 2):145-56.
32. Fetto J, Leali A, Moroz A. Evolution of the Koch model of the biomechanics of the hip: clinical perspective. Journal of Orthopaedic Science. 2002;7(6):724-30.
33. Rubin CT. Skeletal strain and the functional significance of bone architecture. Calcified tissue international. 1984;36 Suppl 1:S11-8.
34. Garrison JG, Slaboch CL, Niebur GL. Density and architecture have greater effects on the toughness of trabecular bone than damage. Bone. 2009;44(5):924-9.
35. Akkus O, Adar F, Schaffler MB. Age-related changes in physicochemical properties of mineral crystals are related to impaired mechanical function of cortical bone. Bone. 2004 Mar;34(3):443-53.
36. Robling AG, Castillo AB, Turner CH. Biomechanical and Molecular Regulation of Bone Remodeling. The Annual Review Biomedical Engineering. 2006 Apr;8:455-98.

37. Riggs CM, Lanyon LE, Boyde A. Functional associations between collagen fibre orientation and locomotor strain direction in cortical bone of the equine radius. Anatomy and embryology. 1993 Mar;187(3):231-8.
38. Mikkola T, Sipila S, Portegijs E, Kallinen M, Alen M, Kiviranta I, et al. Impaired geometric properties of tibia in older women with hip fracture history. Osteoporosis International. 2007 Aug;18(8):1083-90.
39. Haapasalo H, Kontulainen S, Sievanen H, Kannus P, Jarvinen M, Vuori I. Exercise-induced bone gain is due to enlargement in bone size without a change in volumetric bone density: a peripheral quantitative computed tomography study of the upper arms of male tennis players. Bone. 2000 Sep;27(3):351-7.
40. Chalmers J, Ray RD. The Growth of Transplanted Foetal Bones in Different Immunological Environments. The Journal of bone and joint surgery. 1962 Feb;44-B(1):149-64.
41. Baldwin KM, White TP, Arnaud SB, Edgerton VR, Kraemer WJ, Kram R, et al. Musculoskeletal adaptations to weightlessness and development of effective countermeasures. Medicine and science in sports and exercise. 1996 Oct;28(10):1247-53.
42. Collet P, Uebelhart D, Vico L, Moro L, Hartmann D, Roth M, et al. Effects of 1- and 6-month spaceflight on bone mass and biochemistry in two humans. Bone. 1997 Jun;20(6):547-51.
43. Warner SE, Sanford DA, Becker BA, Bain SD, Srinivasan S, Gross TS. Botox induced muscle paralysis rapidly degrades bone. Bone. 2006 Feb;38(2):257-64.
44. Bloomfield SA, Hogan HA, Delp MD. Decreases in bone blood flow and bone material properties in aging Fischer-344 rats. Clinical orthopaedics and related research. 2002 Mar(396):248-57.
45. Kita K, Kawai K, Hirohata K. Changes in bone marrow blood flow with aging. The Journal of Orthopaedic Research. 1987;5(4):569-75.
46. Lahtinen T, Alhava EM, Karjalainen P, Romppanen T. The effect of age on blood flow in the proximal femur in man. The Journal Nuclear Medicine Online. 1981 Nov;22(11):966-72.
47. Prisby RD, Ramsey MW, Behnke BJ, Dominguez JM, 2nd, Donato AJ, Allen MR, et al. Aging reduces skeletal blood flow, endothelium-dependent vasodilation, and NO bioavailability in rats. Journal of Bone Mineral Research. 2007 Aug;22(8):1280-8.
48. Brookes M, Revell WJ. Blood supply of bone : scientific aspects. Revised and updated ed. London ; New York: Springer; 1998.
49. Trueta J, Morgan JD. The vascular contribution to osteogenesis. I. Studies by the injection method. The Journal of bone and joint surgery. 1960 Feb;42-B:97-109.
50. Bridgeman G, Brookes M. Blood supply to the human femoral diaphysis in youth and senescence. Journal of anatomy. 1996 Jun;188 (Pt 3):611-21.
51. Trueta J, Harrison MH. The normal vascular anatomy of the femoral head in adult man. The Journal of bone and joint surgery. 1953 Aug;35-B(3):442-61.
52. Trueta J. The normal vascular anatomy of the femoral head in adult man. 1953. Clinical orthopaedics and related research. 1997 Jan(334):6-14.

53. Kingsmill VJ, Gray CM, Moles DR, Boyde A. Cortical vascular canals in human mandible and other bones. Journal of dental research. 2007 Apr;86(4):368-72.
54. Bousson V, Peyrin F, Bergot C, Hausard M, Sautet A, Laredo JD. Cortical bone in the human femoral neck: three-dimensional appearance and porosity using synchrotron radiation. Journal of Bone Mineral Research. 2004 May;19(5):794-801.
55. Thomas CD, Feik SA, Clement JG. Increase in pore area, and not pore density, is the main determinant in the development of porosity in human cortical bone. Journal of anatomy. 2006 Aug;209(2):219-30.
56. Thomas CD, Feik SA, Clement JG. Regional variation of intracortical porosity in the midshaft of the human femur: age and sex differences. Journal of anatomy. 2005 Feb;206(2):115-25.
57. Stein MS, Feik SA, Thomas CD, Clement JG, Wark JD. An automated analysis of intracortical porosity in human femoral bone across age. Journal of Bone Mineral Research. 1999 Apr;14(4):624-32.
58. O'Brien CA, Jia D, Plotkin LI, Bellido T, Powers CC, Stewart SA, et al. Glucocorticoids act directly on osteoblasts and osteocytes to induce their apoptosis and reduce bone formation and strength. Endocrinology. 2004 Apr;145(4):1835-41.
59. Augat P, Schorlemmer S. The role of cortical bone and its microstructure in bone strength. Journal of Age and Ageing. 2006 Sep;35 Suppl 2:ii27-ii31.
60. Wachter NJ, Augat P, Krischak GD, Sarkar MR, Mentzel M, Kinzl L, et al. Prediction of strength of cortical bone in vitro by microcomputed tomography. Clinical biomechanics (Bristol, Avon). 2001 Mar;16(3):252-6.
61. Bell KL, Loveridge N, Reeve J, Thomas CD, Feik SA, Clement JG. Super-osteons (remodeling clusters) in the cortex of the femoral shaft: influence of age and gender. The anatomical record. 2001 Dec 1;264(4):378-86.
62. Commonwealth of Australia. A Picture of Osteoporosis in Australia. Canberra: Australian Institute of Health and Welfare; 2008. p. 1-36.
63. Ritchie RO, Koester KJ, Ionova S, Yao W, Lane NE, Ager JW. Measurement of the toughness of bone: A tutorial with special reference to small animal studies. Bone. 2008 Jun 28.
64. Bouxsein ML, Karasik D. Bone geometry and skeletal fragility. Current osteoporosis reports. 2006 Jun;4(2):49-56.
65. Garden RS. Low-Angle Fixation in Fracture of the Femoral Head. Journal of Bone and Joint Surgery. 1961;43B(4):647-63.
66. Frandsen PA, Andersen E, Madsen F, Skjodt T. Garden's classification of femoral neck fractures. An assessment of inter-observer variation. The Journal of bone and joint surgery. 1988 Aug;70(4):588-90.
67. Bagger YZ, Tanko LB, Alexandersen P, Qin G, Christiansen C. Radiographic measure of aorta calcification is a site-specific predictor of bone loss and fracture risk at the hip. Journal of internal medicine. 2006 Jun;259(6):598-605.
68. Zerahn B, Olsen C, Stephensen S, Kanstrup IL, Schwarz Lausten G. Bone loss after hip fracture is correlated to the postoperative degree of mobilisation. Archives of orthopaedic and trauma surgery. 1998;117(8):453-6.

69. Fox KM, Magaziner J, Hawkes WG, Yu-Yahiro J, Hebel JR, Zimmerman SI, et al. Loss of bone density and lean body mass after hip fracture. Osteoporosis International. 2000;11(1):31-5.
70. Dirschl DR, Henderson RC, Oakley WC. Accelerated bone mineral loss following a hip fracture: a prospective longitudinal study. Bone. 1997 Jul;21(1):79-82.
71. Wehren LE, Hawkes WG, Hebel JR, Orwig D, Zimmerman SI, Fox KM, et al. Predictors of bone loss after hip fracture. Osteoporosis International. 2004 Feb;15(2):125-31.
72. Magaziner J, Wehren L, Hawkes WG, Orwig D, Hebel JR, Fredman L, et al. Women with hip fracture have a greater rate of decline in bone mineral density than expected: another significant consequence of a common geriatric problem. Osteoporosis International. 2006;17(7):971-7.
73. Inman VT. Functional Aspects of the Abductor Muscles of the Hip. The Journal of Bone and Joint Sugery. 1947 July 1, 1947;29(3):607-19.
74. Poole KE, Reeve J, Warburton EA. Falls, fractures, and osteoporosis after stroke: time to think about protection? Stroke; a journal of cerebral circulation. 2002 May;33(5):1432-6.
75. Devine A, Dhaliwal SS, Dick IM, Bollerslev J, Prince RL. Physical activity and calcium consumption are important determinants of lower limb bone mass in older women. Journal of Bone Mineral Research. 2004 Oct;19(10):1634-9.
76. Marcus EL, Menczel J. Higher prevalence of osteoporosis among female Holocaust survivors. Osteoporosis International. 2007 May 11.
77. Filardi S, Zebaze RM, Duan Y, Edmonds J, Beck T, Seeman E. Femoral neck fragility in women has its structural and biomechanical basis established by periosteal modeling during growth and endocortical remodeling during aging. Osteoporosis International. 2004 Feb;15(2):103-7.
78. Makovey J, Nguyen TV, Naganathan V, Wark JD, Sambrook PN. Genetic effects on bone loss in peri- and postmenopausal women: a longitudinal twin study. Journal of Bone Mineral Research. 2007 Nov;22(11):1773-80.
79. Tse KY, Macias BR, Meyer RS, Hargens AR. Heritability of bone density: regional and gender differences in monozygotic twins. Journal of Orthopaedic Research. 2009 Feb;27(2):150-4.
80. Zhai G, Andrew T, Kato BS, Blake GM, Spector TD. Genetic and environmental determinants on bone loss in postmenopausal Caucasian women: a 14-year longitudinal twin study. Osteoporosis International. 2009 Jun;20(6):949-53.
81. Kaneps AJ, Stover SM, Lane NE. Changes in canine cortical and cancellous bone mechanical properties following immobilization and remobilization with exercise. Bone. 1997 Nov;21(5):419-23.
82. Leblanc AD, Schneider VS, Evans HJ, Engelbretson DA, Krebs JM. Bone mineral loss and recovery after 17 weeks of bed rest. Journal of Bone Mineral Research. 1990 Aug;5(8):843-50.
83. Weinreb M, Patael H, Preisler O, Ben-Shemen S. Short-term healing kinetics of cortical and cancellous bone osteopenia induced by unloading during the reloading period in young rats. Virchows Archiv. 1997 Dec;431(6):449-52.

84. Donahue SW, Galley SA, Vaughan MR, Patterson-Buckendahl P, Demers LM, Vance JL, et al. Parathyroid hormone may maintain bone formation in hibernating black bears (Ursus americanus) to prevent disuse osteoporosis. The Journal of experimental biology. 2006 May;209(Pt 9):1630-8.
85. McGee ME, Maki AJ, Johnson SE, Nelson OL, Robbins CT, Donahue SW. Decreased bone turnover with balanced resorption and formation prevent cortical bone loss during disuse (hibernation) in grizzly bears (Ursus arctos horribilis). Bone. 2008;42(2):396-404.
86. Walser M. Ion association. VI. Interactions between calcium, magnesium, inorganic phosphate, citrate and protein in normal human plasma. The Journal of clinical investigation. 1961 Apr;40:723-30.
87. Favus MJ, Goltzman D. Chapter 21. Regulation of Calcium and Magnesium. Primer. 2008;7(1):104-8.
88. Bronner F, Farach-Carson MC. Bone formation. London; New York: Springer; 2004.
89. Seeman E. Pathogenesis of bone fragility in women and men. Lancet. 2002 May 2002;359:1841 - 50.
90. Lonnroos E, Kautiainen H, Karppi P, Hartikainen S, Kiviranta I, Sulkava R. Incidence of second hip fractures. A population-based study. Osteoporosis International. 2007 Sep;18(9):1279-85.
91. WHO. Assessment of Fracture Risk and its Application to Screening for Postmenopausal Osteoporosis: World Health Organisation1994 1994. Report No.: Series No. 843.
92. Schapira D, Schapira C. Osteoporosis: the evolution of a scientific term. Osteoporosis International. 1992 Jul;2(4):164-7.
93. Webber CE. Photon absorptiometry, bone densitometry and the challenge of osteoporosis. Physics in medicine and biology. 2006 Jul 7;51(13):R169-85.
94. Armelagos GJ. Disease in Ancient Nubia. Science. 1969 Jan;163(3864):255-9.
95. Lees B, Molleson T, Arnett TR, Stevenson JC. Differences in proximal femur bone density over two centuries. Lancet. 1993 Mar 13;341(8846):673-5.
96. Mays SA. Age-related cortical bone loss in women from a 3rd-4th century AD population from England. American journal of physical anthropology. 2006 Apr;129(4):518-28.
97. Barbier S, Ecochard R, Schott AM, Colin C, Delmas PD, Jaglal SB, et al. Geographical variations in hip fracture risk for women: strong effects hidden in standardised ratios. Osteoporosis International. 2009 Mar;20(3):371-7.
98. WHO. Assessment of fracture risk and its application to screening for postmenopausal osteoporosis. Report of a WHO Study Group. World Health Organization technical report series1994. p. 1-129.
99. Riggs BL, Melton LJ, 3rd. Involutional osteoporosis. The New England journal of medicine. 1986 Jun 26;314(26):1676-86.
100. Damilakis J, Maris TG, Karantanas AH. An update on the assessment of osteoporosis using radiologic techniques. European radiology. 2007 Jun;17(6):1591-602.

101. Pasco JA, Seeman E, Henry MJ, Merriman EN, Nicholson GC, Kotowicz MA. The population burden of fractures originates in women with osteopenia, not osteoporosis. Osteoporosis International. 2006;17(9):1404-9.
102. Schuit SC, van der Klift M, Weel AE, de Laet CE, Burger H, Seeman E, et al. Fracture incidence and association with bone mineral density in elderly men and women: the Rotterdam Study. Bone. 2004 Jan;34(1):195-202.
103. Blake GM, Fogelman I. The role of DXA bone density scans in the diagnosis and treatment of osteoporosis. Postgrad Medical Journal. 2007 Aug;83(982):509-17.
104. Recker R, Lappe J, Davies KM, Heaney R. Bone remodeling increases substantially in the years after menopause and remains increased in older osteoporosis patients. Journal of Bone Mineral Research. 2004 Oct;19(10):1628-33.
105. Reid IR. Chapter 19. Menopause. Primer. 2008;7(1):95-7.
106. Riis BJ, Hansen MA, Jensen AM, Overgaard K, Christiansen C. Low bone mass and fast rate of bone loss at menopause: equal risk factors for future fracture: a 15-year follow-up study. Bone. 1996 Jul;19(1):9-12.
107. Blain H, Carriere I, Favier F, Jeandel C, Papoz L. Body weight change since menopause and percentage body fat mass are predictors of subsequent bone mineral density change of the proximal femur in women aged 75 years and older: results of a 5 year prospective study. Calcified tissue international. 2004 Jul;75(1):32-9.
108. Bolotin HH. Inaccuracies inherent in dual-energy X-ray absorptiometry in vivo bone mineral densitometry may flaw osteopenic/osteoporotic interpretations and mislead assessment of antiresorptive therapy effectiveness. Bone. 2001;28(5):548-55.
109. Wright VJ. Osteoporosis in men. Journal of the American Acadamy of Orthopaedic Surgeons. 2006 Jun;14(6):347-53.
110. Orwoll ES. Chapter 62. Osteoporosis in Men. Primer. 2008;7(1):286-9.
111. Chiu GR, Araujo AB, Travison TG, Hall SA, McKinlay JB. Relative contributions of multiple determinants to bone mineral density in men. Osteoporosis International. 2009 Mar.
112. Bonjour JP, Theintz G, Law F, Slosman D, Rizzoli R. Peak bone mass. Osteoporosis International. 1994;4 Suppl 1:7-13.
113. Berenson AB, Rahman M, Wilkinson G. Racial difference in the correlates of bone mineral content/density and age at peak among reproductive-aged women. Osteoporosis International. 2009 Aug;20(8):1439-49.
114. Johnston CC, Jr., Slemenda CW. Peak bone mass, bone loss and risk of fracture. Osteoporos International. 1994;4 Suppl 1:43-5.
115. Cooper C, Westlake S, Harvey N, Javaid K, Dennison E, Hanson M. Review: developmental origins of osteoporotic fracture. Osteoporosis International. 2006;17(3):337-47.
116. Bonjour JP, Chevalley T, Rizzoli R, Ferrari S. Gene-environment interactions in the skeletal response to nutrition and exercise during growth. Med Sport Sci. 2007;51:64-80.
117. Riggs BL. Overview of osteoporosis. The Western journal of medicine. 1991 Jan;154(1):63-77.

118. Rizzoli R, Bianchi ML, Garabedian M, McKay HA, Moreno LA. Maximizing bone mineral mass gain during growth for the prevention of fractures in the adolescents and the elderly. Bone. 2010 Feb;46(2):294-305.
119. Burrows M, Baxter-Jones A, Mirwald R, Macdonald H, McKay H. Bone mineral accrual across growth in a mixed-ethnic group of children: are Asian children disadvantaged from an early age? Calcified tissue international. 2009 May;84(5):366-78.
120. Wetzsteon RJ, Petit MA, Macdonald HM, Hughes JM, Beck TJ, McKay HA. Bone structure and volumetric BMD in overweight children: a longitudinal study. Journal of Bone Mineral Research. 2008 Dec;23(12):1946-53.
121. Wren TA, Kim PS, Janicka A, Sanchez M, Gilsanz V. Timing of peak bone mass: discrepancies between CT and DXA. The Journal of clinical endocrinology and metabolism. 2007 Mar;92(3):938-41.
122. Bolotin HH. The significant effects of bone structure on inherent patient-specific DXA in vivo bone mineral density measurement inaccuracies. Medical physics. 2004 Apr;31(4):774-88.
123. Heaney RP, Abrams S, Dawson-Hughes B, Looker A, Marcus R, Matkovic V, et al. Peak bone mass. Osteoporosis International. 2000;11(12):985-1009.
124. Burghardt AJ, Kazakia GJ, Laib A, Majumdar S. Quantitative assessment of bone tissue mineralization with polychromatic micro-computed tomography. Calcified tissue international. 2008 Aug;83(2):129-38.
125. Meganck JA, Kozloff KM, Thornton MM, Broski SM, Goldstein SA. Beam hardening artifacts in micro-computed tomography scanning can be reduced by X-ray beam filtration and the resulting images can be used to accurately measure BMD. Bone. 2009;45(6):1104-16.
126. Cameron JR, Sorenson J. Measurement of Bone Mineral in Vivo: an Improved Method. Science. 1963 Oct 11;142:230-2.
127. Watt DE. Optimum photon energies for the measurement of bone mineral and fat fractions. British Journal of Radiology. 1975 Apr;48(568):265-74.
128. Sorenson JA. Effects of nonmineral tissues on measurement of bone mineral content by dual-photon absorptiometry. Medical physics. 1990 Sep-Oct;17(5):905-12.
129. Bolotin HH. DXA in vivo BMD methodology: An erroneous and misleading research and clinical gauge of bone mineral status, bone fragility, and bone remodelling. Bone. 2007 Jul;41(1):138-54.
130. Matkovic V, Jelic T, Wardlaw GM, Ilich JZ, Goel PK, Wright JK, et al. Timing of peak bone mass in Caucasian females and its implication for the prevention of osteoporosis. Inference from a cross-sectional model. The Journal of clinical investigation. 1994 Feb;93(2):799-808.
131. Souza A, Udupa JK, Saha PK. Volume rendering in the presence of partial volume effects. IEEE transactions on medical imaging. 2005 Feb;24(2):223-35.
132. Mattsson S, Thomas BJ. Development of methods for body composition studies. Physics in medicine and biology. 2006 Jul 7;51(13):R203-28.
133. Doube A. Are DEXA results reproducible? New Zealand Medical Journal. [Letter]. 2005 Apr;118(1212).
134. Andresen R, Haidekker MA, Radmer S, Banzer D. CT determination of bone mineral density and structural investigations on the axial skeleton for

estimating the osteoporosis-related fracture risk by means of a risk score. British Journal of Radiology. 1999 June 1, 1999;72(858):569-78.
135. Braillon PM. Quantitative computed tomography precision and accuracy for long-term follow-up of bone mineral density measurements: a five year in vitro assessment. Journal of Clinical Densitometry. 2002 Fall;5(3):259-66.
136. Mindways SI. QCT PRO Bone Mineral Densitometry Software. CTXA Hip BMD Application Module [serial on the Internet]. 2005 [cited 2007 01 Dec 2007]; (Version 4.0).
137. Sekhon K, Kazakia GJ, Burghardt AJ, Hermannsson B, Majumdar S. Accuracy of volumetric bone mineral density measurement in high-resolution peripheral quantitative computed tomography. Bone. 2009;45(3):473-9.
138. Cody DD, Gross GJ, J. Hou F, Spencer HJ, Goldstein SA, P. Fyhrie D. Femoral strength is better predicted by finite element models than QCT and DXA. Journal of biomechanics. 1999;32(10):1013-20.
139. Buie HR, Campbell GM, Klinck RJ, MacNeil JA, Boyd SK. Automatic segmentation of cortical and trabecular compartments based on a dual threshold technique for in vivo micro-CT bone analysis. Bone. 2007;41(4):505-15.
140. Gleick J. Genius : Richard Feynman and modern physics. London: Little, Brown; 1992.
141. Hiroshima-shi Nagasaki-shi Genbaku Saigaishi Hensh Iinkai. Hiroshima and Nagasaki, the physical, medical, and social effects of the atomic bombings. New York: Basic Books; 1981.
142. AAPM. AAPM Report No. 96 The Measurement, Reporting, and Management of Radiation Dose in CT. NY: American Association of Physicists in Medicine2008.
143. Mettler FA, Jr., Bhargavan M, Faulkner K, Gilley DB, Gray JE, Ibbott GS, et al. Radiologic and nuclear medicine studies in the United States and worldwide: frequency, radiation dose, and comparison with other radiation sources--1950-2007. Radiology. 2009 Nov;253(2):520-31.
144. Kalef-Ezra JA. Risk factors for spinal bone mineral densitometry. Radiation Protection Dosimetry. 1996;66(Nos 1-4):315-7.
145. Kusama T, Kai M, Yabuuchi E, Bessho Y. Dose estimates for patients receiving radiation from various instruments used for measuring bone mass and density. Radiation Protection Dosimetry. 1995;58(2):149-51.
146. Kolta S, Quiligotti S, Ruyssen-Witrand A, Amido A, Mitton D, Bras AL, et al. In vivo 3D reconstruction of human vertebrae with the three-dimensional X-ray absorptiometry (3D-XA) method. Osteoporosis International. 2008 Feb;19(2):185-92.
147. Njeh CF, Fuerst T, Hans D, Blake GM, Genant HK. Radiation exposure in bone mineral density assessment. Applied Radiation and Isotopes. 1999 Jan;50(1):215-36.
148. McCollough CH, Schueler BA. Calculation of effective dose. Medical physics. 2000;27(5):828-37.
149. Trichopoulos D, Li FP, Hunter DJ. What causes cancer? Scientific American. 1996 Sep;275(3):80-7.

150. Cardis E, Vrijheid M, Blettner M, Gilbert E, Hakama M, Hill C, et al. Risk of cancer after low doses of ionising radiation: retrospective cohort study in 15 countries. BJM. 2005 Jul 9;331(7508):77.
151. Manske SL, Liu-Ambrose T, de Bakker PM, Liu D, Kontulainen S, Guy P, et al. Femoral neck cortical geometry measured with magnetic resonance imaging is associated with proximal femur strength. Osteoporosis International. 2006 Oct;17(10):1539-45.
152. Fanucci E, Manenti G, Masala S, Laviani F, Di Costanzo G, Ludovici A, et al. Multiparameter characterisation of vertebral osteoporosis with 3-T MR. La Radiologia medica. 2007 Mar;112(2):208-23.
153. Ecklund K, Vajapeyam S, Feldman HA, Buzney CD, Mulkern RV, Kleinman PK, et al. Bone Marrow Changes in Adolescent Girls with Anorexia Nervosa. Journal of Bone Mineral Research. 2009 Aug 4.
154. Barrack RL, Hip Society (U.S.), Knee Society (U.S.), American Academy of Orthopaedic Surgeons. Orthopaedic knowledge update. Hip and knee reconstruction 3. 3rd ed. Rosemont, IL: American Academy of Orthopaedic Surgeons; 2006.
155. Ruff CB, Hayes WC. Subperiosteal expansion and cortical remodeling of the human femur and tibia with aging. Science. 1982 Sep 3;217(4563):945-8.
156. Ruff CB, Hayes WC. Cross-sectional geometry of Pecos Pueblo femora and tibiae--a biomechanical investigation: II. Sex, age, side differences. American journal of physical anthropology. 1983 Mar;60(3):383-400.
157. Ruff CB, Hayes WC. Cross-sectional geometry of Pecos Pueblo femora and tibiae--a biomechanical investigation: I. Method and general patterns of variation. American journal of physical anthropology. 1983 Mar;60(3):359-81.
158. Rivadeneira F, Zillikens MC, De Laet CE, Hofman A, Uitterlinden AG, Beck TJ, et al. Femoral neck BMD is a strong predictor of hip fracture susceptibility in elderly men and women because it detects cortical bone instability: the Rotterdam Study. Journal of Bone Mineral Research. 2007 Nov;22(11):1781-90.
159. Beck TJ, Oreskovic TL, Stone KL, Ruff CB, Ensrud K, Nevitt MC, et al. Structural adaptation to changing skeletal load in the progression toward hip fragility: the study of osteoporotic fractures. J Bone Miner Res. 2001 Jun;16(6):1108-19.
160. Ahlborg HG, Johnell O, Turner CH, Rannevik G, Karlsson MK. Bone loss and bone size after menopause. The New England journal of medicine. 2003 Jul 24;349(4):327-34.
161. Waters RL, Perry J, Antonelli D, Hislop H. Energy cost of walking of amputees: the influence of level of amputation. The Journal of bone and joint surgery. 1976 January 1, 1976;58(1):42-6.
162. Kleerekoper M. Osteoporosis prevention and therapy: preserving and building strength through bone quality. Osteoporosis International. 2006 Dec;17(12):1707-15.
163. Plotkin LI, Weinstein RS, Parfitt AM, Roberson PK, Manolagas SC, Bellido T. Prevention of osteocyte and osteoblast apoptosis by bisphosphonates and calcitonin. The Journal of clinical investigation. 1999 Nov;104(10):1363-74.

164. van Beek ER, Cohen LH, Leroy IM, Ebetino FH, Löwik CWGM, Papapoulos SE. Differentiating the mechanisms of antiresorptive action of nitrogen containing bisphosphonates. Bone. 2003;33(5):805-11.
165. Liberman UA. Long-term safety of bisphosphonate therapy for osteoporosis: a review of the evidence. Drugs & aging. 2006;23(4):289-98.
166. Hochberg MC, Greenspan S, Wasnich RD, Miller P, Thompson DE, Ross PD. Changes in Bone Density and Turnover Explain the Reductions in Incidence of Nonvertebral Fractures that Occur during Treatment with Antiresorptive Agents. Journal of Clinical Endocrinology and Metabolism. 2002 April 1, 2002;87(4):1586-92.
167. Delmas PD, Seeman E. Changes in bone mineral density explain little of the reduction in vertebral or nonvertebral fracture risk with anti-resorptive therapy. Bone. 2004;34(4):599-604.
168. Benhamou CL. Effects of osteoporosis medications on bone quality. Joint Bone Spine. 2007 Jan;74(1):39-47.
169. Mellstrom DD, Sorensen OH, Goemaere S, Roux C, Johnson TD, Chines AA. Seven years of treatment with risedronate in women with postmenopausal osteoporosis. Calcified tissue international. 2004 Dec;75(6):462-8.
170. Ste-Marie LG, Sod E, Johnson T, Chines A. Five years of treatment with risedronate and its effects on bone safety in women with postmenopausal osteoporosis. Calcified tissue international. 2004 Dec;75(6):469-76.
171. Grynpas MD, Kasra M, Renlund R, Pritzker KP. The effect of pamidronate in a new model of immobilization in the dog. Bone. 1995 Oct;17(4 Suppl):225S-32S.
172. Abbott T. PBS extension to benefit osteoporosis patients. Canberra: Health and Aging; 2006.
173. Lenart BA, Neviaser AS, Lyman S, Chang CC, Edobor-Osula F, Steele B, et al. Association of low-energy femoral fractures with prolonged bisphosphonate use: a case control study. Osteoporosis International. 2009 Aug;20(8):1353-62.
174. Parker D. The Economic Impact of Australia's Ageing Population. CEDA State of the Nation Conference; 14 June 2007; Canberra2007.
175. Cigolle CT, Langa KM, Kabeto MU, Tian Z, Blaum CS. Geriatric conditions and disability: the Health and Retirement Study. Annals of Internal Medicine. 2007 Aug 7;147(3):156-64.
176. Melbourne Uo. The Burden of Brittle Bones Epidemiology, Cost & Burden of Osteoporosis in Australia 2007: University of Melbourne2007.
177. Johnson TR, Krauss B, Sedlmair M, Grasruck M, Bruder H, Morhard D, et al. Material differentiation by dual energy CT: initial experience. European radiology. 2007 Jun;17(6):1510-7.
178. Hounsfield GN. Computerized transverse axial scanning (tomography). 1. Description of system. British Journal of Radiology. 1973 Dec;46(552):1016-22.
179. Kalender WA. X-ray computed tomography. Physics in medicine and biology. 2006 Jul 7;51(13):R29-43.
180. Kalender WA, Seissler W, Klotz E, Vock P. Spiral volumetric CT with single-breath-hold technique, continuous transport, and continuous scanner rotation. Radiology. 1990 July 1, 1990;176(1):181-3.

181. Toshiba. Toshiba features Aquilion One CT. HealthImaging.com; 2007; Available from: http://www.healthimaging.com/index.php?option=com_articles&view=conference&id=publication:37:article:15554:section:24&division=hiit.
182. Schaller S, Flohr T, Klingenbeck K, Krause J, Fuchs T, Kalender WA. Spiral interpolation algorithm for multislice spiral CT--part I: theory. IEEE transactions on medical imaging. 2000 Sep;19(9):822-34.
183. Toshiba. Aquilion 16 Multislice Helical CT Scanner2006.
184. Zeman RK. Helical/spiral CT : a practical approach. New York: McGraw-Hill, Inc., Health Services Division; 1995.
185. Mori I, Suzuki T. Development of Advanced Multislice CT Scanner Aquilion. Medical Review. [Company Journal]. 2002;4:1-8.
186. Hsieh J. Tomographic reconstruction for tilted helical multislice CT. IEEE transactions on medical imaging. 2000 Sep;19(9):864-72.
187. Lewis MA. Multislice CT: opportunities and challenges. British Journal of Radiology. 2001 Sep;74(885):779-81.
188. Rankin SC. Spiral CT: vascular applications. European Journal of Radiology. 1998 Aug;28(1):18-29.
189. Coyne M. Discussions on the formation of the VIFM MDCT scanning protocol. In: Hislop-Jambrich J, editor. Verbal ed2008.
190. Rydberg J, Liang Y, Teague SD. Fundamentals of multichannel CT. Radiologic Clinics of North America. 2003;41(3):465-74.
191. Seeram E. Computed tomography : physical principles, clinical applications, and quality control. 2nd ed. Philadelphia: W.B. Saunders; 2001.
192. Dalrymple NC, Prasad SR, Freckleton MW, Chintapalli KN. Informatics in radiology (infoRAD): introduction to the language of three-dimensional imaging with multidetector CT. Radiographics. 2005 Sep-Oct;25(5):1409-28.
193. Rubin GD. 3-D imaging with MDCT. European Journal of Radiology. 2003 Mar;45 Suppl 1:S37-41.
194. Catphan. Catphan 500 and 600 Manual2006 2/5/08].
195. ARPANSA. Radiation Protection in the Medical Applications of Ionizing Radiation - Code of Practice. In: Australia Co, editor.2008. p. 1-44.
196. AAPM. AAPM Report No. 39 Specification and Acceptance Testing of Computed Tomography Scanners. NY: American Institute of Physics1993.
197. Curry TS, Dowdey JE, Murry RC, Christensen EE. Christensen's physics of diagnostic radiology. 4th ed. Philadelphia: Lea & Febiger; 1990.
198. Bricault I, Ferretti G. A general tool for the evaluation of spiral CT interpolation algorithms: revisiting the effect of pitch in multislice CT. IEEE transactions on medical imaging. 2005 Jan;24(1):58-69.
199. Beutel J, Kim Y, Horii SC. Handbook of Medical Imaging, Volume 3: Display and PACS. SPIE, editor: SPIE Press; 2000.
200. Mettler FA, Jr., Wiest PW, Locken JA, Kelsey CA. CT scanning: patterns of use and dose. Journal of Radiological Protection. 2000 Dec;20(4):353-9.
201. Brenner DJ, Hall EJ. Computed tomography--an increasing source of radiation exposure. New England Journal of Medicine. 2007 Nov 29;357(22):2277-84.

202. Groves AM, Owen KE, Courtney HM, Yates SJ, Goldstone KE, Blake GM, et al. 16-detector multislice CT: dosimetry estimation by TLD measurement compared with Monte Carlo simulation. British Journal of Radiology. 2004 Aug;77(920):662-5.
203. Geleijns J, Jessen KA, Panzer W, Shrimpton PC, Tosi G, Bongartz G, et al. Eurpopean Guidelines on Quality Criteria for Computed Tomography. Office for Official Publications of the European Communities; 2000.
204. Augat P, Eckstein F. Quantitative Imaging of Musculoskeletal Tissue. Annual Review of Biomedical Engineering. 2008 May 8.
205. Guglielmi G, Schneider P, Lang TF, Giannatempo GM, Cammisa M, Genant HK. Quantitative computed tomography at the axial and peripheral skeleton. European radiology. 1997 Feb 21;7(10):32-42.
206. Nazarian A, Snyder BD, Zurakowski D, Muller R. Quantitative micro-computed tomography: A non-invasive method to assess equivalent bone mineral density. Bone. 2008 Apr 30.
207. Gluer CC. Chapter 30. Quantitative Computed Tomography in Children and Adults. Primer. 2008;7(1):158-63.
208. O'Donnell C, Rotman A, Collett S, Woodford N. Current status of routine post-mortem CT in Melbourne, Australia. Forensic Science Medicine and Pathololgy. 2007.
209. Anderson JF, Read JW, Steinweg J. Atlas of imaging in sports medicine. Sydney: McGraw-Hill; 1998.
210. Clark KC, Whitley AS. Clark's positioning in radiography. 12th ed. London: Arnold; 2005.
211. VIFM. 2008-09 Annual Report. Melbourne: VIFM2010.
212. Komar DA, Grivas C. Manufactured populations: what do contemporary reference skeletal collections represent? A comparative study using the Maxwell Museum documented collection. American journal of physical anthropology. 2008 Oct;137(2):224-33.
213. Navarro MC, Sosa M, Saavedra P, Lainez P, Marrero M, Torres M, et al. Poverty is a risk factor for osteoporotic fractures. Osteoporosis International. 2009 Mar;20(3):393-8.
214. Brennan SL, Henry MJ, Wluka AE, Nicholson GC, Kotowicz MA, Williams JW, et al. BMD in Population-Based Adult Women Is Associated With Socioeconomic Status. Journal of Bone and Mineral Research. 2009;24(5):809-15.
215. Peat JK. Health science research : a handbook of quantitative methods. Crows Nest, N.S.W.: Allen & Unwin; 2001.
216. Mardia KV, Kent JT, Bibby JM. Multivariate analysis. London ; New York: Academic Press; 1979.
217. Follet H, Boivin G, Rumelhart C, Meunier PJ. The degree of mineralization is a determinant of bone strength: a study on human calcanei. Bone. 2004 May;34(5):783-9.
218. Seeman E, Delmas PD. Bone quality--the material and structural basis of bone strength and fragility. The New England journal of medicine. 2006 May 25;354(21):2250-61.
219. Ammann P, Rizzoli R. Bone strength and its determinants. Osteoporosis International. 2003;14 Suppl 3:S13-8.

220. Bousson V, Le Bras A, Roqueplan F, Kang Y, Mitton D, Kolta S, et al. Volumetric quantitative computed tomography of the proximal femur: relationships linking geometric and densitometric variables to bone strength. Role for compact bone. Osteoporosis International. 2006;17(6):855-64.
221. Cann CE. Quantitative CT for determination of bone mineral density: a review. Radiology. 1988 Feb;166(2):509-22.
222. Jarvinen TL, Kannus P, Sievanen H. Bone quality: Emperor's new clothes. Journal of musculoskeletal & neuronal interactions. 2008 Jan-Mar;8(1):2-9.
223. Adams J, Bishop N. Chapter 29. DXA in Adults and Children. Primer. 2008;7(1):152-8.
224. Mayhew PM, Thomas CD, Clement JG, Loveridge N, Beck TJ, Bonfield W, et al. Relation between age, femoral neck cortical stability, and hip fracture risk. Lancet. 2005 Jul 9-15;366(9480):129-35.
225. Crabtree N, Loveridge N, Parker M, Rushton N, Power J, Bell KL, et al. Intracapsular hip fracture and the region-specific loss of cortical bone: analysis by peripheral quantitative computed tomography. Journal of Bone Mineral Research. 2001 Jul;16(7):1318-28.
226. Goldman LW. Principles of CT: multislice CT. Journal of Nuclear Medicine Technology. 2008 Jun;36(2):57-68; quiz 75-6.
227. Kalender WA. Effective dose values in bone mineral measurements by photon absorptiometry and computed tomography. Osteoporosis International. 1992 Mar;2(2):82-7.
228. Shrimpton PC, Jones DG. NRPB-SR250: Normalised Organ Doses for X-Ray Computed Tomography Calculated Using Monte Carlo Techniques. In: Board NRP, editor. NRPB-SR2502008.
229. Guthrie JR, Ebeling PR, Hopper JL, Barrett-Connor E, Dennerstein L, Dudley EC, et al. A prospective study of bone loss in menopausal Australian-born women. Osteoporosis International. 1998;8(3):282-90.
230. McNitt-Gray MF. AAPM/RSNA Physics Tutorial for Residents: Topics in CT. Radiation dose in CT. Radiographics. 2002 Nov-Dec;22(6):1541-53.
231. Khoo BC, Brown K, Cann C, Zhu K, Henzell S, Low V, et al. Comparison of QCT-derived and DXA-derived areal bone mineral density and T scores. Osteoporosis International. 2009 Sep;20(9):1539-45.
232. Brown JK, Cann CE, Prince RL. Age Effects on Hip Structure: Results in 636 women aged 20-97. ASBMR 2007; Hawaii2007.
233. Faulkner KG, Gluer CC, Grampp S, Genant HK. Cross-calibration of liquid and solid QCT calibration standards: corrections to the UCSF normative data. Osteoporosis International. 1993 Jan;3(1):36-42.
234. Burr DB, Piotrowski G, Martin RB, Cook PN. Femoral mechanics in the lesser bushbaby (Galago senegalensis): structural adaptations to leaping in primates. The anatomical record. 1982 Mar;202(3):419-29.
235. Steele CR, Zhou LJ, Guido D, Marcus R, Heinrichs WL, Cheema C. Noninvasive determination of ulnar stiffness from mechanical response--in vivo comparison of stiffness and bone mineral content in humans. Journal Biomechical Engineering. 1988 May;110(2):87-96.

236. Marjanovic EJ, Ward KA, Adams JE. The impact of accurate positioning on measurements made by peripheral QCT in the distal radius. Osteoporosis International. 2009 Jul;20(7):1207-14.
237. Loveridge N, Power J, Reeve J, Boyde A. Bone mineralization density and femoral neck fragility. Bone. 2004 Oct;35(4):929-41.
238. Poole KE, Compston JE. Osteoporosis and its management. BMJ (Clinical research ed. 2006 Dec 16;333(7581):1251-6.
239. Hansson B, Karambatsakidou A. Relationships between entrance skin dose, effective dose and dose area product for patients in diagnostic and interventional cardiac procedures. Radiation Protection Dosimetry. 2000;90(Nos 1-2):141-4.
240. RSNA. Safety: Radiation Exposure in X-ray Examinations. RSNA; 2009 [updated June 10th 2009; cited 2009 06 August 2009]; Available from: http://www.radiologyinfo.org/en/safety/index.cfm?pg=sfty_xray.
241. Carey DP, Smith DT, Martin D, Smith G, Skriver J, Rutland A, et al. The bi-pedal ape: plasticity and asymmetry in footedness. Cortex. 2009 May;45(5):650-61.
242. Coren S, Halpern DF. Left-handedness: a marker for decreased survival fitness. Psychological Bulletin. 1991 Jan;109(1):90-106.
243. ABS. How Australians Measure Up. Canberra: Australian Bureau of Statistics; 1995. p. 1-48.
244. Nurzenski MK, Briffa NK, Price RI, Khoo BC, Devine A, Beck TJ, et al. Geometric indices of bone strength are associated with physical activity and dietary calcium intake in healthy older women. Journal of Bone Mineral Research. 2007 Mar;22(3):416-24.
245. Feik SA, Thomas CD, Bruns R, Clement JG. Regional variations in cortical modeling in the femoral mid-shaft: sex and age differences. American journal of physical anthropology. 2000 Jun;112(2):191-205.
246. Lauretani F, Bandinelli S, Griswold ME, Maggio M, Semba R, Guralnik JM, et al. Longitudinal changes in BMD and bone geometry in a population-based study. Journal of Bone Mineral Research. 2008 Mar;23(3):400-8.
247. Eklund F, Nordström A, Björnstig U, Nordström P. Bone mass, size and previous fractures as predictors of prospective fractures in an osteoporotic referral population. Bone. 2009;45(4):808-13.
248. Kiel DP, Rosen CJ, Dempster D. Chapter 20. Age-Related Bone Loss. Primer. 2008;7(1):98-103.
249. Lou Bonnick S. HSA: Beyond BMD with DXA. Bone. 2007;41(1, Supplement 1):S9-S12.
250. Ito M, Wakao N, Hida T, Matsui Y, Abe Y, Aoyagi K, et al. Analysis of hip geometry by clinical CT for the assessment of hip fracture risk in elderly Japanese women. Bone.46(2):453-7.
251. Simpson G, Hartrick GS. Use of thoracic computed tomography by general practitioners. Medical Journal of Australia. 2007 Jul 2;187(1):43-6.
252. Upton AC. The state of the art in the 1990's: NCRP Report No. 136 on the scientific bases for linearity in the dose-response relationship for ionizing radiation. Health Physics. 2003 Jul;85(1):15-22.

253. Royal HD. Effects of low level radiation-what's new? Seminars in Nuclear Medicine. 2008 Sep;38(5):392-402.
254. Reid IR. Relationships between fat and bone. Osteoporosis International. 2008 May;19(5):595-606.
255. Travison TG, Araujo AB, Esche GR, Beck TJ, McKinlay JB. Lean mass and not fat mass is associated with male proximal femur strength. Journal of Bone Mineral Research. 2008 Feb;23(2):189-98.
256. Scheuer L. Application of osteology to forensic medicine. Clinical anatomy (New York, NY. 2002 Jun;15(4):297-312.
257. Rissech C, Schaefer M, Malgosa A. Development of the femur--Implications for age and sex determination. Forensic science international. 2008;180(1):1-9.
258. Mall G, Graw M, Gehring K, Hubig M. Determination of sex from femora. Forensic science international. 2000 Sep;113(1-3):315-21.
259. Auerbach BM, Ruff CB. Limb bone bilateral asymmetry: variability and commonality among modern humans. Journal of Human Evolution. 2006 Feb;50(2):203-18.
260. Hauser R, Smolinski J, Gos T. The estimation of stature on the basis of measurements of the femur. Forensic science international. 2005 Jan;147(2-3):185-90.
261. Gehring KD, Haffner HT, Weber D, Graw M. Investigations on the reliability of determining an individual's age from the proximal femur. Homo. 2002;52(3):214-20.
262. Tuniz C, Gillespie R, Jones C. The bone readers : atoms, genes and the politics of Australia's deep past. Crows Nest, N.S.W.: Allen & Unwin; 2009.
263. ABS. 2004-05 Overweight and Obesity in Australia. Canberra: Australian Bureau of Statistics; 2008. p. 1-44.
264. Rollet E. De la mensuration des os longs des membres. Theses pour le doctorat en medecine liere. 1888;Series 43:1-128.
265. Formicola V. Stature reconstruction from long bones in ancient population samples: an approach to the problem of its reliability. American journal of physical anthropology. 1993 Mar;90(3):351-8.
266. Trotter M, Gleser G. The effect of ageing on stature. American journal of physical anthropology. 1951;9(3):311-24.
267. Trotter M, Gleser GC. Estimation of stature from long bones of American Whites and Negroes. American journal of physical anthropology. 1952 Dec;10(4):463-514.
268. Wheatley BP. An evaluation of sex and body weight determination from the proximal femur using DXA technology and its potential for forensic anthropology. Forensic science international. 2005 Jan 29;147(2-3):141-5.
269. Robinson C, Eisma R, Morgan B, Jeffery A, Graham EA, Black S, et al. Anthropological Measurement of Lower Limb and Foot Bones Using Multi-Detector Computed Tomography. Journal of Forensic Science. 2008 Sep.
270. Milos A, Selmanovic A, Smajlovic L, Huel RL, Katzmarzyk C, Rizvic A, et al. Success rates of nuclear short tandem repeat typing from different skeletal elements. Croation Medical Journal. 2007 Aug;48(4):486-93.

271. Davoren J, Vanek D, Konjhodzic R, Crews J, Huffine E, Parsons TJ. Highly effective DNA extraction method for nuclear short tandem repeat testing of skeletal remains from mass graves. Croation Medical Journal. 2007 Aug;48(4):478-85.
272. ICMP. DNA. ICMP; 2008 [cited 2008 08 October 2008]; ICMP website of dna service]. Available from: http://www.ic-mp.org/activities/technical-assistance/dna/.
273. Primorac D, Andelinovic S, Definis-Gojanovic M, Drmic I, Rezic B, Baden MM, et al. Identification of war victims from mass graves in Croatia, Bosnia, and Herzegovina by use of standard forensic methods and DNA typing. Journal of Forensic Science. 1996 Sep;41(5):891-4.
274. Bertelsen PK, Clement JG, Thomas CD. A morphometric study of the cortex of the human femur from early childhood to advanced old age. Forensic science international. 1995 Jun 30;74(1-2):63-77.
275. Watanabe Y, Konishi M, Shimada M, Ohara H, Iwamoto S. Estimation of age from the femur of Japanese cadavers. Forensic science international. 1998 Nov 30;98(1-2):55-65.
276. Lynnerup N, Frohlich B, Thomsen JL. Assessment of age at death by microscopy: unbiased quantification of secondary osteons in femoral cross sections. Forensic science international. 2006 May 15;159 Suppl 1:S100-3.
277. Lynnerup N, Thomsen JL, Frohlich B. Intra- and inter-observer variation in histological criteria used in age at death determination based on femoral cortical bone. Forensic science international. 1998 Feb 16;91(3):219-30.
278. WHO. Physical status: the use and interpretation of anthropometry. Report of a WHO Expert Committee. World Health Organization technical report series. 1995;854:1-452.
279. Appropriate body-mass index for Asian populations and its implications for policy and intervention strategies. Lancet. 2004 Jan 10;363(9403):157-63.
280. Bass WM. Human osteology: a laboratory and field manual. 3rd ed. Columbia, Mo.: Missouri Archaeological Society; 1987.
281. Mays SA. Asymmetry in Metacarpal Cortical Bone in a Collection of British Post-Mediaeval Human Skeletons. Journal of Archaeological Science. 2002;29(4):435-41.
282. Schranz D. Age determination from the internal structure of the humerus. American journal of physical anthropology. 1959 Dec;17(4):273-7.
283. Acsadi G, Nemekseri J. History of human life span and mortality. Budapest: Akademiai Kiado; 1970.
284. El-Kaissi S, Pasco JA, Henry MJ, Panahi S, Nicholson JG, Nicholson GC, et al. Femoral neck geometry and hip fracture risk: the Geelong osteoporosis study. Osteoporosis International. 2005 Oct;16(10):1299-303.
285. Kuiper JW, Van Kuijk C, Grashuis JL. Distribution of trabecular and cortical bone related to geometry. A quantitative computed tomography study of the femoral neck. Investigative radiology. 1997 Feb;32(2):83-9.
286. Covino SW, Mitnick RJ, Shprintzen RJ, Cisneros GJ. The accuracy of measurements of three-dimensional computed tomography reconstructions. Journal of Oral Maxillofacial Surgery. 1996 Aug;54(8):982-90; discussion 90-1.

287. Benazzi S, Maestri C, Parisini S, Vecchi F, Gruppioni G. Sex assessment from the acetabular rim by means of image analysis. Forensic science international. 2008 Aug 8.
288. Janus ED, Laatikainen T, Dunbar JA, Kilkkinen A, Bunker SJ, Philpot B, et al. Overweight, obesity and metabolic syndrome in rural southeastern Australia. Medical Journal of Australia. 2007 Aug 6;187(3):147-52.
289. Mandal MK. Left handedness: Facts and figures across cultures*. Psychology and Developing Societies. [Sage Publications]. 2001;13(2):20.
290. Hulme PA, Boyd SK, Ferguson SJ. Regional variation in vertebral bone morphology and its contribution to vertebral fracture strength. Bone. 2007;41(6):946-57.
291. Brooks RA. A quantitative theory of the Hounsfield unit and its application to dual energy scanning. JournaL of Computer Assisted Tomography. 1977 Oct;1(4):487-93.
292. Clarke MS. The effects of exercise on skeletal muscle in the aged. Journal of musculoskeletal & neuronal interactions. 2004 Jun;4(2):175-8.
293. Yang RS, Chieng PU, Tsai KS, Liu TK. Symmetry of bone mineral density in the hips is not affected by age. Nuclear Medicine Communications. 1996 Aug;17(8):711-6.
294. Jantz LM, Jantz RL. Secular change in long bone length and proportion in the United States, 1800-1970. American journal of physical anthropology. 1999 Sep;110(1):57-67.
295. Yang KT, Yang AD. Evaluation of activity of epiphyseal plates in growing males and females. Calcified tissue international. 2006 Jun;78(6):348-56.
296. O'Neill TW, Grazio S, Spector TD, Silman AJ. Geometric measurements of the proximal femur in UK women: secular increase between the late 1950s and early 1990s. Osteoporosis International. 1996;6(2):136-40.
297. Peleg S, Dar G, Medlej B, Steinberg N, Masharawi Y, Latimer B, et al. Orientation of the human sacrum: anthropological perspectives and methodological approaches. American journal of physical anthropology. 2007 Jul;133(3):967-77.
298. Kantor S. Serial scanning for BMD. In: Hislop-Jambrich J, editor. Email ed. Melbourne2009. p. 1.
299. Ebbesen EN, Thomsen JS, Beck-Nielsen H, Nepper-Rasmussen HJ, Mosekilde L. Vertebral bone density evaluated by dual-energy X-ray absorptiometry and quantitative computed tomography in vitro. Bone. 1998;23(3):283-90.
300. Beck TJ, Ruff CB, Warden KE, Scott WW, Jr., Rao GU. Predicting femoral neck strength from bone mineral data. A structural approach. Investigative radiology. 1990 Jan;25(1):6-18.
301. ABS. Causes of Death, Australia, 2006. Canberra: Australian Bureau of Statistics; 2006.
302. ABS. Muskuloskeletal Conditions in Australia: A Snapshot, 2001. Canberra: Australian Bureau of Statistics; 2001.
303. AIHW. Arthritis and osteoporosis in Australia 2008. In: Welfare AIoHa, editor. Canberra: National Centre for Monitoring Arthritis and Musculoskeletal Conditions; 2008. p. 1-172.

304. ABS. Health Indicators, 2009. Canberra: Australian Bureau of Statistics; 2009.
305. Prokop M. New challenges in MDCT. European radiology. 2005 Dec;15 Suppl 5:E35-45.
306. Curtis JR, Taylor AJ, Matthews RS, Ray MN, Becker DJ, Gary LC, et al. "Pathologic" fractures: should these be included in epidemiologic studies of osteoporotic fractures? Osteoporosis International. 2009 Nov;20(11):1969-72.
307. Rittweger J, Simunic B, Bilancio G, Gaspare De Santo N, Cirillo M, Biolo G, et al. Bone loss in the lower leg during 35 days of bed rest is predominantly from the cortical compartment. Bone. 2009;44(4):612-8.
308. Fei X, Du X, Li P, Liao J, Shen Y, Li K. Effect of dose-reduced scan protocols on cardiac coronary image quality with 64-row MDCT: a cardiac phantom study. European Journal of Radiology. 2008 Jul;67(1):85-91.